IOWA STATE UNIVERSITY
Digital Repository

Retrospective Theses and Dissertations

Iowa State University Capstones, Theses and Dissertations

1-1-2004

Slope reinforcement using soil displacement grouted micropiles

Mark Jason Thompson
Iowa State University

Follow this and additional works at: https://lib.dr.iastate.edu/rtd

Recommended Citation

Thompson, Mark Jason, "Slope reinforcement using soil displacement grouted micropiles" (2004). *Retrospective Theses and Dissertations*. 20291.
https://lib.dr.iastate.edu/rtd/20291

This Thesis is brought to you for free and open access by the Iowa State University Capstones, Theses and Dissertations at Iowa State University Digital Repository. It has been accepted for inclusion in Retrospective Theses and Dissertations by an authorized administrator of Iowa State University Digital Repository. For more information, please contact digirep@iastate.edu.

www.manaraa.com

Slope reinforcement using

soil displacement grouted micropiles

by

Mark Jason Thompson

A thesis submitted to the graduate faculty

in partial fulfillment of the requirements for the degree of

MASTER OF SCIENCE

Major: Civil Engineering (Geotechnical Engineering)

Program of Study Committee:
David White (Major Professor)
Vernon Schaefer
Thomas Rudolphi

Iowa State University
Ames, Iowa
2004

Copyright © Mark Jason Thompson, 2004. All rights reserved.

Graduate College

Iowa State University

This is to certify that the master's thesis of

Mark Jason Thompson

has met the thesis requirements of Iowa State University

Signatures have been redacted for privacy

TABLE OF CONTENTS

LIST OF FIGURES

LIST OF TABLES

LIST OF ABBREVIATIONS AND SYMBOLS

General		Units
c	cohesion	kPa
ϕ	internal friction angle	degrees
γ	unit weight of soil	kN/m^3
E_S	soil modulus	kN/m^2
b	pile diameter	mm
EI	pile stiffness	$kN\text{-}m^2$
M_u	moment capacity	kN-m
D_1	center-to-center spacing	m
D_2	clear spacing	m
Limit Resistance Curves		
z	depth	m
Z_S	depth to sliding surface	m
P_u	ultimate soil pressure	kN/m
F_S	limit soil resistance	kN
F_S'	limit soil resistance	kN/m
$F_{S,max}$	maximum F_S value, at the pile tip elevation	kN
F_A	limit anchorage resistance	kN
F_A'	limit anchorage resistance	kN/m
F_M	limit member resistance	kN
F_M'	limit member resistance	kN/m
F_R	composite limit resistance	kN
F_R'	composite limit resistance	kN/m
M_{max}	maximum moment developed in pile	kN-m
α	ultimate soil pressure reduction factor	

SDGM Design

FS	factor of safety	
ΣF_D	driving forces of slope (per unit length)	kN/m
ΣF_R	resisting forces of slope (per unit length)	kN/m
ΔF_R	total stabilizing force (per unit length)	kN/m
n	required number of pile rows	

ABSTRACT

Remediation of slope failures requires stabilization alternatives that address causes of slope instability. Slope reinforcement using pile stabilization practices can be an effective method of remediation in preventing slope movements in weak soils where enhanced drainage does not provide adequate stability. Soil load transfer to pile elements from the downslope soil movement, as occurs in the slope failures, is a complex soil-structure interaction problem. The significant differences in existing design procedures of pile stabilization suggest that the stabilizing mechanisms are not fully understood. The downslope soil movement of slope failures induces unique, unknown lateral load distributions along stabilizing piles. The reliable estimation of these load distributions is important, because the influence of piles on the global stability of the slope depends directly on the pile loading condition.

Soil-structure interactions for small-diameter piles subject to lateral soil movement were investigated by conducting full-scale pile load tests, in which piles installed through a shear box were indirectly loaded by uniform lateral translation of soil. Instrumentation of the shear boxes and pile reinforcement indicated the load distributions that developed along the piles. The load test analyses which succeeded the pile load tests support the claim that the distributed loads which are achieved during pile loading vary linearly with depth. The product of the analysis, which answers a central question of the research, is directly incorporated into the proposed design methodology for soil displacement grouted micropiles.

It is apparent from the pile load tests that small-diameter pile elements provide effective passive resistance to lateral soil movement. The proposed, non-proprietary remediation technology, if implemented into current slope remediation practices, offers an alternative that gives consideration to cost constraints, schedule constraints, and constructability concerns of local transportation agencies.

CHAPTER 1

INTRODUCTION

INDUSTRY PROBLEM

Socioeconomic Issues of Slope Instability

Failures of slopes occur throughout the world and contribute to economic and casualty losses. These losses, intuitively proportional to the magnitude of failure, are direct and indirect costs to individuals and institutions. Direct costs include the replacement and maintenance of structures and transportation facilities. Indirect costs include loss of tax revenues on properties devalued as a result of slope failures and loss of industrial and agricultural productivity due to the damage of land (Spiker and Gori 2003). The impact of slope failures on these losses is often undervalued. The U.S. Geological Survey (Spiker and Gori 2003) estimates that the United States, every year, experiences in excess of $1 billion in damages and approximately 50 deaths; worldwide, slope failures cause 100's of billions of dollars in damage and 100's of thousands of deaths. More locally, the annual cost for remediation and maintenance of slopes often exceeds state and county transportation budgets. The U.S. Geological Survey is leading a newly-developed, 10-year plan to "substantially reduce the risk of loss of life, injuries, economic costs, and destruction of natural and cultural resources caused by landslides and other ground-failure hazards" (Spiker and Gori 2003). Current understanding of such socioeconomic losses therefore justifies the allocation of funds needed for slope stability research.

The need for slope stability research and the development of new remediation technologies is evidenced by a survey of Iowa county engineers conducted in 2001. Table 1 provides the percent of Iowa counties having experienced the presented slope failure conditions (e.g. frequency, soil type, etc). Select survey results are shown graphically in Figure 1.

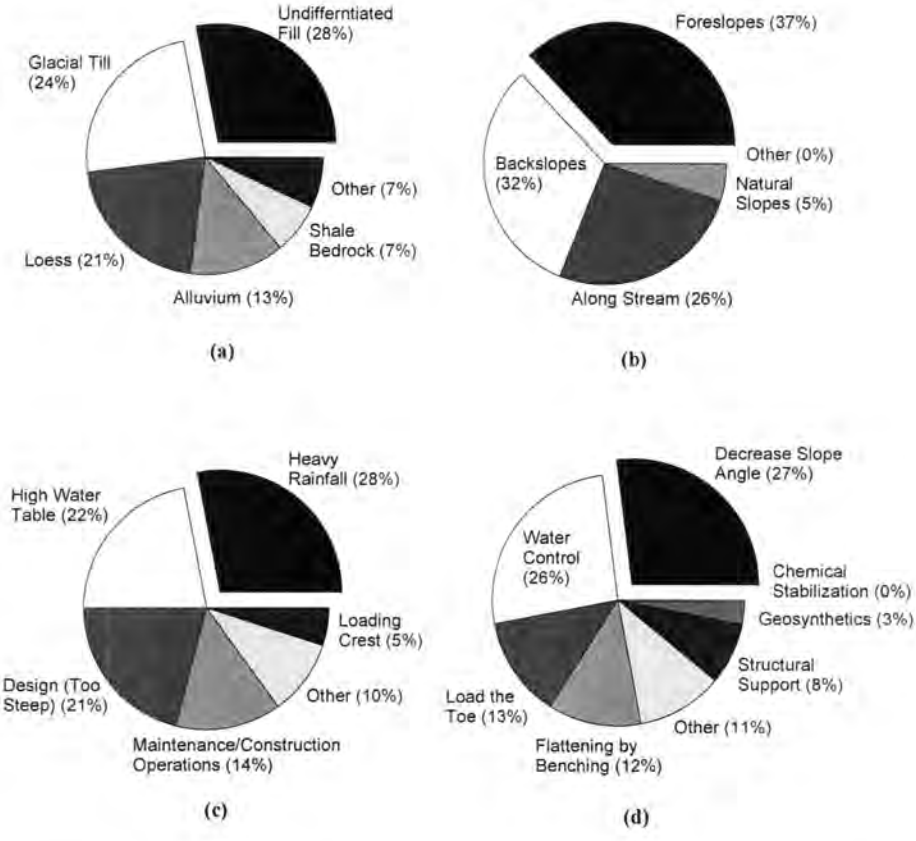

Figure 1 – Conditions of Iowa Slope Failures (after Lohnes et al. 2001)
(a) Soil Types; (b) Location; (c) Cause; (d) Remediation of Slope Failures

Table 1 – Conditions of Iowa Slope Failures (after Lohnes et al. 2001)

Landslide Frequency	**1 - 5**	**6 - 10**	**11 - 15**	**15 +**	—
	44%	25%	14%	17%	—
Soil Types	**Fill**	**Glacial Till**	**Loess**	**Alluvium**	**Shale Bedrock**
	28%	24%	21%	13%	7%
Landslide Location	**Foreslope**	**Backslope**	**Along Stream**	**Natural Slope**	—
	37%	32%	26%	5%	—
Probable Causes	**Heavy Rainfall**	**High Water Table**	**Poor Design**	**Human Activity**	**Loading Crest**
	28%	22%	21%	14%	5%
Slope Angle	**< 1:1**	**1:1 - 2:1**	**2:1 - 3:1**	**3:1 - 4:1**	**> 4:1**
	18%	49%	29%	3%	1%
Slope Height	**1 - 10 ft**	**11 - 20 ft**	**21 - 30 ft**	**> 30 ft**	—
	25%	41%	21%	13%	—
Remediation / Preventative Method	**Flattening**	**Water Control**	**Load Toe**	**Benching**	**Structural Support**
	27%	26%	13%	12%	8%

Research Problem Statement

Slope instability continues to pose problems for highway systems in Iowa. Failures occur on both new embankment foreslopes and cut backslopes. The failures occur because identifying factors that affect stability at a particular location, such as soil shear strength values, ground water surface elevations, and negative influences from construction activities are often difficult to discern and measure. The U.S. Geological Survey (Spiker and Gori 2003) recognizes that hazard identification is a cornerstone of landslide hazard mitigation. Once a failure occurs or a potential failure is identified, highway agencies need information and knowledge of which methods of remediation will be most effective to stabilize the slope. Ideally, these stability problems can be discovered and addressed before a slope failure occurs. When remediation is necessary, however, options are needed that give consideration to the remediation goals, cost constraints, environmental constraints, schedule constraints, and constructability. Newly-developed technologies for the repair of nuisance slope failures and maintenance of state transportation infrastructure are ideally simple, rapid, and cost-effective.

RESEARCH GOAL

Development of Slope Remediation Technology

Research was conducted to develop a new innovation in slope stabilization for Iowa soil conditions. The research group conceived soil displacement grouted micropiles (SDGM) as small-diameter, grouted columns that are easily and rapidly constructed. The slope stabilization alternative was to be sufficiently developed to implement into current slope remediation practices of state and county transportation agencies in Iowa.

TECHNICAL PROBLEM

Load Transfer of Piles Subject to Lateral Soil Movement

Soil load transfer to relatively stiff pile elements from the downslope soil movement as occurs in a slope failure is a complex soil-structure interaction problem. The downslope soil movement of slope failures induces unique, unknown lateral load distributions along stabilizing piles that are a function of soil type, pile size, pile spacing, and relative movement between the pile and soil. The reliable estimation of these load distributions and resolution of the technical problem are important, because the influence of piles on the global stability of an unstable slope depends directly on the loading.

Lateral soil movement described herein refers to the movement associated with slope failures, as opposed to the movement associated with settling embankments, excavation operations, or tunneling operations. The applicability of piles for stabilization of the latter movement is beyond the scope of the research and not considered.

Preceding Research Investigations

Several investigators (e.g. Broms 1964, Reese et al. 1974, Ito and Matsui 1975, Poulos 1995) have studied the interaction of piles subject to lateral soil movement. The methods for pile stabilization exhibit significant differences, suggesting that the stabilizing mechanisms are not fully understood. The present research aims to evaluate the existing analytical methods, focusing on the applicability of the methods to slender, small-diameter micropiles. Full-scale pile load tests facilitate the evaluation and subsequent recommendation of a "best", most applicable method.

RESEARCH OBJECTIVES

Measure and Interpret Loads Induced by Lateral Soil Movement

Soil-structure interactions for small-diameter piles subject to lateral soil movement are investigated by conducting full-scale pile load tests. Proposed pile load tests are conducted in a manner similar to large-scale direct shear tests, where piles installed through a shear box into existing ground are indirectly loaded by uniform lateral translation of soil. Instrumented shear boxes aid the evaluation of stress-strain relationships of "reinforced" soil. Instrumentation of pile reinforcement (i.e. strain gauges) provides bending moment profiles and offers evidence of the distributed loads developed along the pile. The determination of loads induced by lateral soil movement and characterization of load transfer is the principal objective for resolving the technical problem and achieving the overall research goal.

Measure Material Properties of Soil and Pile Elements

Soils are complicated engineering materials because the material properties are highly variable and must often be estimated for geotechnical engineering design and analysis. Common laboratory tests to evaluate soil shear strength parameters for slope stability analyses include direct shear tests and triaxial compression tests, considering drained and/or undrained conditions. Because laboratory tests can be expensive and time consuming, the Iowa Borehole Shear Test (BST) is an alternative in-situ test that provides shear strength parameters on an effective stress or drained basis. High quality shear strength parameters, obtained from the aforementioned tests, are principal inputs for evaluating slope stability, with and without reinforcement.

The material properties associated with pile elements are less variable than soil and are predicted to a higher degree of certainty with fewer laboratory tests. Although combining concrete and reinforcing steel to achieve a more effective composite material complicates the

evaluation of engineering properties, established methods are available for predicting the performance of the composite material.

Knowledge of soil and pile material properties is necessary for the analysis of pile load tests and facilitates the prediction of pile behavior with analytical and finite element methods.

Predict Pile Behavior Associated with Lateral Soil Movement

The prediction of pile behavior associated with downslope soil movement is important to the development of the proposed remediation technology. The potential implementation of the technology requires that design engineers use existing resources (e.g. analytical methods, computer software) to reproduce the response of a pile subject to the loading conditions of slope reinforcement. The development of the SDGM stabilization design methodology, for example, relies on closed-form analytical methods to predict pile behavior including maximum moment and shear forces. The design method also incorporates conventional limit equilibrium methods to determine the factor of safety against slope instability. The research project evaluated existing analytical models and the ability of the models to predict pile loading conditions. The research project employed computer software (LPILE) to identify and calibrate the pile response subject to the given loading conditions.

Develop SDGM Stabilization Design Methodology

The implementation of SDGM stabilization requires a rational procedure for designing micropiles and the micropile stabilization system for given slope failure conditions. The design procedure for SDGM remediation draws upon concepts of existing remediation methods, but demonstrates the unique behavior of soil reinforced by soil displacement grouted micropiles. The research objective is particularly important, because technical literature offers little guidance to engineers designing pile-stabilized slopes.

Demonstrate Stability of Pile-Stabilized Slopes

The demonstration of pile-stabilized slope stability incorporates the achievement of the preceding research objectives. The demonstration involves the validation of proposed analytical methods with measured pile behavior, the prediction of pile behavior with methods already employed by geotechnical design engineers, and sample designs that utilize the proposed design methodology.

RESEARCH SIGNIFICANCE

Development of Slope Remediation Technology

Research funded by the Iowa Highway Research Board was conducted with the primary goal of developing the aforementioned slope remediation alternative. Demonstration of the stability of pile-stabilized slopes, inclusive of a reliable design methodology, assists state transportation agencies with incorporating pile stabilization systems into slope remediation practices. Pile stabilization can be more effective and more appropriate than conventional stabilization practices (i.e. excavation, drainage).

Continuation of Research on Piles Subject to Lateral Soil Movement

The present research follows the work of Reese et al. (1974), Ito and Matsui (1975), and Poulos (1995). The full-scale pile load tests of controlled soil type, pile size, and pile spacing offer a unique data set that explores the respective influences on piles subject to lateral soil movement. Every effort was made to perform research that was collectively innovative and practical.

DOCUMENT ORGANIZATION

Chapter 1 – Introduction

Chapter 1 provides an introduction to the problem of slope instability and the use of small-diameter micropiles for the stabilization of shallow slope failures. The research goals and objectives are discussed with a focus on how the investigation resolves the technical issues associated with pile-stabilized slopes. In addition to the benefits of the research project, the section provides a framework for how the research findings will be implemented.

Chapter 2 – Background

Chapter 2 presents a comprehensive review of literature. The principal objective of the literature review is the more complete understanding of slope stability and slope remediation alternatives. The review of literature demonstrates the vast scope of current remedial methods. The conceptual understanding of each remedial method, including pile stabilization, reveals considerations that are important to the development of new remediation technologies and soil displacement grouted micropiles, in particular.

Chapter 3 – Research Testing Methods

Chapter 3 details the conception, preparation, and performance of experimental tests for characterizing load transfer of piles subject to lateral soil movement. The chapter offers an overview of soil displacement grouted micropiles and explains the development of the comprehensive testing program. The testing program, which includes laboratory and field tests, is completed to satisfy the research objectives of measuring properties of engineering materials and evaluating the loads induced on piles subject to uniform lateral translation of soil. Additionally, results from laboratory testing are presented in Chapter 3.

Chapter 4 – Load Test Results

Chapter 4 provides the results from load tests on piles subject to lateral soil movement. The material of the chapter supports the discussion of results and design methodology of the subsequent chapters. The following load test results are presented:

- Shear box load-displacement relationship
- Pile head load-displacement relationship
- Shear box rotation and tilt
- Relative displacement of shear box and pile head
- Pile moment distributions
- Photogrammetry
- Soil sampling with in-situ testing devices

Chapter 5 – Load Test Analysis and Discussion of Results

Chapter 5 presents the load test analysis, which was performed to: (1) determine the load distributions induced on piles due to lateral soil movement, (2) determine the ultimate soil pressure as a function of depth, and (3) verify the predicted structural performance of piles under the loading condition of slope reinforcement. The analysis, accomplished by comparing observed behavior of pile load tests with predicted behavior for trial load distributions applied to the piles, incorporates existing analytical models of pile-stabilized slopes and evaluates the applicability of the methods to soil displacement grouted micropile stabilization in Iowa soils.

Chapter 6 – SDGM Design Methodology

Chapter 6 establishes a protocol for designing pile-stabilized slopes, making use of the preceding load test data and results. The design method incorporates limit states of the matrix soil and the proposed pile, such that the design method is based on failure of the soil

or structural failure of the pile. The design method extends the determination of the resisting force of a single pile to the determination of the influence of multiple piles on global slope stability. The proposed design method involves evaluating the stability of a failing slope with common limit equilibrium methods and using prepared design charts for calculating a new factor of safety for the pile-stabilized slope.

Chapter 7 – Conclusions

Chapter 7 presents the conclusions of the research investigation. The conclusions address the research goals and objectives, and indicate the successes for each phase of the research project.

Chapter 8 – Recommendations

Chapter 8 provides recommendations regarding how the research is to be implemented in the immediate and long-term future. The author recommends that the design methodology be further explored by means of pilot studies of stabilizing slope failures in Iowa. The implementation of the design method and process of slope monitoring provides critical evidence as to whether the proposed remediation alternative is an effective and viable option for slope stabilization in Iowa.

CHAPTER 2

BACKGROUND

INTRODUCTION

The purpose of the background is to summarize important concepts of slope stability and slope stabilization. Slope stability is a basic subject of geotechnical engineering. Slope stabilization with pile elements, however, is a specialized subject of geotechnical engineering and the focus of only limited research. The background is divided into five sections, where each section more closely relates to the load transfer of piles subject to lateral soil movement than the preceding section. Understanding of the concepts aids the performance of research and the development of new remediation technologies.

Complicating Issues of Pile-Stabilized Slopes

Stabilization of unstable slopes with pile elements is complicated by factors affecting pile performance under the loading conditions of slope reinforcement and factors controlling the influence of piles on global slope stability. The research group acknowledges the following complicating issues of pile-stabilized slopes:

- **Prediction of load distributions along piles** – The load development on piles subject to downslope soil movement, presented earlier as the research technical problem, is important; because the influence of piles on the global stability of an unstable slope depends directly on the loading. This issue is the focus of performed experimental and analytical work and is addressed throughout the document.

- **Influence of soil type** – Understanding the influence of soil type is important for designing pile stabilization. The engineering properties of soil – soil shear strength parameters, in particular – control the stability of the unreinforced slope and the required reinforcement capacity. Stress-strain behavior of slope soils and the determination of an ultimate soil pressure profile with depth facilitate the development of limit resistances considering failure of soil above the failure surface, failure of soil due to insufficient anchorage, and structural failure of the pile elements.
- **Influence of pile size and spacing** – The influence of pile size and spacing on slope and pile stability of reinforced slopes is evidenced by the dependence of pile behavior on the reinforcement parameters. Load-displacement (p-y) curves, which are used to relate pile displacement and soil response, are most reliably back-calculated from pile load tests and are found to vary with pile size and spacing.
- **Pile orientation** – The orientation of piles with respect to slope and failure surfaces affects the performance of reinforcement and the influence of reinforcement on slope stability. The resultant stabilizing force of a pile does not necessarily act in the same direction as the failure surface, and only one directional component of the force acts to oppose slope movement. Also of consequence, skin friction achieved by pile elements potentially reduces the normal stress between the unstable and stable soil masses, resulting in reduced soil shear resistance. The research group recognizes, however, that the stabilization potential of slender pile elements is optimized by altering the inclination of the piles to develop axial loads (i.e. tension or compression), reducing the loads responsible for pile bending. Heavily-reinforced piles may benefit from mobilization of tension, whereas lightly-reinforced piles may benefit from mobilization of compression. The research group performing tests on soil displacement grouted micropiles, for this study, did not evaluate the influence of pile orientation on pile behavior. The pile and the resistance developed along the pile

were perpendicular and parallel to the shear plane, respectively. Battered (i.e. non-vertical) piles accept axial loads due to the mobilization of skin friction along the length of piles subject to soil movement. The performance of pile load tests on battered piles is the next most important task for improving remediation with soil displacement grouted micropiles.

- **Truncation of piles** – The truncation of piles likely increases the capacity of the reinforcement system. Aside from potential reductions in the total applied load on the pile, the moment development in a truncated pile is reduced due to the shortened moment-arm on which the load acts. This benefit is particularly important for slope stabilization with slender pile elements, because the moment capacity of the pile sections controls the failure mode of the stabilization system.
- **Soil arching** – Soil arching refers to the transfer of loads from weak elements to strong, stiff elements. The phenomenon is applicable to pile-stabilized slopes, where deforming soil indirectly transfers load to stiff pile elements. Soil arching is generally regarded as a contributor to the capacity of the slope reinforcement. Unfortunately, designers of pile stabilization do not fully understand the conditions necessary for soil arching to occur or the quantitative effects of soil arching on the stability of reinforced slopes.
- **Stress concentrations** – The loads developed on piles subject to downslope movement are induced by displacement. The imposition of displacement compatibility between piles and adjacent soil result in stress concentrations of which current design methodologies fail to consider. The difference in stiffness between soil and steel-reinforced concrete involve a requisite difference in mobilized stresses, for a given displacement.

The preceding issues of pile-stabilized slopes, several of which are addressed by the current research project, are illustrated in Figure 2.

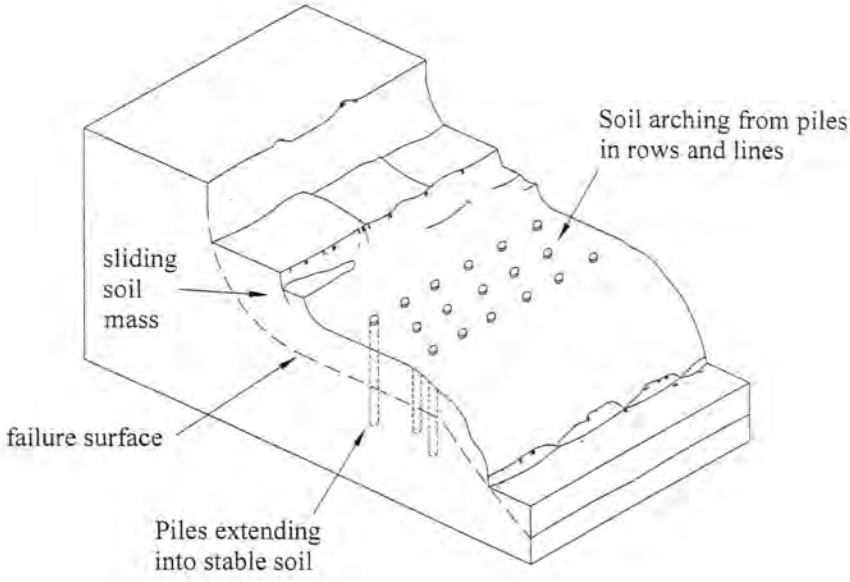

(a)

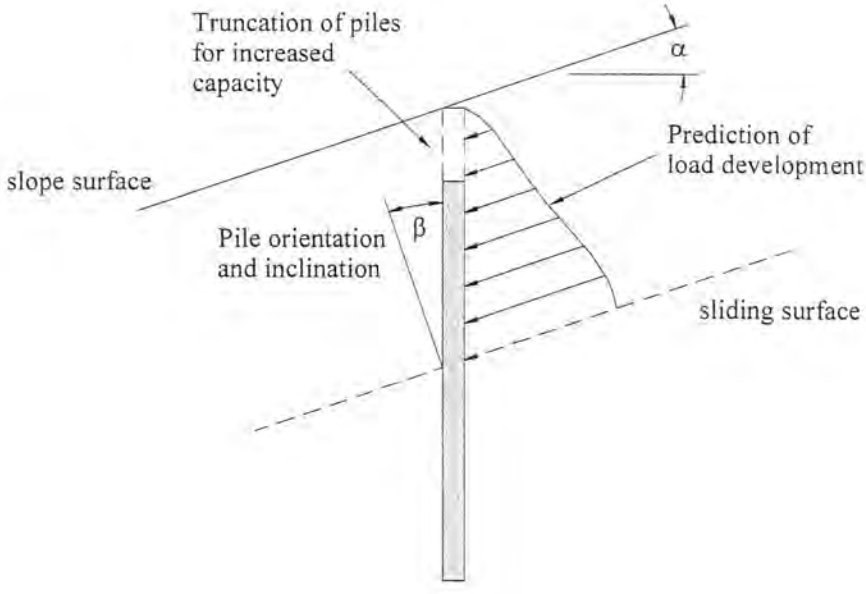

(b)

Figure 2 – Issues of Pile-Stabilized Slopes

(a) Plan view; (b) Elevation view

CONCEPTS OF SLOPE STABILITY

Factors of Safety and Slope Stability

Factors of safety (FS) are used to quantitatively indicate the adequacy of the stability of slopes. By definition, the factor of safety is the ratio of forces resisting slope movement to forces driving slope movement. The definition is presented in the following equation:

$$FS = \frac{\Sigma F_R}{\Sigma F_D} \tag{1}$$

or

$$FS = \frac{\Sigma M_R}{\Sigma M_D}$$

where F_R = forces resisting slope movement,

F_D = forces driving slope movement

M_R = moment resisting slope movement, and

M_D = moment driving slope movement

When the forces driving movement equal the forces resisting movement, the factor of safety equals unity (FS = 1.0) and the slope approaches failure.

Qualitatively, slopes are stable, marginally stable, or actively unstable (Crozier 1986). Popescu (1994) interprets the stages of stability as follows: "stable slopes are those where the margin of stability is sufficiently high to withstand all destabilizing forces; marginally stable slopes are those which will fail at some time in response to destabilizing forces; and actively unstable slopes are those in which destabilizing forces produce continuous or intermittent movement." The stages are naturally applied to a continuum based on the probability of failure.

Factors Influencing Slope Stability

Popescu (1994) classified the causal factors of slope failures as either preparatory causal factors or triggering causal factors. Preparatory causal factors are influences that promote slope instability without actually initiating movement. Triggering causal factors are influences that elicit movement. A negative influence, such as water, is potentially a preparatory and a triggering causal factor. In general, however, preparatory causal factors are long term influences and triggering causal factors are short term influences. Figure 3 illustrates the effects of negative influences on the stability of a slope. The figure also incorporates the stages of stability.

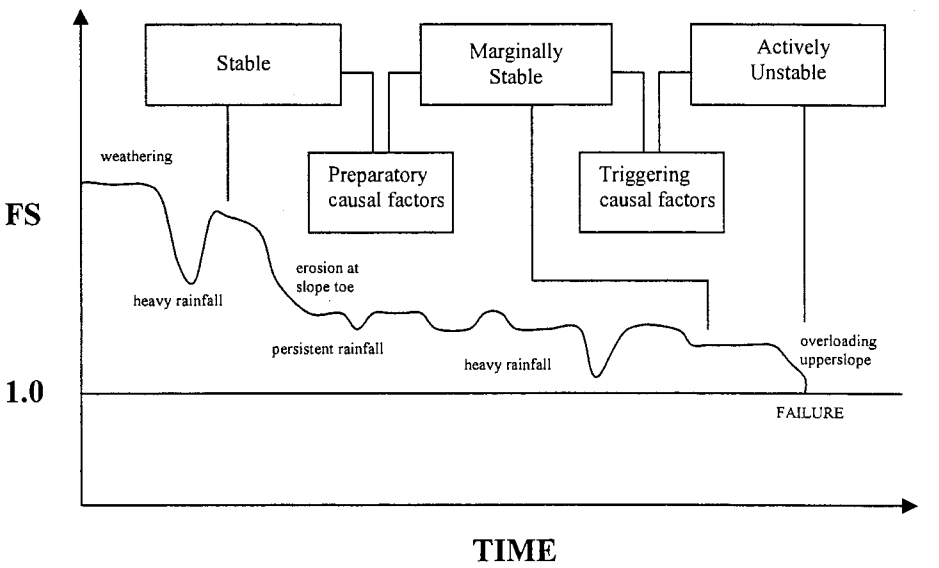

Figure 3 – Effects of Causal Factors on Slope Stability (reproduced from Popescu 1994)

Analyzing the Stability of Slopes

Limit equilibrium methods are popular with geotechnical engineers, and the various methods are commonly used in developing slope stability software. Limit equilibrium methods for determining the stability of slopes divide a slide-mass into *n* slices. Each slice is

subjected to a force system that is resolved with equilibrium equations (Abramson et al. 2002). A factor of safety is computed with the forces driving and resisting slope failure.

Solutions to limit equilibrium systems are, in actuality, statically indeterminate. Consequently, simplifying assumptions are established to make the problems determinate. These assumptions help differentiate the various limit equilibrium methods. Table 2 provides the static equilibrium conditions satisfied by the methods.

Table 2 – Conditions Satisfied by Limit Equilibrium Methods (Abramson et al. 2002)

	Force Equilibrium		**Moment**
Method	**x**	**y**	**Equilibrium**
Ordinary method of slices	No	No	Yes
Bishop's simplified	Yes	No	Yes
Janbu's simplified	Yes	Yes	No
Lowe and Darafiath's	Yes	Yes	No
Corps of Engineers	Yes	Yes	No
Spencer's	Yes	Yes	Yes
Bishop's rigorous	Yes	Yes	Yes
Janbu's generalized	Yes	Yes	No
Sarma's	Yes	Yes	Yes
Morgenstern-Price	Yes	Yes	Yes

Recent developments of finite element methods are being applied to geotechnical engineering projects and slope stability problems in particular. Finite element methods produce solutions which incorporate complex stress distributions from within a slope. Limit equilibrium methods oversimplify lateral stresses, and the solutions fail to consider the stress history of the slope soils. Practically, the advantage of finite element analysis over limit equilibrium methods is that the aforementioned assumptions regarding interslice forces and locations of failure surfaces are unnecessary to generate a solution. The assumptions of limit equilibrium methods are more consequential when the slope stability analysis incorporates

piles or geosynthetic reinforcement, such that finite element analysis is best suited for research applications or large-scale engineering projects.

The finite element method is used to evaluate slope stability with the following two methods: gravity load increase or more commonly shear strength reduction (FLAC 2004). The shear strength reduction method effectively lowers the shear strength parameters of soil by a reduction factor that just causes the slope to fail. Where SRF is the strength reduction factor, Equation 2 and Equation 3 are used to generate modified shear strength parameters.

$$c_f = \frac{c}{SRF} \tag{2}$$

$$\phi_f = \tan^{-1}\left(\frac{\tan\phi}{SRF}\right) \tag{3}$$

Practicing engineers still employ limit equilibrium methods more often than finite element methods. Solutions of finite element methods require thorough understanding of slope soil behavior and, thus, necessitate extensive soil exploration programs. This gathering of information consumes time and economic resources. Also, finite element solutions can be prohibitively expensive with regards to computational resources. Slope stability programs that employ limit equilibrium methods evaluate the stability of slopes in a fraction of the time that is required for finite element method programs. Nevertheless, the rapid advancement in computing technologies requires that engineers become familiar with finite element analysis. In all likelihood, engineers will eventually utilize finite element analysis in professional fields of engineering practice and research.

OVERVIEW OF IOWA SOIL CONDITIONS

Relationship Between Geology and Slope Stability

The relationship between geology and slope stability is important to geologists and geotechnical engineers. The following geological elements are of particular concern to geotechnical engineers: soil origin; engineering properties of soil such as unit weight, moisture content, and strength; and stress history of soil. Geology influences slope stability in terms of soil and rock properties and the contact interfaces of two soil or rock types (Lohnes et al. 2001). For example, a dense soil with low shear strength is highly susceptible to slope failure. The driving forces associated with the high unit weight likely exceed the resisting forces of the soil. Additionally, a geologic contact between two soil types is a potential slope failure plane. As a result of this relationship, the current research project examined the distribution of soil types in Iowa.

Lohnes et al. (2001) divided Iowa into three significantly different geological regions. North central Iowa, western Iowa, and eastern Iowa are composed of glacial till, friable loess, and plastic loess, respectively. Furthermore, alluvium and weathered shale exist in portions of Iowa and are susceptible to slope instability.

Loess

The source of loess in the Midwest is fine rock flour produced by the grinding processes of continental glaciers. The fine-grained rock flour was deposited on floodplains and, upon drying, subsequently transported by wind to deposition locations. Therefore, "the Missouri and Mississippi rivers and their tributaries are the principal sources of [Iowan] loess deposits" (Anderson 1998).

Loess is an eolian soil, and the transportation agent is responsible for several consequences of soil deposition. As the distance between the source and deposition location increases, the texture of loess changes from silty loam through silty clay loam to silty clay

(Davidson 1960). Specifically, the average particle size of loess decreases and the plasticity of loess increases. The differentiations between individual loess deposits in Iowa have been established and documented by Davidson (1960). The engineering properties of loess vary and cannot be used indiscriminately for the purposes of design and analysis of slopes.

Glacial Till

The origin of glacial till in Iowa is drift deposits of the Wisconsinan Glacial Stage. The Sheldon Creek Formation was established approximately 25,000 to 38,000 years ago and succeeded by the Dow Formation, established approximately 15,000 years ago (Anderson 1998). Deposits of glacial till reflect the progress of glaciers in the central lowland. "Glacial ice surged into Iowa and reached its terminal position in Des Moines" (Anderson 1998). The region is appropriately referred to as the Des Moines Lobe.

Glacial till is comprised of unsorted, unstratified, and generally heterogeneous material (Abramson et al. 2002). High density, high strength, and low compressibility are indicative of the glacier deposits. Also associated with glacial till are erratics – rocks that are foreign to the local area. "The large erratics of Iowa are of igneous and metamorphic origins" (Anderson 1998).

Alluvium

Alluvium is most commonly found in floodplains that are occasionally submerged by excess water caused by heavy rains and/or rapidly melting snow. Alluvial deposits are established when soil particles settle out of flowing or standing water. Soil particles settle when the flow of water is insufficient to maintain the suspension of particles. Thus, "the deposits are generally of relatively narrow particle size range regardless of whether they consist of cobbles and gravels from rushing rivers and creeks, sands from moderately moving rivers, or clays from sluggish rivers, or from precipitation water moving in sheets down the

sides of gentle slopes" (Abramson et al. 2002). The deposition environment and resulting soil characteristics promote potential landslides.

Weathered Shale

Weathering of shale is achieved through mechanical and chemical processes (Mitchell 1993). Overburden stresses and relative movement contribute to the disintegration of shale rock, and oxidation alters the chemical composition of the soil. These changes are evidenced by widely varying soil appearance. Weathered shale is particularly susceptible to slope failure when the slope experiences a change in groundwater conditions (Abramson et al. 2002). Wetting of the slope, attributed to heavy rainfall or melting snow, "softens clay and weathered shale, thus providing lubricated sliding surfaces, and [simultaneously] increases the weight of the material" (Abramson et al. 2002). These effects synergistically reduce the factor of safety of slope stability.

SLOPE STABILITY REMEDIATION METHODS

Remedial methods for arresting slope movement must consider the specific causal factors contributing to slope instability. Beyond this fundamental notion, the selection of an appropriate remedial method must also address engineering and economic feasibility, as well as social and environmental acceptability (Popescu 1994).

The principal objective of discussing possible solutions to slope instability is to demonstrate the vast scope of conventional and unconventional remedial methods. The conceptual understanding of each remedial method reveals considerations that are beneficial in the development of new remediation technologies, specifically soil displacement grouted micropiles.

Excavation

The most intuitive remedial method involves the excavation of failed slopes. The addition and removal of soil from a slope undoubtedly influence the resisting and driving forces of a slope failure and consequently alter the stability of a slope. As a result of the relative simplicity of the method, regional departments of transportation make use of the method. While the excavation method often includes benching or buttressing, the most commonly used method for repairing slopes involves slope flattening.

Slope flattening involves a change in slope geometry, such that the stability of the new slope is improved. Although effective, the remedial method is difficult to achieve along transportation corridors where right-of-way limits do not allow the change. The method is not used for remediation when the acquisition of right-of-way is too time consuming and/or too expensive. Figure 4 illustrates the slope flattening method for increasing slope stability.

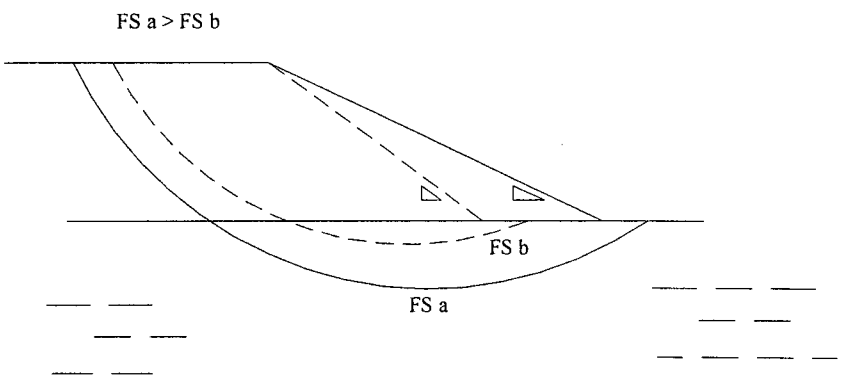

Figure 4 – Slope Flattening for Slope Stabilization

Horizontal Drainage

Groundwater seepage is regarded as a potential cause of failure for nearly all geotechnical engineering projects, and groundwater is a contributing factor to slope instability. Specifically, water contributes to slope failures when the rate of drainage is

inadequate and the slope experiences an increase in pore water pressure (Forrester 2001). The stability of slopes is dependent on surface and subsurface drainage, especially when a slope has experienced a previous slope failure (Lohnes 2001). The methods for controlling *surface* water (e.g. ditches, permeable aprons, and crack sealing) provide a path for water to flow, as opposed to infiltration and consequential slope saturation. *Subsurface* drainage, removal of water from within a slope, can be effectively achieved with trench drains, drainage galleries, and wells.

The University of Missouri-Rolla recently explored the use of horizontal wick drains as a means of subsurface drainage and unconventional slope remediation. An initial assessment of the method suggests that the wick drains successfully lower water levels and enhance the stability of slopes (Santi 2001).

Wick drains were installed with a sequential process whereby wicks were loaded into a push pipe and driven into a vertical cut in a slope (Santi 2001). The push pipe was pulled from the slope, and a sacrificial anchor ensured that the wick drain remain in the slope. The problems associated with installing horizontal wick drains included buckling of the push pipe and excessive damage to drive plates. The problems were easily resolved with the use of larger diameter push pipes and an attached pipe section at the leading end of the push pipe, respectively.

Bioengineering

Bioengineering uses living materials to construct structures that perform some engineering function (Polster 2003). When bioengineering remediation incorporates geosynthetics, the approach is referred to as biotechnical engineering. In addition to slope stabilization and erosion control, however, bioengineering offers the following benefits: reduction of maintenance costs, enhancement of opportunities for wildlife habitat and

ecological diversity, and improved aesthetic quality through naturalization of the slope (Sotir and Gray 1996).

The use of bioengineering as a remedial method is demonstrated by the planting of black locust seedlings by the Civil Engineering Department at Ohio State University (Wu 1995). Black locust seedlings were planted on a rebuilt clay embankment, and the resulting slope stability was compared with a stable section of an embankment where black locust trees already existed. The significant stabilizing mechanism was the growing root system of the trees, such that the evaluation of slope stability required that researchers examine the roots at different periods in their development. Four years after the initial planting of the seedlings, the roots were excavated and examined. Figure 5 illustrates the establishment of a root system at one, two, four, and five years.

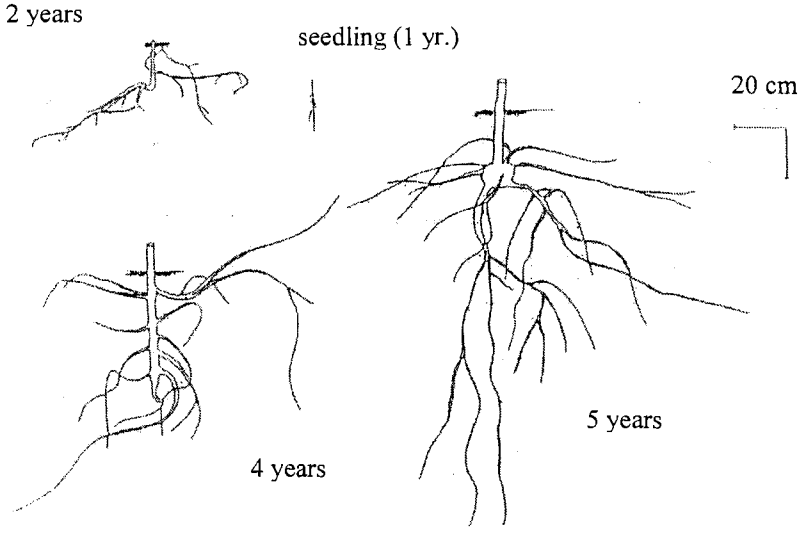

Figure 5 – Roots of Black Locust Seedlings (Wu 1995)

Researchers concluded that the contribution of roots to the increase in shear strength constituted a remedial method and successfully stabilized the clay embankment.

Furthermore, investigators speculate that the factor of safety continually increases as the root system matures.

Bioengineering is considered a specialty remedial method, as opposed to a regularly-used remedial method for slope stabilization. The disadvantages of bioengineering as a remedial method for slope instability involve performance dependent on environmental conditions, obstructed slope inspection and slope failure identification, and general unfamiliarity with horticulture and plant science of geotechnical engineers.

Geosynthetic Reinforcement

Geosynthetics offer an effective reinforcement method for slope stabilization (Holtz et al. 1997). The method is particularly effective when the cost of fill or limited right-of-way make steep slopes desirable, or when low quality fill is used as the construction material (Holtz et al. 1997). Figure 6 presents some applications for reinforced slopes.

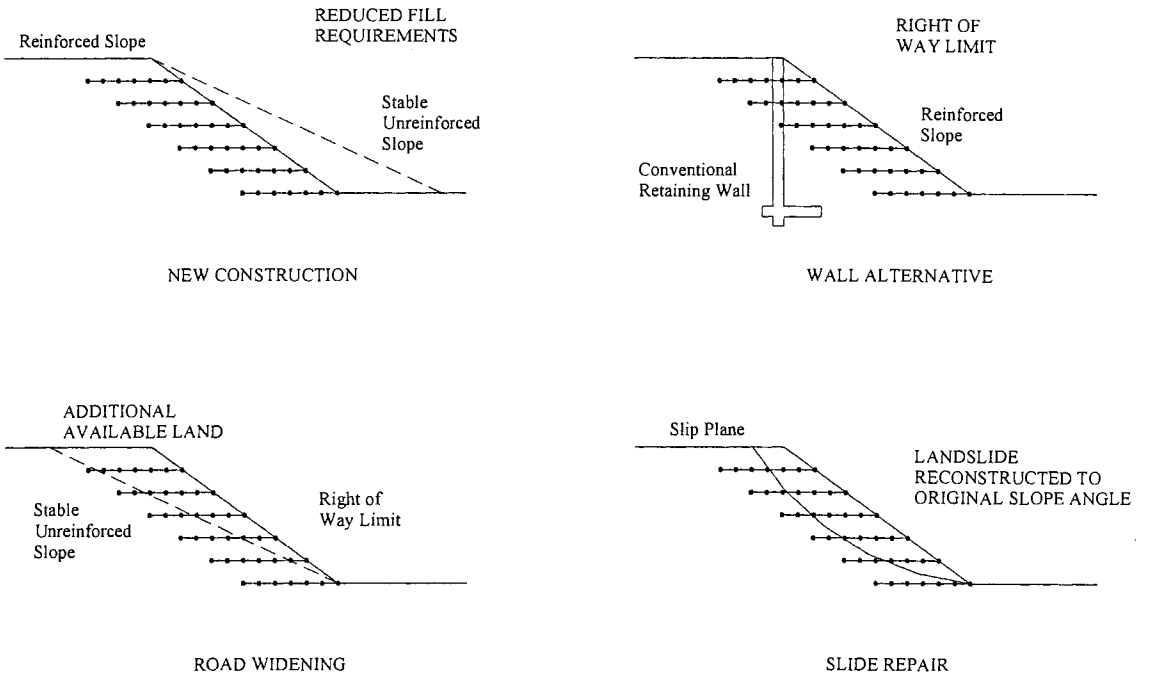

Figure 6 – Applications of Reinforced Slopes (reproduced from Holtz et al. 1997)

Elias et al. (2001) recognized several advantages of using reinforced slopes, as opposed to alternative remedial methods. Reinforced slopes allow the use of failed material, and the requirements for fill of reinforced slopes are relatively relaxed when compared to those for non-reinforced slopes. The use of reinforced slopes provides a method for building over weak foundations, and reinforced slopes tolerate large horizontal and vertical deflections.

Reinforced slopes require that appropriately selected geosynthetics be placed across existing or potential failure planes. The reinforcement significantly increases the strength along the failure surface and, consequently, results in a deeper failure plane. The deeper failure plane corresponds to a longer failure surface, and the resulting resisting forces are increased. The factor of safety is increased accordingly.

Soil Nailing

Soil nailing is an in-situ reinforcing of unstable soil (Elias and Juran 1991). The soil improvement method, most commonly used for stabilizing slopes or earth retaining structures, consists of installing steel bars into a slope or cut face. Inclusions (i.e. nails) create a stable mass of soil, and the stable earth resists failure of the soil behind it. Fundamental soil nailing concepts are employed by multiple applications. Common applications of soil nailing include the stabilization of cut slopes, the retrofit of bridge abutments, and the excavation of earth retaining structures.

The research group explored the French method for designing slope stabilization with soil nails, because the method accounts for the influence of inclusion inclination. The method considers tensile resistance, shearing capacity, and bending stiffness of the nails in evaluating the influence of the nails on the stability of the reinforced soil mass. The mobilized limit forces are calculated according to the principle of maximum plastic work considering the failure criterion (Elias and Juran 1991), and the intersection of the failure criteria gives an envelope in the plane (T_n, T_c) (normal and shear force, respectively), as shown in Figure 7. The normal and shear forces developed in an inclusion at failure are determined by drawing a line that is perpendicular to the line representing the nail inclination and tangent to the composite failure envelope.

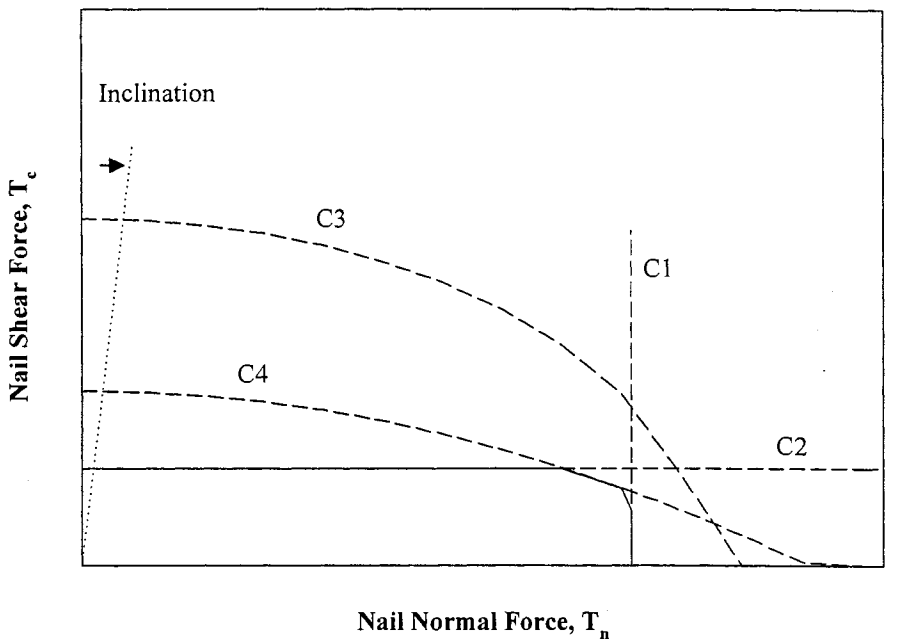

Figure 7 – Failure Envelope of Soil Nail Multicriteria (after Schlosser and Francois 1991)

Equations for the failure criteria are provided below, which correspond to the multicriteria of Figure 7.

Soil-nail skin friction criterion (C1):

$$T_n \leq q_s \pi D L_a$$

Soil-nail lateral pressure criterion (C2):

$$T_c \leq \frac{D}{2} l_o p_u$$

Failure of the nail, following allowable stress design (C3, C4):

$$\left(\frac{T_n}{R_n}\right)^2 + \left(\frac{T_c}{R_c}\right)^2 + \left|\frac{M}{M_o}\right| \leq 1$$

$$T_c \leq b\left(\frac{M_o}{l_o}\right)\left[1-\left(\frac{T_n}{R_n}\right)^2\right] + c\, D_c\, l_o\, p_u$$

where q_s = soil - nail unit skin friction

D = nail diameter

L_a = nail length beyond failure surface

l_o = transfer length

p_u = ultimate lateral soil pressure

R_n = nail tensile capacity

R_c = nail shear capacity

M_o = nail moment capacity

Investigations on the effects of soil nail inclination were conducted by shearing soil reinforced with battered inclusions (see Figure 8). The study results indicate that an inclusion orientated at 30 degrees to mobilize tension provides optimum shear strength increase (normalized with normal load).

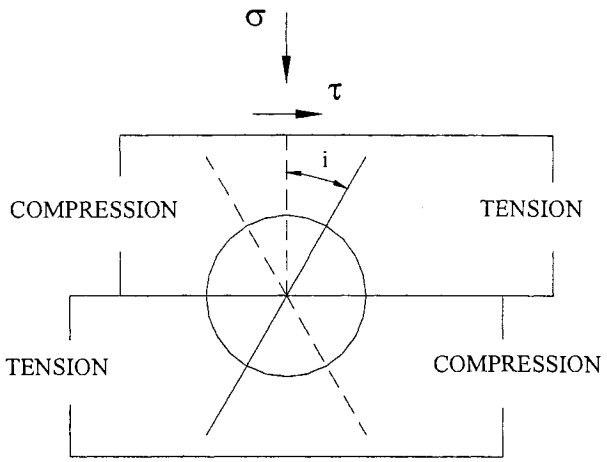

(a)

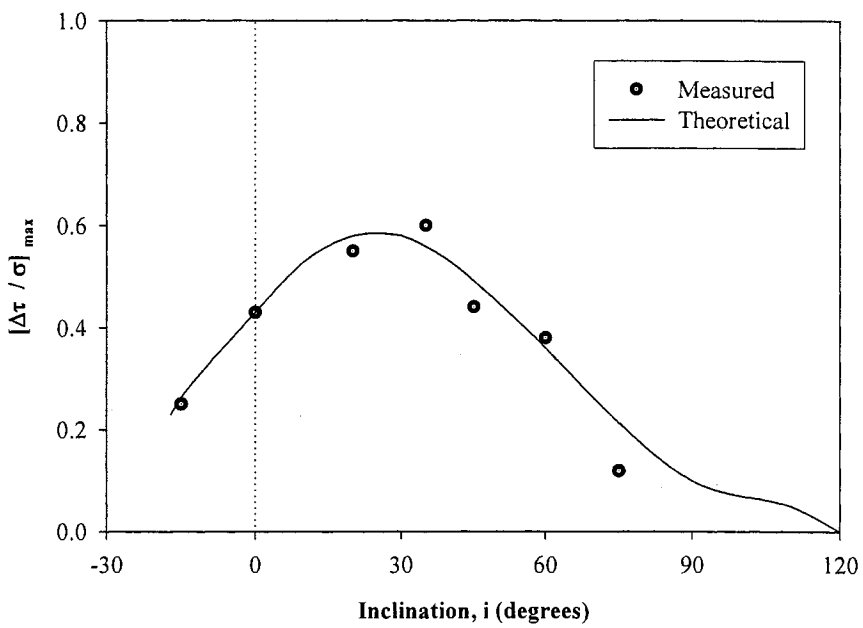

(b)

Figure 8 – Influence of Inclusion Orientation on Soil Reinforcement (after Schlosser and Francois 1991)

The soil nail launcher has recently been developed as a means for rapid installation of the inclusions. The launcher, originally used by the British military to launch nerve gas canisters, uses compressed air to throw the inclusion into slopes or cut faces at velocities approaching 220 miles per hour. The installation method is a consequence of the interaction of the soil and nail tip at high velocities. Shock waves are generated during installation, causing the soil to seemingly jump away from the nail in elastic compression (Barrett et al. 2003). After the nail comes to rest, the soil rebounds towards the nail and high pull-out capacities are achieved. The principal advantages of launching soil nails over the conventional method of drilling and grouting soil nails therefore include high production rates, low impact access, and high pull-out capacity.

Recycled Plastic Pins

The Department of Civil and Environmental Engineering at the University of Missouri-Columbia recently explored the possibility of using recycled plastic pins to stabilize slopes (Loehr et al. 2003). The remediation technology uses the fundamental concept of installing piles through a failure surface, such that pins provide sufficiently large resisting forces to arrest surficial slope movement. The remediation technology is innovative, however, in that the pins are constructed of recycled plastic.

An initial assessment of the remediation technology revealed promising stabilizing performance of the structural members, yet potential problems with the construction method of the slope stabilization. As the research group attempted to drive the recycled plastic pins vertically into the slope, an unacceptable number of pins were broken. Unstable operation of installation equipment further complicated the installation of recycled plastic pins. The use of more efficient equipment and contractor experience, however, resolved these construction issues. Significantly fewer construction complications were experienced in succeeding research phases.

The proposed slope reinforcement technology (i.e. SDGM stabilization) is similar to the preceding slope remediation alternative, and a technical evaluation of slope stabilization using recycled plastic pins is provided under the *Methodology of Slope Stabilization with Piles* section of Chapter 2.

CASE HISTORIES OF SLOPE STABILIZATION WITH PILES

Compaction Grout Columns

Compaction grout columns closely resemble auger-cast piles except that compaction grout columns laterally displace the soil, whereas auger-cast piles generate spoil material that requires disposal. Low slump grout with approximate 28-day compressive strength of 3,000 psi is pumped into the ground under high pressure (300-500 psi) to form a relatively cylindrical grout column (Benedict et al. 2001). Irregularities in the columns are normal and expected. The columns accept vertical and lateral loads, such that the method is commonly used for densification of foundation soils, raising and leveling of structures and foundation elements, and mitigation of liquefaction potential. The use of compaction grout columns for slope stabilization is effectively demonstrated by a case study, where compaction grout columns were employed to provide adequate stability and acceptable settlement behavior for an Amtrak track extension. The use of compaction grout columns for track support was initially documented by Benedict et al. (2001).

In order to meet the sight distance requirements of high-speed electrified passenger rail service, a track extension was to be constructed along a wetland underlain by organic soils. The two concerns related to the thick peat layer were global stability and the potential for excessive settlement. Geotechnical analyses suggested that significant consolidation and secondary settlements of the peat layer would require future track maintenance issues. Also, a global stability analysis indicated a factor of safety of approximately unity against slope failure. Several ground improvement alternatives were considered. However, due to

overhead clearance limitations and the need to address stability and settlement issues, compaction grout columns were used for the project. The objective was therefore to design the compaction grout columns as structural members to transfer the train and ballast loads through the thick peat layer to the dense sand stratum.

The design of column sections was based on slope stability, where the stability of the embankment was the controlling design aspect. Due to the large shear forces expected in the compaction grout columns, reinforcement was provided with No. 8 steel rebar. Steel reinforcement was more economical than using high strength grouts or installing additional compaction grout columns. Furthermore, using higher strength grout potentially exposed the compaction grout columns to undetected deficiencies in installation and, consequently, required more rigorous quality control practices.

A pre-blended grout mix design was developed and included Type II cement, fly ash, sand, and bentonite. Slump and compression tests verified the adequacy of the mix design, such that following a trial column installation, construction commenced on the embankment. A total of 289 compaction grout columns were installed at equilateral spacing of 6 feet. Beyond checking slope stability and settlement, engineers observed that by transferring the loads from the trains to the sand stratum axially, the reduction of driving forces correspondingly reduced the potential for slope stability failure.

Rammed Aggregate Piers

Geopier Rammed Aggregate Piers were originally developed to carry foundation loads and reduce settlement of supported structures. The Rammed Aggregate Piers perform well, because the unique construction process alters the post-construction properties of the engineering materials. Matrix soil is laterally prestressed and pier elements develop high strength and stiffness during construction (Wong et al. 2004). Currently, soil reinforcement with Rammed Aggregate Piers is incorporated into the stabilization of retaining walls and

highway embankments. Wong et al. (2004) documents the use of Rammed Aggregate Piers to improve the global stability and bearing capacity of the Sienna Parkway Mechanically Stabilized Earth (MSE) Wall in Missouri City, Texas. The ensuing discussion focuses on the effect of the piers on global stability as it relates to multiple global stability applications.

The design of the Sienna Parkway required that the road cross above existing railroad lines. Proposed MSE walls with maximum heights exceeding 30 feet facilitated the grade changes. The project site consisted of soft to very stiff clay extending to depths of approximately 40 feet. The clay was underlain by medium dense sandy silt and silty sand. The groundwater table was located at a depth of 15 below the grade, and water contents of surface soils ranged from 15 to 35 percent. Field and laboratory tests indicated that undrained shear strengths ranged from 0.5 ksf to 4.5 ksf.

Global stability analyses were completed for the placement of MSE walls on the unreinforced soils using conventional limit equilibrium methods. The analyses suggested that wall heights exceeding 27 feet resulted in long-term factors of safety less than the target factor of safety of 1.3. Rammed Aggregate Piers were selected to increase the shear resistance of the foundation soils based on cost and speed of pier installation.

Rammed Aggregate Piers are installed through potential failure surfaces to increase the shear strength parameter values and, consequently, increase the factor of safety against sliding. Composite shear strength parameter values of the reinforced foundation soils are determined by calculating the weighted average of shear strength parameters of pier elements and matrix soil based on an areas ratio. Composite shear strength parameters for reinforced soil are determined with the following equations:

$$c_{comp} = c_g R_a + c_m \cdot (1 - R_a) \tag{4}$$

$$\phi_{comp} = \tan^{-1}[R_a \tan\phi_g + (1 - R_a)\tan\phi_m] \tag{5}$$

where c_g and ϕ_g are the shear strength parameters of the aggregate, c_m and ϕ_m are the shear strength parameters of the matrix soil, and R_a is the area ratio of pier elements to the reinforced soil footprint. Wong notes that significant axial loading of Rammed Aggregate Piers results in stress concentration at pier tips, such that further increase in the composite shear strength is potentially employed for stability calculations.

Field and laboratory tests (e.g. full-scale direct shear tests, triaxial shear tests) indicate engineering properties of *Geopier* Rammed Aggregate Piers. Test results indicate a friction angle of approximately 49 degrees for piers constructed from open-graded stone and a friction angle of approximately 52 degrees for piers constructed from well-graded stone (Fox and Cowell 1998). The use of Rammed Aggregate Piers for reinforcing the soils under the Sienna Parkway MSE walls resulted in a composite friction angle of 23.7 degrees and a composite cohesion of 180 psf with an area replacement ratio (R_a) of approximately 10 percent.

Global stability analyses were performed for the placement of MSE walls on the pier-reinforced soil. The long-term factors of safety exceeded 1.3. Piers were installed with 7-ft center-to-center spacing and to depths of 16 feet.

Lime Columns

Quicklime (CaO) or hydrated lime ($Ca(OH)_2$), when introduced to soils containing clay minerals, initiate cation exchange, flocculation/agglomeration, carbonation, and continuing pozzolanic reactions. Generally accepted consequences of these stabilization mechanisms include reduced plasticity, increased volumetric stability, and increased strength. The increase in soil shear strength due to lime columns can be expressed by estimating the average shear strength along a potential failure surface (Abramson et al. 2002), which is estimated with the following equation:

$$c_{avg} = c_u \cdot (1-a) + \frac{S_{col}}{a} \quad (6)$$

where c_u = undrained shear strength of soil,

S_{col} = average shear strength of stabilized clay, and

a = relative column area = $\frac{\pi D^2}{4S^2}$

Lime columns are placed over a sufficiently large area of the slope, such that the factor of safety against slope movement is greater than the minimum required by the governing agency. Additional stabilizing mechanisms, although more difficult to quantify, include dehydration of clay, generation of negative pore water pressure, and lateral consolidation of the soil in the shear plane caused by pile expansion (Rogers and Glendinning 1997).

Rogers and Glendinning (1997) discussed the applicability of lime columns to shallow failures and demonstrated the fundamental mechanisms of the stabilization method. Rogers and Glendinning recognized that the normal stresses acting on the failure surface of a shallow failure are usually small. Consequently, a significant change in friction angle is required to increase the frictional resistance of the sliding soil. Small changes in the cohesion of soil, however, have a noticeable effect on the stability of the slope, such that the relatively large increase in cohesion of slopes stabilized with lime columns adequately increases the factor of safety against slope movement. The remedial method typically requires that one third of the slope area be stabilized with lime columns.

Bored Piles

Davies et al. (2003) documented the pile stabilization and slope monitoring of a landslide on the M25 Highway in England.

The wettest winter in English history resulted in a slope failure on the M25 Highway around London. The failure extended 260 feet upslope from the highway and threatened 650

feet of the slope along the transportation corridor. The slope was marginally stable and responded rapidly to rainfall events. Months after the initial failure, rainfall triggered additional movements. The investigation, design, construction, and monitoring programs were fast tracked to stabilize the slope before the next wet season.

The Flint Hall Farm Cutting was constructed between 1976 and 1979. Site investigation indicated that the failure surface was within a stiff to very stiff gray fissured clay (Gault), with overlying Head deposits mantling the upper portion of the slope. The engineering properties of the soils are provided in Table 3.

Table 3 – Engineering Properties of M25 Slope Failure Soils

	Shear Strength		**Typical Properties**		
Soil Type	**ϕ' (deg)**	**c' (kPa)**	**c_u (kPa)**	**PI**	**w/c**
Head	14	0.0	50.0	—*	40
Gault	24	1.0	100.1	45	35
Residual Gault	14	0.0	50.0	—*	—*

Notes:
* Data not available

The governing transportation agency specified a stabilization design life of 60 years. The design was therefore unable to employ drainage alternatives as the sole means for preventing further slope movement due to likely blockage of the drainage structures with time. Moreover, the counterforts installed during construction of the slope failed to prevent the landslide. Rather, a structural solution of pinning the sliding soil to the underlying Gault clay with piles was adopted.

The design of piles for stabilizing the slope began by establishing the location of piles on the slope and the pile lengths. Piles were installed one third of the way up the failure and extended 52 feet into the ground. The establishment of the variables reduced the number of permutations for the pile design. Pile spacing was then selected to maximize soil arching

between the piles and minimize the flow of soil between piles. Piles with 3.3-ft diameters, spaced at 8.2 feet offered the aforementioned benefits over other pile size and spacing configurations.

The structural design of piles concluded the stabilization design. The design incorporated the method proposed by Viggiani (1981). The method ensures pile stability by adjusting proposed pile sizes and capacities until the controlling failure mechanism of the stabilization is failure of the soil around the piles. The failure mode offers a non-brittle failure mechanism, which is preferable over the brittle failure mechanism of the development of a plastic hinge in a pile section. Ultimately, seventy four piles were installed to stabilize the slope. Post-construction monitoring indicated that despite heavy winter rainfall events sufficient to remobilize failure, the slope was effectively stabilized.

Type "A" In-Situ Earth Reinforcement Technique Walls

Type "A" In-Situ Earth Reinforcement Technique (INSERT) Walls (Pearlman and Withiam 1992) control the movement of unstable slopes by providing passive resistance mobilized in a pattern of vertical and near vertical reinforcing elements installed through a slope failure surface. The pile elements are generally connected at the slope surface with a reinforced pile cap, which provides added stiffness for relatively shallow failure planes. Pile diameters range in size from five to nine inches, and the pile elements are reinforced with centered steel rebar or steel pipes (see Figure 9). Pile elements installed with pipe reinforcement have significantly more capacity than pile elements installed with a centralized reinforcing bar. The slope stabilization applications of Type "A" INSERT walls are illustrated in Figure 9.

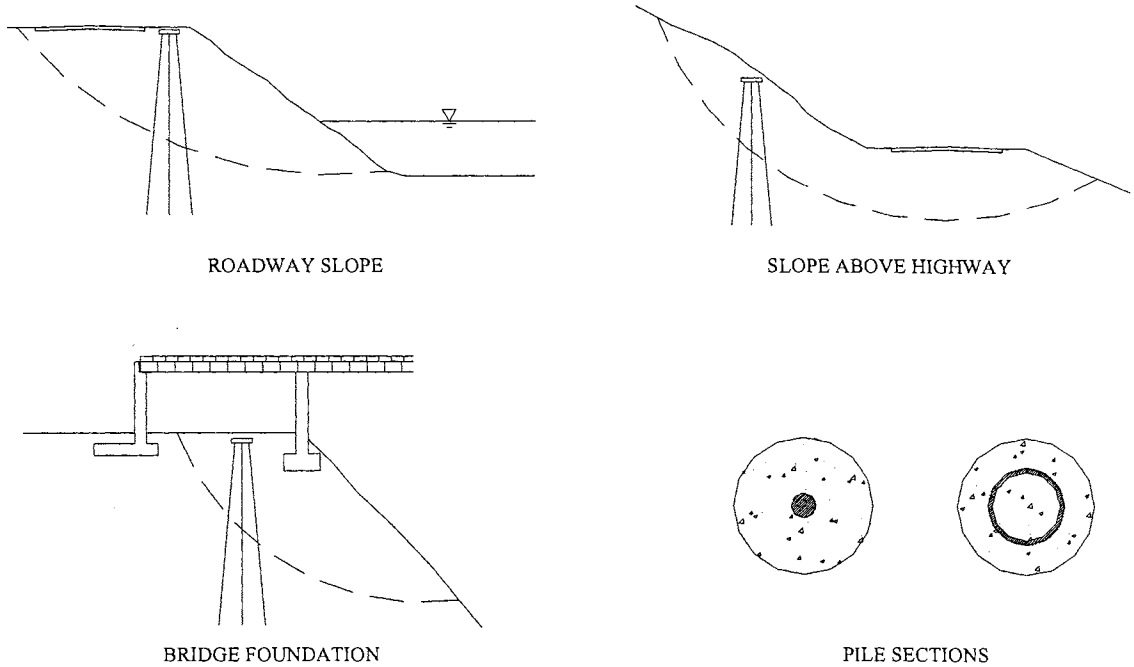

Figure 9 – Typical Configurations and Applications for Type "A" INSERT Walls (reproduced from Pearlman and Withiam 1992)

The procedure for designing Type "A" INSERT walls considers structural failure of the piles and plastic failure of slope soil. The procedure uses a method proposed by Fukuoka (1977) for evaluating the bending moments developed in piles oriented perpendicular to a failure plane. Plastic failure of soil around the piles is analyzed using the method proposed by Ito and Matsui (1975). Pearlman and Withiam (1992) notes that the surface area to cross-sectional area ratio of slender pile elements is large and small-diameter piles are efficient at mobilizing skin friction. The piles generally have higher axial capacity than lateral capacity. For this reason, pile elements of Type "A" INSERT walls are battered. The design methodology, however, does not quantitatively indicate the effect pile inclination on the stability of the reinforced slope.

Pearlman and Withiam (1992) documented the use of Type "A" INSERT walls to stabilize a slope in Kentucky. The U.S. Army Corps of Engineers observed a moving slope

downhill from a bridge abutment and above a land pier supporting an historic railroad bridge. Continued slope movement threatened the stability of the structure.

The slope soil conditions, determined from soil exploration, consisted of medium stiff to stiff silty clay with shale bedrock ($\phi = 19°$, $c = 0$, $\gamma = 125$ pcf). The wall design (resembling the BRIDGE FOUNDATION application of Figure 9) consisted of 5.5-in diameter piles, reinforced with No. 11 and 14 rebar. The pile density required to achieve stability was calculated at 0.75 piles per lineal foot, in which piles were oriented from 19° to minus 5° with vertical. Following pile construction, a reinforced cap beam of dimensions 35 ft x 5 ft x 3 ft (L x W x T) was constructed to provide stiffness to the pile wall. Slope monitoring during construction and following construction indicated that lateral displacements were less than one inch.

METHODOLOGY OF SLOPE STABILIZATION WITH PILES

Behavior of Laterally Loaded Piles

Lateral loading of piles is most commonly encountered in geotechnical engineering practice with lateral earth pressure, wind loads, seismic loads, and eccentric vertical loads on columns (Coduto 2001). Developed solutions to these problems of laterally loaded piles involve specified loading and boundary conditions. Given soil and pile properties (i.e. stiffness), pile behavior is classified and subsequently described with any of several available methods (e.g. equivalent cantilever, elastic continuum, and p-y method).

Classification of pile behavior is aided by the determination of characteristic length, R or T, determined with the following equations (Das 1999):

$$R = \sqrt[4]{\frac{EI}{E_s}}, \text{ constant } E_s \text{ with depth} \quad (7)$$

$$T = \sqrt[5]{\frac{EI}{E_s}}, \text{ linearly increasing } E_s \text{ with depth} \quad (8)$$

where EI = pile stiffness, and

E_s = soil elastic modulus

A pile is *short* when the pile length is less than twice the characteristic length (i.e. 2 R or 2 T). A short pile experiences rigid behavior and fails by means of rotation about a point near the pile tip. A pile is *long* when the pile length exceeds 3.5 R (4 T, linearly increasing E_s). A long pile experiences flexible behavior and fails by means of pile bending, most commonly associated with exceeding of the pile moment capacity and development of a plastic hinge. The failure modes of free-headed piles are illustrated in Figure 10.

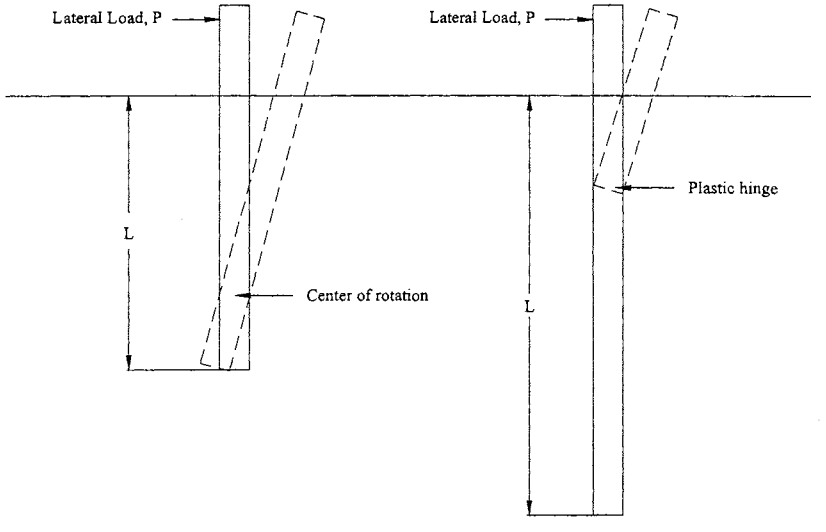

Figure 10 – Failure Modes of Free-Headed Piles (after Broms 1964)
(a) Short (rigid); (b) Long (flexible)

Nonlinear Subgrade Reaction Method (p-y Method)

The load-displacement behavior of piles subject to lateral loads is complicated by the interdependence of pile displacement and soil response. Pile displacement depends on the soil response, and soil response depends on pile displacement. Consequently, problems of laterally loaded piles cannot be solved solely by means of static equilibrium, but rather require the solution to a differential equation (COM624 1993). The principal differential equation relating pile displacement and soil response is provided below. Progressive differentiation and integration of the following equations aid in the development of relationships between pile displacement, shear, and moment.

$$EI\frac{d^4y}{dx^4} = p \tag{9}$$

$$EI\frac{d^3y}{dx^3} = V \tag{10}$$

$$EI\frac{d^2y}{dx^2} = M \tag{11}$$

where x = length coordinate

EI = flexural rigidity of pile

y = pile displacement

p = lateral soil resistance

V = pile shear

M = pile moment

The differential equations are valid, irregardless of the pile section and material properties. Reese and Allen (1977), however, presents several limiting assumptions of the relationships, as follows:

- The beam material is linearly elastic and has the same moduli in tension and compression.
- Plane sections through the beam normal to its axis remain plane after the beam is bent.
- The beam has a plane of symmetry parallel to its longitudinal axis, and loads and reactions lie in that plane.
- Deflections of the beam are small in relation to its span length.
- Forces are applied without shock or impact.

The soil response to lateral loading of piles is efficiently and practically depicted with a series of nonlinear elastic springs, as shown in Figure 11. The load-displacement property of each spring, actually representing the load-displacement behavior of soil, is defined by a p-y curve (Coduto 2001). The units of lateral soil resistance, p, are force per length (of the pile). The units of displacement, y, are length (in the direction of loading, perpendicular to the pile). The p-y curve is nonlinear, because the lateral soil resistance approaches an ultimate soil pressure after which soil resistance remains relatively constant with increasing pile displacement. Excluding effects of stress concentration, soil is incapable of inducing pile loads that exceed the ultimate soil pressure. An illustrative definition of the p-y relationship is shown in Figure 12.

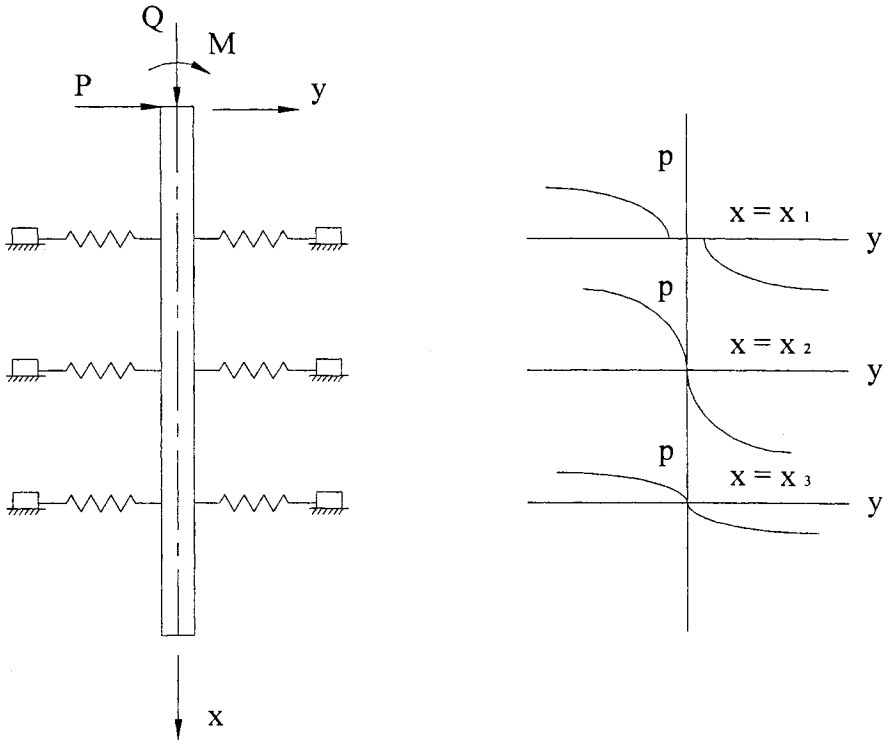

Figure 11 – Nonlinear Elastic Spring of p-y Model (reproduced from Reese and Allen 1977)

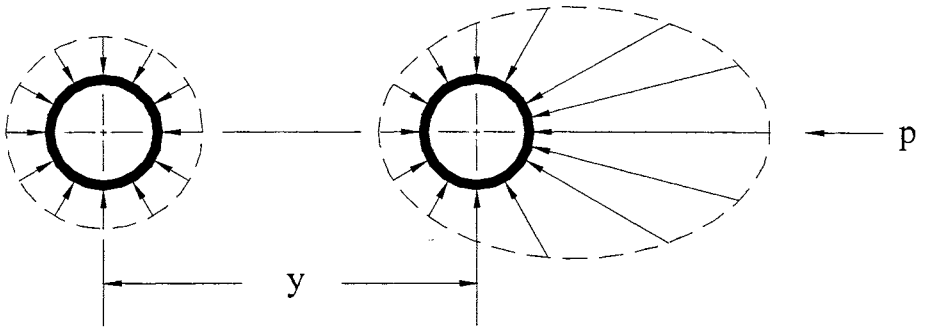

Figure 12 – Illustrative Definition of Load-Displacement (p-y) Relationship (reproduced from Reese et al. 1974)

Soil profiles are represented by multiple p-y curves that vary with depth, and the series of curves seemingly imply that the behavior of soil at a particular depth is independent of soil behavior at other depths (Reese et al. 1974). *Experimentation* suggests that the pile deflection which occurs at a particular depth influences the soil response at that depth and not the soil response above or below the pile deflection. The load-displacement behavior of soil is reliably modeled with *discrete* mechanisms.

The p-y relationship is highly empirical and includes effects of soil type, loading type, pile type, pile size, and pile spacing. The empirical quality of the p-y relationship requires that p-y curves be back-calculated from full-scale pile load tests or *approximated* from the stress-strain relationship of soil measured in laboratory triaxial compression tests. Additional load test data for correlation of p-y curves with standard soil properties further facilitates understanding of the p-y relationship. Recently, p-y curves have been developed from in-situ tests such as the Pressuremeter Test (PMT) (Robertson et al. 1985), Dilatometer Test (DMT) (Robertson et al. 1989), and Cone Penetrometer Test (CPT) (Robertson and Campanella 1983). The more innovative methods for developing p-y curves are important, because large projects often require site-specific p-y curves. The use of in-situ testing

methods for approximating p-y curves is often more cost-effective than conducting full-scale pile load tests.

Prediction of Load-Displacement Behavior with LPILE Software

Several software programs are capable of analyzing the behavior of laterally loaded piles. The present research project employed LPILE 4.0, an engineering software program distributed by ENSOFT, Inc (Reese and Wang 2000). LPILE analyzes pile response (i.e. moment, shear, and deflection) to the application of provided loading and boundary conditions. The program also indicates whether a pile is structurally stable, where piles experience structural failure if the shear or moment force developed from lateral loading exceeds the shear or moment capacity of the pile.

Soil behavior is easily modeled with p-y curves in LPILE. The program applies recommended p-y curves for various soil types and offers the option to input user-defined p-y curves for more advanced analyses. The application of p-y curves to design practices with LPILE is important, because any design method must consider the nonlinear response of soil to lateral loading (Reese and Wang 2000).

Application of Laterally Loaded Pile Behavior to Slope Stabilization

Piles installed in failing slopes arrest or slow the rate of slope movement. Each pile element offers passive resistance to downslope soil movement by transferring the loads developed along the pile to stable soil below the failure surface. The load transfer of piles depends principally on the magnitude and rate of slope movement, because the pressures developed between piles and soil observe the load-displacement (i.e. stress-strain) relationship of the engineering materials. In fact, Walker and Fell (1987) recognizes that the installation of passive piles does not guarantee an end to slope movement. Unstable soil continues to slide until sufficient resisting forces are developed along the pile to discontinue the movement. Alternatively, piles installed in a marginally stable slope to increase the

factor of safety against sliding are potentially unloaded, where the shear strength of soil along possible failure surfaces is sufficient to oppose triggering causal factors of slope movement (i.e. soil shear strength carries load of soil mass). The loads developed on passive piles due to downslope soil movement are therefore limited by the resisting force required to arrest slope movement or the pressure that causes yielding of the pile and/or surrounding soil.

Recognizing the relationship between slope movement and loads developed along pile elements is important to understanding how the pile elements contribute to the stabilization resisting force of the unstable slope. Poulos (1995) presents a method for analyzing piles in soil undergoing lateral movement. The analysis assumes a soil movement profile and cycles through a series of equations to obtain the pressure due to pile-soil interaction. The finite difference method imposes displacement compatibility and elastic soil conditions, whereby the elastic soil condition is abandoned for elements experiencing lateral pressure in excess of soil yield pressure. However, the prediction of slope movement (i.e. input for finite difference method) is difficult and therefore fails to aid the determination of pile loading conditions for slope stabilization. Investigators instead incorporate a limit state methodology in analyzing the stability of pile-stabilized slopes. Lateral soil movements of slope failures assumingly induce load distributions along stabilizing piles that cause the local soils to fail (i.e. ultimate soil pressure). Ultimate soil pressures are a function of soil type, pile size, and pile spacing. Investigators have presented analytical models for estimating the loads, but a model has yet to acquire absolute acceptance by the geotechnical engineering community for the design of pile-stabilized slopes.

Existing Analytical Models for Ultimate Soil Pressure

Design methods for pile-stabilized slopes consistently assume that sliding soil moves sufficiently to mobilize the ultimate soil pressure (Reese and Wang 2000). The ultimate soil pressure (i.e. design load) is therefore applied to the pile directly or as an equivalent loading

condition. The assumption aids in the structural design of proposed piles and nearly ensures pile stability for reliably-determined ultimate soil pressures. But the prediction of ultimate soil pressure is complicated, and Ito et al. (1981) advises that an accurate estimation of the lateral resistance is essential for stability analyses. An overestimation of ultimate soil pressure results in a conservative pile stability and an unconservative slope stability. Alternatively, an underestimation of ultimate soil pressure results in a conservative slope stability and an unconservative pile stability.

Ultimate soil pressures are most easily and most reliably obtained from p-y relationships. By definition, the ultimate soil pressure is the limiting soil resistance. Unfortunately, p-y curves necessitate prohibitively-expensive pile load tests. Based on failure mechanisms of soil (e.g. plasticity, viscous flow, wedge), investigators have established approximations for limiting soil resistance in terms of standard soil properties and stress conditions.

Ultimate Soil Pressure in Cohesive Soil

The ultimate soil pressure in cohesive soil is generally regarded to be a function of undrained shear strength, as illustrated in Figure 13. Approximations are of the following form:

$$p_u = k \cdot s_u \cdot d \qquad (12)$$

where p_u = ultimate soil pressure per unit length of pile,

k = lateral load factor,

s_u = undrained shear strength, and

d = pile diameter

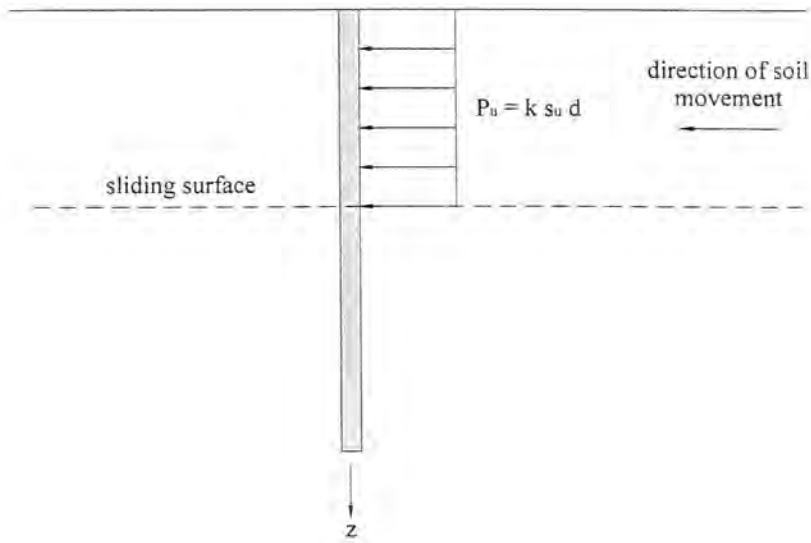

Figure 13 – Ultimate Soil Pressures in Cohesive Soil

Broms (1964) proposes a lateral load factor of nine on the basis of a plasticity solution for a frictionless circular pile. The ultimate soil pressure is zero from the ground surface to a depth of 1.5 d and is then constant with depth assuming constant undrained shear strength with depth. Poulos and Davis (1980) conclude that the ultimate soil pressure varies linearly from 2 s_u at the ground surface to 8 to 12 s_u at a depth of 3 d. at which point the ultimate soil pressure remains constant. The reduced soil pressures near the ground surface account for the formation of gaps behind the piles.

Investigators obtained various empirical values for k in experimental load tests. Lateral load factors were as low as 2.8 (Viggiani 1981) and as high as 12 (Poulos and Davis 1980; Bransby and Springman 1999). Moreover, investigators developed different empirical factors for explaining group effects. Pan et al. (2002) used reduced k values for piles in a row, such that k values are proportional to pile spacing.

Ultimate Soil Pressure in Cohesionless Soil

Broms (1964) analyzes piles in cohesionless soil with the following assumptions: (1) the active earth pressure acting on the back of the pile is neglected, (2) the distribution of passive pressure along the front of the pile is equal to three times the Rankine passive pressure, and (3) the shape of the pile section has no influence on the distribution of ultimate soil pressure. The distribution of soil resistance is proportional to the passive lateral earth pressure and of the following form, where N = 3:

$$P_u = N \sigma_v K_p d \qquad (13)$$

where P_u = ultimate soil pressure per unit length of pile,

N = lateral load factor,

σ_v = vertical overburden pressure,

K_p = Rankine coefficient of passive lateral earth pressure, and

d = pile diameter

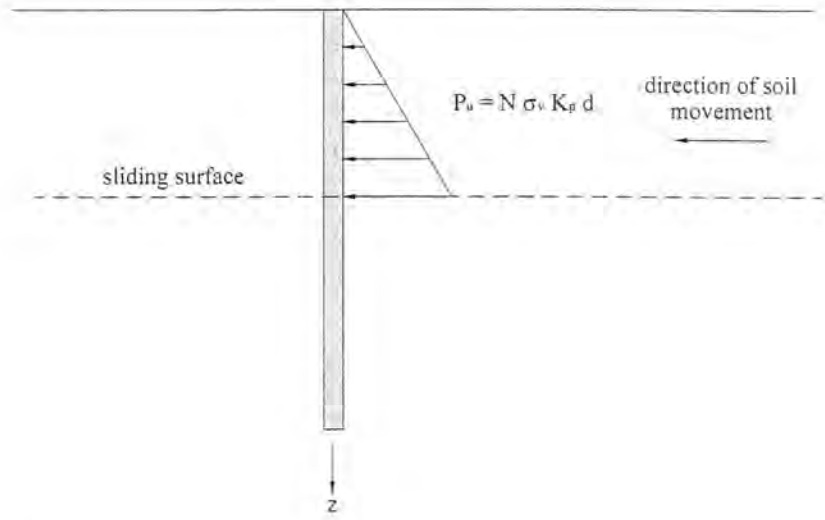

Figure 14 – Ultimate Soil Pressures in Cohesionless Soil

The analyses of Brinch Hansen (1961), presented in the ensuing section, incorporate lateral load factors that vary with depth. Brinch Hansen supports the lateral load factor of Broms as a reasonable to conservative approximation for ultimate soil pressure at intermediate depths (Poulos and Davis 1980).

Reese et al. (1974) established an alternative model for ultimate soil pressure in cohesionless soil. The model incorporates potential failure modes of cohesionless soil including the development of a passive wedge near the ground surface and horizontal flow around a pile. For horizontal flow, the stress σ_1 (see Figure 15 (b)) must be equal or larger than the minimum active earth pressure (Reese and Wang 2000). Failure to satisfy this condition results in failure of the soil by slumping. Free bodies for each failure mode are diagrammed in Figure 15. The forces of the free bodies are resolved with equilibrium equations. The ultimate soil pressures for sand near the ground surface and at considerable depths are computed with Equations (14) and (15), respectively. The ultimate soil pressure distribution for laterally loaded piles in sand is the minimum of p_{ct} and p_{cd}.

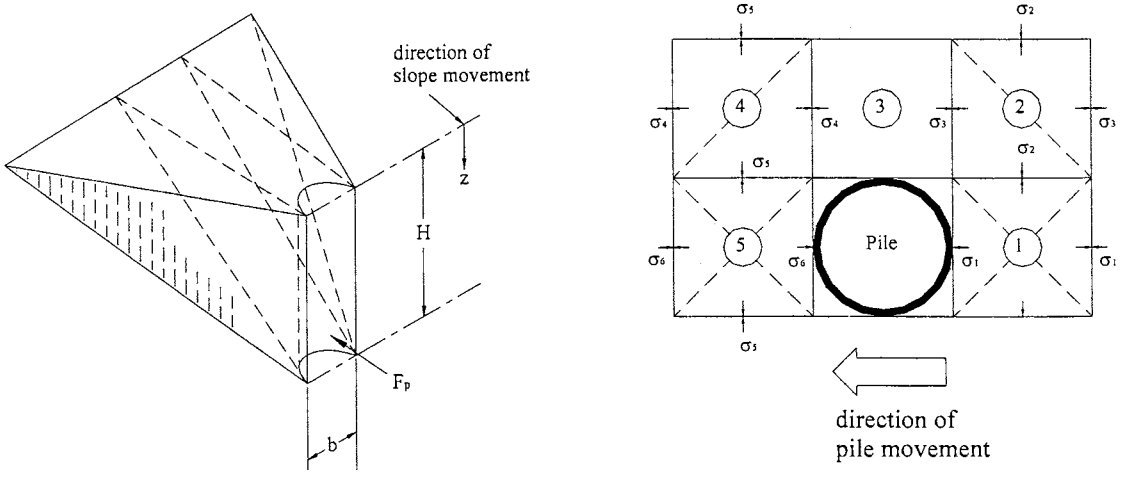

Figure 15 – Failure Modes of Cohesionless Soil (reproduced from Reese et al. 1974)
(a) Passive Wedge-Type Failure, (b) Lateral Flow Around Pile

$$p_{ct} = \gamma \cdot z \left[\frac{K_o \, z \tan\phi \sin\beta}{\tan(\beta - \phi)\cos\alpha} + \frac{\tan\beta}{\tan(\beta - \phi)}(d + z \tan\beta \tan\alpha)\right. \tag{14}$$

$$\left. + K_o \, z \tan\beta \, (\tan\phi \sin\beta - \tan\alpha) - K_a \, d\right]$$

where z = depth,

d = pile diameter,

$\beta = 45 + \frac{\phi}{2}$,

$\alpha = \frac{\phi}{3}$ to $\frac{\phi}{2}$ for loose sand, and

$\alpha = \phi$ for dense sand

$$p_{cd} = A[\gamma \cdot z \, K_a \, d \, (\tan^8\beta - 1) + \gamma \cdot z \, K_o \, d \tan\phi \tan^4\beta] \tag{15}$$

where A = empirical adjustment factor

Ultimate Soil Pressure in $\phi - c$ Soil

Brinch Hansen (1961) explored ultimate soil pressure for the more general case of soils that possess both cohesion and friction. Based on earth pressure theory, the ultimate soil pressure is determined with the following equation:

$$p_u = q \, K_q + c \, K_c \tag{16}$$

where q = vertical overburden pressure,

c = cohesion, and

K_c, K_q = factors that are a function of ϕ and $\frac{z}{d}$

The passive earth pressure coefficients due to soil unit weight and cohesion (K_q and K_c, respectively) are determined with equations or prepared charts. For friction angles from 0 to 30 degrees, K_c varies from 3 to 30 and K_q varies from 1 to 8.

Ito and Matsui (1975) derived an equation for ultimate soil pressure that, in addition to the engineering properties of soil, incorporates the size and spacing of stabilizing piles. The method facilitates direct evaluation of soil pressures acting on a *row* (i.e. group) of piles, as opposed to the determination of a load reduction factor to account for grouped piles. The method, based on theory of plastic deformation, makes the primary assumptions that: (1) the soil layer becomes plastic only in the soil just around the piles, in which the Mohr-Coulomb yield criterion is applied; (2) the soil layer is in a plane-strain condition; and (3) piles are rigid.

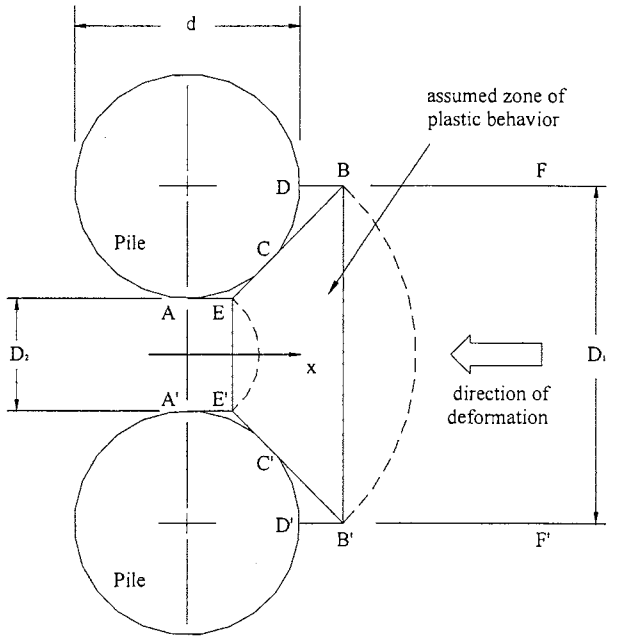

Figure 16 – State of Plastic Deformation at Piles (reproduced from Ito and Matsui 1975)

The soil pressure developed on a pile (i.e. force per unit length of pile) as a function of depth is determined with the following equation:

$$p_u(z) = c\,D_1\left(\frac{D_1}{D_2}\right)^{J_1}\left[\frac{1}{N_\phi \tan\phi}\left\{e^{\frac{D_1-D_2}{D_2}J_3} - 2N_\phi^{1/2}\tan\phi - 1\right\} + \frac{J_2}{J_1}\right] \qquad (17)$$

$$- c\left\{D_1\frac{J_2}{J_1} - 2D_2 N_\phi^{-1/2}\right\} + \frac{\sigma_v}{N_\phi}\left\{D_1\left(\frac{D_1}{D_2}\right)^{J_1}\cdot e^{\frac{D_1-D_2}{D_2}J_3} - D_2\right\}$$

where $N_\phi = \tan^2\left(\frac{\pi}{4}+\frac{\phi}{2}\right)$,

$J_1 = N_\phi^{1/2}\tan\phi + N_\phi - 1$,

$J_2 = 2\tan\phi + 2N_\phi^{1/2} + N_\phi^{-1/2}$,

$J_3 = N_\phi \tan\phi \tan\left(\frac{\pi}{8}+\frac{\phi}{4}\right)$,

D_1 = center-to-center spacing of piles, and

D_2 = clear spacing between piles

Evaluation of Slope Stabilization Using Recycled Plastic Pins

The University of Missouri-Columbia recently developed a slope remediation alternative using recycled plastic pins. Recycled plastic pins consist of nearly 40 percent sawdust and are fabricated with post-size dimensions. The research program engaged a comprehensive materials testing program focusing on tension, compression, shear, and flexural strengths of the recycled plastic. The research group also investigated interface friction and bending creep of the pins. Recycled plastic pins were ultimately characterized as "weak" reinforcement elements, as opposed to "strong" reinforcement elements such as steel pipes (Loehr et al. 2000). The pins were regarded as adequate nonetheless, because soil resistance often controls slope stability.

The research program acknowledged the potential of slope stabilization with small pile elements and established the feasibility of soil displacement grouted micropiles as a slope remediation alternative. The analysis and design procedure for SDGM stabilization draws upon the succeeding concepts of recycled plastic pin stabilization. The design must demonstrate the unique behavior of soil reinforced by soil displacement grouted micropiles, but the stabilizing mechanisms and failure modes are common to other slender piles.

The influence of recycled plastic pins on the global stability of a slope is evaluated with the conventional definition of limit equilibrium factor of safety. The direct resistance of a pile element, F_R, increases the factor of safety over that of an unreinforced slope. The factor of safety for a reinforced slope is determined with the following equation:

$$FS = \frac{\Sigma F_R + \Delta F_R}{\Sigma F_D} \tag{18}$$

where ΔF_R = limit resistance of piles,

ΣF_R = resisting forces of slope, and

ΣF_D = driving forces of slope

The design and analysis of pile-stabilized slopes is readily supplemented by existing limit equilibrium methods for evaluating slope stability. Research efforts therefore focus on the determination of ΔF_R. The University of Missouri-Columbia presents a procedure for finding the limit resistance of a pile as a function of sliding depth (i.e. depth to failure surface).

The design methodology of slope stabilization using recycled plastic pins involves finding the limit lateral resistance of individual reinforcing members. The procedure considers the following limit states (Loehr and Bowders 2003):

- "failure of soil around or between reinforcing members – referred to as the 'limit soil resistance',
- structural failure of reinforcing members in shear or bending due to loads applied from the soil mass – referred to as the 'limit member resistance', and
- failure of soil due to insufficient anchorage length – referred to as the 'limit anchorage resistance'."

The determination of each limit state is discussed in the ensuing sections.

Limit Soil Resistance

The proposed design method employs the model for ultimate soil pressure originally proposed by Ito and Matsui (1975), as previously presented. The ultimate soil pressure of the model increases linearly with depth. The design method assumes that the ultimate soil pressure is mobilized along the entire length of pile subject to lateral soil movement, and the *limit* soil pressure is integrated from the ground surface to potential sliding depths. The integration with units of force is called the limit soil resistance, F_R. The limit soil resistance increases as the depth to the sliding surface increases, because the length over which the ultimate soil pressure is integrated increases. The integration of ultimate soil pressure and the limit soil resistance curve is shown in Figure 17 (a) and (b), respectively.

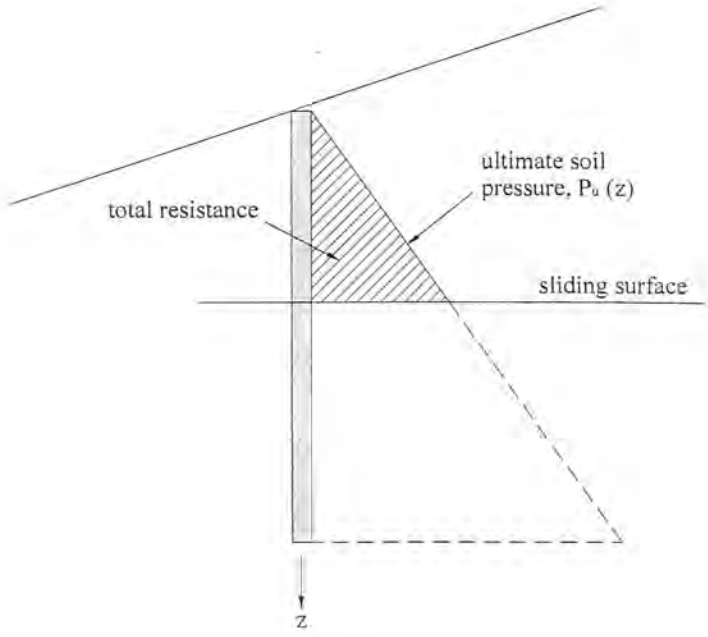

(a)

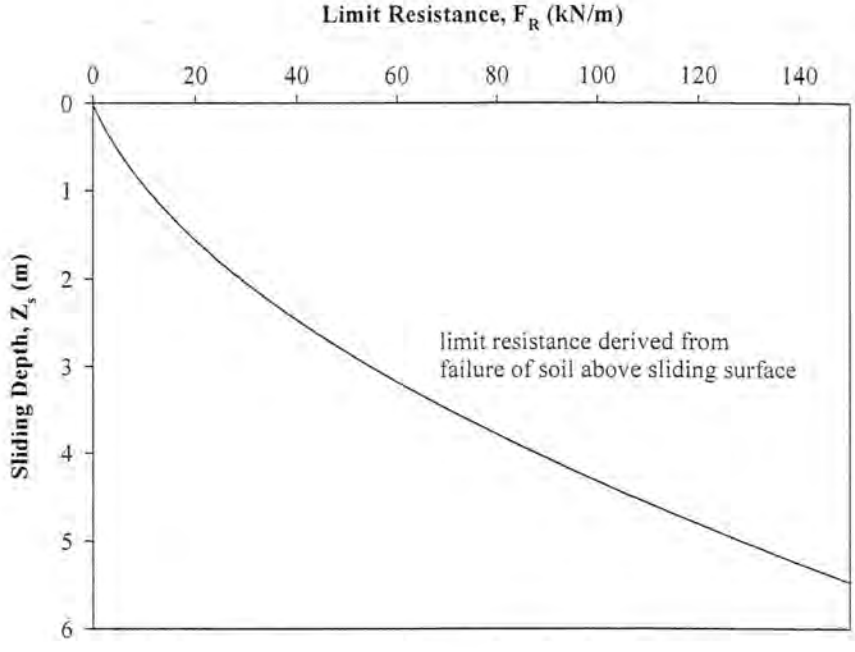

(b)

Figure 17 – Limit Soil Resistance (after Loehr and Bowders 2003)

(a) Integration for limiting soil pressure; (b) Limit soil resistance curve

Limit Anchorage Resistance

Incorporation of limit anchorage resistance ensures that pile elements do not induce passive failure of the soil below the sliding surface. For potential sliding depths, the limit soil pressure is integrated from the depth of the sliding surface to the bottom of the pile. The limit anchorage resistance decreases as the depth to the sliding surface increases (for a given pile length), because the length over which the ultimate soil pressure is integrated decreases. Clearly, piles that extend only to the failure surface offer no resistance to slope movement. The integration of ultimate soil pressure and the limit anchorage resistance curve is shown in Figure 18 (a) and (b), respectively.

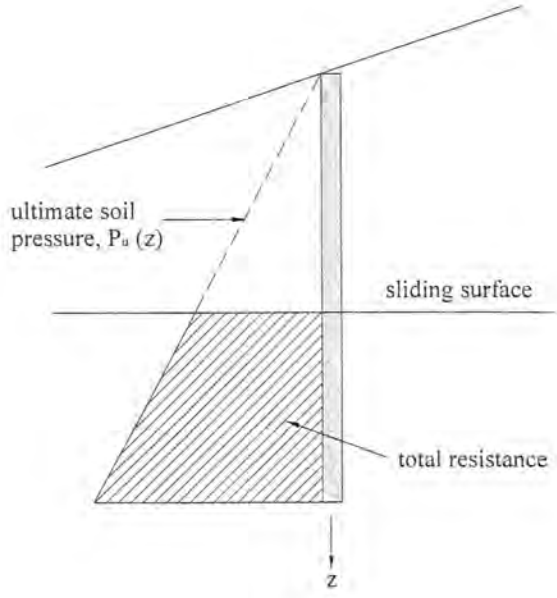

(a)

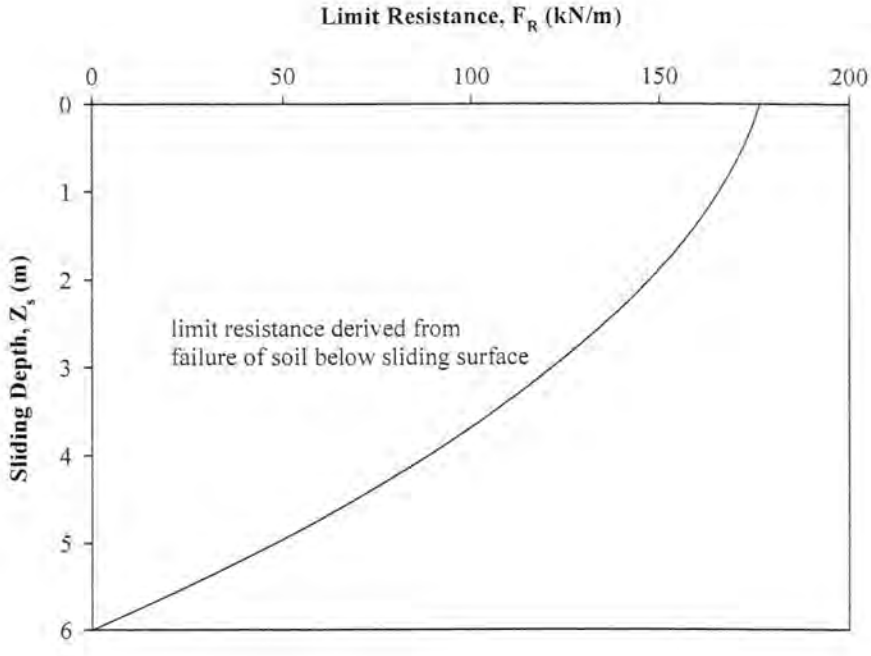

(b)

Figure 18 – Limit Anchorage Resistance (after Loehr and Bowders 2003)

(a) Integration for limiting anchorage resistance; (b) Limit anchorage resistance curve

Limit Member Resistance

The development of a limit member resistance curve to account for the structural capacity of pile elements uses the ultimate soil pressure and a reduction factor, where the application of the ultimate soil pressure may lead to bending moments or shear forces that exceed the capacity of the reinforcing member (Loehr and Bowders 2003). The reduction factor, α, is the factor by which the ultimate soil pressure is applied to the pile element that just causes the pile to fail in either bending or shear (see Figure 19). The maximum moment (or maximum shear) developed by the factored soil pressure distribution equals the moment capacity (or shear capacity) of the pile section, observing that the limit member resistance represents the maximum load that is carried by the pile.

The limit *member* resistance curve is developed similarly to the limit *soil* resistance curve, where the former uses the factored soil pressure distribution along the pile and the latter uses the unfactored soil pressure distribution along the pile. The factored ultimate soil pressure distribution is integrated from the ground surface to the potential sliding depth, such that the length over which the factored soil pressure is integrated increases with sliding depth. The limit member resistance decreases with sliding depth, however, because α decreases with sliding depth. The reduction factor, inversely proportional to the maximum moment developed in the pile, decreases with sliding depth; because the moment arm of an equivalent loading condition increases. As the moment arm increases, the calculated maximum moment increases. For this reason, at intermediate sliding depths where α is less than 1.0, member resistance controls the reinforcement capacity.

The establishment of the reduction factor and use of the factor to modify the soil pressure distribution is illustrated in Figure 19. The limit member resistance curve is provided in Figure 20.

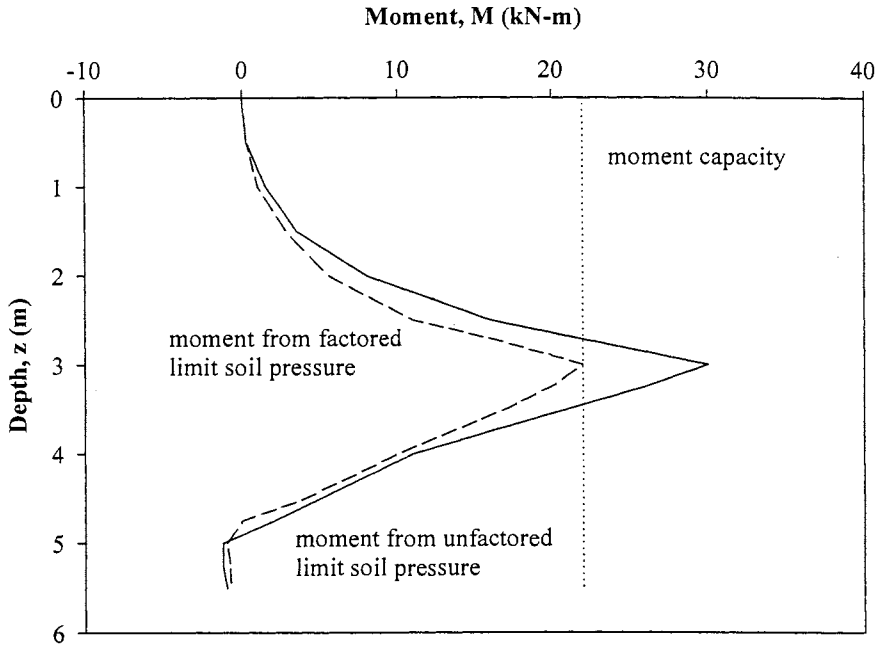

(a)

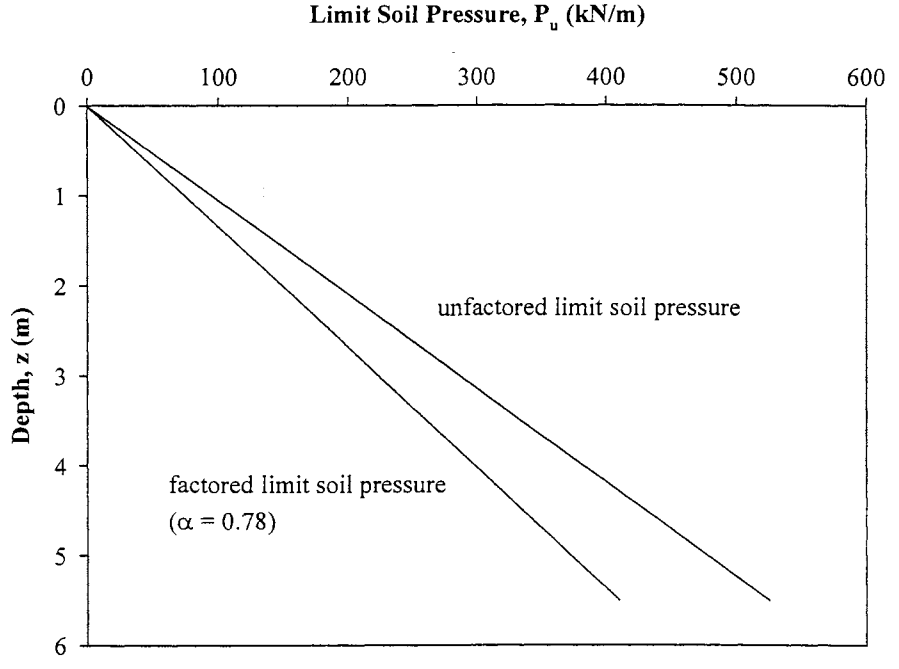

(b)

Figure 19 – Factored Pressure Distributions (after Loehr and Bowders 2003)
(a) Determination of reduction factor, α; (b) Factored limit soil pressure

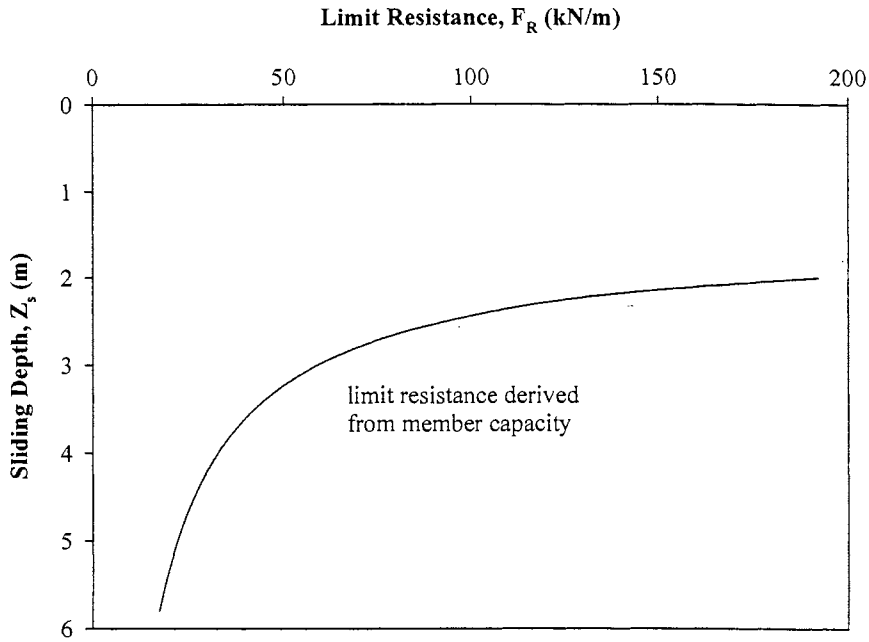

Figure 20 – Limit Member Resistance Curve (after Loehr and Bowders 2003)

Composite Limit Resistance Curve

For each limit state (soil resistance, anchorage resistance, and member resistance), a factored or unfactored limit soil pressure is determined and appropriately integrated to find the respective limit resistance for a given sliding depth. The limit resistance of the system is the least of the three limit states considered. Figure 21 shows typical distributions of limit resistance and a composite limit lateral resistance.

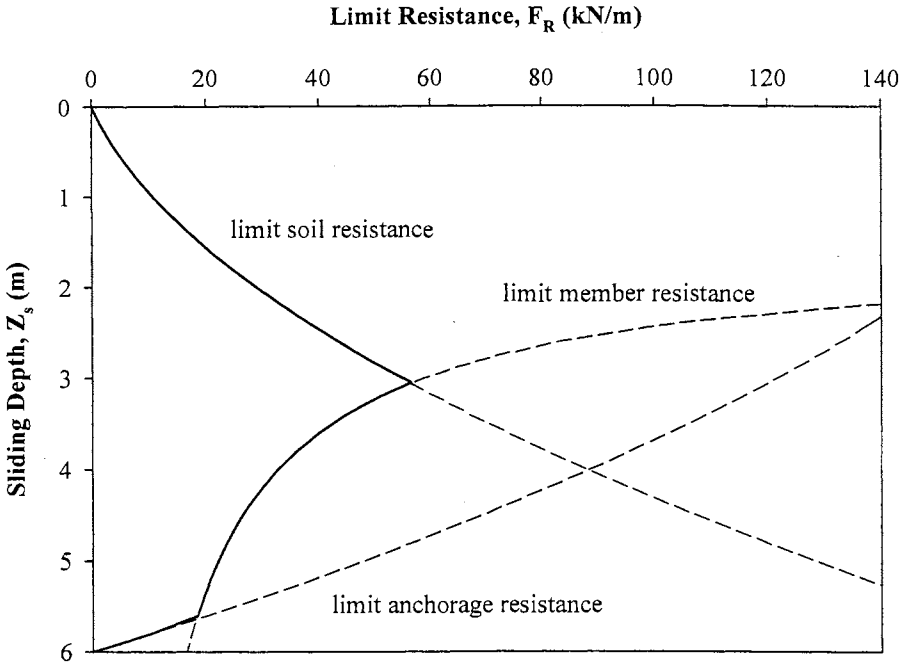

(a)

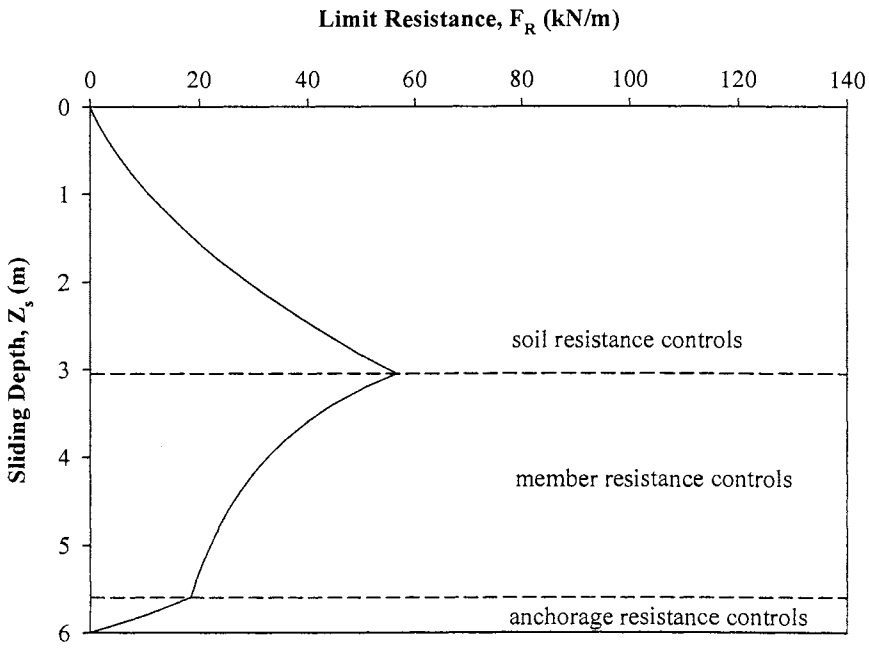

(b)

Figure 21 – Limit Resistance Distributions for Recycled Plastic Pins (after Loehr 2003)

A complete assessment of the use of recycled plastic pins for slope stabilization is premature given that the most recent test section was stabilized in 2003. Five test sites were instrumented with slope inclinometers and pore pressure sensors. Additionally, the reinforcing members of several sites were instrumented to monitor the loads and deflections of the members. It is the understanding of the author that investigators from the University of Missouri-Columbia are participating in an ongoing effort to monitor the stability of the reinforced slopes to provide evidence of the effectiveness of the stabilization scheme.

CHAPTER 3

RESEARCH TESTING METHODS

INTRODUCTION

The current research program aims to develop a rapid, cost effective, and simple remediation system that can be implemented into slope stabilization practices for a wide range of slope failure conditions. The non-proprietary remediation technology consists of soil displacement grouted micropiles (SDGM), and the experimental testing establishes soil displacement grouted micropiles as a feasible remediation alternative.

The ensuing sections summarize the conception, preparation, and performance of experimental tests for characterizing load transfer of piles subject to lateral soil movement. More specifically, Chapter 3 details the development of the comprehensive testing program, which includes laboratory and field tests.

DEVELOPMENT OF TESTING PROGRAM

Overview of Soil Displacement Grouted Micropiles

Micropiles can be classified as displacement or replacement piles. Displacement piles are generally driven or vibrated into the ground, whereas replacement piles are placed in predrilled boreholes. Soil displacement grouted micropiles, however, exhibit the characteristics of both pile types. A column of soil is laterally displaced with a reverse pitch auger, and grout is subsequently placed in the borehole. The feature contributes to the stabilizing mechanisms of the remediation method, because the locally compacted soil offers

increased shear strength at the failure surface and increased soil resistance along the entire length of the installed pile.

The stabilizing mechanisms unique to soil displacement grouted micropiles are reflected in the installation process of the pile elements. The anticipated installation method is illustrated in Figure 22.

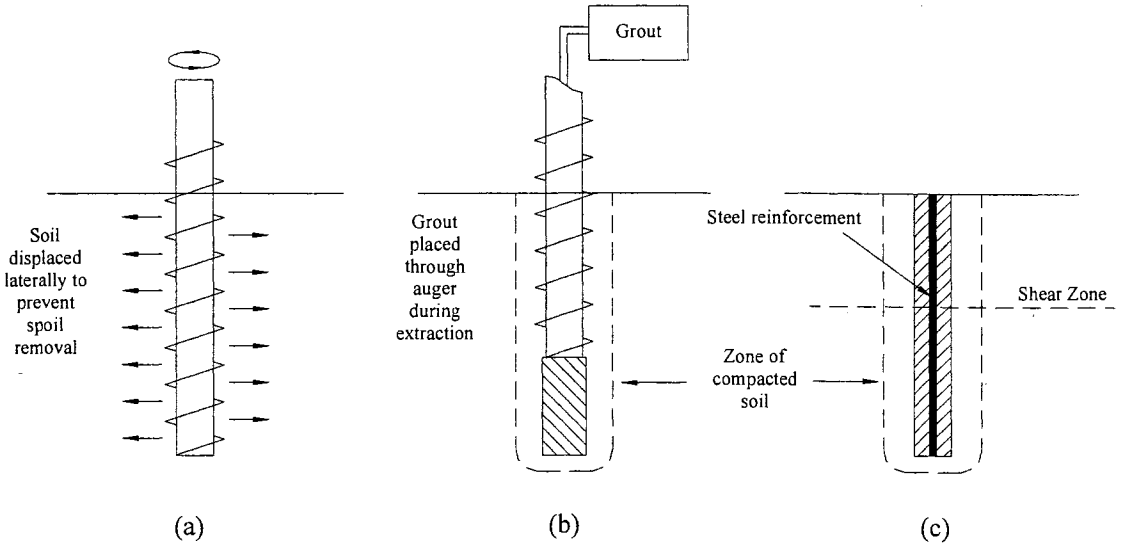

Figure 22 – Construction Sequence of SDGM System

(a) Lateral displacement of soil due to reverse pitch auger;
(b) Placement of grout concurrent with removal of auger;
(c) Finished SDGM through failure surface

The auger prepares the borehole for placement of grout, and the matrix soil is forced laterally outward or vertically downward. The local soils densify, and soil-pile system experiences increased strength. Upon reaching the desired pile depth, grout is placed through the hollow-stem auger concurrent with the removal of the auger. The unreinforced, grouted pile is subsequently reinforced with steel rebar or a steel pipe to improve the structural capacity of

the pile element. A steel-reinforced, grouted micropile (i.e. soil displacement grouted micropile) surrounded by a zone of dense soil remains at the end of construction.

The soil displacement grouted micropile system was developed as a simple remediation technology. The research group, at inception of the research project, speculated that the method would be used by state and county highway construction and maintenance crews to repair nuisance slope failures and stabilize unstable slopes. Beyond being easily constructed, however, soil displacement grouted micropiles offer benefits related to the stabilizing mechanisms of the remediation system. The remediation system employs a larger number of small-diameter micropiles, as opposed to fewer large-diameter drilled piers. The system offers redundancy, such that the failure of one micropile is less critical than the failure of one tensioned anchor in a retaining structure. Moreover, the likely failure mode of soil displacement grouted micropiles is preferable over the failure modes of other remediation methods, in that the slope structure deforms in smaller increments and offers evidence of movement prior to catastrophic failure. The deformations are ideally observed with the slope monitoring program; and, when necessary, additional piles are installed to prevent further slope movement or increase the factor of safety for global stability to accommodate increased performance requirements of the slope (i.e. building of structures adjacent to slope).

Development of Test Plan

The testing program for evaluating soil displacement grouted micropiles as a feasible slope reinforcement alternative involved laboratory and field testing. The laboratory testing program was completed to satisfy the research objective of measuring material properties of soil and pile elements. The field testing program was completed to satisfy the research objective of measuring loads induced by lateral soil movement. Laboratory tests and field

tests were performed with representative Iowa soils (e.g. loess, glacial till, and weathered shale).

The laboratory testing program consisted of determining properties of soil and grout samples. The following laboratory tests sufficiently characterized soil and potential grout mixtures:

- soil classification tests, including grain size distribution and Atterberg limits;
- soil compaction characteristics;
- unconfined compression tests;
- direct shear tests for effective soil shear strength parameters, c and ϕ;
- consolidated-undrained triaxial compression tests for empirical development of p-y curves; and
- compression tests on grout samples (mixtures of Portland cement, sand, fly ash, chemical admixtures, water, and air) for the determination of elastic modulus, ultimate compressive strength, and rate of strength development

The field testing program consisted of measuring the shear strength of soil reinforced with pile elements. The pile load tests were performed in a manner similar to large-scale direct shear tests. The direct shear boxes, constructed large enough to minimize the influence of box boundaries, contained compacted soil with known properties and piles that extended into existing ground. The shear boxes were pushed laterally to impose uniform lateral translation of soil and model the movement of a unit "cell" of a sliding soil mass. The interface of the shear box and the at-grade elevation resembled the failure surface of a slope failure, and the soil below grade resembled the stable soil of a slope in which piles are installed to provide passive resistance to movement. Instrumentation of the direct shear boxes (displacement gauges and load cell) was installed to measure the load-displacement response of the reinforced soil. Instrumentation of the pile reinforcement (strain gauges)

indirectly indicated the loads induced on the piles due to lateral soil movement and the pile response to the loads. Figure 23 shows the large-scale direct shear test set-up.

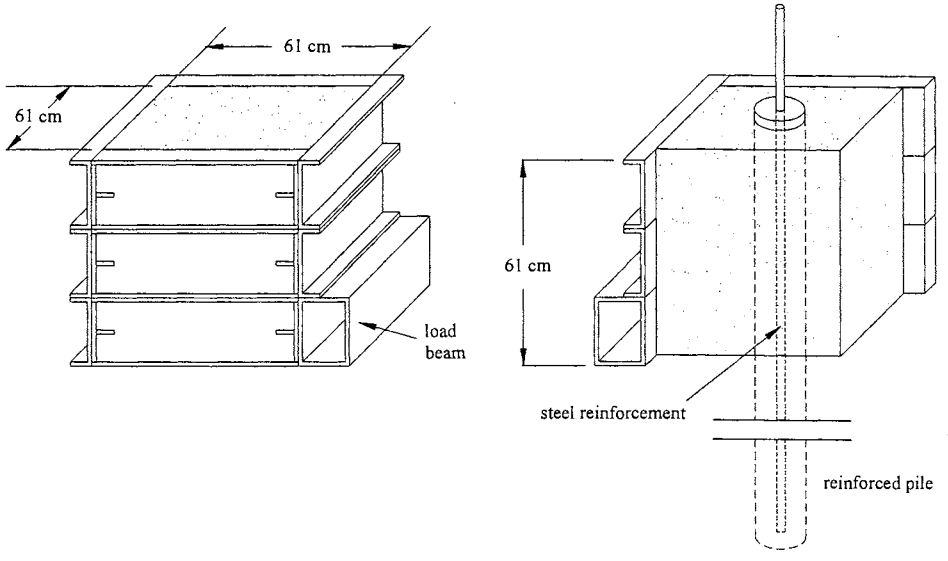

Figure 23 – Large-Scale Direct Shear Test Set-Up

Preliminary analyses of proposed pile diameters and steel reinforcement were performed to determine critical pile lengths and demarcate rigid piles from flexible piles. Figure 24 provides pile head deflection vs. pile length, where a uniformly distributed load was applied to the uppermost two feet of each pile. Pile lengths greater than 1.8 meters (L/D = 12-14) resulted in flexible pile behavior, evidenced by stabilization of pile head deflection. Based on this information, the research group decided that each pile would extend 1.5 meters into existing ground, resulting in total pile lengths of 2.1 meters.

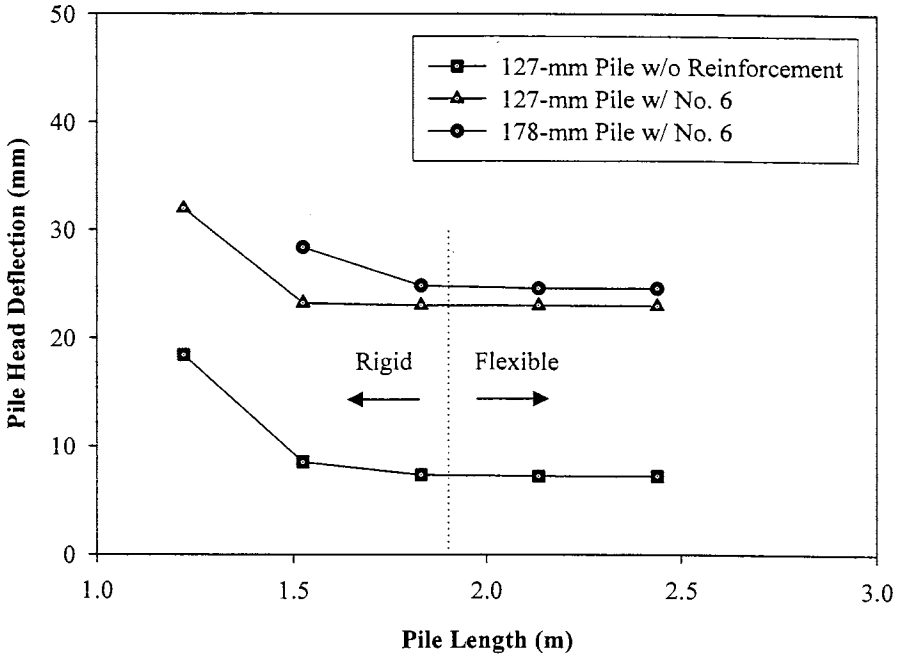

Figure 24 – Pile Head Deflection vs. Length for Determination of Critical Pile Length

The research testing plan is diagrammed in Figure 25 and shows the tests that were performed on soil, pile materials, and reinforced soil. The figure also summarizes how each test aids the desired analyses of piles subject to lateral soil movement.

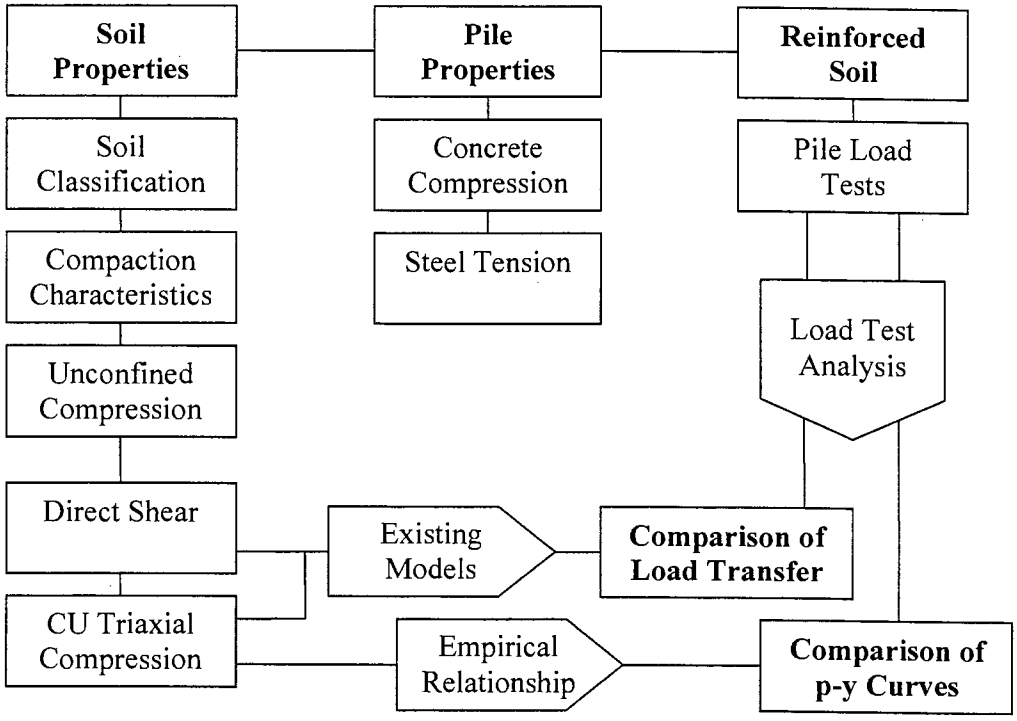

Figure 25 – Research Testing Plan

Test Location, Personnel, and Duration

The research testing program was completed at Iowa State University by the author under the supervision of his major advisor. Laboratory tests were performed at the Gerald Olson Soil Mechanics Laboratory, and pile load tests were conducted at the Spangler Geotechnical Experimentation Site (SGES). Previous research investigations have been performed at the SGES. The site soil conditions, inclusive of p-y curves developed from full-scale pile load tests, have been documented (Hong, 2003). The soil profile and p-y curves of the uppermost soil layers are provided in Appendix A. Engineering properties of the non-stratified glacial till are provided in Table 4.

Table 4 – SGES Engineering Properties

Soil Parameter	Range of Values
Density	1920 to 2160 kg/m^3
Cohesion	20 to 210 kPa
Friction Angle	19 to 31 degrees
OCR	1.5 to 4
LL, PI	30 - 40% and 10 - 20%
Soil Classification	CL
Permeability	10^{-4} to 10^{-5} cm/s
Modulus	5,000 to 17,000 kPa

Laboratory testing was conducted during the fall and spring semesters of the 2003-2004 academic year, concurrent with the review of literature and preliminary analyses. The field investigation was conducted during the summer of 2004. Pile load tests were prepared and performed in May and June, respectively.

Soil Acquisition

For the research, the state of Iowa was divided into three upland regions of different topography and surface geology. Soils from each region (e.g. glacial till, loess, and weathered shale) were collected for use in the testing program. The soils were characterized with laboratory testing and also used in pile load tests. Employment of the same soils in laboratory and field testing was necessary for pile load test data interpretation and analysis.

The north central portion of the state is comprised of glacial till from the Des Moines Lobe Glaciation. Glacial till was obtained in Ames, Iowa.

The western portions of the state, adjacent to the Missouri River floodplain, have deep loess soils that form very steep hillslopes and narrow drainage divides. The western Iowa loess is often referred to as friable loess. Figure 26 illustrates the loess deposits with a photograph of the Loess Hills.

Figure 26 – Loess Hills of Western Iowa

Loess was obtained from a cut section in the Loess Hills of western Iowa. The loess source (Turin, Iowa) is shown in Figure 27.

(a)

(b)

Figure 27 – Loess Source (Turin, Iowa)

Weathered shale was obtained from a slope failure near Luther, Iowa. The weathered shale source, shown in Figure 28, is located on Highway E57 next to the Des Moines River.

(a)

(b)

Figure 28 – Weathered Shale Source (Luther, Iowa)

LABORATORY TESTING PROGRAM

Soil Classification

Gradation analysis and Atterberg limit tests were performed on each soil sample according to ASTM D 2487 [Test Method for Classification of Soils for Engineering Purposes] and ASTM D 4318 [Standard Standard Test Method for Liquid Limit, Plastic Limit, and Plasticity Index of Soils] (ASTM 2000), respectively. The Atterberg limits for each soil are provided in Table 5. The gradation analysis of each soil is provided in Table 6 and Figure 29.

Table 5 – Atterberg Limits

Soil Type	LL	PL	PI
Loess	29	23	6
Glacial Till	24	15	9
Weathered Shale	35	24	11

Table 6 – Gradation Analysis, Based on USCS

Soil Type	Gravel (> 2.00 mm)	Sand (> 0.075 mm)	Silt (> 0.002 mm)	Clay (< 0.002 mm)
Loess	0.0	2.9	90.9	6.2
Glacial Till	1.4	46.3	37.7	14.6
Weathered Shale	0.0	9.1	51.7	39.2

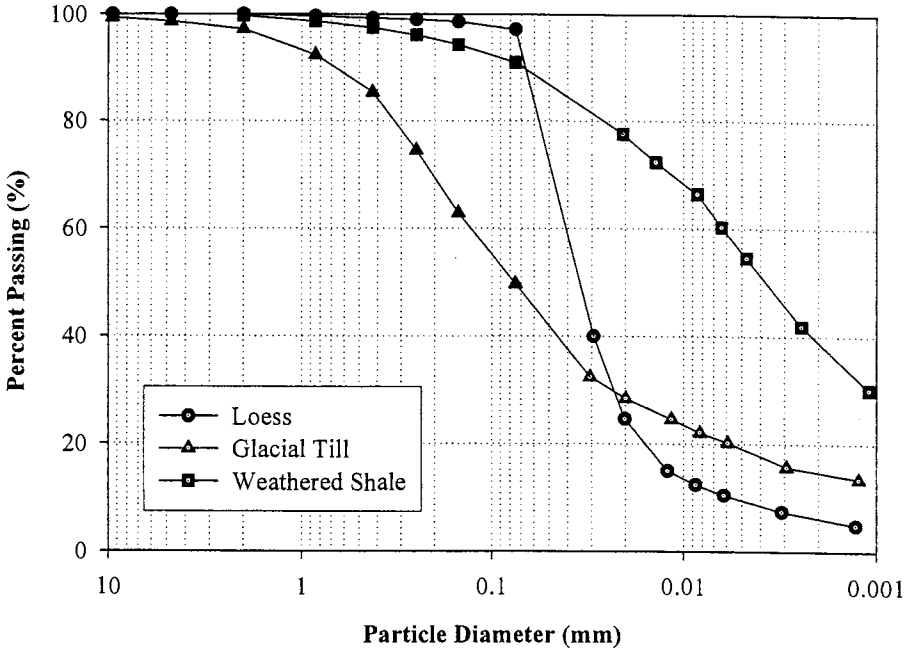

Figure 29 – Grain Size Distribution Curve

Each soil was classified according to the Unified Soil Classification System (USCS), the AASHTO classification system, and the United States Department of Agriculture (USDA) textural classification system. Soil classifications are provided in Table 7.

Table 7 – Soil Classifications

	USCS		AASHTO		USDA
Soil Type	**Group Symbol**	**Group Name**	**Classification**	**GI***	**Textural Classification**
Loess	ML	Silt	A-4	(6)	Silt loam
Glacial Till	CL	Sandy lean clay	A-4	(2)	Sandy loam
Weathered Shale	CL	Lean clay	A-6	(11)	Silty clay loam

Notes:

* Group Index = $0.01\ (F_{200} - 35)\ [0.2 + 0.005\ (LL - 40)] + 0.01\ (F_{200} - 15)\ (PI - 10)$

Moisture and Density Properties

The specific gravity was determined for each soil type. The tests were performed according to ASTM C 128 [Specific Gravity and Absorption of Fine Aggregate] (ASTM 2002). Specific gravities are provided in Table 8.

Table 8 – Specific Gravities

Soil Type	G_s
Loess	2.72
Glacial Till	2.66
Weathered Shale	2.69

The compaction moisture-density relationship was developed with the standard Proctor test, performed according to ASTM D 698, Method A [Standard Test Method for Determining the Moisture-Density Relations of Soils and Soil-Aggregate Mixtures] (ASTM 2000). The maximum dry unit weights and optimum moisture contents are provided in Table 9, and the Proctor curves are shown in Figure 30.

Table 9 – Maximum Dry Unit Weights and Optimum Moisture Contents

Soil Type	w_{opt} (%)	$\gamma_{d\ max}$ (kN/m^3)
Loess	18	15.55
Glacial Till	14	17.75
Weathered Shale	18	16.65

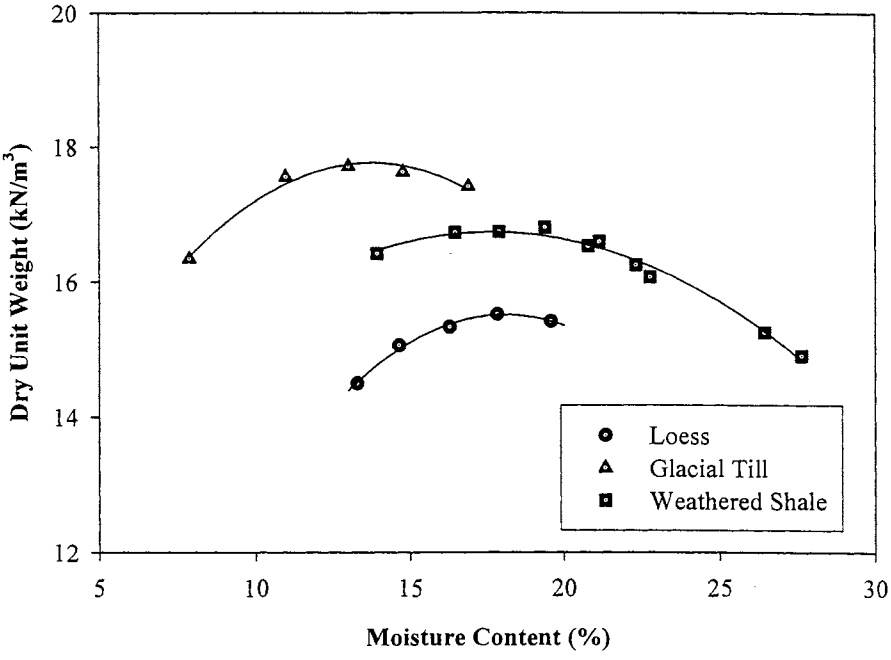

Figure 30 – Graph of Dry Unit Weight vs. Moisture Content

Upon acquisition of soil samples, moisture contents were measured for the in-situ moisture of the soil. The natural moisture contents, provided in Table 10, were used as the conditions for subsequent test preparation.

Table 10 – Natural Moisture Contents

Soil Type	$w_{natural}$ (%)
Loess	8.6
Glacial Till	11.8
Weathered Shale	21.8

Direct Shear Test

Direct shear tests were performed on each sample to determine effective cohesion, c, and effective internal friction angle, ϕ. Samples were compacted, saturated under load, and subsequently sheared at a rate that would avoid build-up of excess pore water pressures. The loess and glacial till samples were sheared at 1.27 mm per minute, and the less-permeable weathered shale samples were sheared at 0.025 mm per minute. The shear strength parameters are provided in Table 11, and the failure envelopes are shown in Figure 31.

Table 11 – Shear Strength Parameters from Direct Shear Tests

			Compaction	
Soil Type	**ϕ (deg)**	**c (kPa)**	**γ_d (kN/m^3)**	**w (%)**
Loess	28	25	14.9	14
Glacial Till	31	31	17.8	12
Weathered Shale	21	24	16.3	22

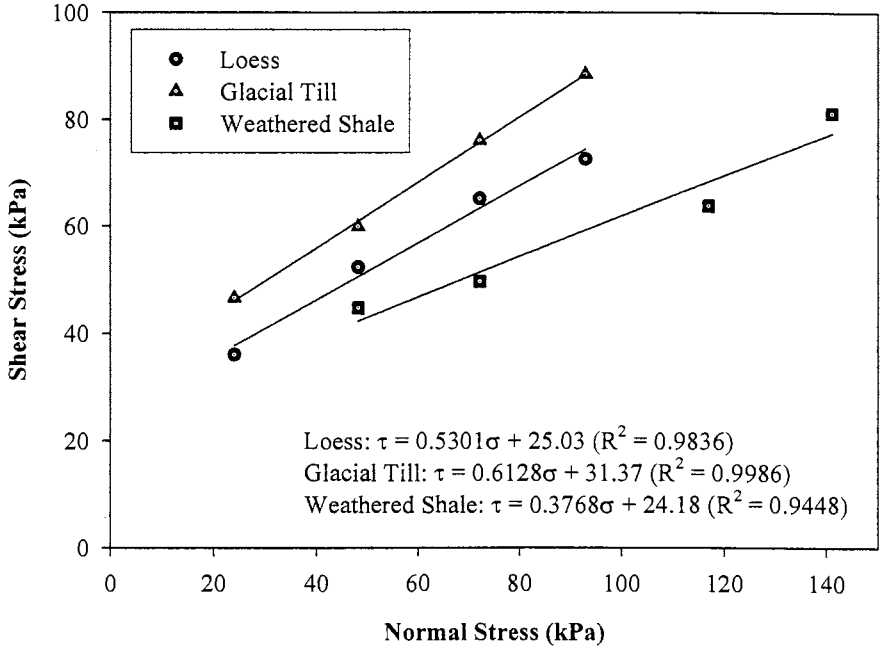

Figure 31 – Direct Shear Test Failure Envelopes

Unconfined Compression Test

The unconfined compression test is a unique case of the triaxial test. In this instance, the confining pressure, σ_3, equals zero. The soil sample experiences considerable deformation as an axial load is applied. The unconfined compression strength, q_u, is commonly used as an indicator for the consistency of saturated clays (Das, 1999). Additionally, the unconfined compression strength indicates the value of the undrained shear strength, s_u. Equation (19) defines the relationship between undrained shear strength and unconfined compression strength. The equation is valid for clays, which routinely assume the undrained friction angle, ϕ, equals zero for the design of foundations.

$$s_u = \frac{q_u}{2} \tag{19}$$

where s_u = undrained shear strength

q_u = unconfined compression strength

Average unconfined compressive strengths are provided in Table 12.

Table 12 – Unconfined Compressive Strength

	Unconfined Strength (kPa)		Compaction		
Soil Type	**Average**	**Std Dev**	**γ_d (kN/m^3)**	**w (%)**	**n**
Loess	19.3	6.6	15.6	31	3
Glacial Till	105.5	9.8	20.0	17	5
Weathered Shale	8.0	—*	16.0	23	1

Notes:
* Data not available
n = number of tests

Typical stress-strain relationships for unconfined compression tests in loess, glacial till, and weathered shale are provided in Figures 32 through 34.

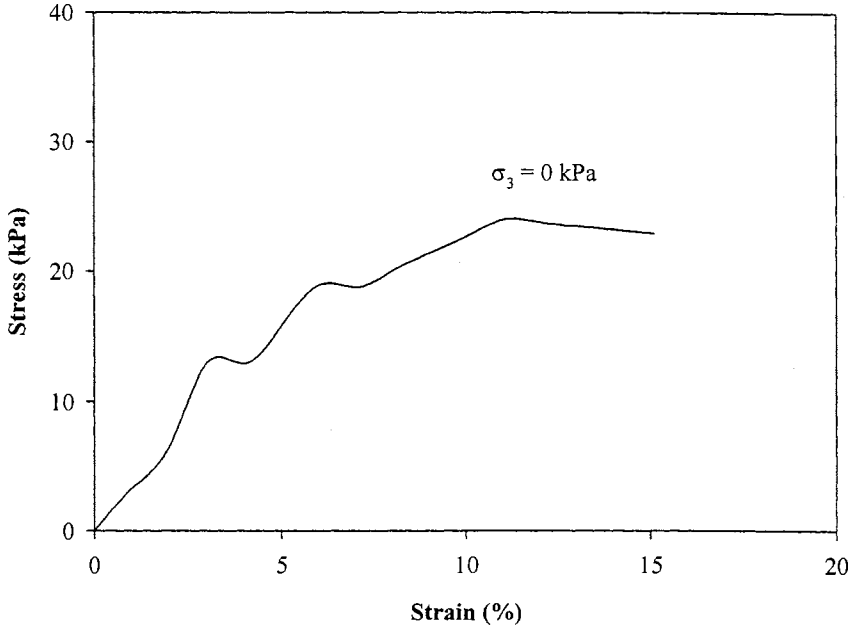

Figure 32 – Unconfined Compression Test Stress-Strain Relationship for Loess

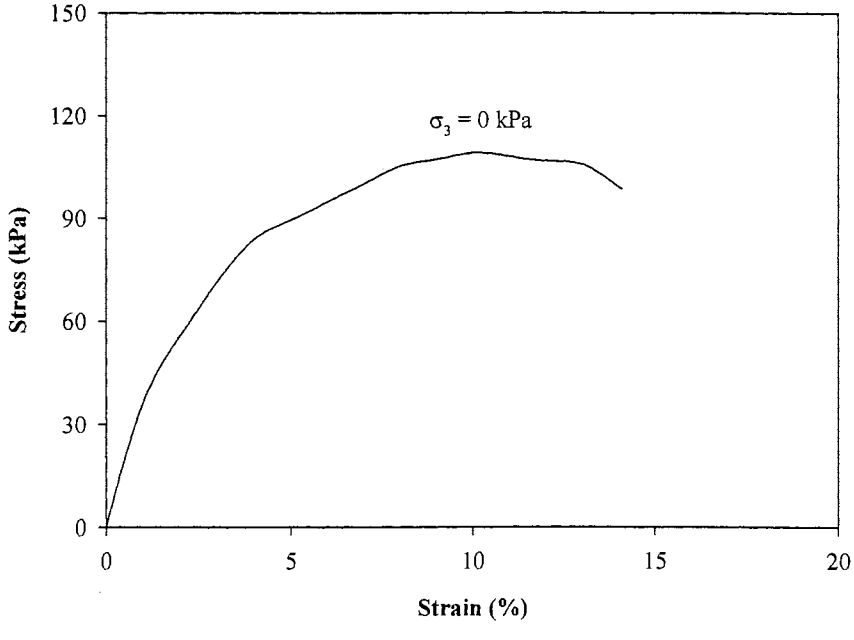

Figure 33 – Unconfined Compression Test Stress-Strain Relationship for Glacial Till

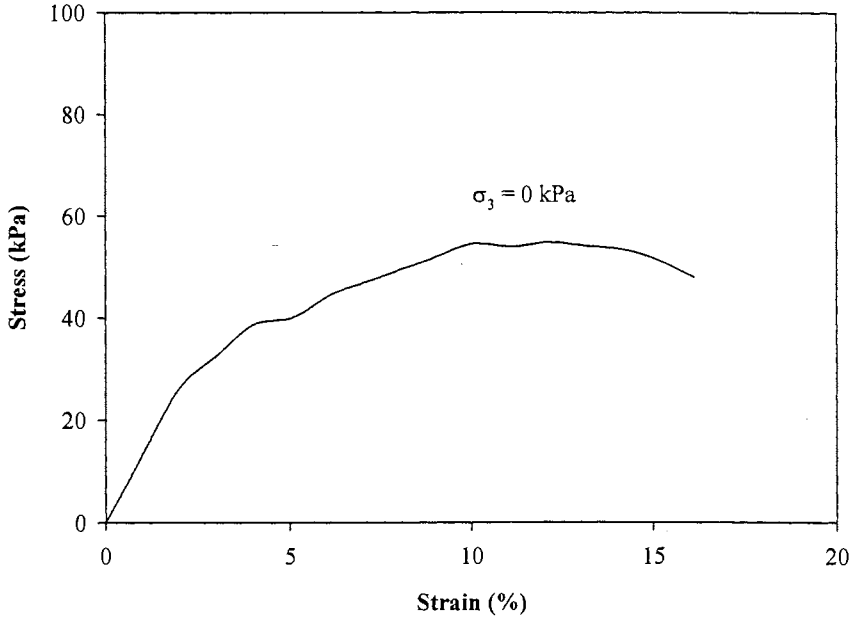

Figure 34 – Unconfined Compression Test Stress-Strain Relationship for Weathered Shale

Consolidated-Undrained (CU) Triaxial Test

Consolidated-undrained (CU) triaxial tests were performed as part of the field testing program. CU triaxial tests were performed on a single specimen for each soil type. Each of the three test specimens (one specimen per soil type) was saturated and subsequently consolidated at 34.5 kPa. The specimen was loaded and the stress-strain behavior was recorded by a data acquisition system. Following the loading, the specimen was consolidated at 103.5 kPa. The specimen was reloaded and allowed to strain significantly more than at the lower confining pressure. Confining pressures of 34.5 and 103.5 kPa were selected to develop boundary p-y curves from which intermediate load-displacement curves were potentially used for the analysis. The stress-strain relationships for triaxial compression tests in loess, glacial till, and weathered shale are provided in Figures 35 through 37.

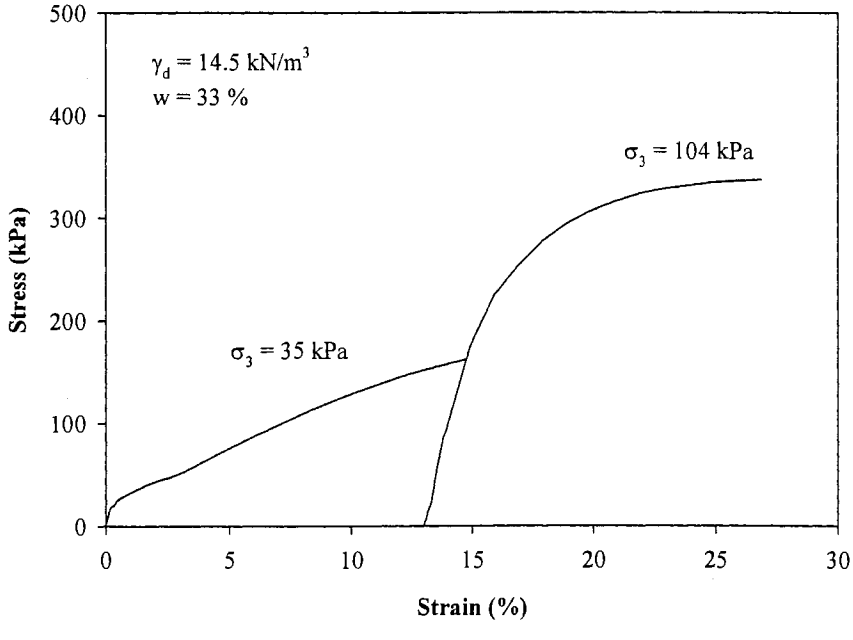

Figure 35 – CU Triaxial Test Stress-Strain Relationship for Loess

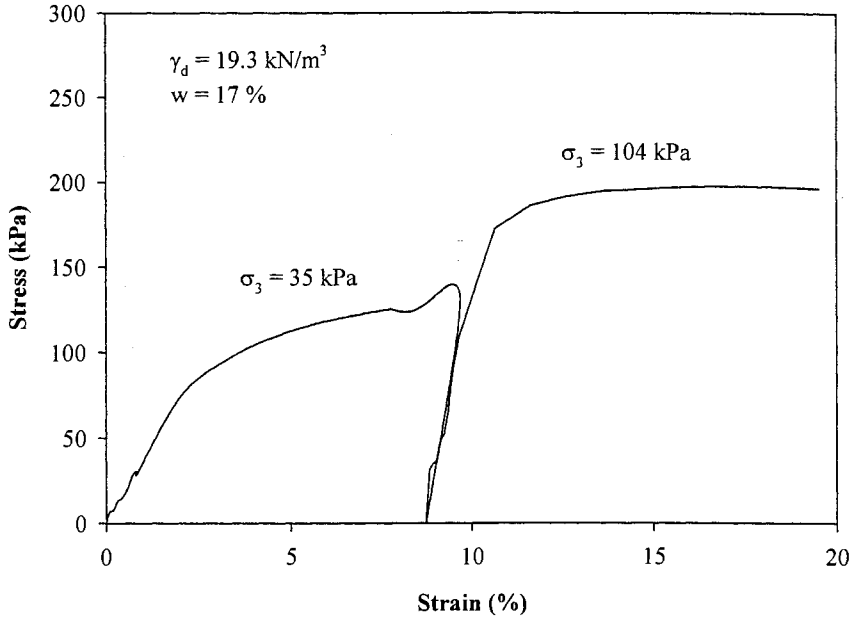

Figure 36 – CU Triaxial Test Stress-Strain Relationship for Glacial Till

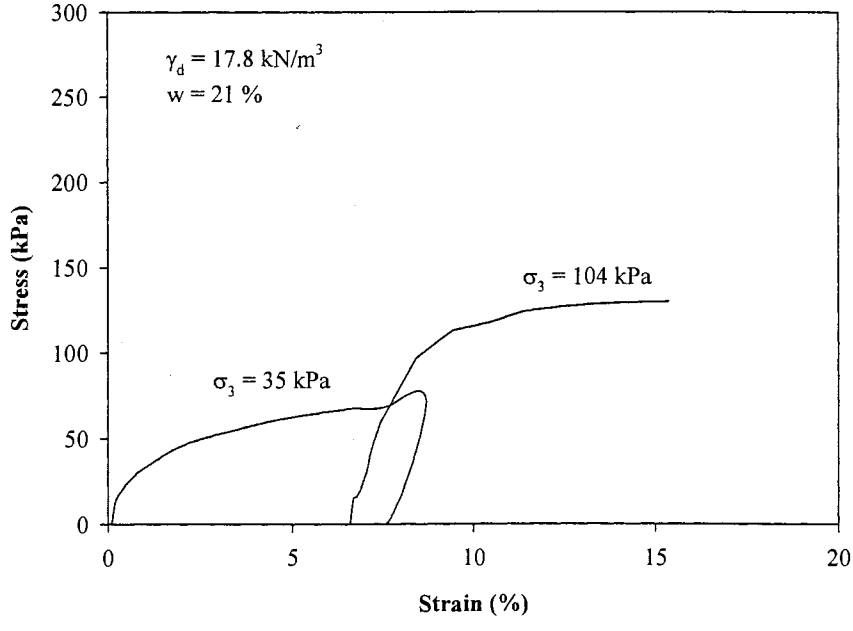

Figure 37 – CU Triaxial Test Stress-Strain Relationship for Weathered Shale

The load-displacement behavior of the triaxial tests, including the behavior of the unconfined compression tests, was used in developing p-y curves for pile load test analyses. The ultimate soil pressure (p_u) and strain at 50 percent of maximum load (ε_{50}) define the shape of p-y curves developed from triaxial compression tests. The p-y curves were developed from an equation of the following form (Reese and Wang 2000):

$$\frac{p}{p_u} = 0.5\left(\frac{y}{y_{50}}\right)^n \tag{20}$$

where p_u = ultimate soil resistance (force/length)

y_{50} = deflection at one - half the ultimate soil resistance (length)

$n = \frac{1}{3}$ for soft clay, proposed by Matlock (1970)

$n = \frac{1}{4}$ for stiff clay, proposed by Reese and Welch (1975)

The ultimate soil resistance, p_u, is the smaller value given by the following equations (Reese and Wang 2000):

$$p_u = \left[3 + \frac{\gamma'}{c_u} + \frac{J}{b}x\right] c_u\, b \tag{21}$$

$$p_u = 9\, c_u\, b \tag{22}$$

where γ' = aveage effective unit weight from ground to p - y curve

x = depth to p - y curve

c_u = undrained shear strength

b = pile diameter

J = empirical coefficient (0.25 for soft clay, 0.5 for medium and stiff clay)

The y_{50} is determined with the following equation:

$$y_{50} = 2.5\,\varepsilon_{50}\,b \qquad (23)$$

Based on strengths from unconfined compression tests, the loess was characterized as soft clay. The glacial till and weathered shale was characterized as stiff clay. Figures 38 through 41 show the p-y curves developed from CU triaxial tests. The p-y curves of Figure 41, those used for the load test analysis, correspond to strengths measured with no confining stress (σ_3 = 0 kPa). The undrained shear strength was assumed to equal one-half of the unconfined compressive strength.

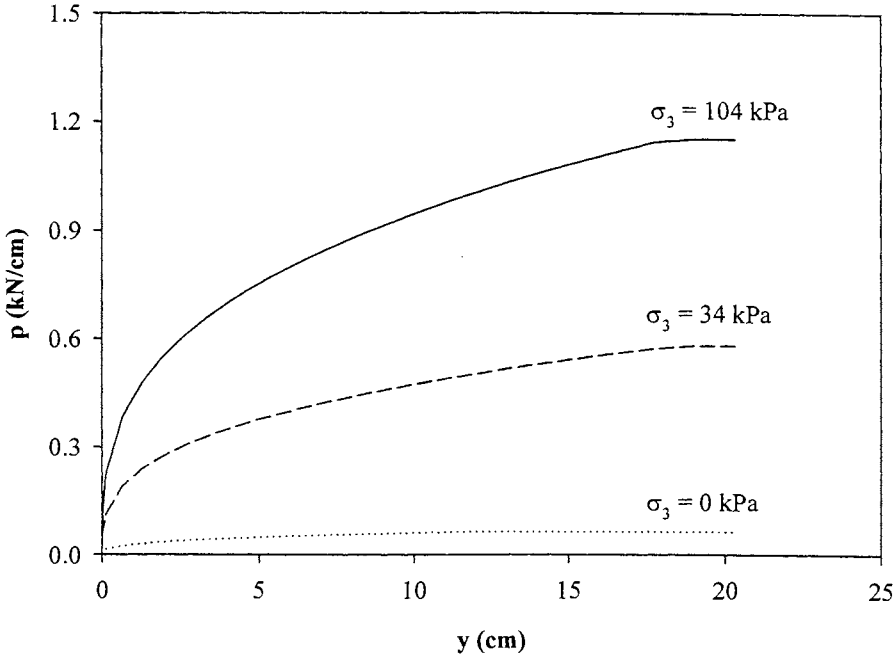

Figure 38 – P-y Curves for Loess

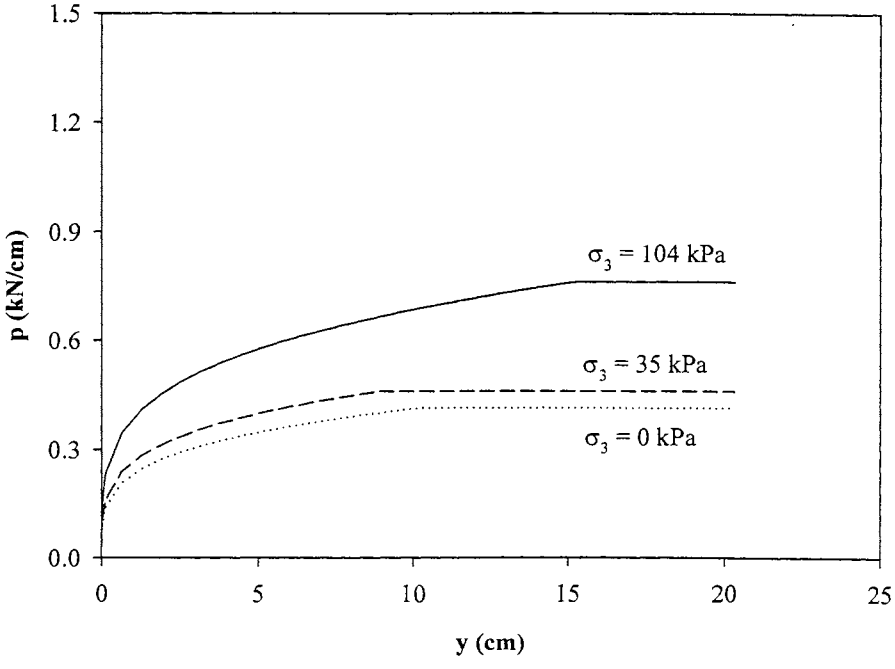

Figure 39 – P-y Curves for Glacial Till

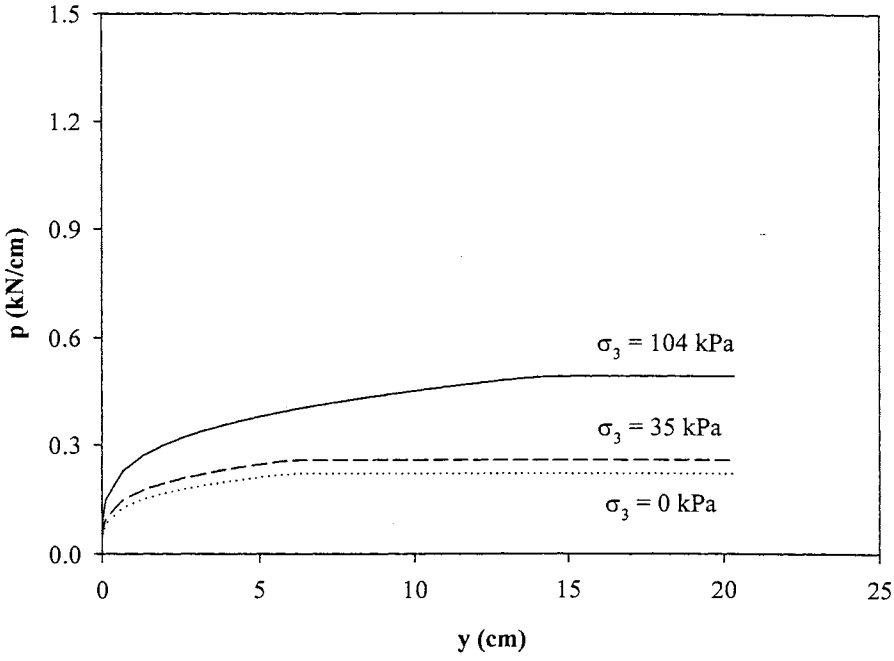

Figure 40 – P-y Curves for Weathered Shale

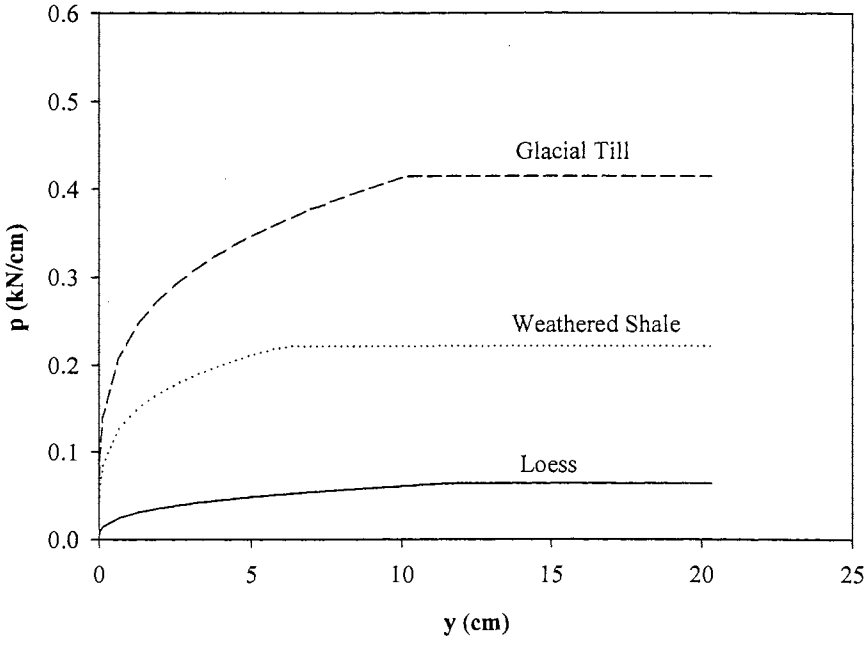

Figure 41 – P-y Curves Used for Load Test Analyses (σ_3 = 0 kPa)

Grout Mix Design

The proposed micropiles employed small diameters (100 to 200 mm), and the workability of a potential grout mix design was of critical importance to the construction and subsequent performance of the piles under the loading conditions of slope reinforcement. The research group evaluated several high-slump grout mixtures for use in soil displacement grouted micropiles. Based principally on self-compacting concrete (SCC) and controlled low-strength material (CLSM), a new mix design was tested and recommended for use in the pile load tests. The proposed mix design satisfied the preliminary performance criteria established by the research group at the onset of the research project in that the grout mixture was highly fluid and achieved sufficiently high compressive strength (27.6 MPa).

The selection of a grout mix design for use in pile load tests evolved from published mix designs for CLSM (CTRE 2003) and SCC (Schlagbaum 2002) of residential and structural applications. The SCC and CLSM mix designs were developed and subjected to preliminary tests. Freshly mixed grout was tested for workability, and hardened grout was tested for compressive strength. The research group subsequently attempted to develop a grout mixture for soil displacement grouted micropiles that exhibited the flow properties of CLSM and the mechanical performance properties of SCC. Mixture proportions and performance properties of each concrete mixture are provided in Table 13.

Table 13 – Preliminary Mixture Proportions and Testing Results

Grout Constituent	**SCC*** **lb/cy**	**CLSM**** **lb/cy**	**SDGM** **lb/cy**
Cement	600	100	600
Fly Ash	n/a	400	125
Fine Aggregate	1340	2600	2700
Coarse Aggregate	1700	n/a	n/a
w/cm	0.55	1.12	0.65
Admixture	**fl oz/cwt**	**fl oz/cwt**	**fl oz/cwt**
HRWR	8	n/a	8
VMA	2	n/a	2
Performance	**MPa**	**MPa**	**MPa**
21-day Strength	54.35	2.68	30.34
Slump (cm)	17.8	27.9	27.4

Notes:
* Schlagbaum (2002)
** Center for Transportation Research and Education (2003)
HRWR = high range water reducer
VMA = viscosity modifying admixture

Concrete sand was obtained from Hallet Materials in Ames, Iowa. The gradation of the sand is provided in Figure 42.

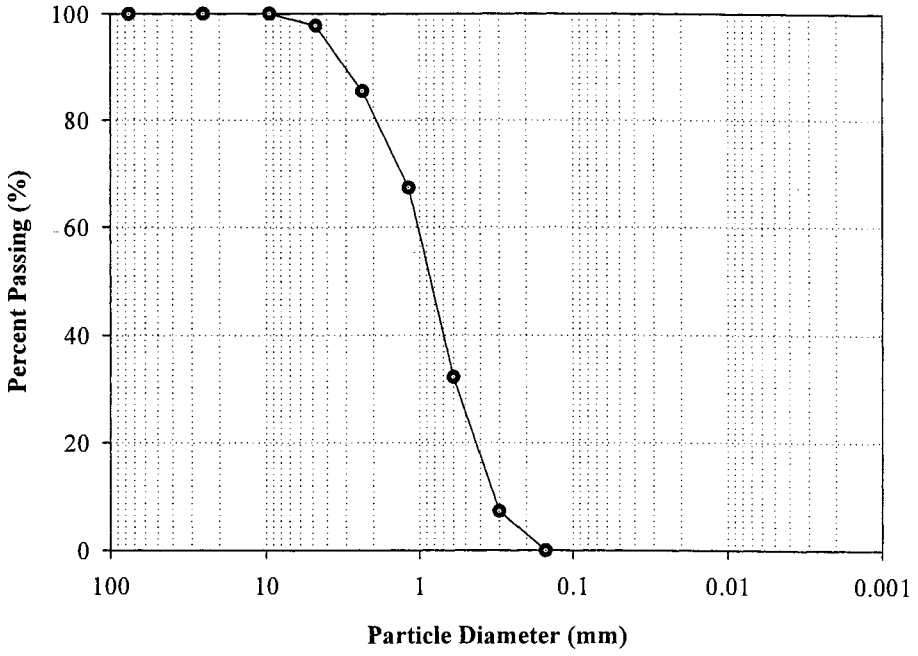

Figure 42 – Concrete Sand Gradation

The compressive strength development of each flowable grout mix design is provided in Table 14 and Figure 43.

Table 14 – Compressive Strength Development of Concrete Mixtures

Days	CLSM	SCC	SDGM
0	—*	—*	—*
7	1.71	35.38	20.10
14	2.28	47.51	28.74
21	2.68	54.35	30.34
28	—*	—*	30.85

Notes:
Strengths in units of MPa
* Data not available

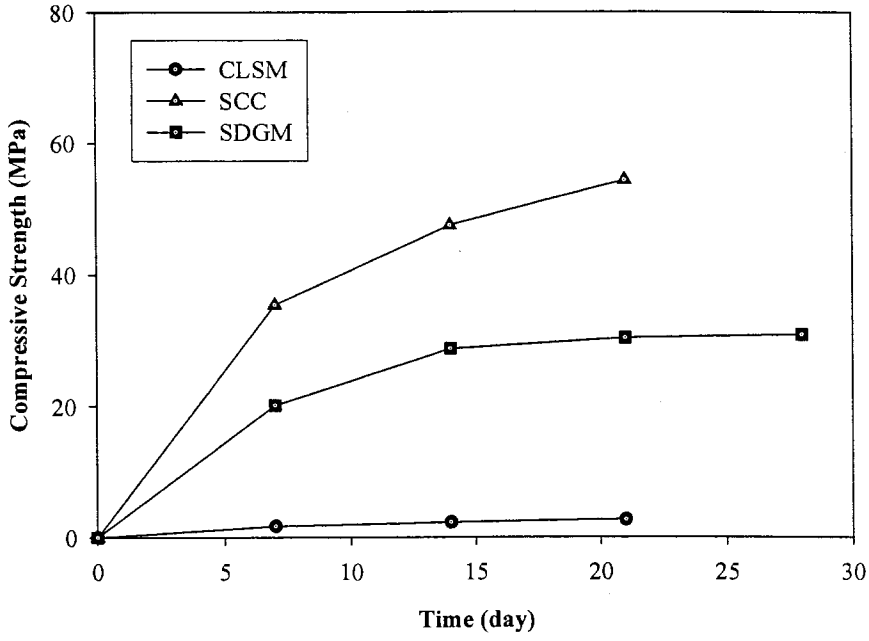

Figure 43 – Strength Development of Grout Mixtures

Sufficient testing has not yet been performed to optimize mechanical and flow properties of the mix design with respect to cost effectiveness. This evaluation is complicated by issues of composite materials, constructability, and costs associated with quality control/assurance practices. The development of more advanced concrete/grout mixtures is beyond the scope of the current research project.

FIELD TESTING PROGRAM

Load Test Plan

The pile load test plan involved the evaluation of soil type, pile size, and pile spacing as each parameter relates to the performance of the slope stabilization system. Each reinforcement parameter influences the response of piles subject to lateral soil movement, and the influence of the parameters on pile behavior is evidenced by the dependence of p-y curves on the parameters.

The pile load test plan, provided in Table 15, included seven load tests of 14 unique pile configurations. Direct shear boxes were loaded against each other, such that each test involved the simultaneous loading of two boxes. The full-scale tests were conducted to evaluate the performance of 127-mm and 178-mm piles, reinforced with a centered No. 19 rebar.

Table 15 – Pile Load Test Plan

Test Number	Box Numbers	Soil Types	Pile Sizes*
1	1	Loess	No Pile
	2	Weathered Shale	No Pile
2	3	Glacial Till	No Pile
	4	Loess	114-mm Pile
3	5	Glacial Till	112-mm Pile
	6	Weathered Shale	117-mm Pile
4	7	Weathered Shale	114-mm Pile **
	8	Loess	183-mm Pile
5	9	Glacial Till	178-mm Pile
	10	Weathered Shale	(2) 113-mm Piles
6	11	Loess	(2) 114-mm Piles
	12	Weathered Shale	173-mm Pile
7	13	Glacial Till	(2) 113-mm Piles
	14	Glacial Till	(2) 115-mm Piles

Notes:
All piles with No. 19 rebar
* Measured after pile exhumation
** No pile reinforcement

Site Preparation and Load Test Set-Up

Pile load tests were conducted at the Spangler Geotechnical Experimentation Site. The site was covered by vegetation that required removal prior to testing. Figure 44 shows the clearing of site vegetation with a skid loader. Frequent and heavy rainfall events resulted in difficult working conditions on the flat, bare site. The field testing site was ultimately covered with gravel to facilitate wet-weather access. The presence of gravel, however, had no influence on the test performance and obtained test results.

Pile load tests were laid out prior to excavating control soil pads and compacting soil in shear box forms. The initial test layout ensured that sufficient spacing was available for the necessary load frame and loading system (e.g. load cells, hydraulic cylinders). The use of string lines helped in keeping shear box forms aligned with loading counterparts. Figure 45 shows the initial test layout.

Control soil pads were excavated at each shear box location. The control pads, excavated with dimensions larger than the shear boxes and to depths of 30 centimeters, ensured that all potential failure surfaces during load testing were contained within the soil of known shear strength parameters (i.e. loess, glacial till, weathered shale). A failure surface located at the interface of the existing site soil and the soil of the shear box would likely complicate the evaluation of the load-displacement behavior of laterally-pushed shear boxes. The soil pads served as a means for control to facilitate more reliable load test analyses. Figure 46 shows the manually-excavated control soil pads.

Soil was compacted in the control soil pads and shear box forms with hand tampers. The compaction of soil occurred at approximately natural moisture for each soil type, and the compaction effort was uncontrolled. Soil sampling that followed pile load tests, however, suggested that relatively uniform density was achieved during the preparation of the load tests. The results of the soil sampling investigation (i.e. moisture and density, dynamic cone

penetrometer, unconfined compression, and K_o stepped blade) are described in Chapter 4. Figures 47 and 48 show the compaction of soil in control soil pads and shear box forms, respectively.

Figure 49 shows completed shear box forms containing compacted soil. The forms were elevated approximately 2.5 to 5 centimeters, such that failure surfaces potentially exhibit some thickness.

Piles were installed through the shear box forms approximately 1.5 meters into the existing ground (i.e. 2.1-m pile lengths). Boreholes were prepared with the Iowa State University Mobile B57 drill rig, used principally for relatively shallow soil sampling and site investigation. Figure 50 shows the preparation of boreholes. Smaller-diameter piles were prepared with a 114-mm-diameter auger. Larger-diameter piles were prepared using a hollow-stem auger with a 178-mm outside diameter. Exhumation of piles following the performance of pile load tests indicated that actual/measured pile diameters were of approximately the same dimension as auger diameters.

The developed grout mixture was prepared at the testing site and, upon completion of individual boreholes, bottom-fed into the cavity using a PVC casing. Estimated grout slump ranged from 20 cm to 24 cm, making vibration of the material unnecessary, as planned. Although bottom-feeding the grout mixture through PVC casing prevented segregation and ensured pile integrity and uniformity, the grout mixture was principally bottom-fed to avoid placement of grout through a variable water table. Figure 51 shows the placement of grout through the casing. The strength of grout was verified by performing compression tests on 76-mm-diameter test cylinders. The cylinders from each batch (one batch per pile) were field cured for two days following pile installation and subsequently stored in a humid room. The cylinders were tested on the same day the pile load test was performed. Compressive strengths at the time of pile load testing (approximately 2-3 weeks) ranged from 26.9 MPa to 34.1 MPa. The average compressive strength was 29.6 MPa with a standard deviation of 2.4

Mpa (42 tests). The compressive strengths were used to develop unique moment-curvature graphs for each pile and are provided in Appendix B.

Pile reinforcement (No. 19 bar for all piles) was incorporated into the grouted boreholes immediately following the satisfactory placement of grout. The reinforcement was centered in the borehole with spacers and orientated such that strain gauges were facing the tension-side of the piles. Figure 52 shows several shear box forms with compacted soil and steel-reinforced pile elements. The piles remained undisturbed for approximately two weeks following installation so that the concrete mixture developed adequate strength for loading.

(a)

(b)

Figure 44 – Clearing of Vegetation at SGES

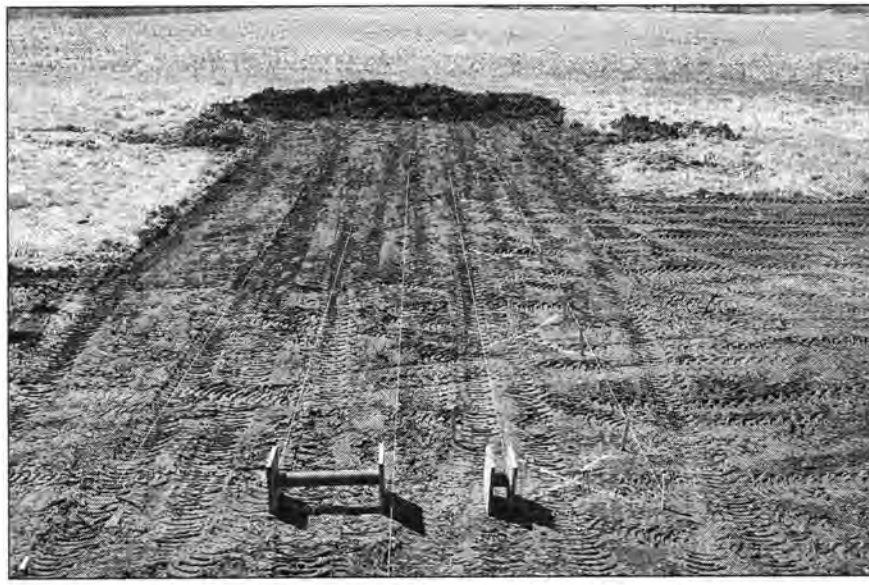

Figure 45 – Test Layout

(a)

(b)

Figure 46 – Excavation of Control Soil Pads

(a)

(b)

Figure 47 – Compaction of Soil in Control Soil Pads

(a)

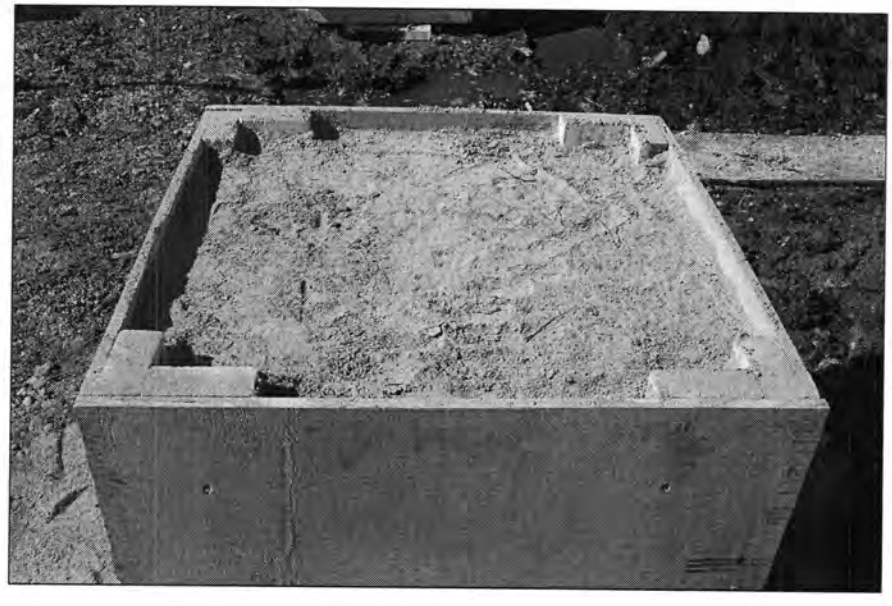

(b)

Figure 48 – Compaction of Soil in Shear Box Forms

Figure 49 – Prepared Soil Forms

(a)

(b)

Figure 50 – Preparation of Borehole

(a) **(b)**

Figure 51 – Placement of Grout through Casing

(a)

(b)

Figure 52 – Reinforced Soil in Forms

Load Test Performance

Large-scale direct shear tests were conducted on the composite system of soil and small-diameter pile elements. The research group measured the load-displacement behavior of shear boxes, the load-displacement behavior of pile heads, and the strain of pile reinforcement (subsequently converted to bending moment for comparison with predicted moment values). The following paragraphs detail the instrumentation that was used to measure loads and deflections, the equipment that was used to apply horizontal loads to the shear boxes, and the data acquisition system.

The displacement of each shear box was measured with three displacement gauges. Two gauges were mounted to the top of the box (left and right), and one gauge was mounted to the bottom of the box (middle). Use of three gauges to measure displacement provided the data set with redundancy and offered evidence of rotation (about vertical axis) and tilt (about horizontal axis) of the box with continued loading. The instrumentation was mounted on wood reference beams, which were attached to fence posts driven into existing ground outside the zone of influence of the test system. The arrangement for measuring displacements is shown in Figure 53.

Displacement gauges were additionally mounted to the section of reinforcement extending above the pile head. The distance between the two gauges was measured, such that the difference in displacement was used to calculate the pile head slope (i.e. rotation) at a given load. The pile head slopes were used to adjust the lower of the displacement gauges for more accurate pile head displacements (i.e. pile head displacement at the soil surface). The use of displacement gauges to measure pile head displacement and slope is shown in Figure 54.

Strain of the pile reinforcement was measured concurrent with load and displacement measurements. Strain gauges were installed on the reinforcement at pre-determined

elevations, based on moment profiles from preliminary analyses. A total of ten strain gauges were used to define the strain and moment profiles of piles during loading. The employed strain gauges were type FLA-3-11, gauge factor 2.13, manufactured by Tokyo Sokki Kenkyujo Co., Ltd. Each gauge level consisted of a single gauge on the tension-side of the reinforcement. The installation of strain gauges is shown in Figure 55.

The loading system of the large-scale direct shear tests included a load frame (pipe struts and steel plates); a pump-controlled, 12-in-stroke hydraulic cylinder; and a load cell. The capacity of the loading system, controlled by the load cell, was 50 kips. The loading system was placed between the shear boxes of a given test, and equivalent loads were simultaneously applied to each shear box by pressurizing the ram cylinder. The loading system is shown in Figure 56.

The electronic deflection measuring devices, the load cell, and strain gauges produce a voltage signal that was monitored through an analog-to-digital data acquisition system. The instrumentation was connected to individual terminal channels of the acquisition hardware, and the system software was programmed to record a measurement reading at 3-second intervals. The data acquisition system, mounted inside a cargo van for protection against inclement weather and transportation of the system around the site, is shown in Figure 57.

Figure 53 – Displacement Gauge Locations on Shear Boxes

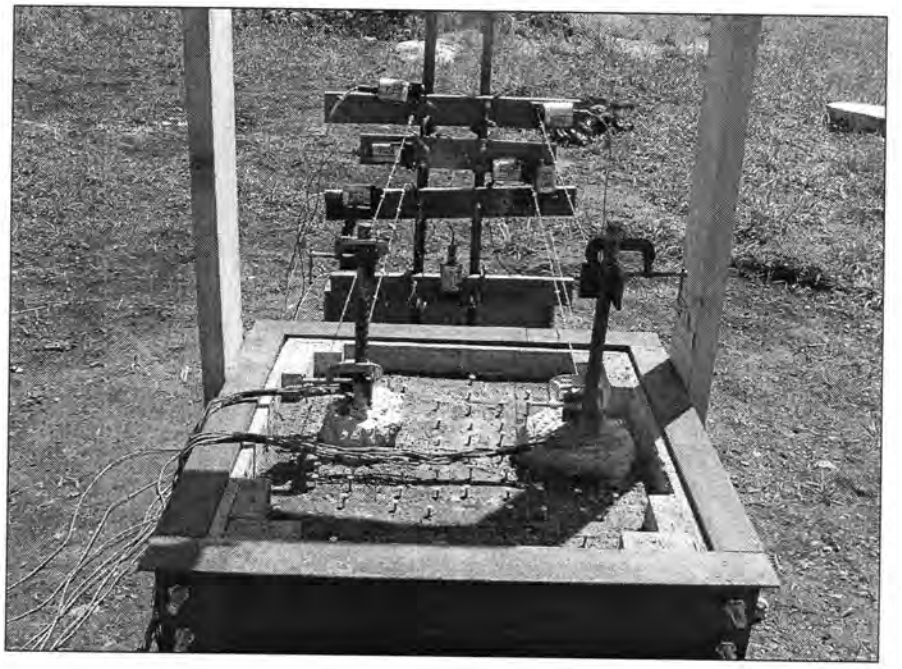

Figure 54 – Displacement Gauge Locations on Piles

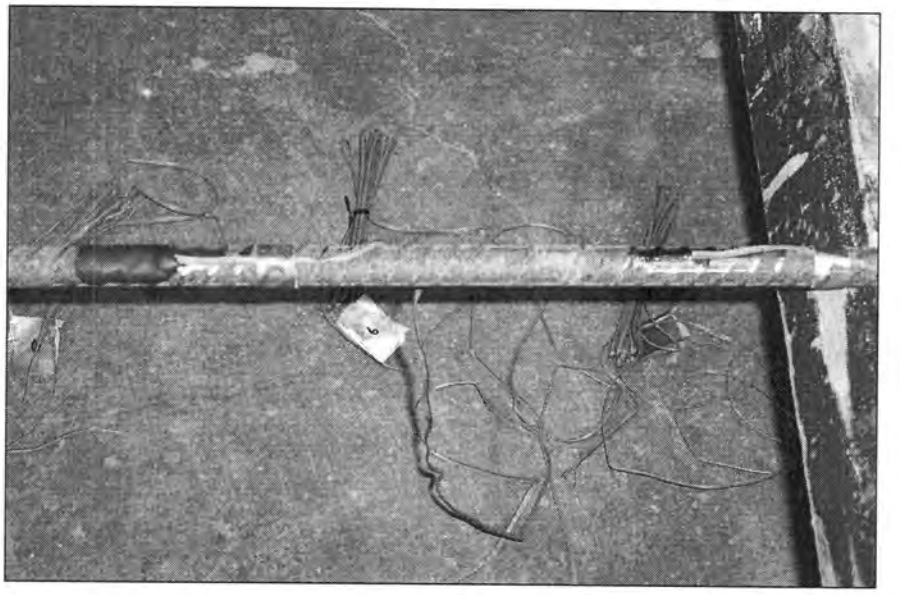

(a)

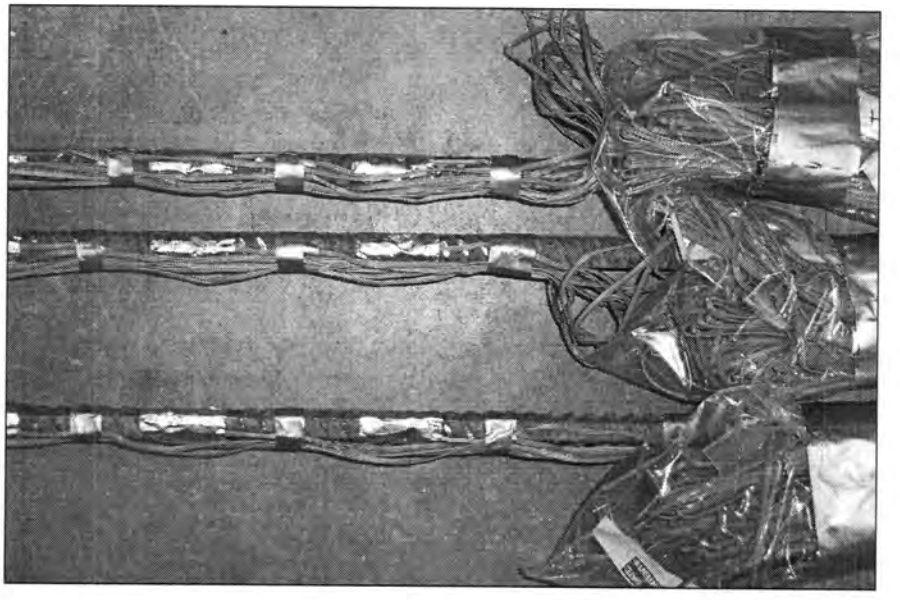

(b)

Figure 55 – Installation of Strain Gauges

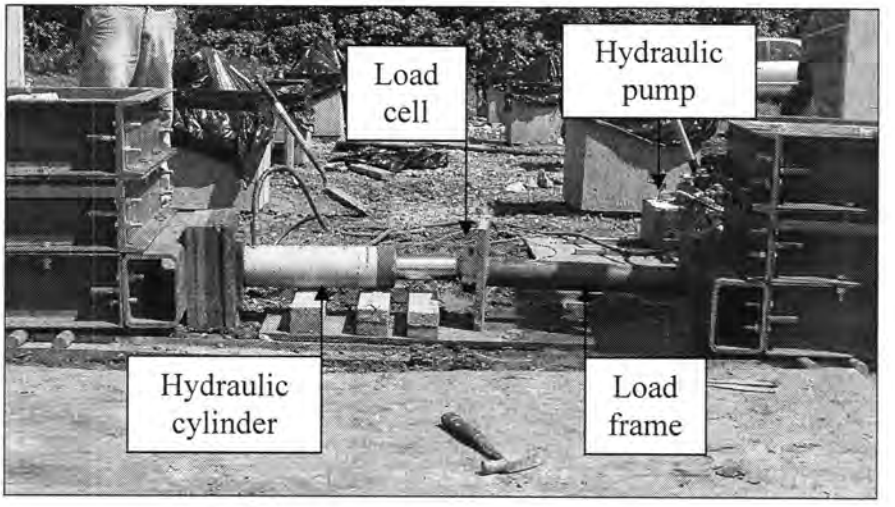

Figure 56 – Pile Load Test Loading System

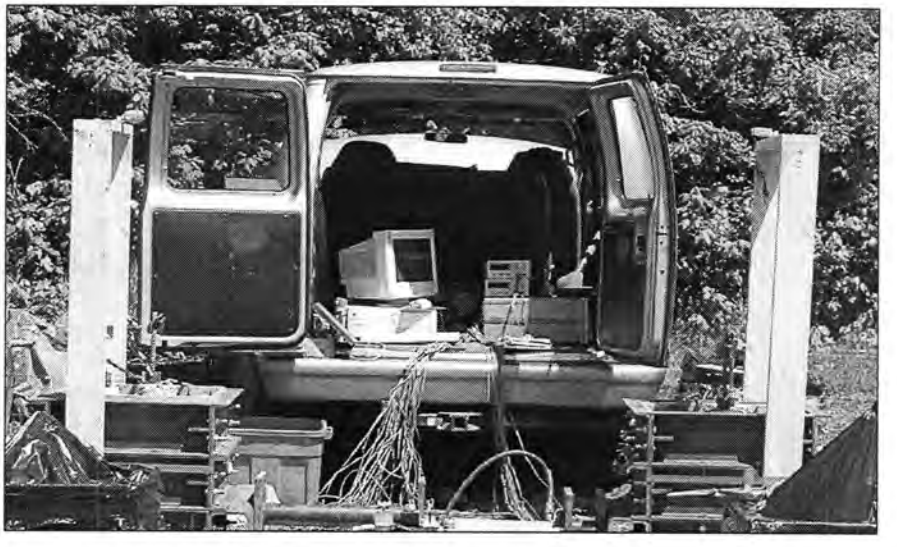

Figure 57 – Data Acquisition System

Pile load tests were performed by monitoring shear box displacements and controlling the load applied to each shear box. Generally, load increments of approximately 1 kN were applied to the system, and the research group monitored the displacements of each shear box at the relatively constant load. The next load increment was applied when the rate of displacement for each box became small. The research group believed that the loading process most accurately offered drained soil behavior, as opposed to undrained soil behavior, because excess pore pressure are more likely to dissipate at slower shearing rates. The test performance method resulted in loading times between 90 and 180 minutes. After a pile load test was completed, the shear boxes and loading system were disassembled and moved to the next test location.

The load-displacement data of Appendix C shows unload-reload cycles. As the shear boxes were pushed laterally, the loading system (e.g. hydraulic cylinder, load cell, load frame) became overextended and increasingly unstable. The applied load of the system was released and, upon adjustment of the loading system, reapplied.

Data Interpretation (Strain-Curvature-Moment Relationship)

Evaluation of pile response is generally completed by examining the deflection, shear, and moment of a pile. The research group wished to compare the moments of pile load tests to the moments predicted by LPILE for given loading conditions. The *strain* of pile reinforcement was measured during the pile load tests, and analysis of the test data required understanding of the relationship between strain and moment for each pile section.

Data interpretation (i.e. conversion of strain to moment) was achieved by evaluating the relation between the moment applied to the pile and the resulting curvature. For the full range of loading, from an unloaded condition to section failure, the relationship examines member ductility, development of plastic hinges, and redistribution of elastic moments that occur in reinforced concrete sections (Nilson 1997). LPILE analyses provide the moment-

curvature relationship, inclusive of pile stiffness and neutral axis positions, for pile sections with specified reinforcement and material properties. A conceptual plot of stiffness (EI) vs. moment is shown in Figure 58. The figure presents four stages of pile behavior for the range of possible loading conditions.

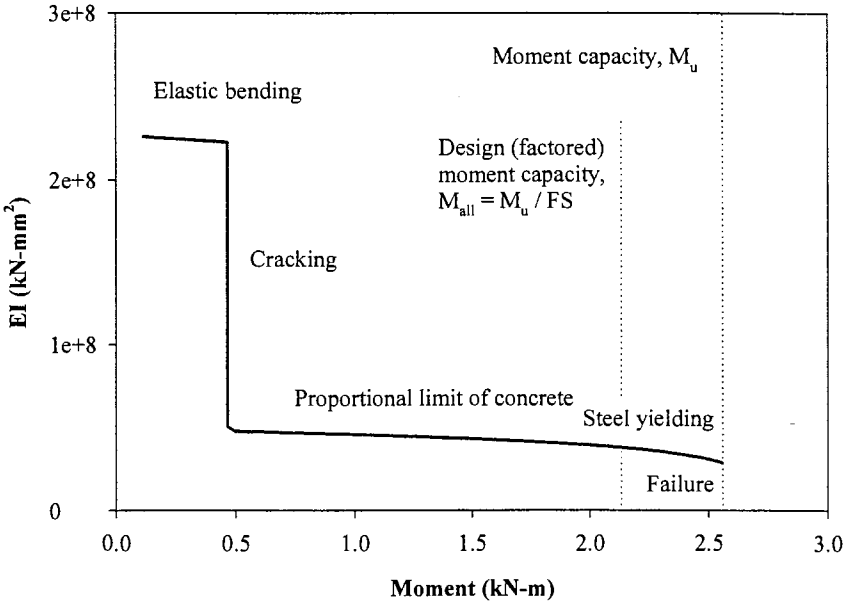

Figure 58 – Pile Stiffness-Moment Relationship

Strain profiles for uncracked and cracked pile sections are shown in Figure 59 to illustrate the relationship between the neutral axis position, curvature, and strain. Given curvature and "maximum" strain, the gauge strain (i.e. strain at tension side of reinforcement) is obtained with the following equation:

$$\varepsilon_{gage} = \varepsilon_{max} - \psi \left(\frac{d_p}{2} \pm \frac{d_b}{2}\right) \tag{24}$$

where ε_{gage} = gauge strain

ε_{max} = strain at top of section, as illustrated

ψ = curvature

d_p = pile diameter

d_b = reinforcement diameter

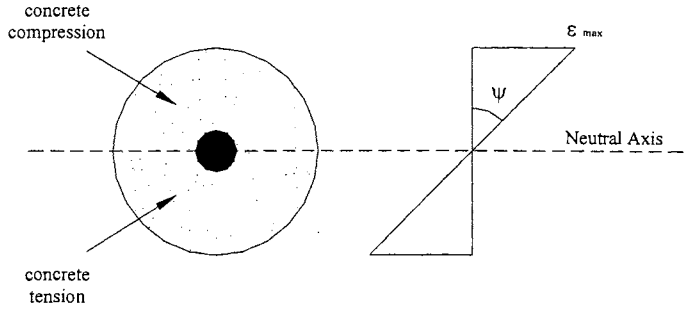

(a)

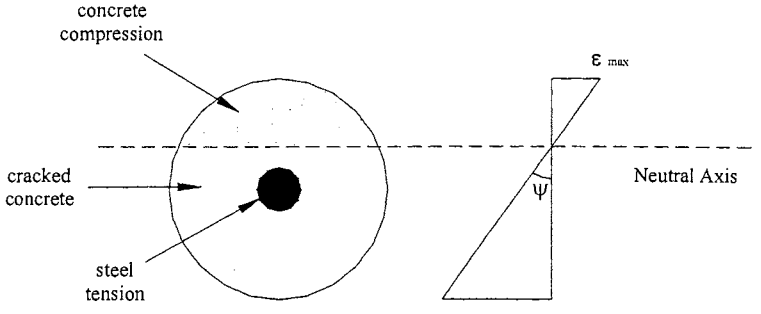

(b)

Figure 59 – Pile Sections with Strain Profiles
(a) uncracked section; (b) cracked section

Equation (24) facilitates the conversion of "maximum" strain and curvature, obtained from LPILE analyses, to gauge strain. A graph of stiffness and gauge strain vs. moment is shown in Figure 60 and is the means by which gauge strain is converted to moment for subsequent comparison with predicted pile response by LPILE. Graphs of pile stiffness and gauge strain vs. moment for specified pile sections and material properties are provided in Appendix B.

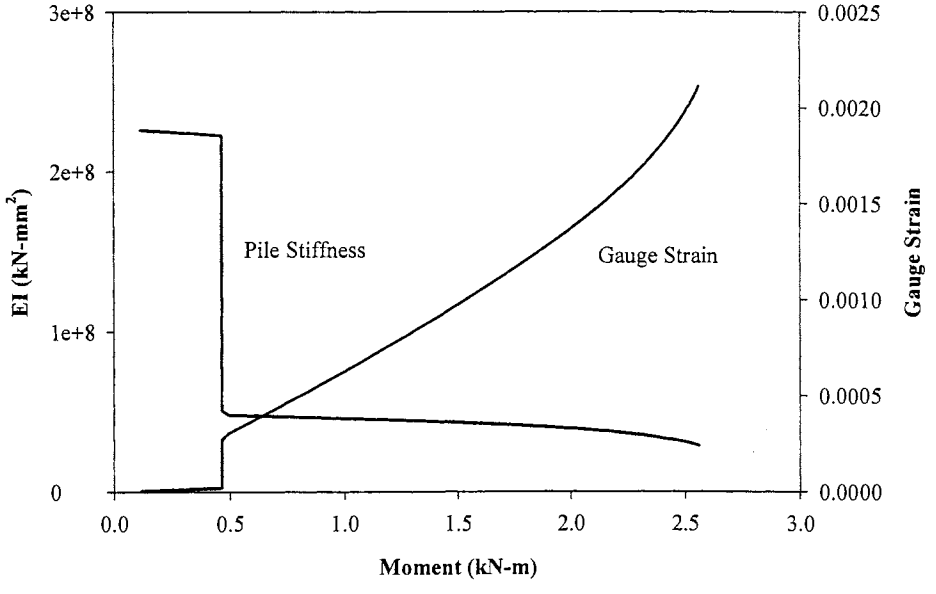

Figure 60 – Graph of Pile Stiffness and Gauge Strain vs. Moment

The conversion of measured strain values to bending moments is demonstrated in Table 16 and Figure 61. The strains of Table 16 are those measured in Pile 14 B upon application of 15.57 kN to the test shear box, and the moments are observed in the moment profiles of Figure 144.

Table 16 – Conversion of Measured Strain to Bending Moment (Pile 14 B)

	15.57 kN	
Depth (cm)	**μS ***	**M** (kN-m)**
13	4	0.108
25	37	0.463
38	114	0.463
51	115	0.463
64	410	0.675
76	1388	1.989
102	1814	2.292
152	6	0.137
178	0	0.008
203	-4	-0.095

Notes:
* μS is measured
** M is obtained from curves
M_{crack} = 0.463 kN-m
M_u = 2.357 kN-m

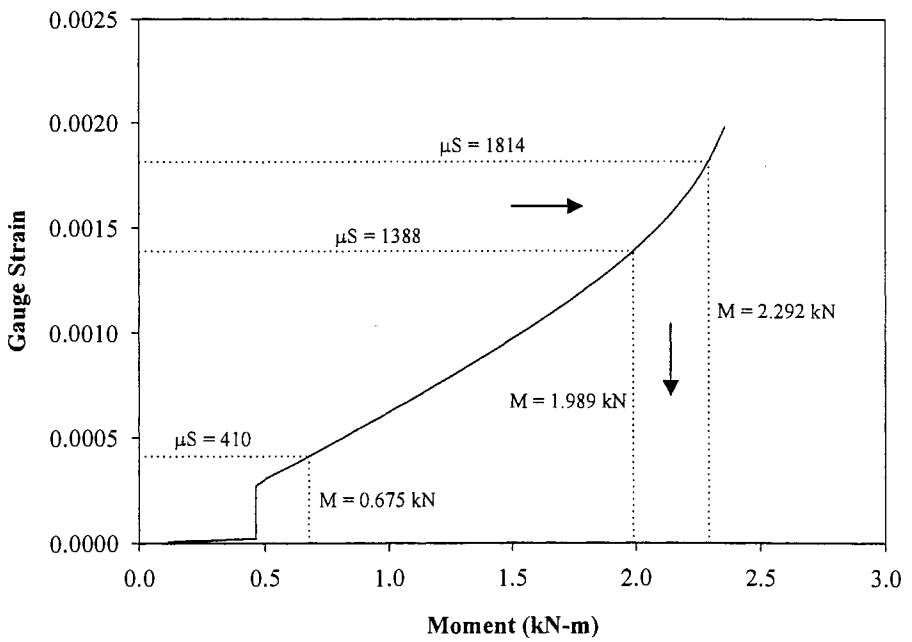

Figure 61 – Conversion of Measured Strain to Bending Moment (Pile 14 B)

The implications of the moment-curvature relationship include structural behavior of the piles subject to a range of loading conditions and the design of piles for lateral loading. The proposed design methodology, presented in Chapter 6, involves the design of piles that experience moment forces that exceed the moment required to crack the concrete on the tension side of the pile section. Further loading mobilizes tension in the steel reinforcement and additional compression in the concrete. Load is distributed to the steel and the concrete until the concrete fails in compression (i.e. concrete crushing). At this point, the load is carried solely by reinforcing steel. The section achieves moment capacity when the reinforcing steel yields, likely due to the development of a plastic hinge.

The design moment capacity (i.e. moment for which piles are subjected) of piles is a basic SDGM stabilization design input, and the design is highly dependent on the structural behavior of pile elements. The design of pile sections that remain uncracked is uneconomical and unnecessary. Rather, more efficient designs accept that concrete cracks under tension loads and target moment development in piles between concrete cracking and steel yielding. The prediction of structural behavior of piles is reliable, and the research group employed the actual moment capacity of the pile and a factor of safety equal to 1.2 for the design moment capacity (i.e. $M_{all} = M_u / 1.2$) (see Figure 58) and calculation of the stabilizing force of the pile.

CHAPTER 4

LOAD TEST RESULTS

INTRODUCTION

This chapter provides the results from load tests on piles subject to lateral soil movement. The material of the chapter facilitates the load test analysis and supports the discussion of results and design methodology of the ensuing chapters.

SHEAR BOX LOAD-DISPLACEMENT RELATIONSHIP

The measured load-displacement relationships of the shear boxes are provided in this section (Figures 62 through 76). The graphs of load vs. displacement for reinforced soil indicate the contribution of the pile to the shear strength of the system. The difference between the reinforced soil load and the unreinforced soil load, for a given shear box displacement, is the load applied to the pile. The values of total load applied to the pile are used for estimating the load distributions along the piles with increasing lateral translation of soil.

The first four figures (see Figures 62 through 65) provide the load-displacement (i.e. stress-strain) behavior of unreinforced soil. Loess, as evidenced by low dry density (14 kN/m^3), exhibited low strength compared to glacial till and weathered shale. Glacial till provided intermediate strength and initial modulus values. Weathered shale exhibited a stiff response to initial shearing and gave the highest peak strength of the three soils. Upon further shearing, the weathered shale exhibited a strain softening behavior and approached a residual strength comparable to the glacial till.

The 115-mm-diameter piles offered considerable resistance to lateral soil movement. Generally, the installation of the single piles resulted in peak loads of 215 to 325 percent of those for tests of unreinforced soil. The use of 178-mm-diameter piles offered additional resistance, beyond that achieved with the smaller pile elements. The installation of larger piles resulted in peak loads of 325 to 390 percent of those for tests of unreinforced soil.

The installation and loading of multiple piles offered some quantitative evidence of soil arching and increased capacity due to group effects. The research group matched the peak loads of multiple piles against peak loads of single piles. The use of grouped piles offered 19 to 105 percent increase in reinforcement capacity. Percent increases of approximately 100 percent indicate a potential influence due to group effects. The research group attributes the low peak loads to not fully mobilizing the pile moment capacities of multiple piles installed in glacial till and weathered shale, as supported by the moment data.

Table 17 provides the peak loads of each test and a comparison of the loads with other tests of the same soil. The presented improvement factors are ratios of peak loads for reinforced and unreinforced tests and tests of one and two piles.

Table 17 – Peak Loads and Improvement Factors

Box	Diameter (mm)	Soil Type	Peak Load (kN)	Improvement Factors	
				Reinforced / Unreinforced	2 Piles / 1 Pile
1	—	L	1.65	—	—
2	—	S	5.47	—	—
3	—	T	4.04	—	—
4*	114	L	5.34	3.24	—
5*	112	T	10.45	2.59	—
6*	117	S	11.70	2.14	—
7*	115	S	6.01	1.10	—
8*	183	L	6.41	3.88	—
9*	178	T	14.10	3.49	—
10**	113	S	13.96	2.55	1.19
11**	114	L	10.94	6.63	2.05
12*	173	S	17.79	3.25	—
13**	113	T	16.01	3.96	1.53
14**	115	T	16.28	4.03	1.56

Notes:
— not applicable
* single pile
** multiple piles
L = loess
T = glacial till
S = weathered shale

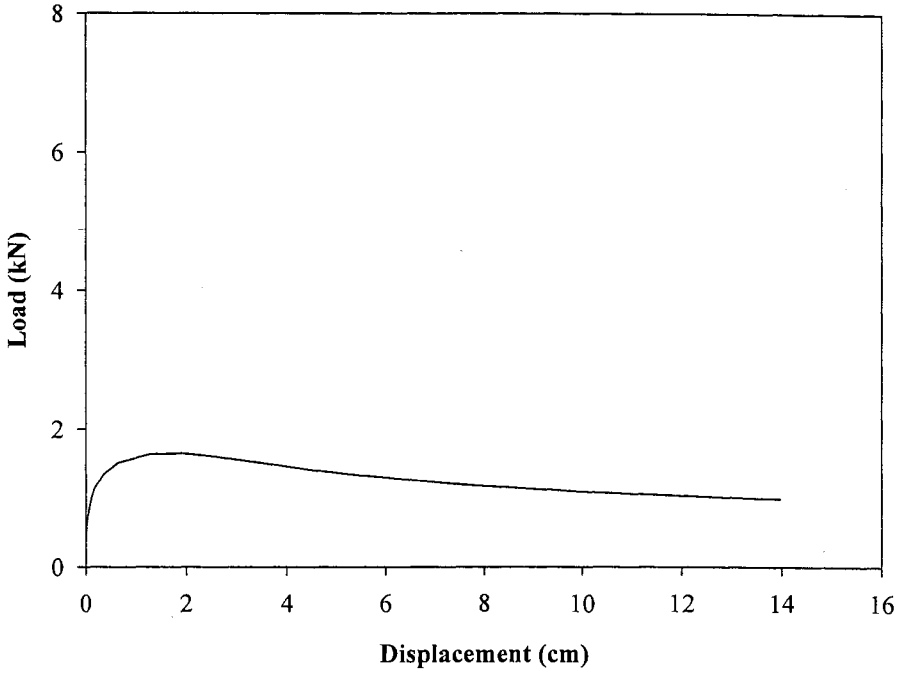

Figure 62 – Graph of Load vs. Displacement for Unreinforced Loess

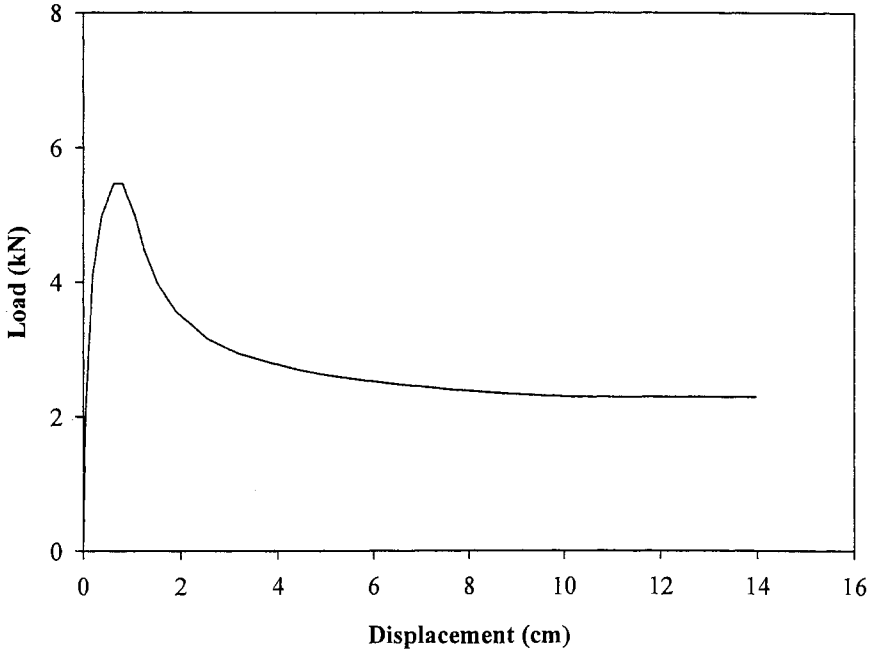

Figure 63 – Graph of Load vs. Displacement for Unreinforced Weathered Shale

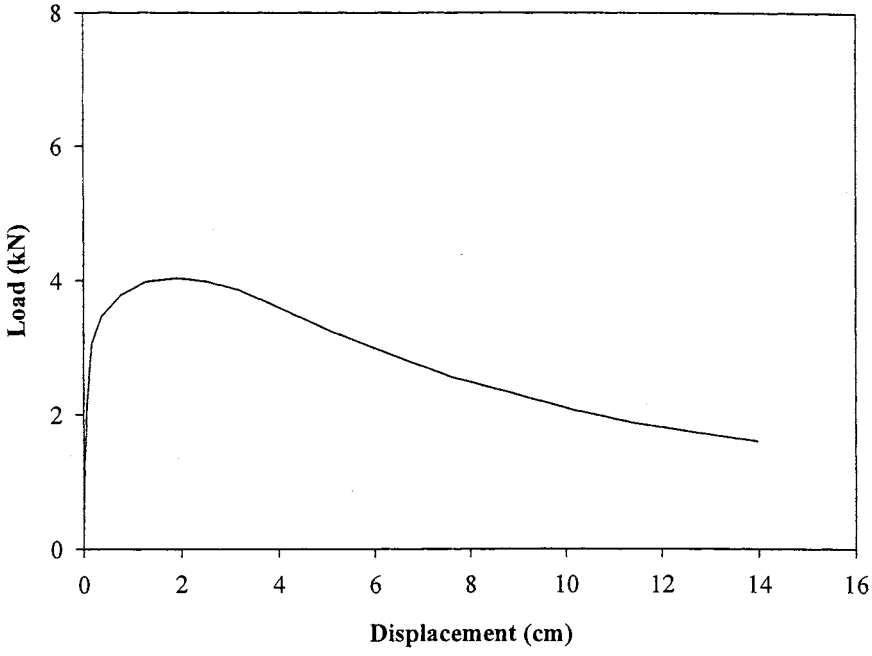

Figure 64 – Graph of Load vs. Displacement for Unreinforced Glacial Till

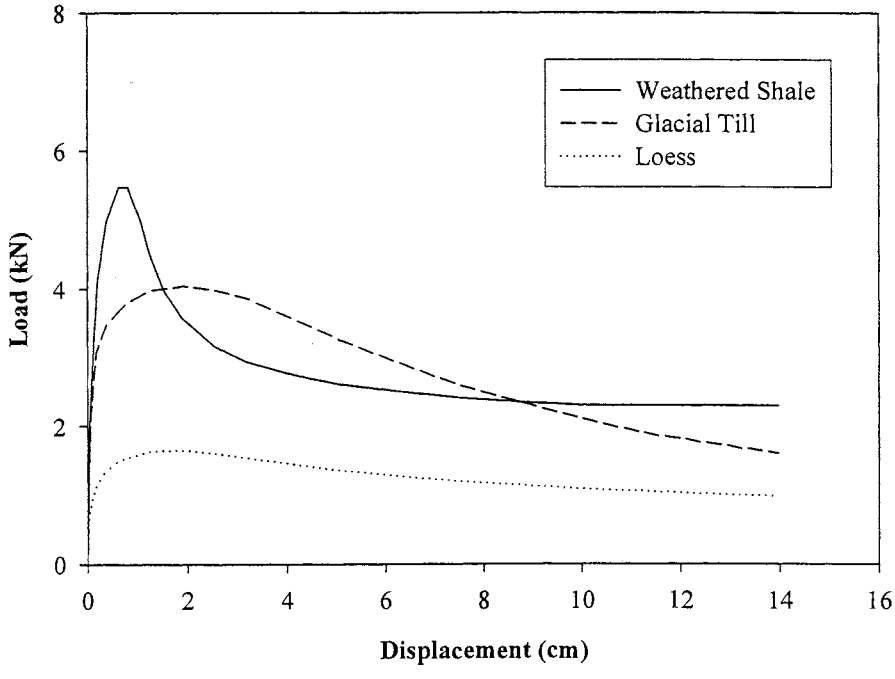

Figure 65 – Graph of Load vs. Displacement for Unreinforced Soils

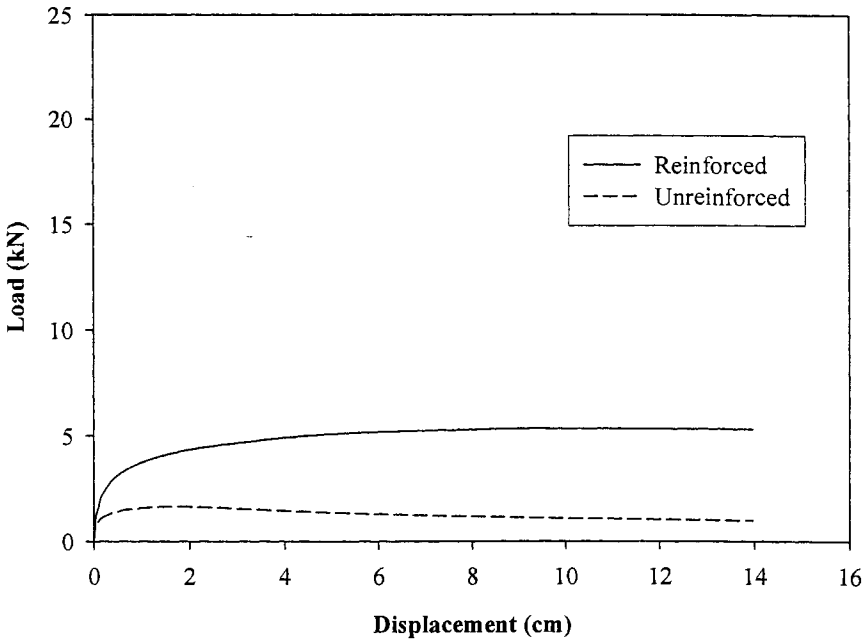

Figure 66 – Graph of Load vs. Displacement for Loess (Pile 4)

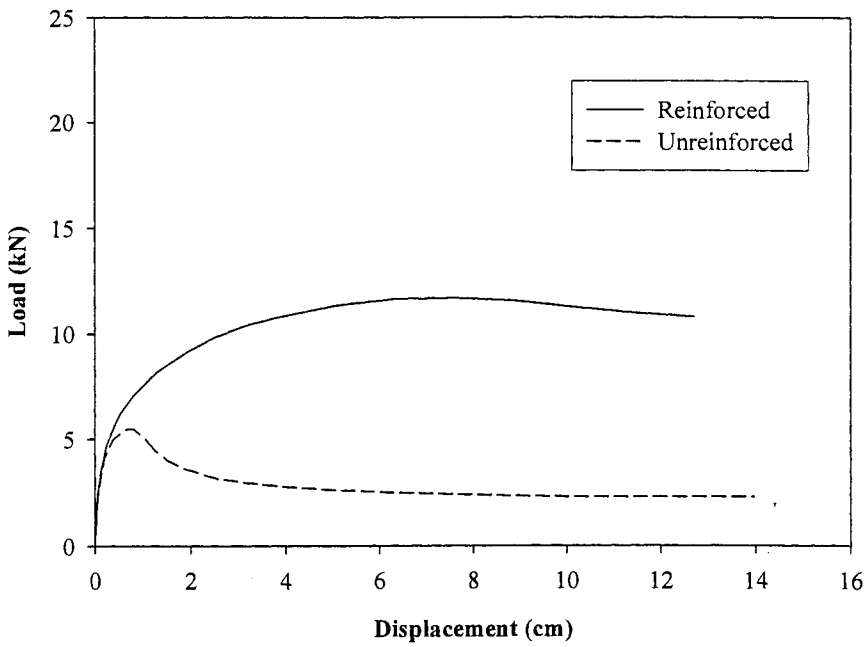

Figure 67 – Graph of Load vs. Displacement for Weathered Shale (Pile 6)

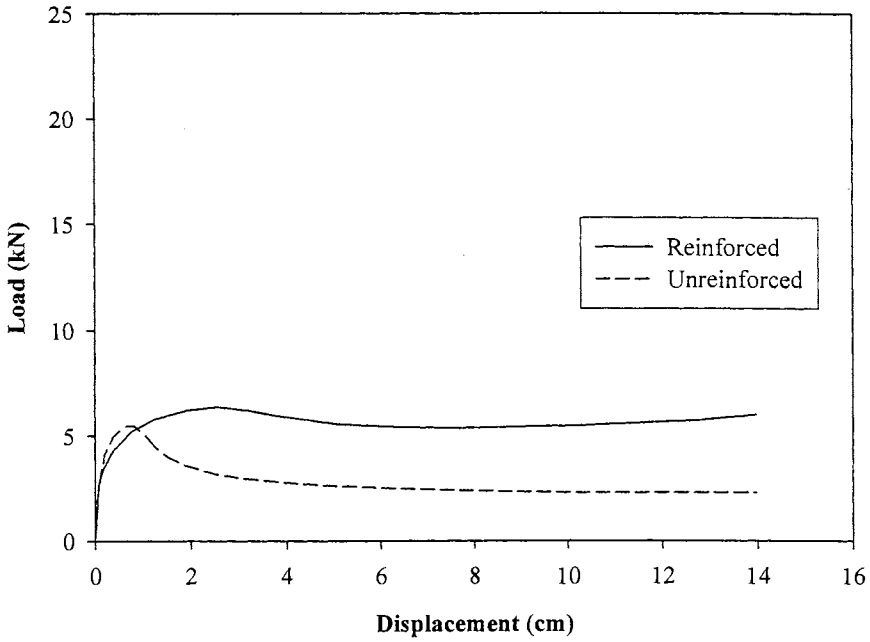

Figure 68 – Graph of Load vs. Displacement for Weathered Shale (Pile 7)

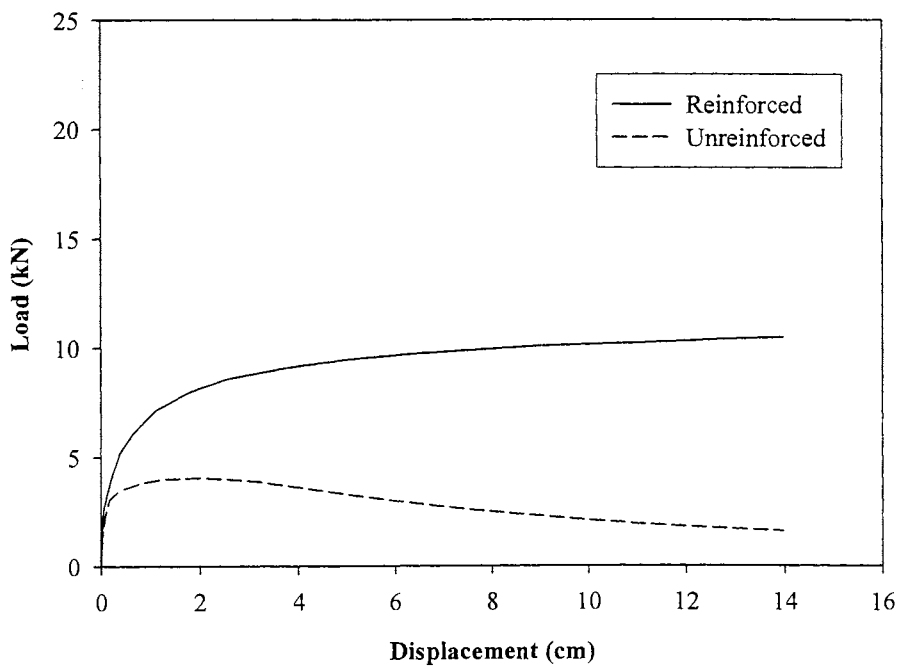

Figure 69 – Graph of Load vs. Displacement for Glacial Till (Pile 5)

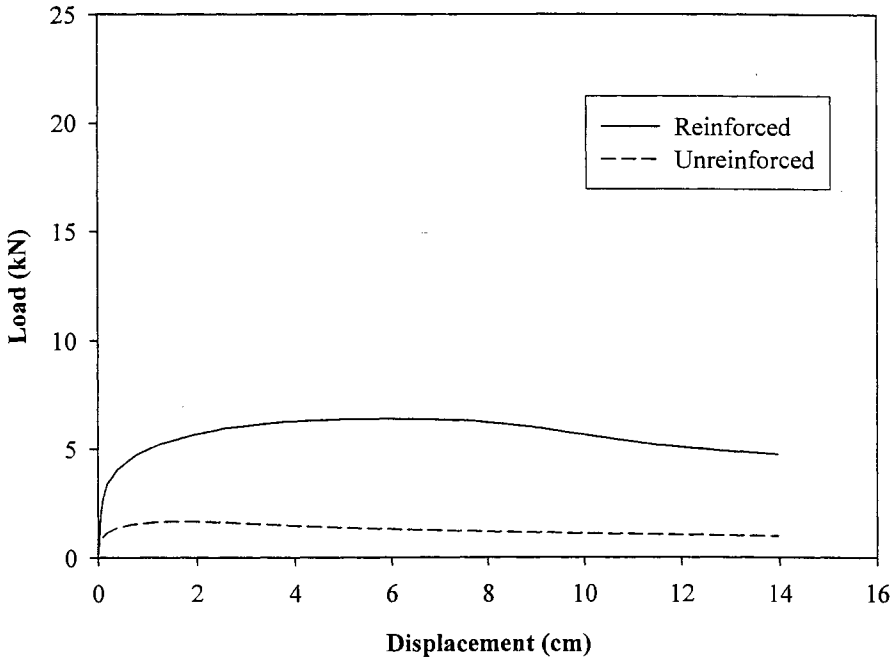

Figure 70 – Graph of Load vs. Displacement for Loess (Pile 8)

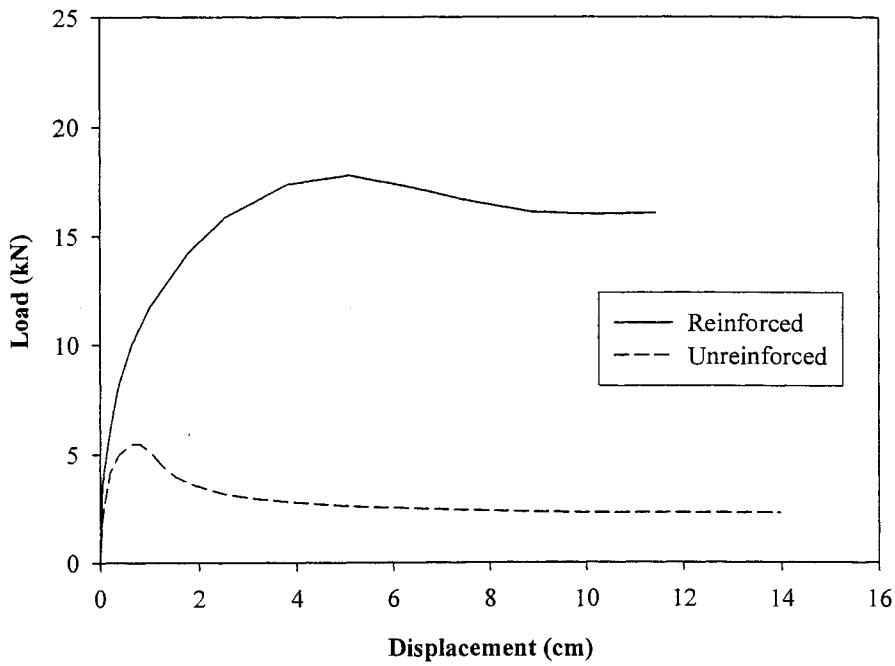

Figure 71- Graph of Load vs. Displacement for Weathered Shale (Pile 12)

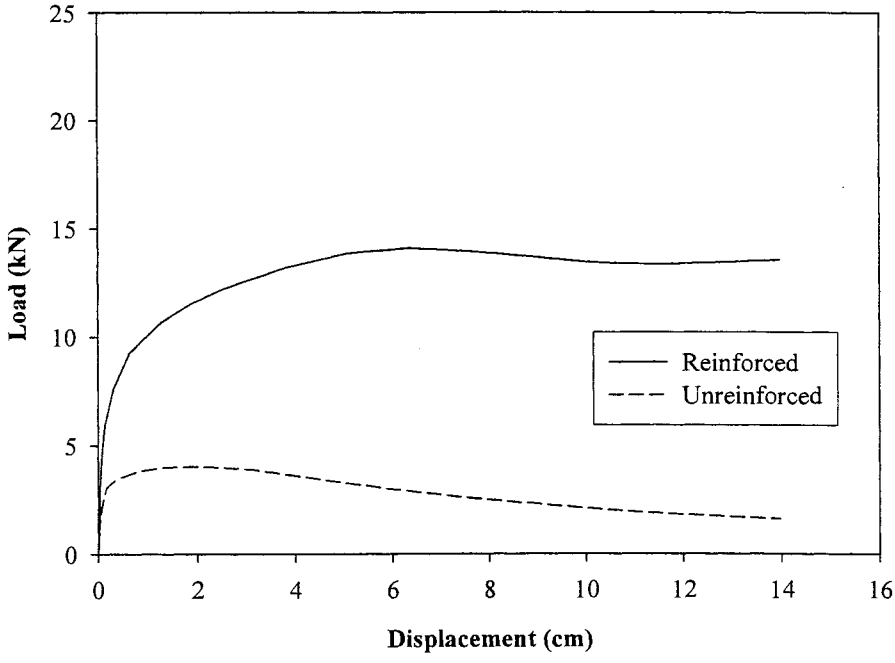

Figure 72 – Graph of Load vs. Displacement for Glacial Till (Pile 9)

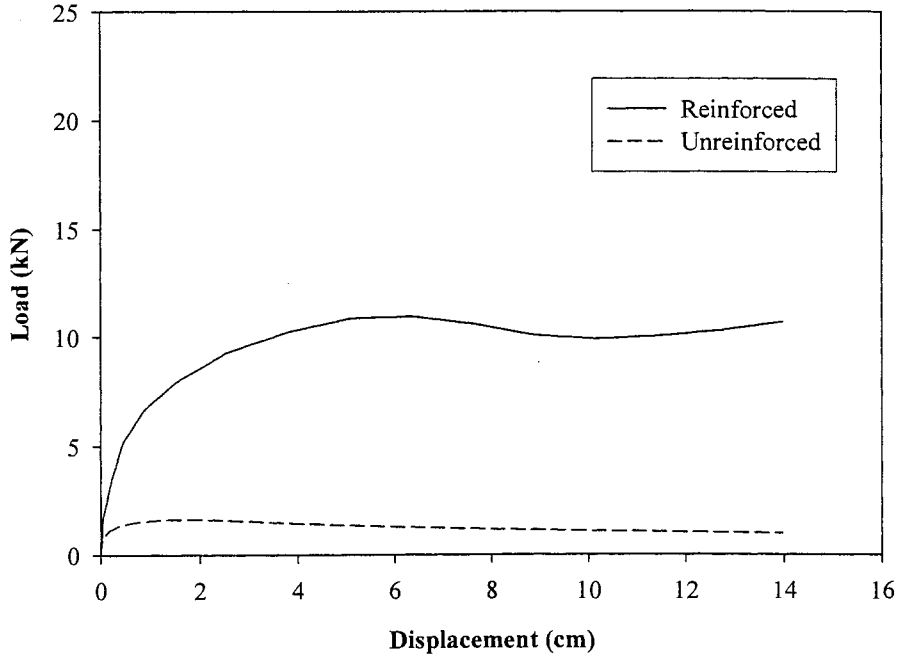

Figure 73 – Graph of Load vs. Displacement for Loess (Piles 11 A and B)

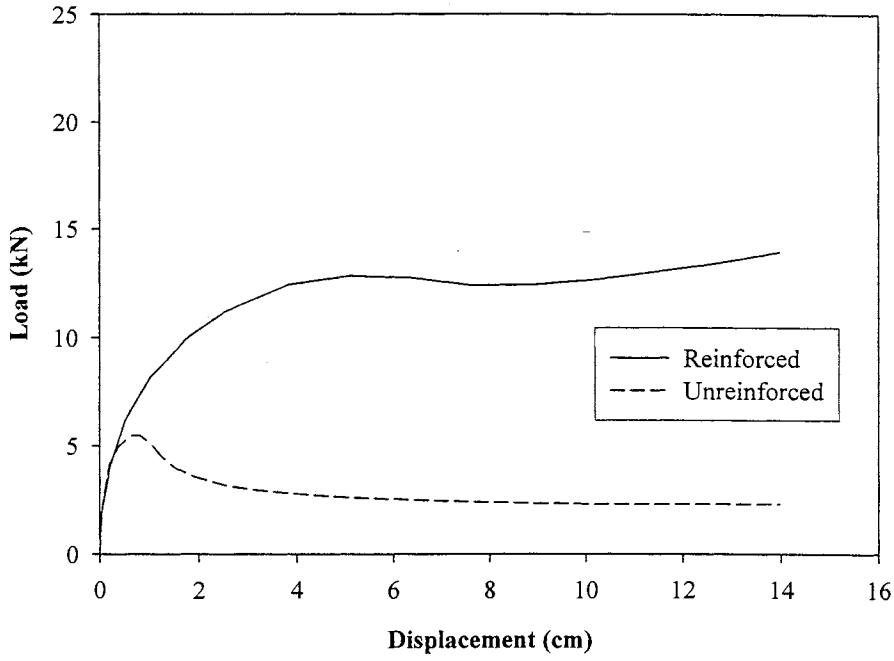

Figure 74 – Graph of Load vs. Displacement for Weathered Shale (Piles 12 A and B)

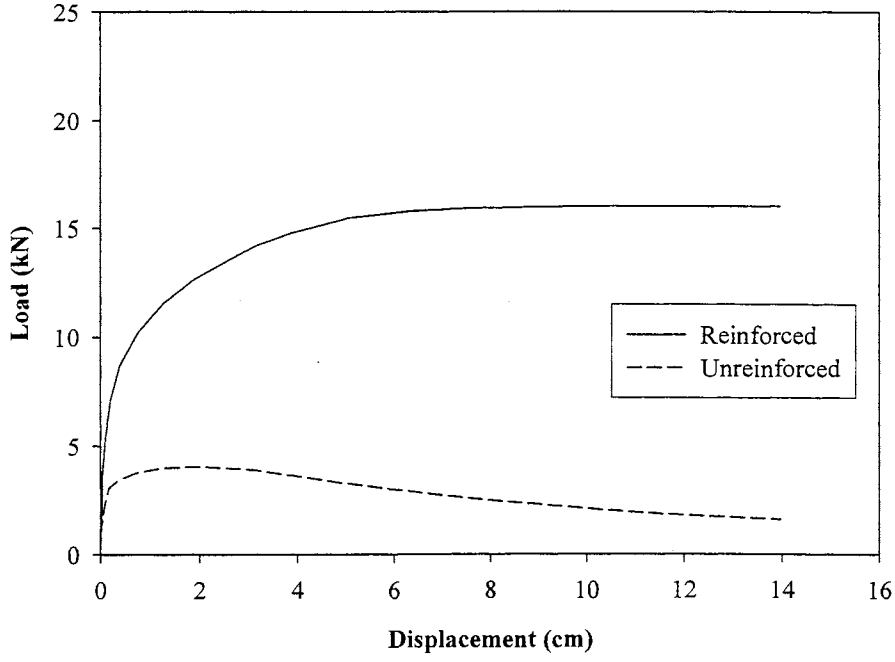

Figure 75 – Graph of Load vs. Displacement for Glacial Till (Piles 13 A and B)

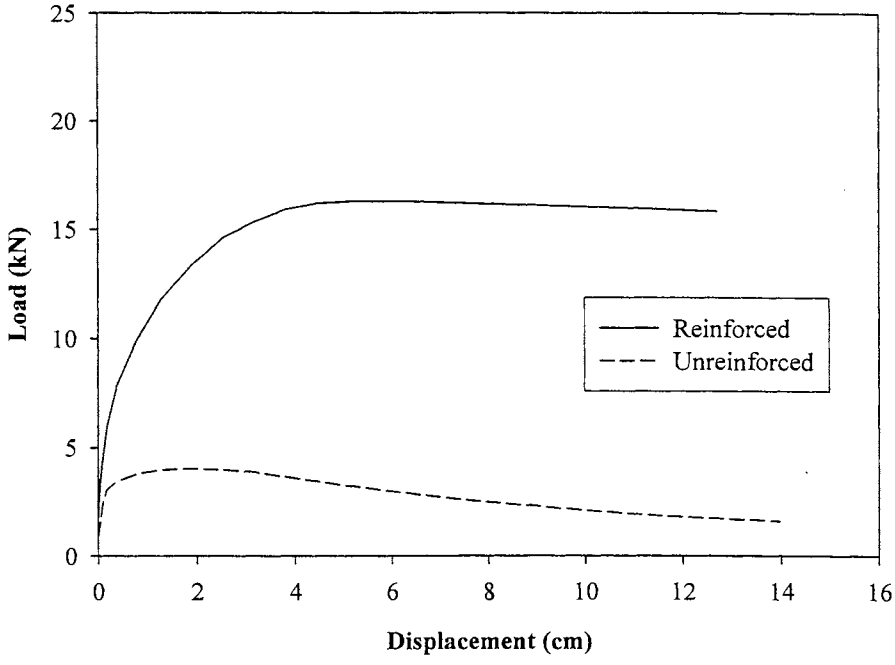

Figure 76 – Graph of Load vs. Displacement for Glacial Till (Piles 14 A and B)

PILE HEAD LOAD-DISPLACMENT RELATIONSHIP

The measured pile head load-deflection relationships are provided in this section. The loads refer to the load applied to the shear box, and the pile head deflection is the displacement measured at the lower-most transducer attached to the pile (i.e. Δx_2 in Figure 77). The pile head deflections of Figures 78 through 87 are *uncorrected* for deflection at the soil surface. Nevertheless, the figures illustrate the pile head load-displacement relationship, where the original data exhibited some scatter and was represented with smoothed curves. Moreover, the lower-most transducers were attached to the piles close to the soil surface, and piles experienced relatively small pile head rotations at pre-peak loads. Consequently, the corrected pile head deflections do not differ considerably from those presented. Based on pile head slope, corrected pile head deflections are adjusted for the pile deflection at the soil surface and used in the analyses of laterally load piles. The calculation of pile head slope and corrected pile head deflection are performed with the following equations:

$$\text{P.H. Slope} = \frac{\Delta x_1 - \Delta x_2}{L} \tag{25}$$

$$\text{P.H. Deflection (corrected)} = \Delta x_2 - \frac{L'}{L}(\Delta x_1 - \Delta x_2) \tag{26}$$

Figure 78 through 87 show the nonlinear pile head load-displacement relationship. The load-displacement curves generally follow those of reinforced soil, as previously presented. The pile head deflections of tests with multiple piles (Figures 84 through 87) are illustrated with a single plot. Within the range of data scatter, the two piles experienced similar pile head deflections. Thus, a single curve was developed to adequately represent the pile head behavior of both piles.

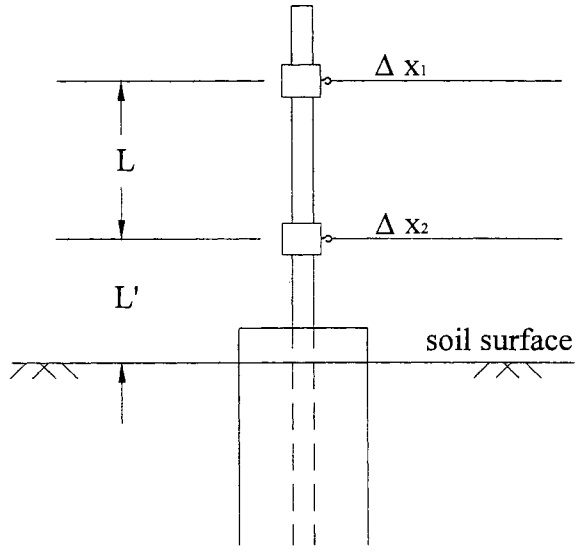

Figure 77 – Measurement and Correction for Pile Head Deflection

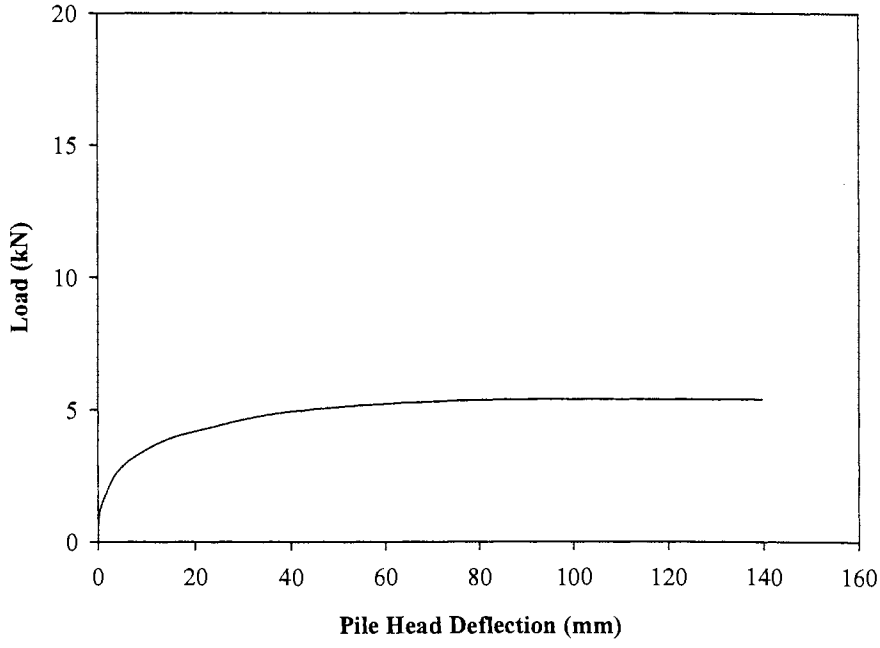

Figure 78 – Pile Head Load-Deflection for Loess (Pile 4)

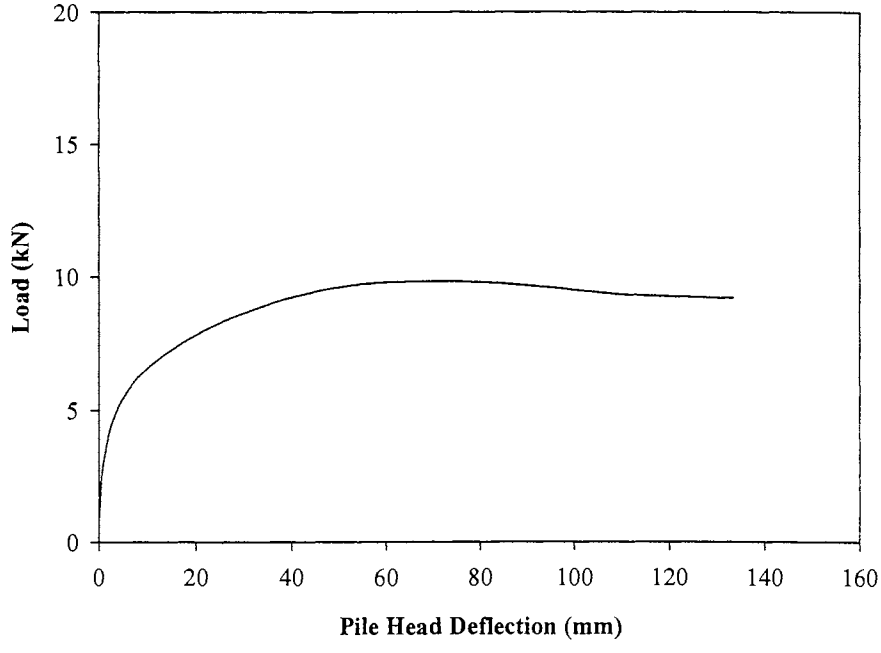

Figure 79 – Pile Head Load-Deflection for Glacial Till (Pile 5)

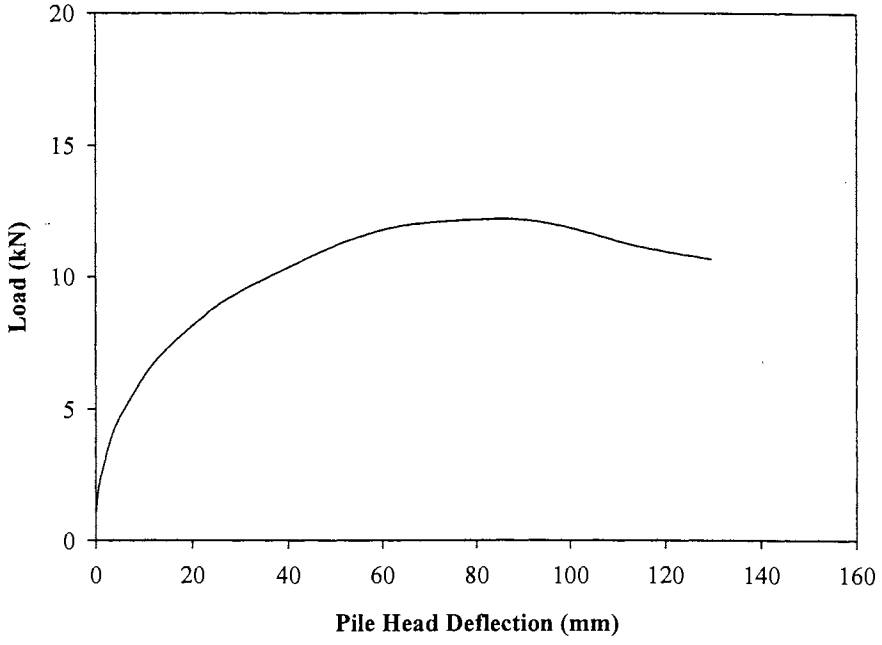

Figure 80 – Pile Head Load-Deflection for Weathered Shale (Pile 6)

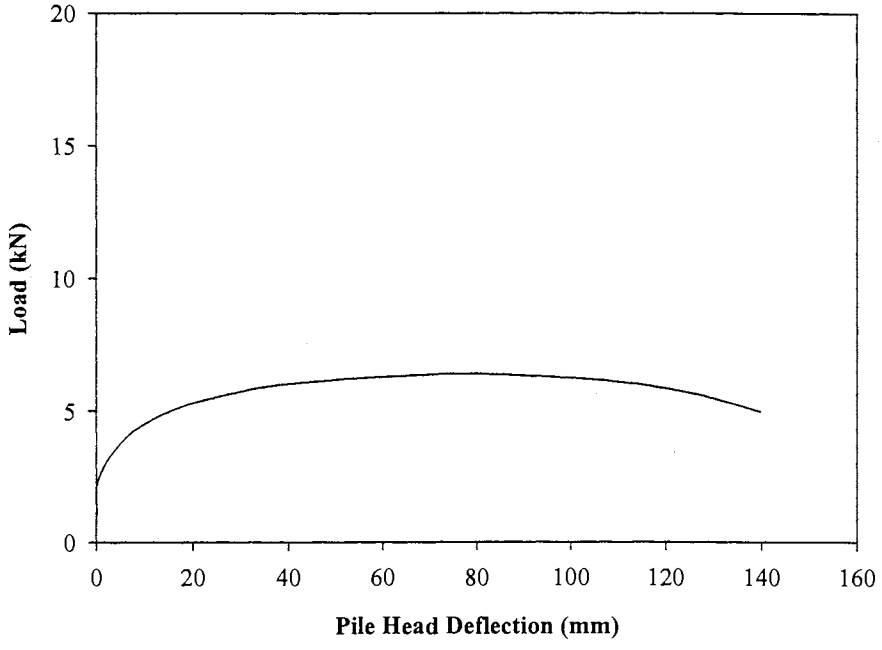

Figure 81 – Pile Head Load-Deflection for Loess (Pile 8)

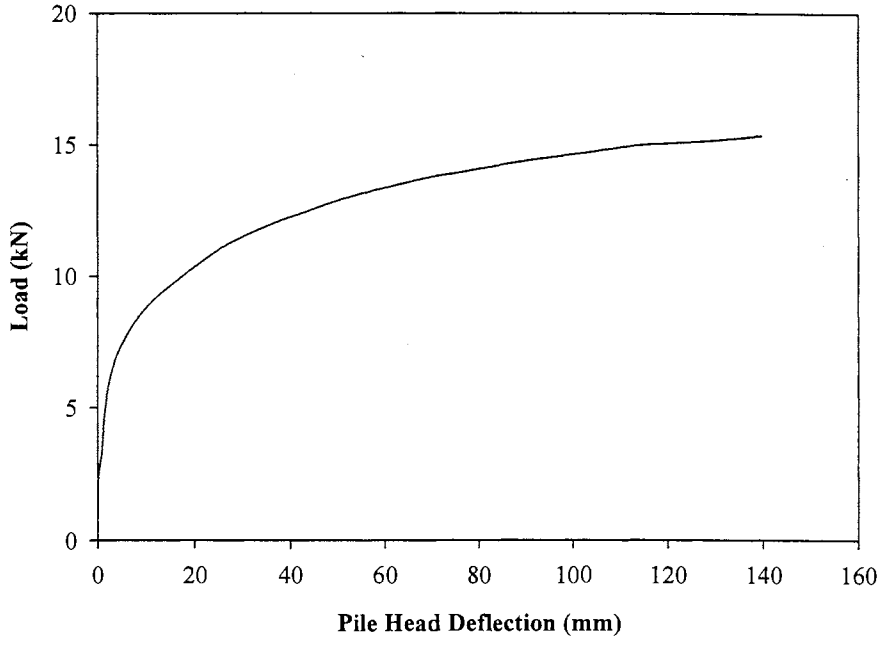

Figure 82 – Pile Head Load-Deflection for Glacial Till (Pile 9)

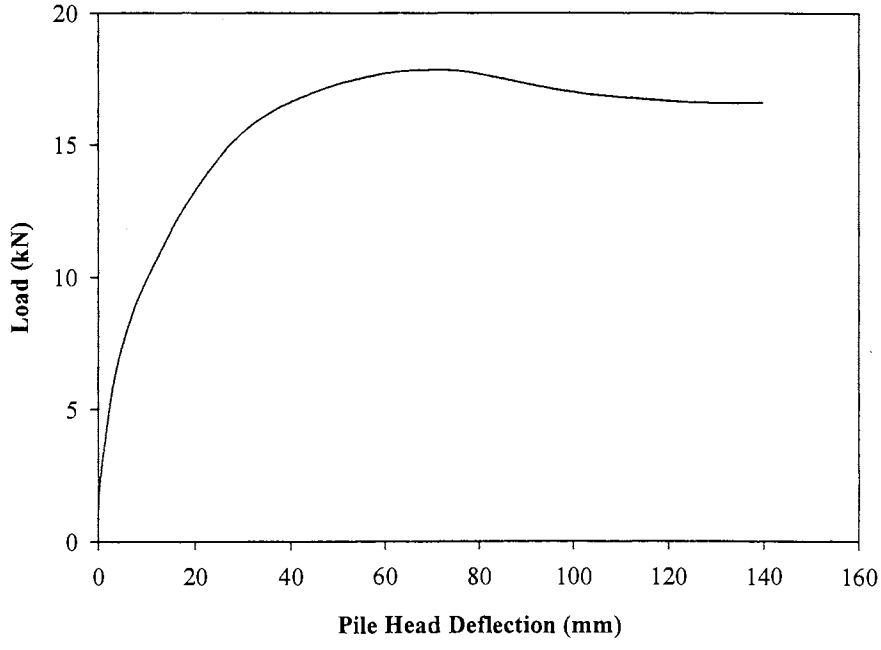

Figure 83 – Pile Head Load-Deflection for Weathered Shale (Pile 12)

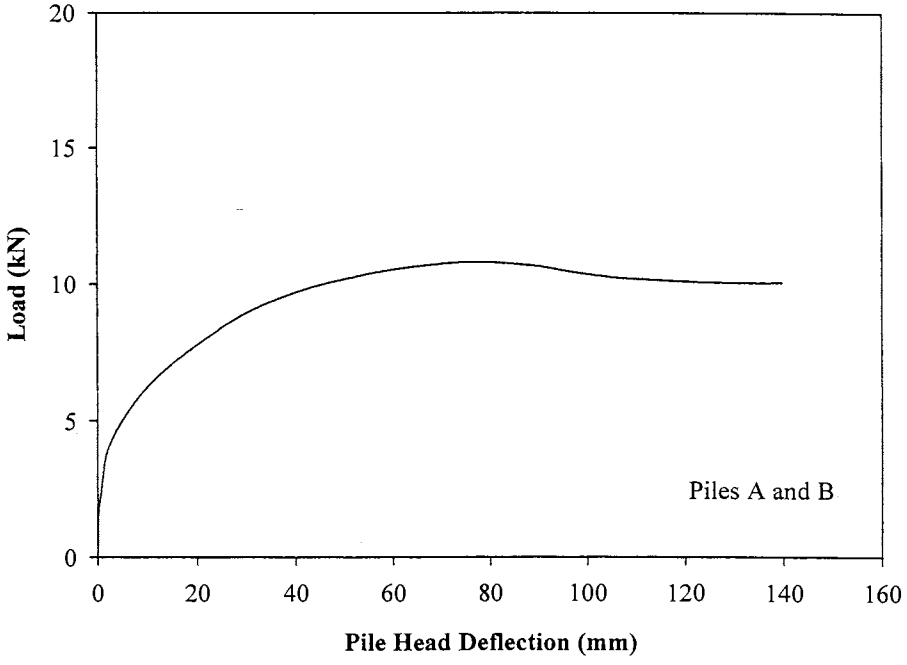

Figure 84 – Pile Head Load-Deflection for Loess (Piles11 A and B)

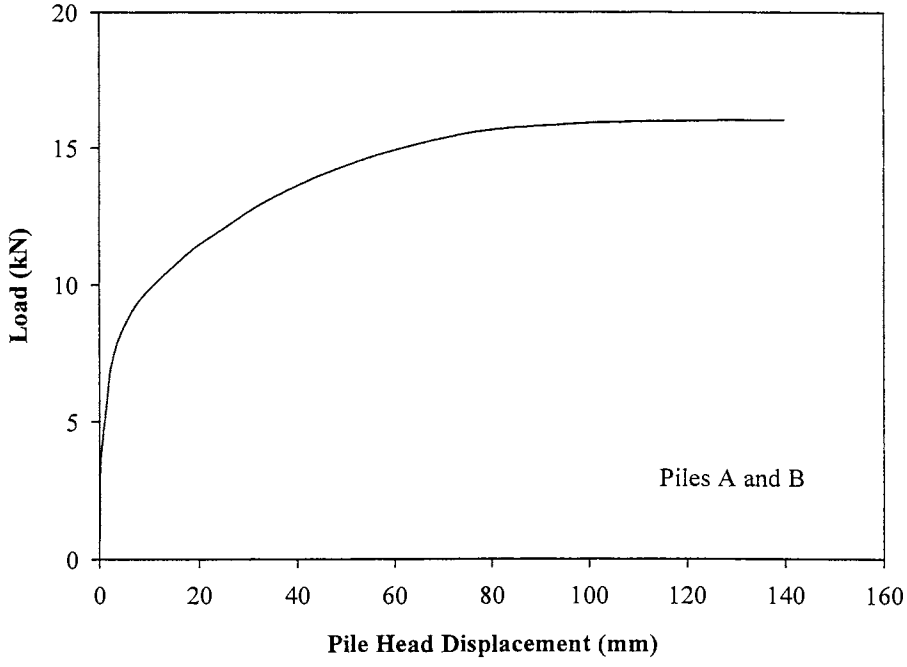

Figure 85 – Pile Head Load-Deflection for Glacial Till (Piles 13 A and B)

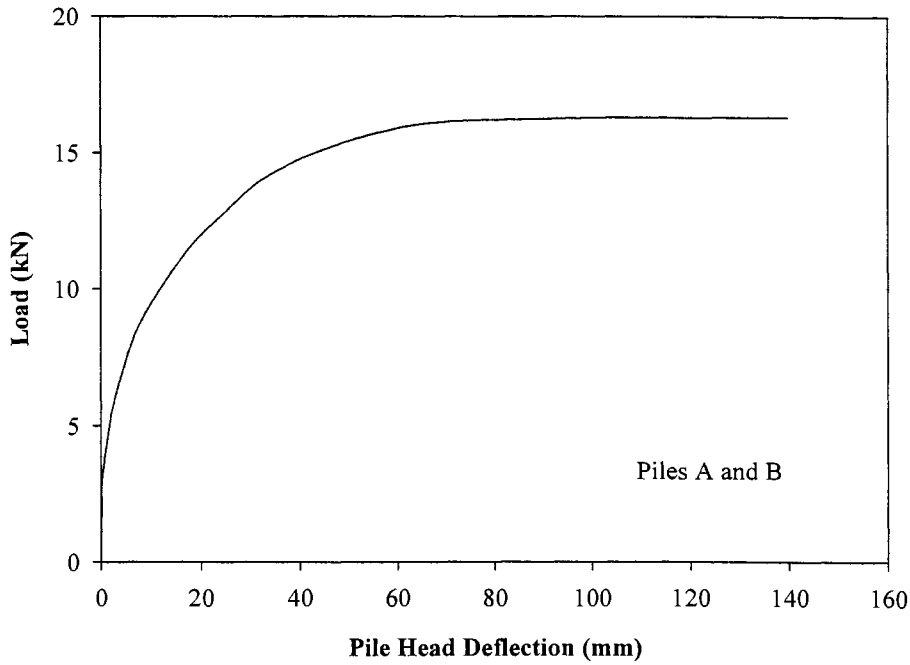

Figure 86 – Pile Head Load-Deflection for Glacial Till (Piles 14 A and B)

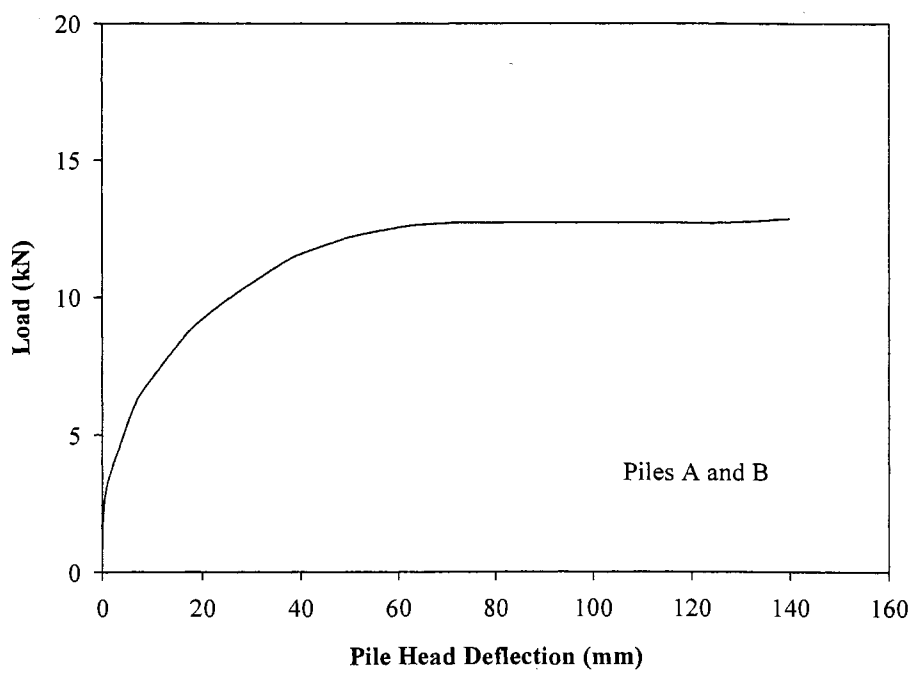

Figure 87 – Pile Head Load-Deflection for Weathered Shale (Piles 10 A and B)

RELATIVE DISPLACEMENT OF SHEAR BOX AND PILE HEAD

The relative displacement of the shear boxes and pile heads are provided in this section. The figures are used to support the observed pile behavior during the performance of the load tests. The research group witnessed the formation of a gap at the front (i.e. load-side) of the pile. The gap formed because the displacement of the pile head, due to rotation of the pile, exceeded the displacement of the surface soil. The development of a gap potentially complicated the load test analyses, because the load distribution along the piles was directly affected by the exposed – and therefore, unloaded – length of pile (see Figure 88). The following discussion on the behavioral stages of pile loading suggests that the gap formation is not an issue for estimating load distributions developed along piles. The research group conducted an analysis on the sensitivity of behavior of piles subject to alternative loading conditions (i.e. distributions) to satisfy residual concerns regarding the effect of small gaps on pile behavior prediction. Pile head deflections and maximum moments are not sensitive to small changes in gap widths (see Chapter 5).

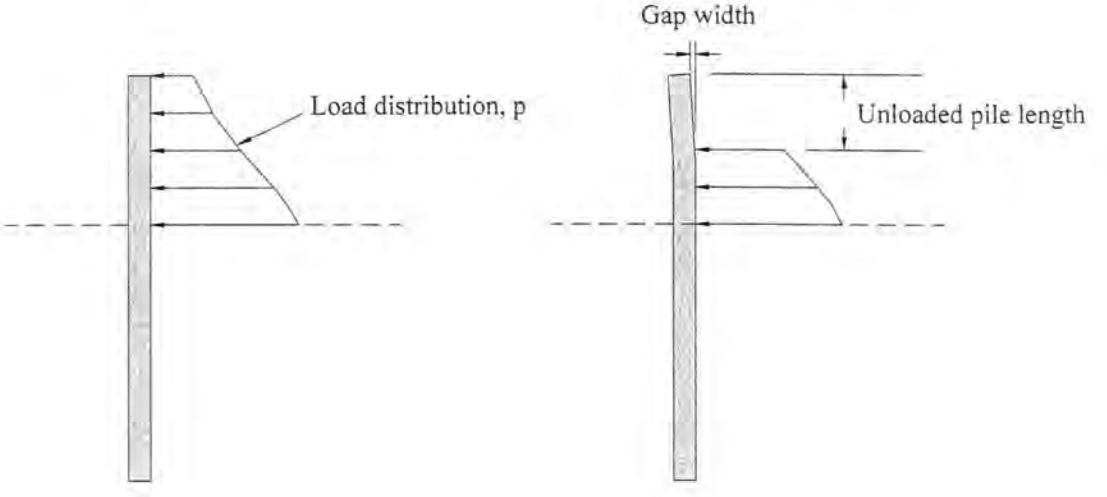

Figure 88 – Effect of Gap Formation on Estimations of Pile Load Distributions

The figures relating gap width (corrected pile head δ – shear box δ), load, and shear box displacement indicate the behavioral stages of piles subject to lateral soil movement and offer evidence for the mobilization of pile moment capacity. Figure 89 illustrates the behavioral stages, as follows:

- Stage 1 – elastic compression of soil and elastic bending of pile
- Stage 2 – mobilization of soil shear stresses and pile flexural stiffness
- Stage 3 – incipient failure due to mobilization of pile moment capacity

Stage 1 is characterized by relatively linear behavior of the soil and the intact pile element. The stress development at the soil-pile interface is insufficient to cause yielding of soil or cracking of the pile, such that a gap of negligible width forms. Stage 2 commences with the development of a bending moment in the pile element that causes the tension-carrying concrete to crack. The pile stiffness immediately drops, and the pile element becomes more flexible. Further loading of the pile causes more rapid pile rotation and pile head deflection. Coincidentally, the gap formation occurs more rapidly. Stage 3 commences with the mobilization of the pile moment capacity. The effect of mobilizing the moment capacity of the pile is similar to that associated with the pile cracking of Stage 2. The principal difference between the stages, however, is that the pile rotation which occurs during Stage 3 occurs under constant load. The failed pile element is incapable of carrying additional load. Gaps of significant width form with the mobilization of pile moment capacity and development of a plastic hinge.

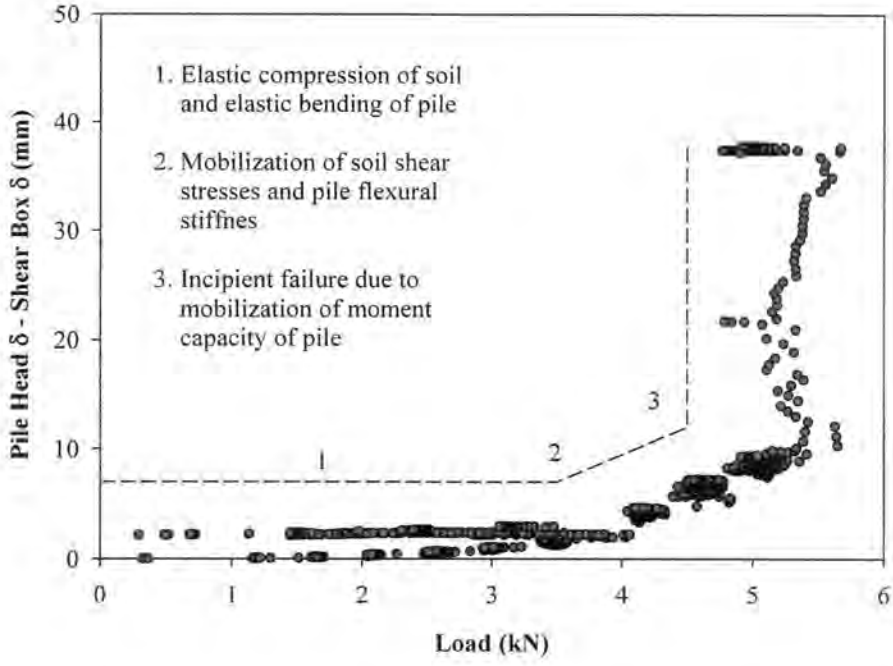

Figure 89 – Behavioral Stages of Piles Subject to Soil Movement (Pile 4)

Figure 90 supports the behavioral stages of piles subject to lateral soil movement and offers additional evidence for the mobilization of pile moment capacities. The data of the figures is concentrated at shear box displacements associated with pre-peak loads. Moreover, the gap widths formed during pre-peak loads remain small. The gap width becomes significant at peak loads, suggesting that the gap formation is caused by pile rotation due to *failure of the pile* during Stage 3. Prediction of pile behavior (e.g. pile head deflection and moment profiles) is performed only for pre-peak loads; and, for this reason, the gap formation *does not* complicate the load test analysis.

Figure 91 provides an alternative approach for supporting the behavioral stages of piles subject to lateral soil movement. The gap width, when plotted against shear box displacement, takes on a bilinear relationship. Interestingly, the data follows Slope I (see Figure 91) for shear box displacements corresponding to pre-peak loads (Stages 1 and 2). Upon mobilization of the pile moment capacity, however, the data follows Slope II for shear

box displacement corresponding to the peak load (Stage 3). In each case of the bilinear rate of gap formation, Slope II is greater than Slope I. The difference in slopes indicates that the gap forms more quickly following mobilization of the pile moment capacity during Stage 3 loading.

Figures 92 through 111 provide the relationship between gap width, load, and shear box displacement for each of the pile load tests. Table 18 provides the loads and slopes of the behavioral stages of loading for each pile load test.

Table 18 – Loads and Slopes of Behavioral Stages of Loading

	Load (kN)			Slope (mm/mm)	
Pile	**Stage 2**	**Stage 3**	**Peak****	**Slope I**	**Slope II**
4	3.8	5.3	5.34	0.18	0.36
5	6.3	10.0	10.45	0.12	*—
6	7.8	10.9	11.70	0.10	0.16
8	5.3	6.3	6.41	0.05	0.11
9	10.0	13.9	14.10	0.12	*—
10	9.7	12.8	13.96	0.12 / 0.21	*—
11	8.0	10.6	10.94	0.11	0.34
12	13.8	16.9	17.79	0.10	*—
13	10.9	15.9	16.01	0.13 / 0.16	*—
14	12.5	16.3	16.28	0.11	*—

Notes:
** peak loads from Table 17
*— bilinear rate of gap formation not apparent

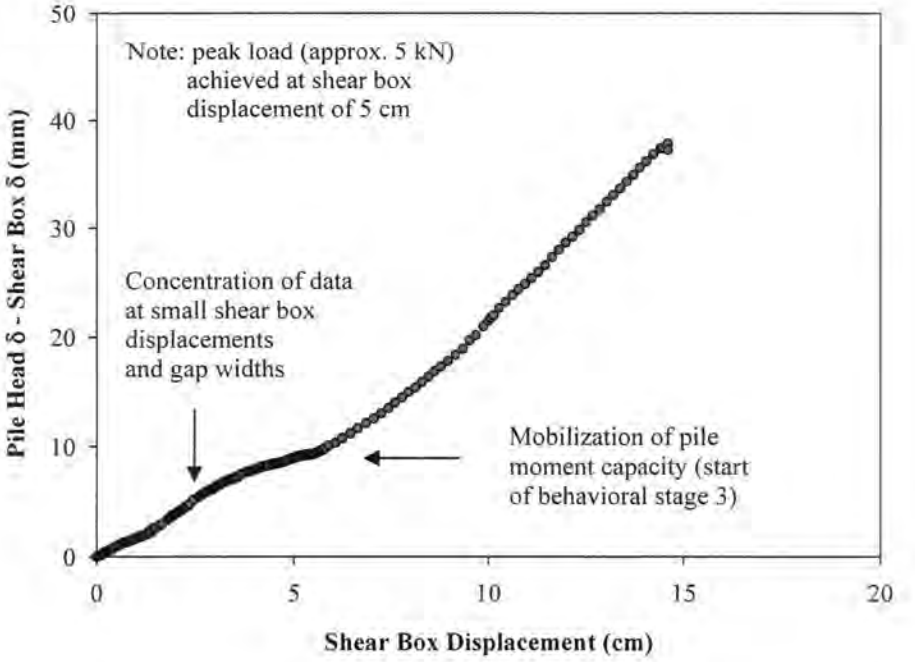

Figure 90 – Evidence for Mobilization of Pile Moment Capacity and Gap Formation (Pile 4)

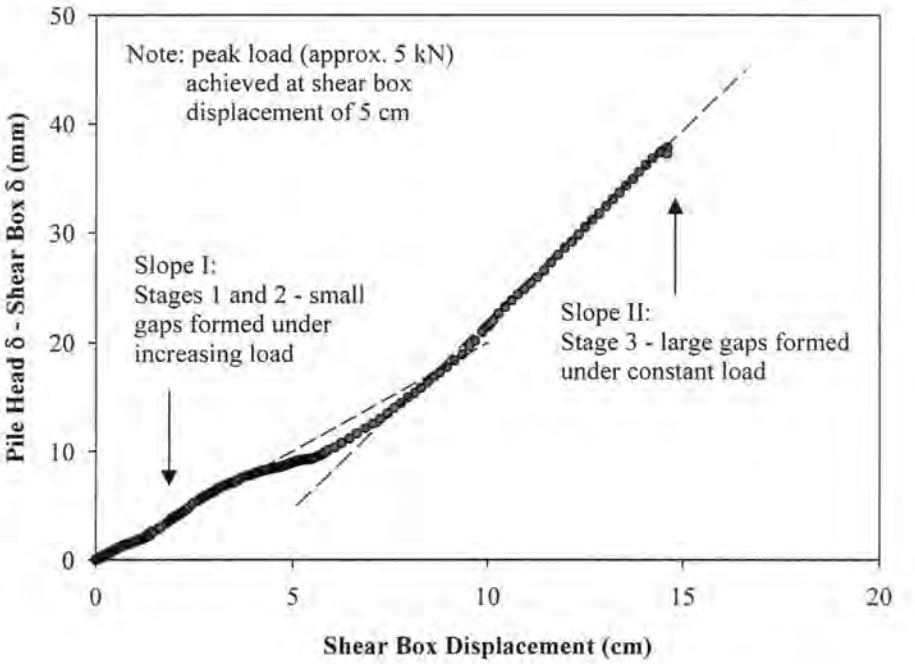

Figure 91 – Bilinear Rate of Gap Formation with Behavioral Stages of Loading (Pile 4)

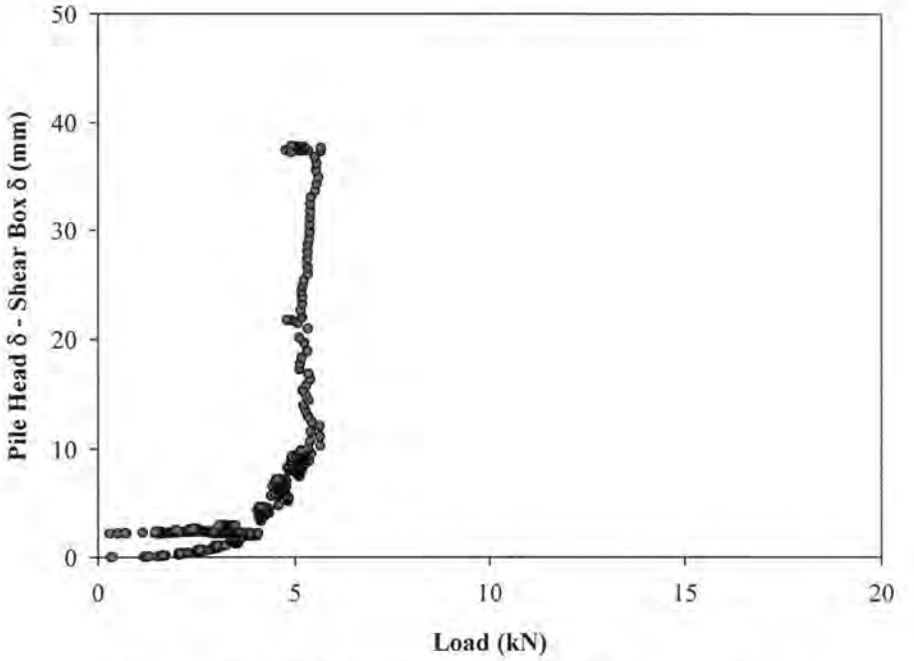

Figure 92 – Relative Displacement for Loess (Pile 4)

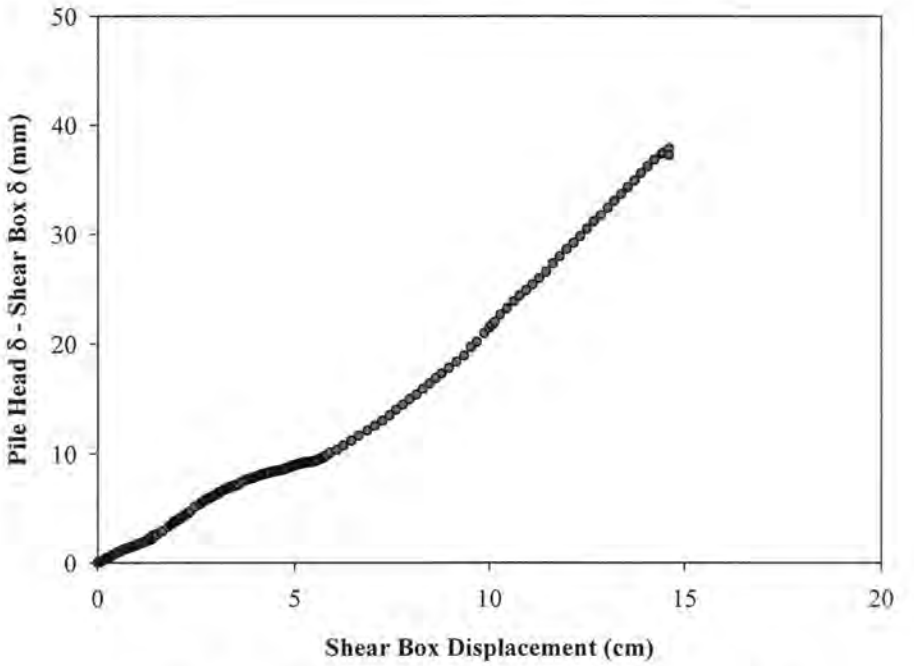

Figure 93 – Relative Displacement for Loess (Pile 4)

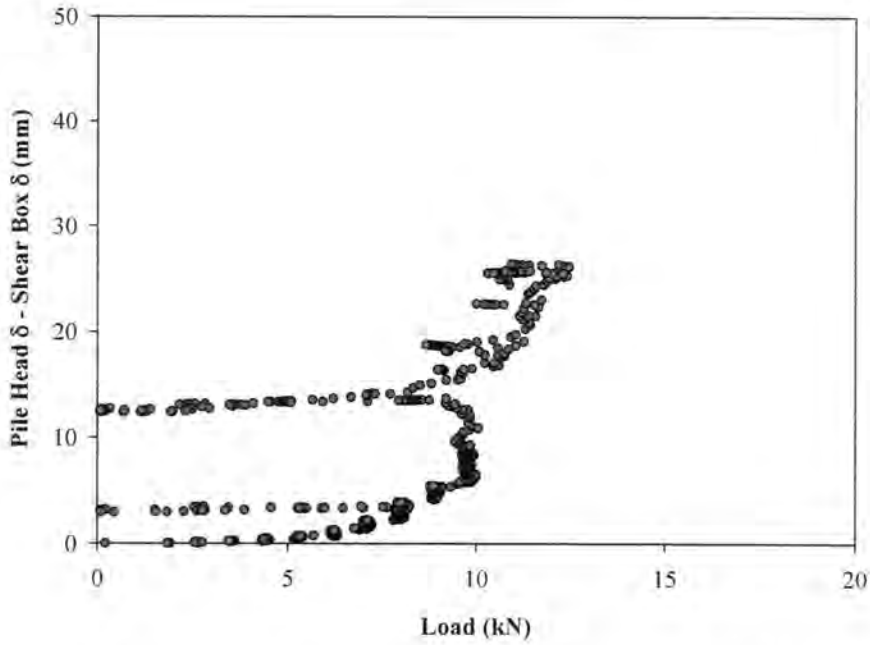

Figure 94 – Relative Displacement for Glacial Till (Pile 5)

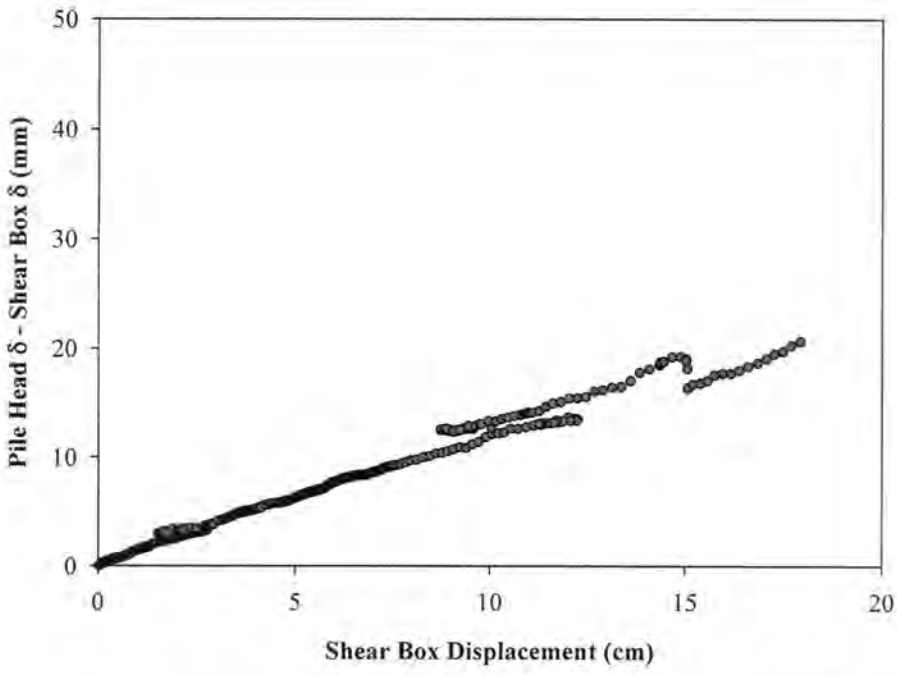

Figure 95 – Relative Displacement for Glacial Till (Pile 5)

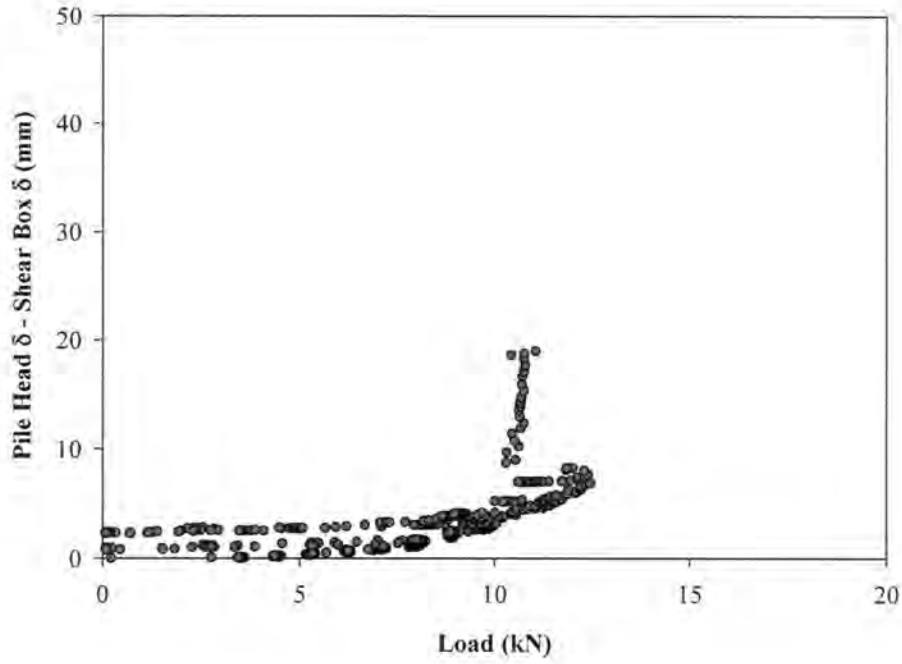

Figure 96 – Relative Displacement for Weathered Shale (Pile 6)

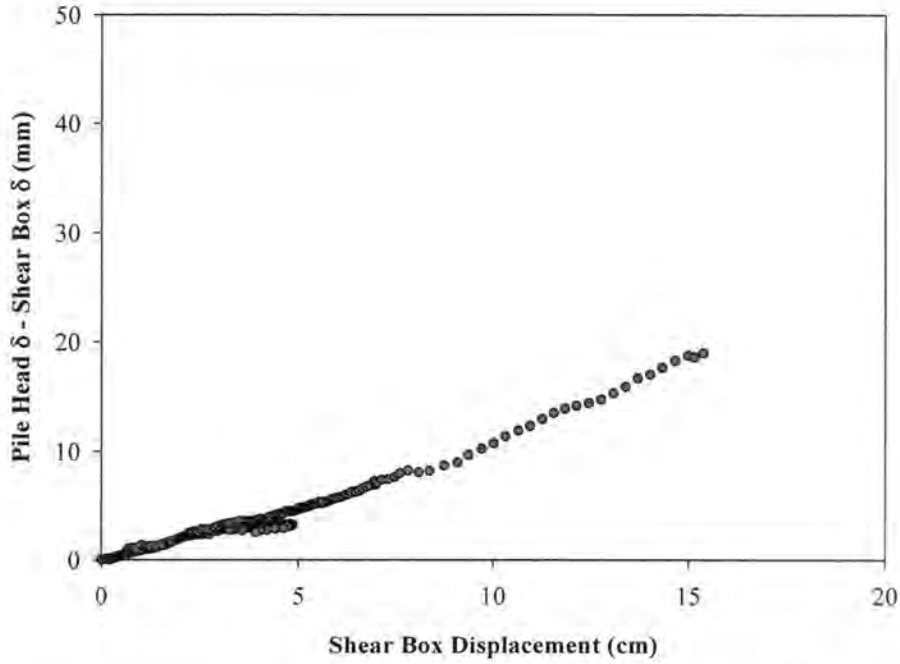

Figure 97 – Relative Displacement for Weathered Shale (Pile 6)

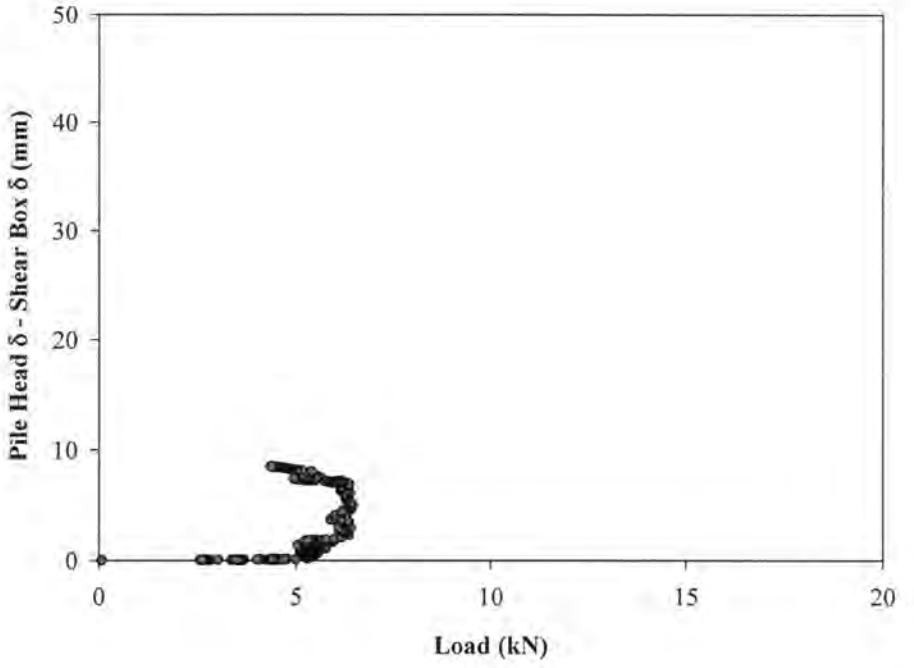

Figure 98 – Relative Displacement for Loess (Pile 8)

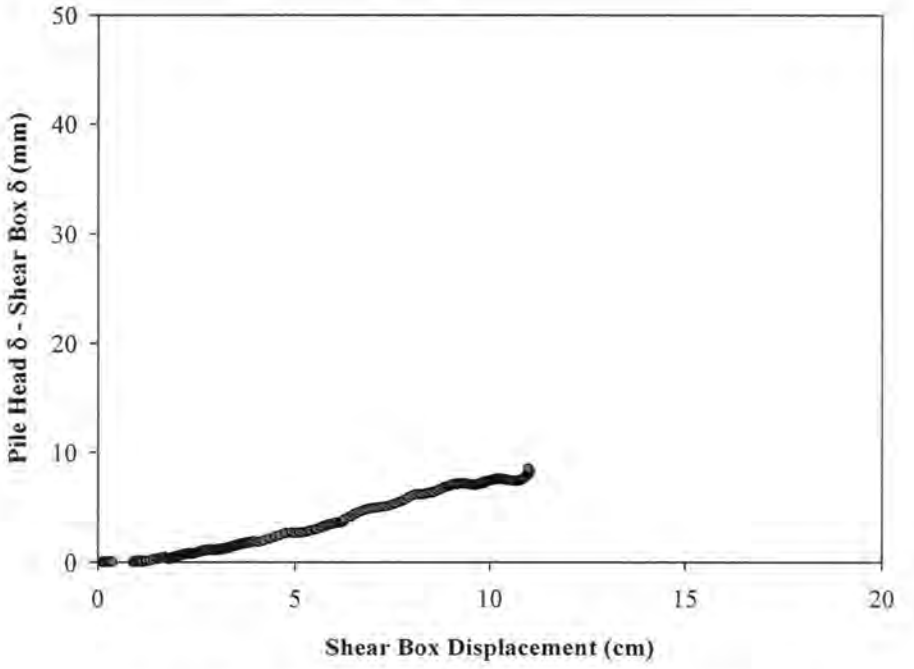

Figure 99 – Relative Displacement for Loess (Pile 8)

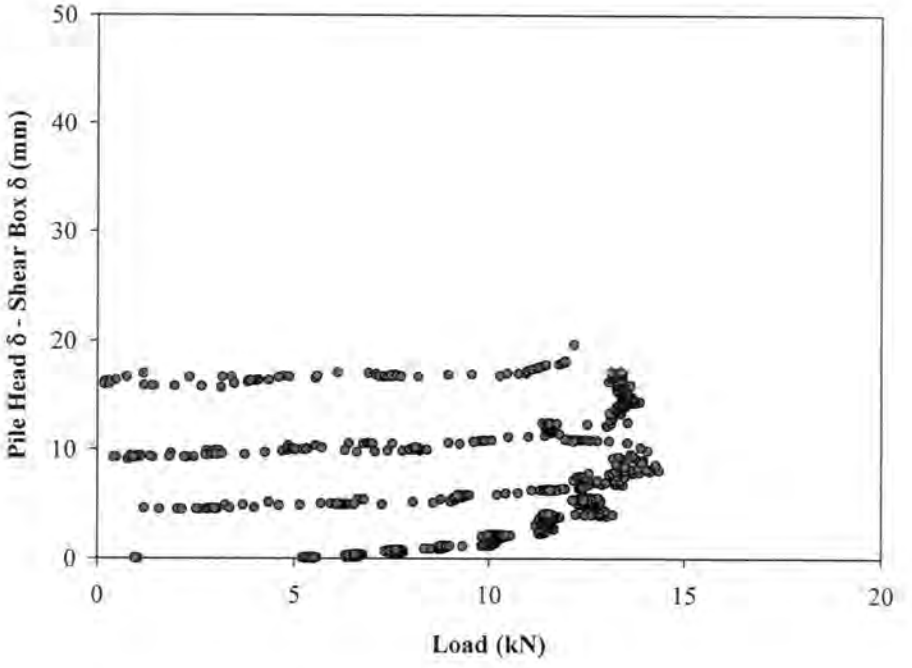

Figure 100 – Relative Displacement for Glacial Till (Pile 9)

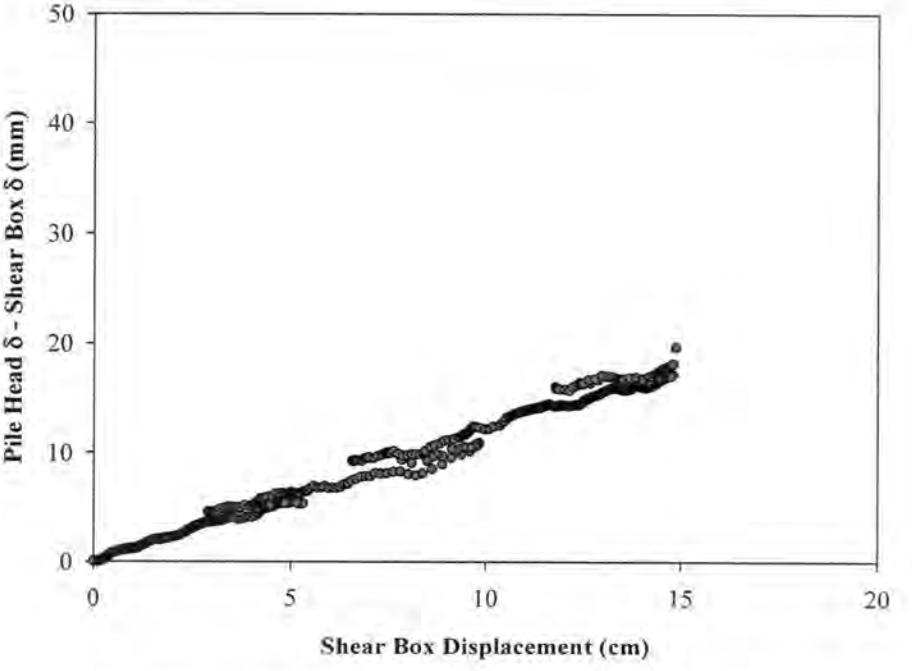

Figure 101 – Relative Displacement for Glacial Till (Pile 9)

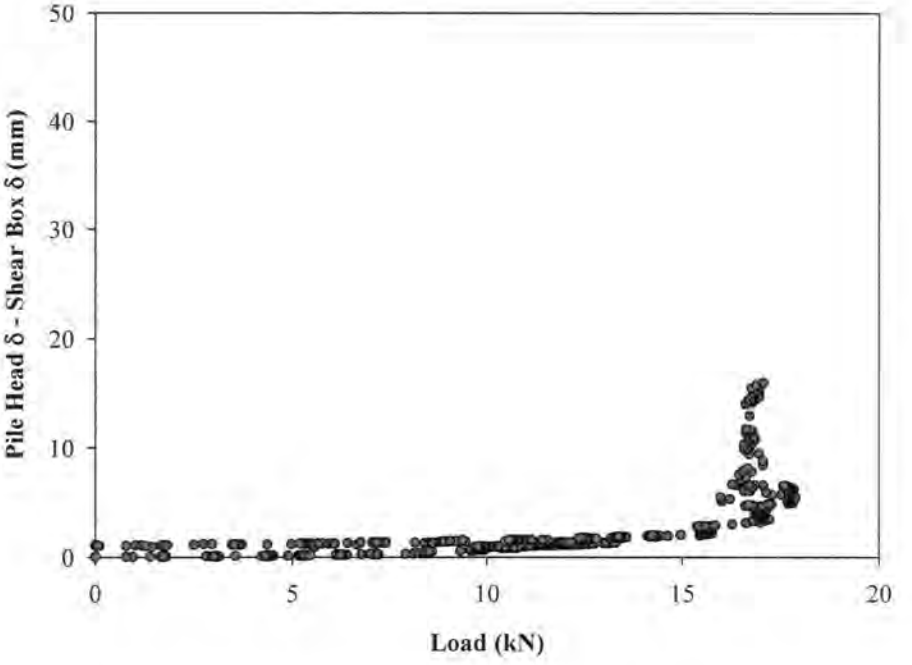

Figure 102 – Relative Displacement for Weathered Shale (Pile 12)

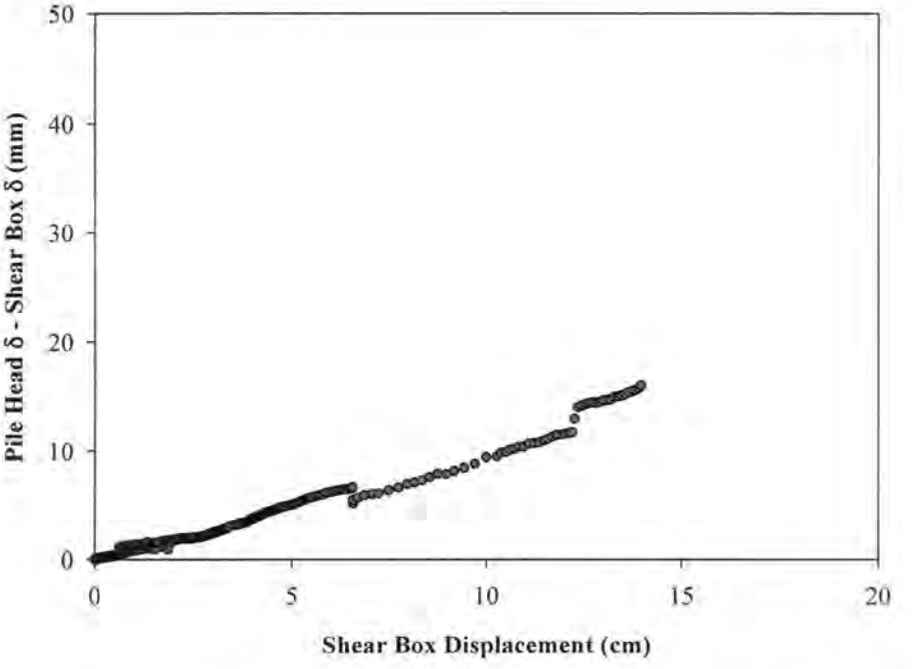

Figure 103 – Relative Displacement for Weathered Shale (Pile 12)

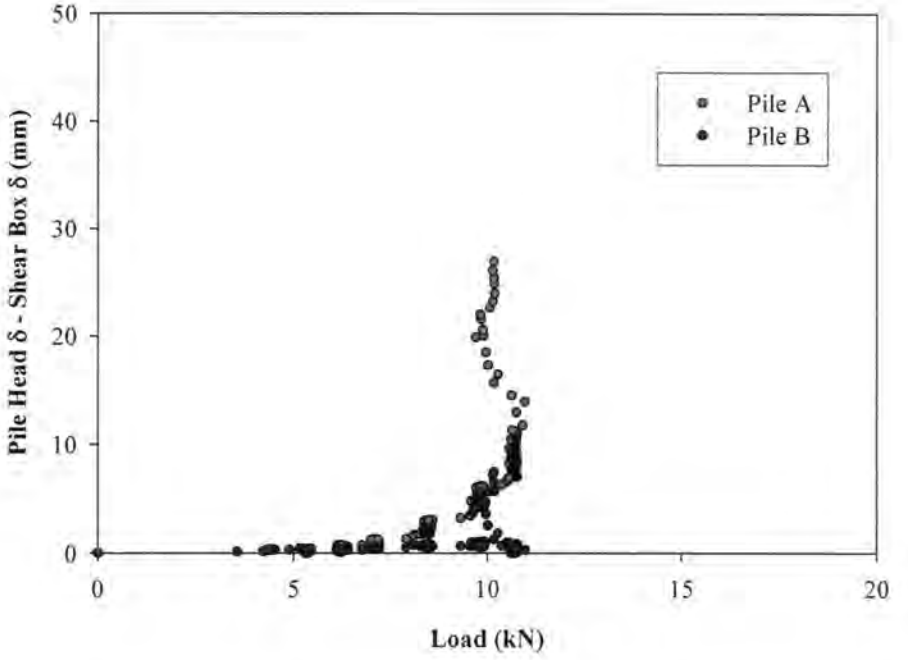

Figure 104 – Relative Displacement for Loess (Piles 11 A and B)

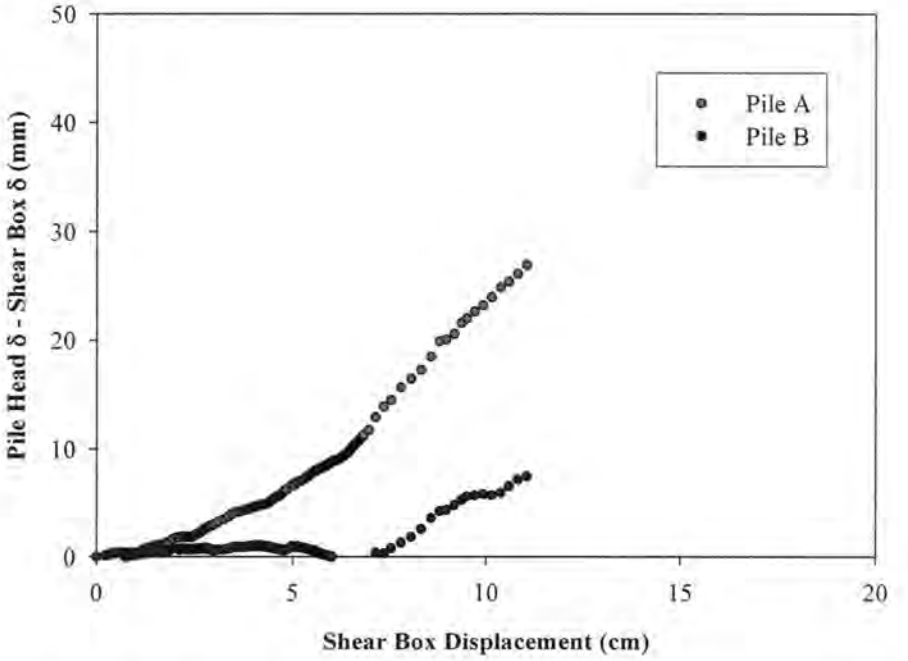

Figure 105 – Relative Displacement for Loess (Piles 11 A and B)

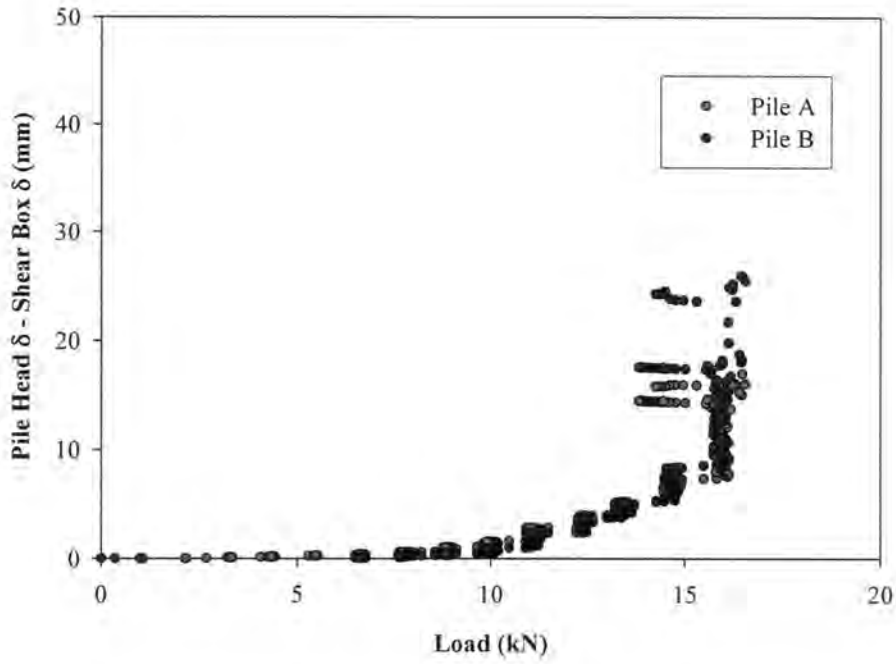

Figure 106 – Relative Displacement for Glacial Till (Piles 13 A and B)

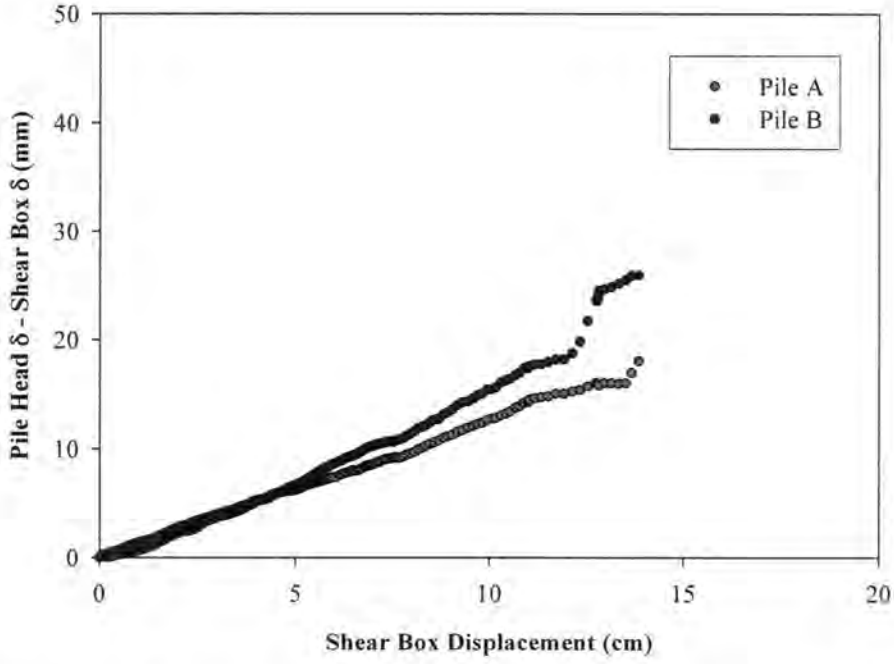

Figure 107- Relative Displacement for Glacial Till (Piles 13 A and B)

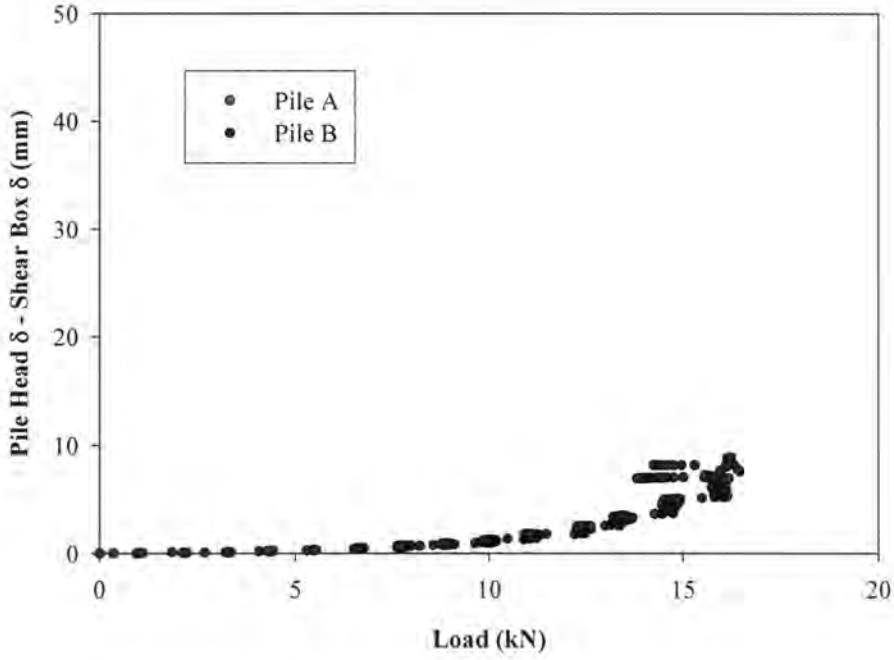

Figure 108 – Relative Displacement for Glacial Till (Piles 14 A and B)

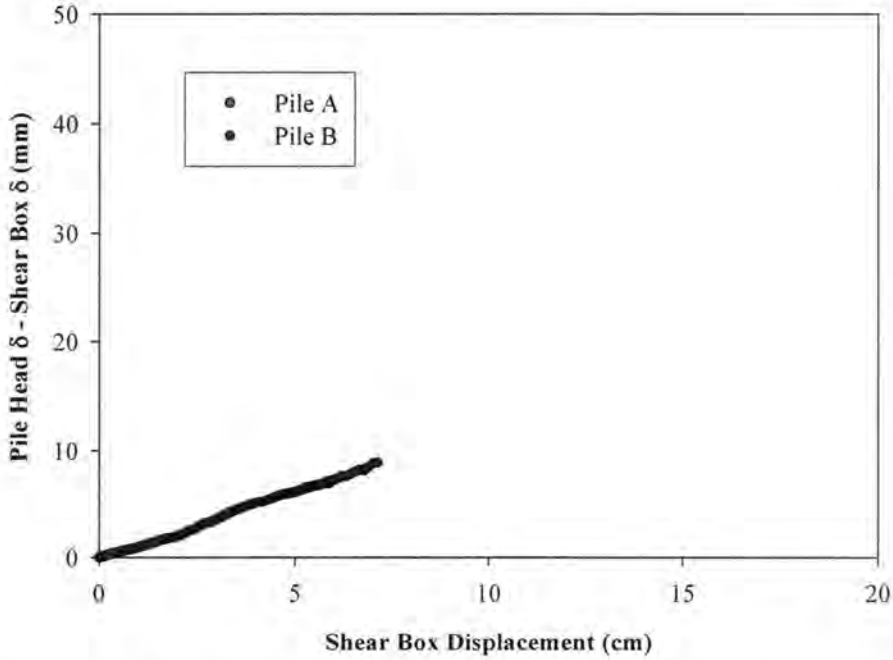

Figure 109 – Relative Displacement for Glacial Till (Piles 14 A and B)

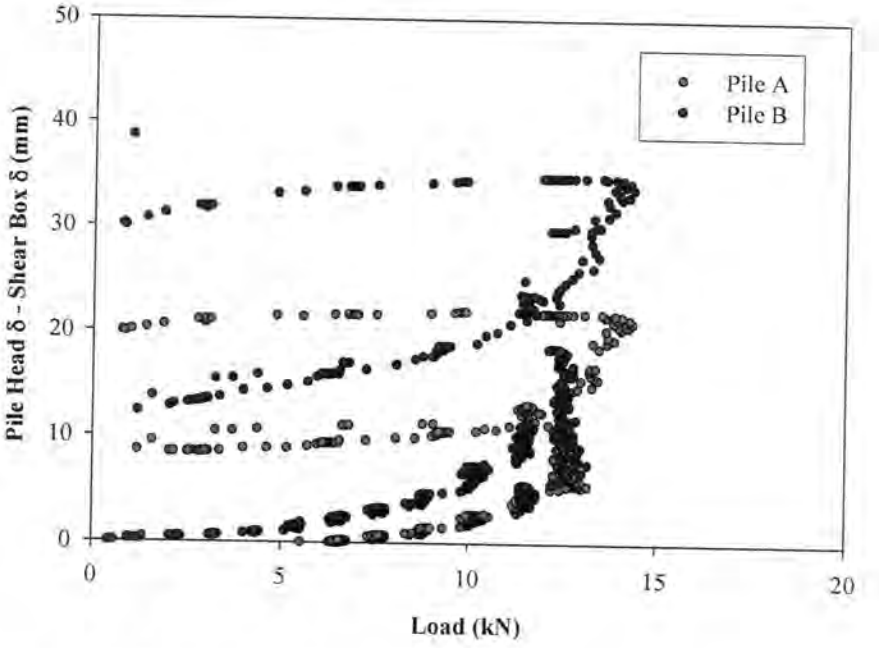

Figure 110 – Relative Displacement for Weathered Shale (Piles 10 A and B)

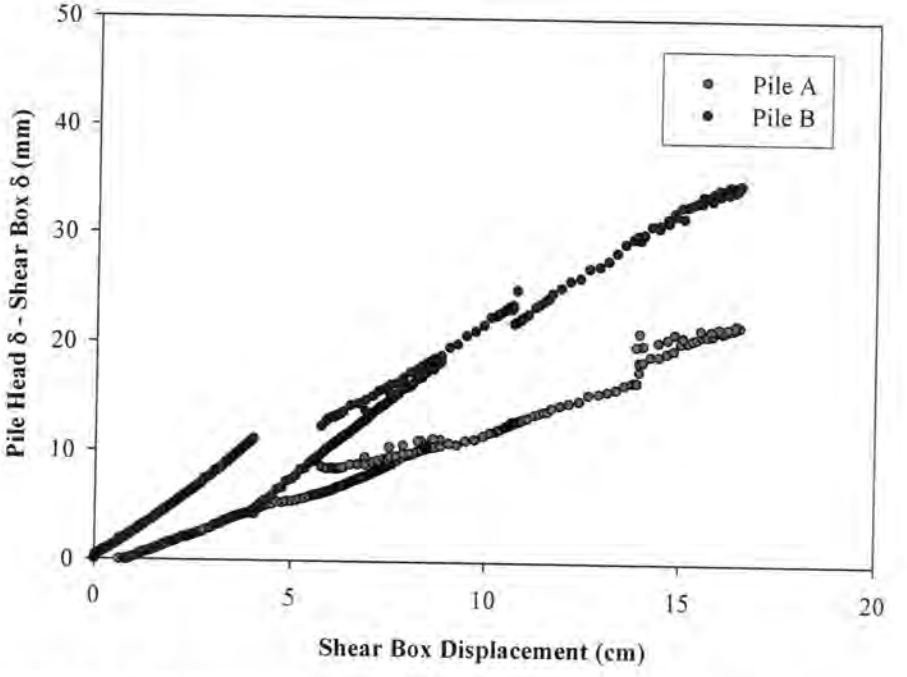

Figure 111 – Relative Displacement for Weathered Shale (Piles A and B)

SHEAR BOX ROTATION AND TILT

The rotation (about vertical axis) and tilt (about horizontal axis) of the direct shear boxes (see Figures 112 and 113) are provided in this section. Figures 114 through 133 are presented to document a possible cause of poor correlation between predicted and measured pile behaviors. A tilted box, for example, potentially subjects the pile element to a component of axial load and alters the pile performance. Ultimately, shear box rotation or tilt was not used to explain pile load test behavior.

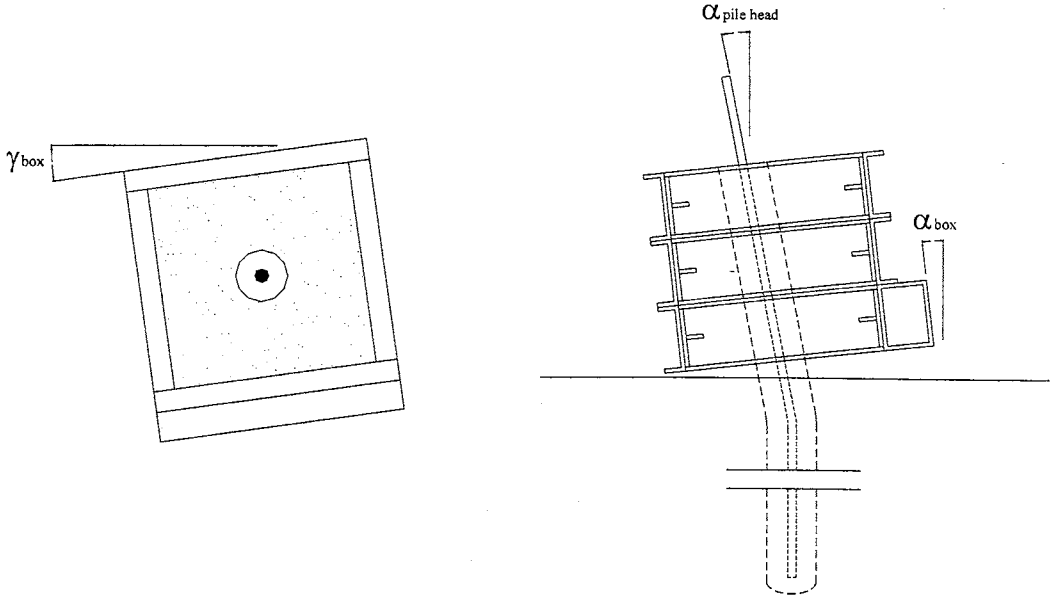

Figure 112 – Shear Box Rotation and Tilt

(a) Plan view (rotation); (b) Elevation view (tilt)

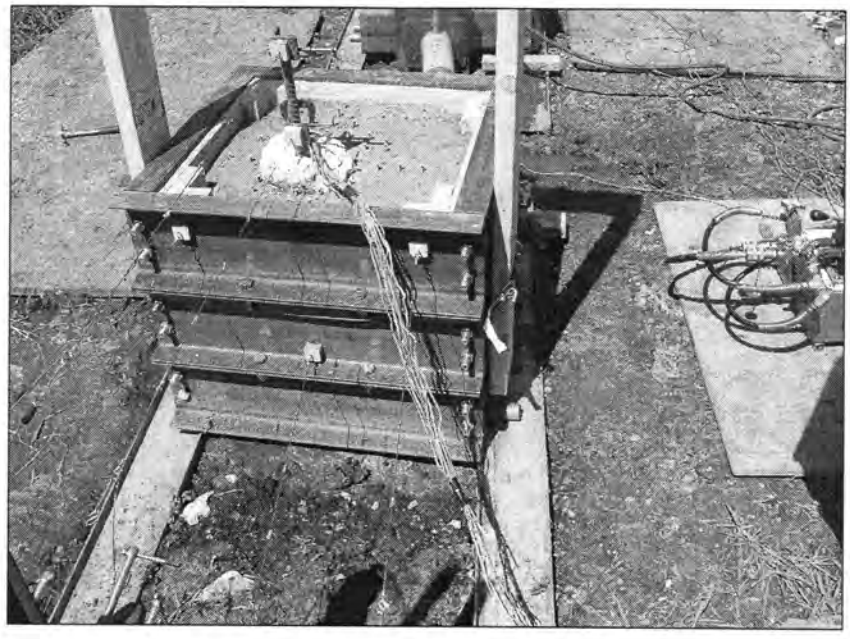

(a)

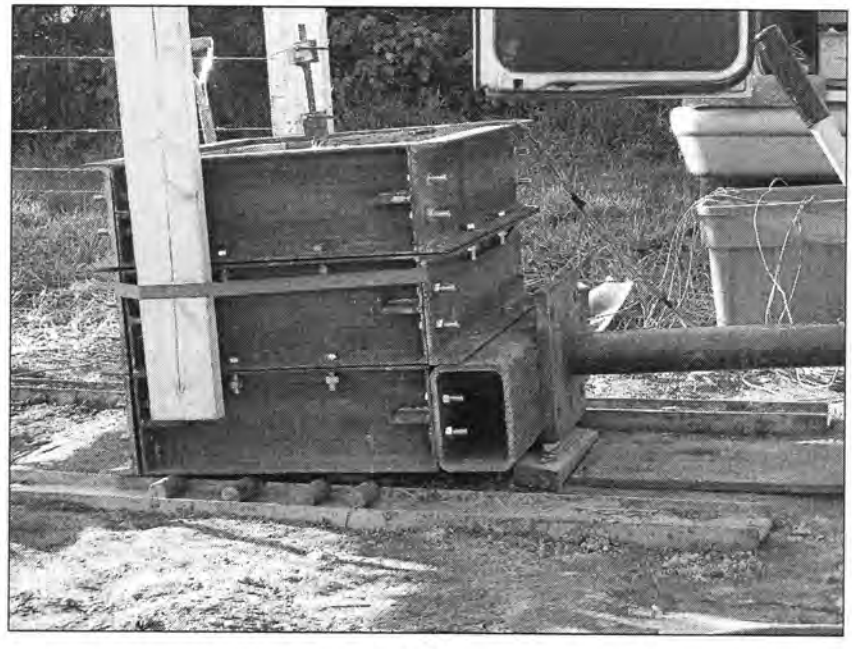

(b)

Figure 113 – Shear Box Rotation and Tilt

(a) Rotation (Box 8); Tilt (Box 5)

Table 19 provides the maximum values of shear box rotation and tilt.

Table 19 – Maximum Shear Box Rotation and Tilt

Box	Rotation	Tilt
4	2.3	0.6
5	1.2	3.5
6	1.8	3.1
8	1.8	0.0
9	0.9	1.6
10	0.9	4.6
11	0.4	0.3
12	1.0	1.2
13	0.7	2.6
14	4.5	3.2

Notes:
All units in degrees

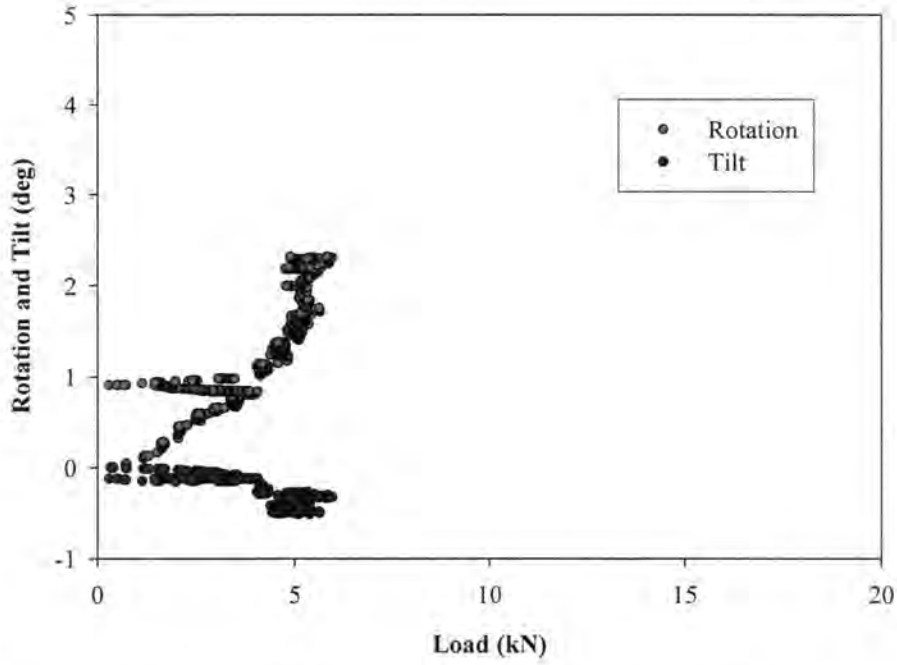

Figure 114 – Graph of Box Rotation and Tilt vs. Load for Loess (Box 4)

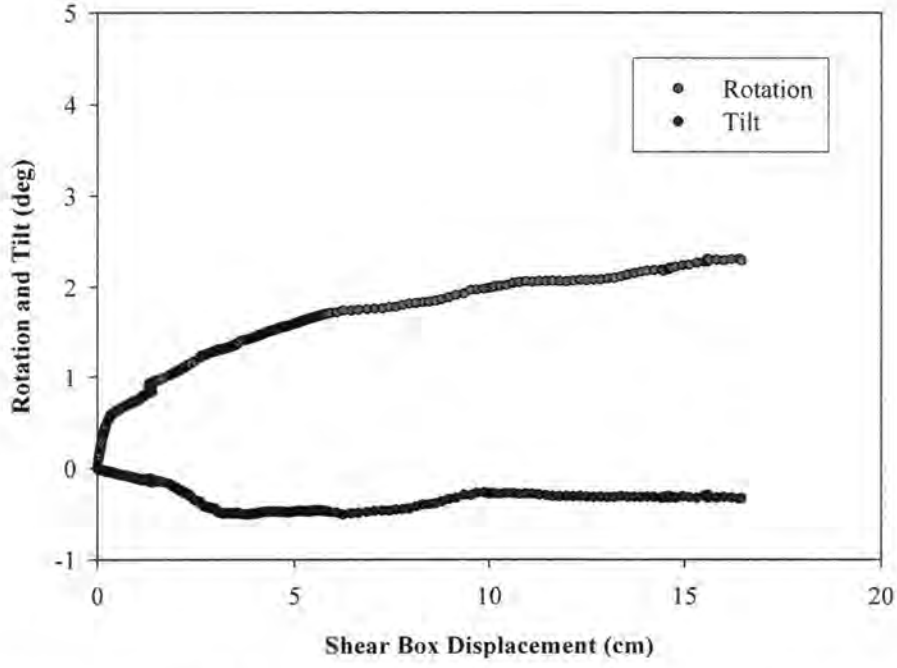

Figure 115 – Graph of Box Rotation and Tilt vs. Displacement for Loess (Box 4)

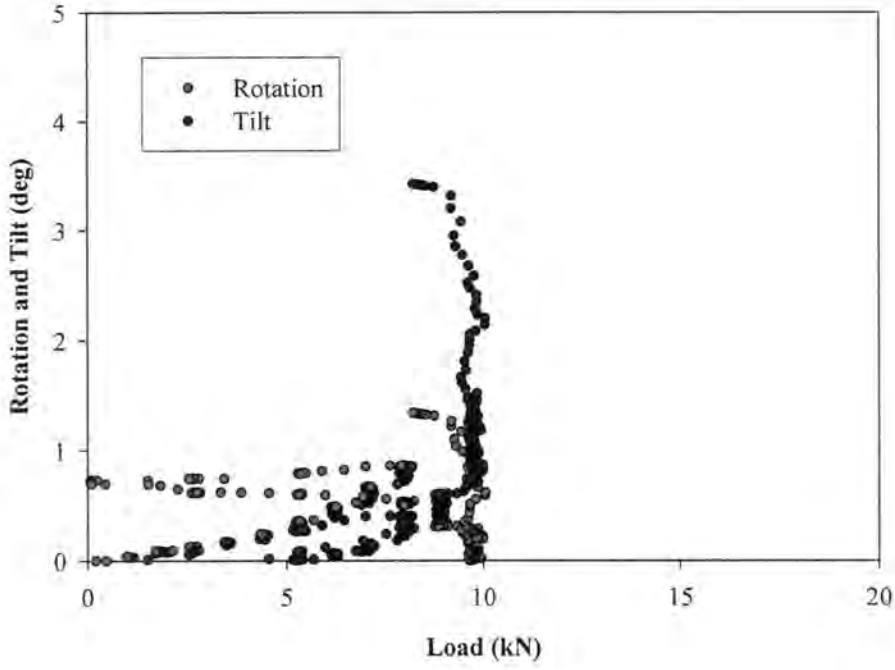

Figure 116 – Graph of Box Rotation and Tilt vs. Load for Glacial Till (Box 5)

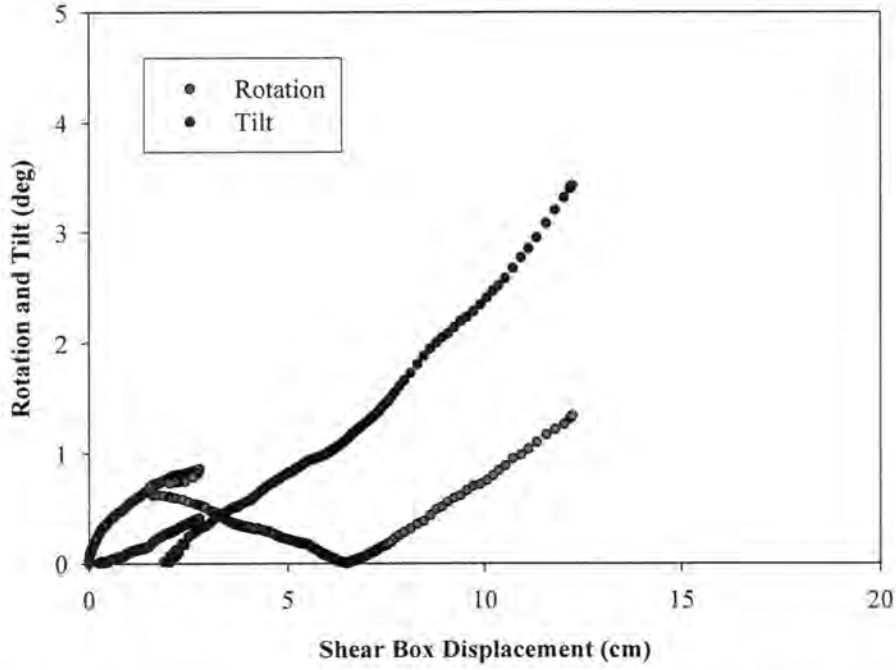

Figure 117 – Graph of Box Rotation and Tilt vs. Displacement for Glacial Till (Box 5)

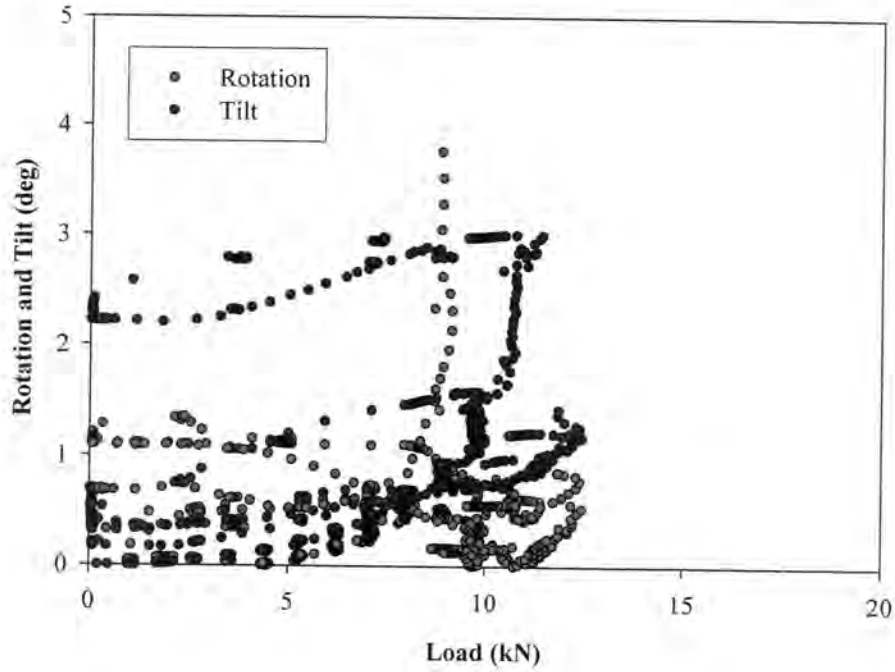

Figure 118 – Graph of Box Rotation and Tilt vs. Load for Weathered Shale (Box 6)

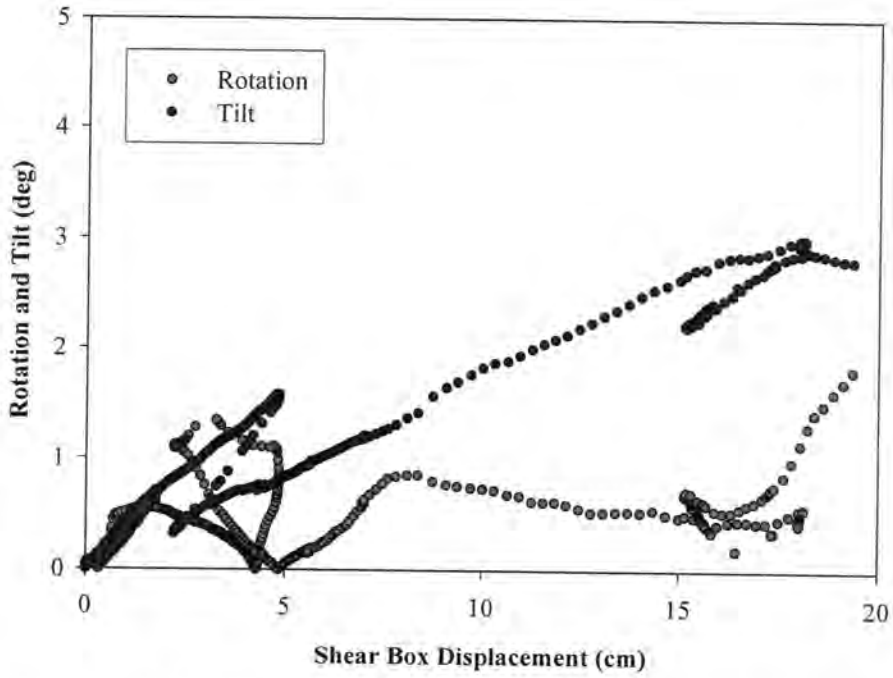

Figure 119 – Graph of Box Rotation and Tilt vs. Displacement for Weathered Shale (Box 6)

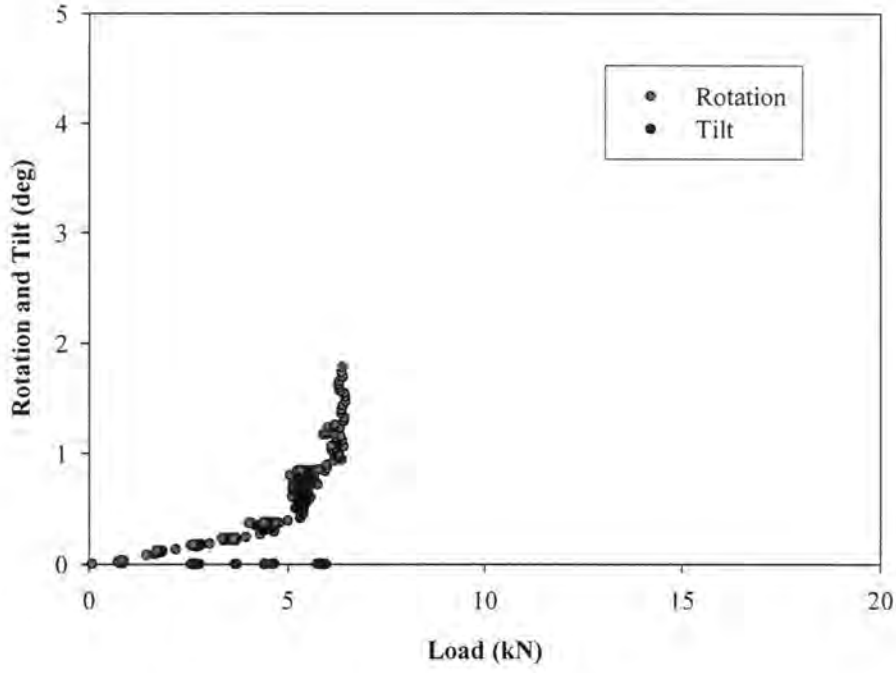

Figure 120 – Graph of Box Rotation and Tilt vs. Load for Loess (Box 8)

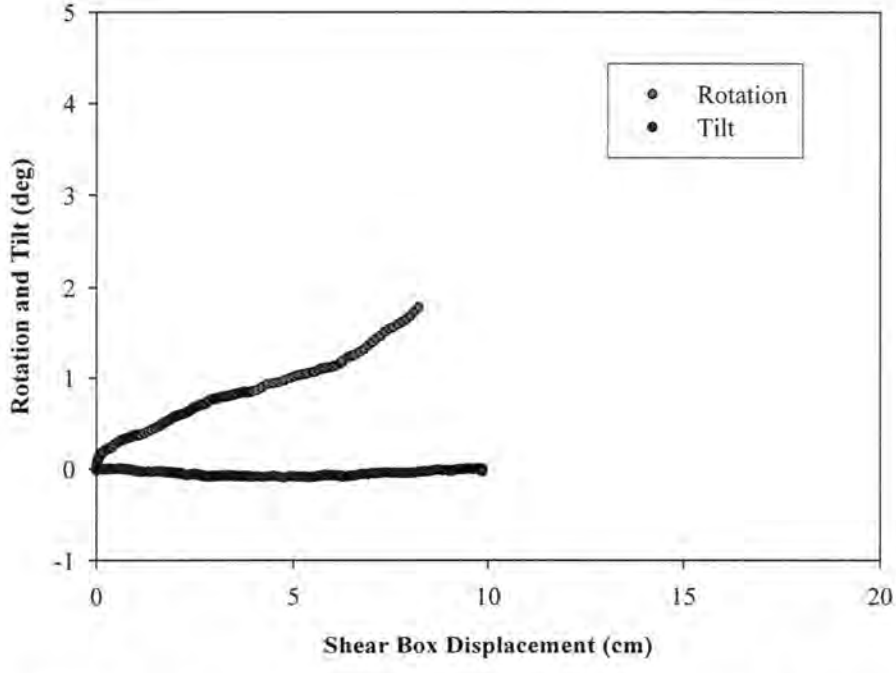

Figure 121 – Graph of Box Rotation and Tilt vs. Displacement for Loess (Box 8)

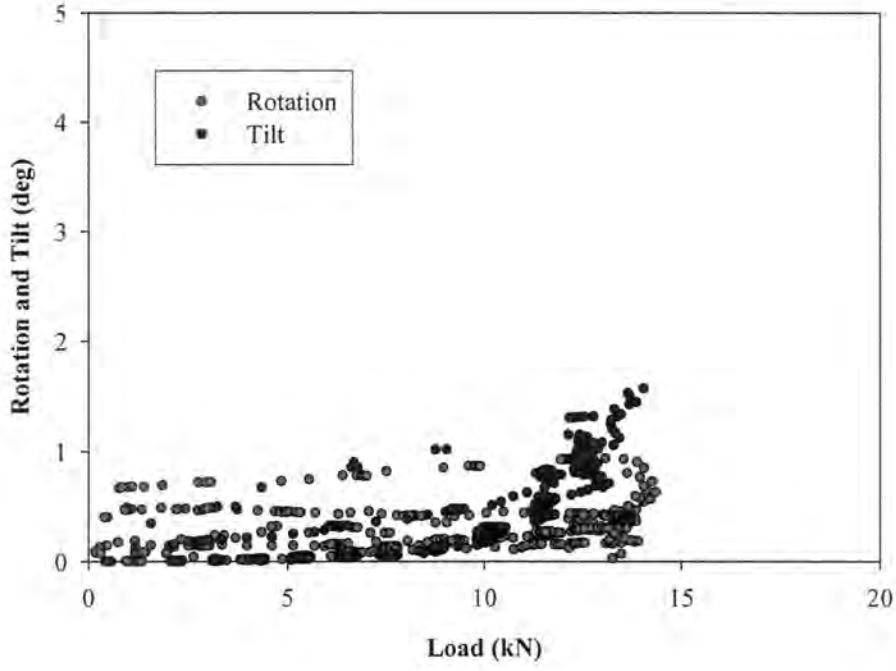

Figure 122 – Graph of Box Rotation and Tilt vs. Load for Glacial Till (Box 9)

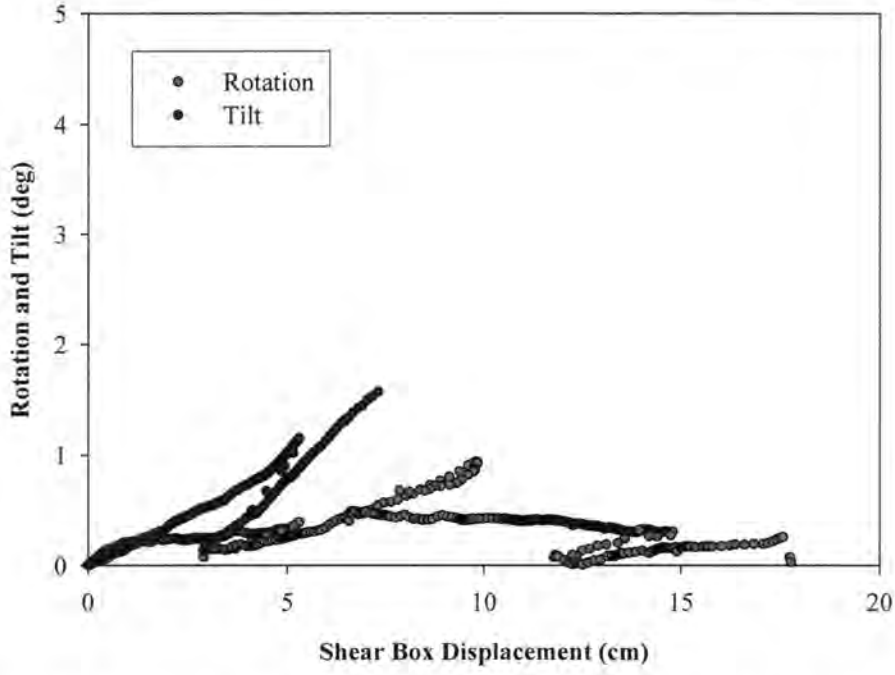

Figure 123 – Graph of Box Rotation and Tilt vs. Displacement for Glacial Till (Box 9)

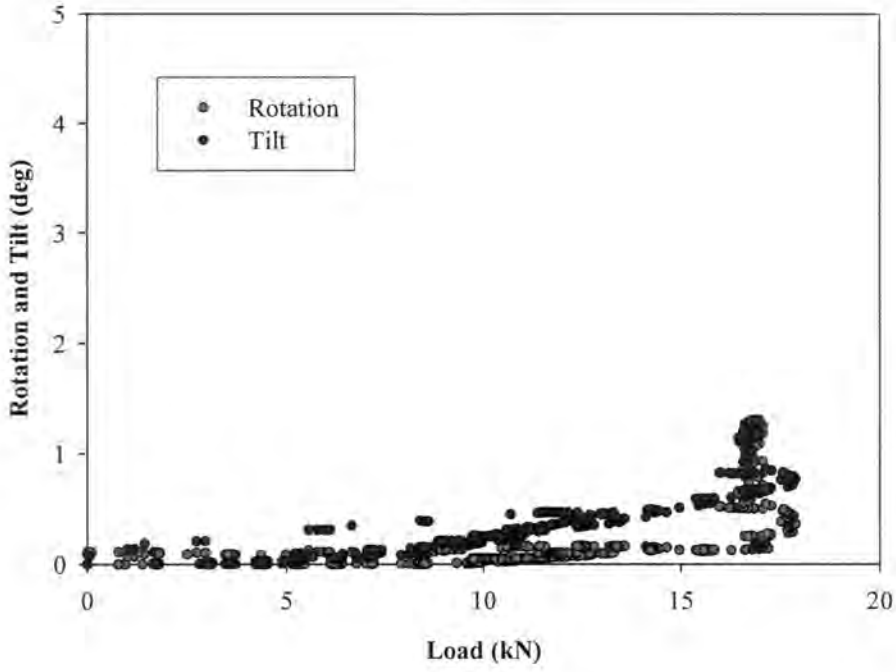

Figure 124 – Graph of Box Rotation and Tilt vs. Load for Weathered Shale (Box 12)

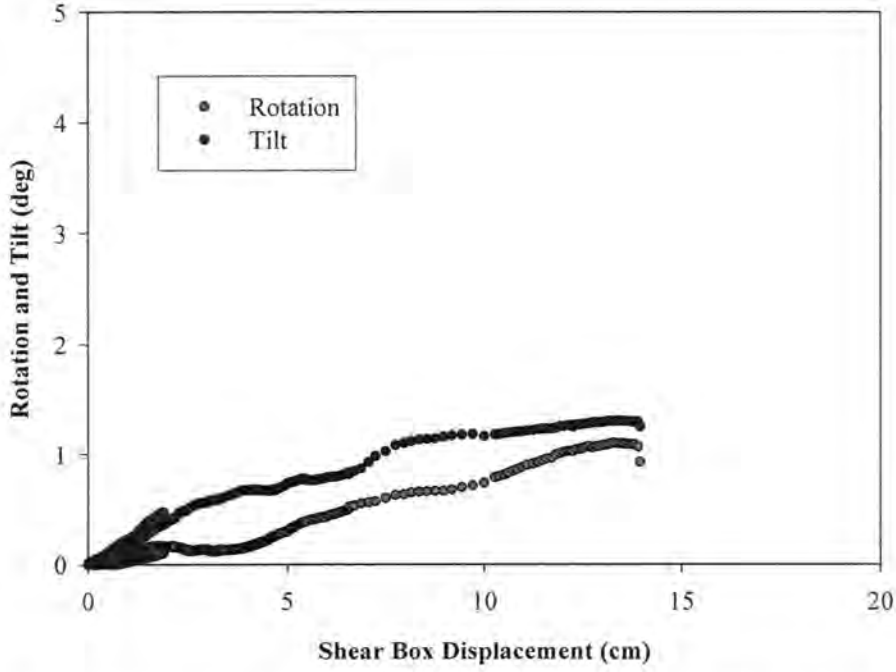

Figure 125 – Graph of Box Rotation and Tilt vs Displacement for Weathered Shale (Box 12)

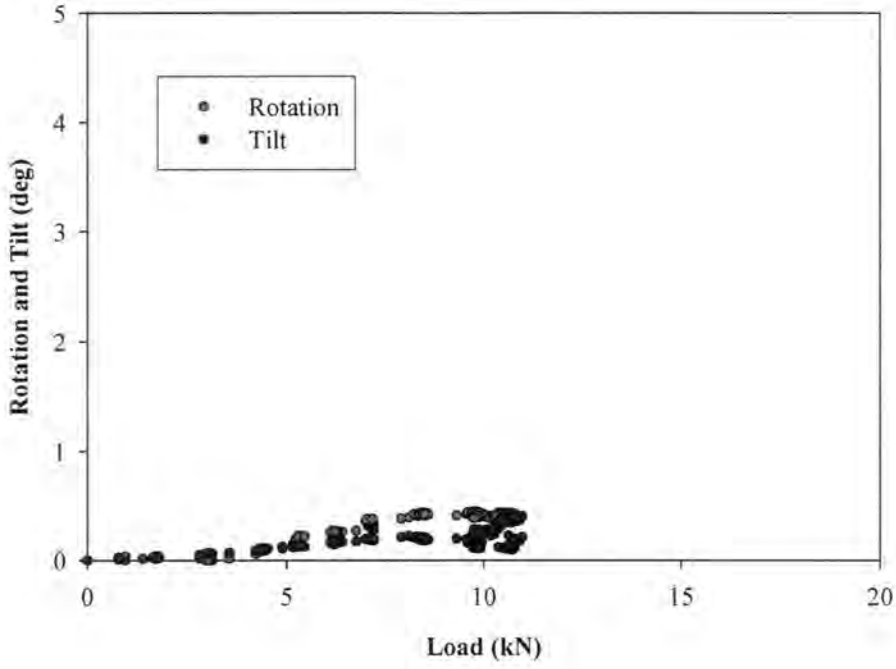

Figure 126 – Graph of Box Rotation and Tilt vs. Load for Loess (Box 11)

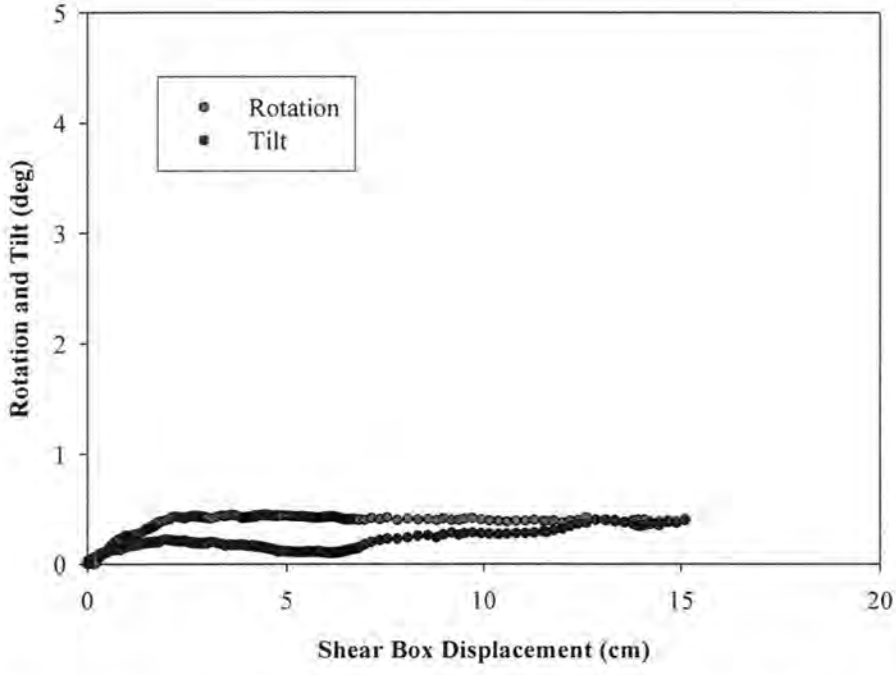

Figure 127 – Graph of Box Rotation and Tilt vs. Displacement for Loess (Box 11)

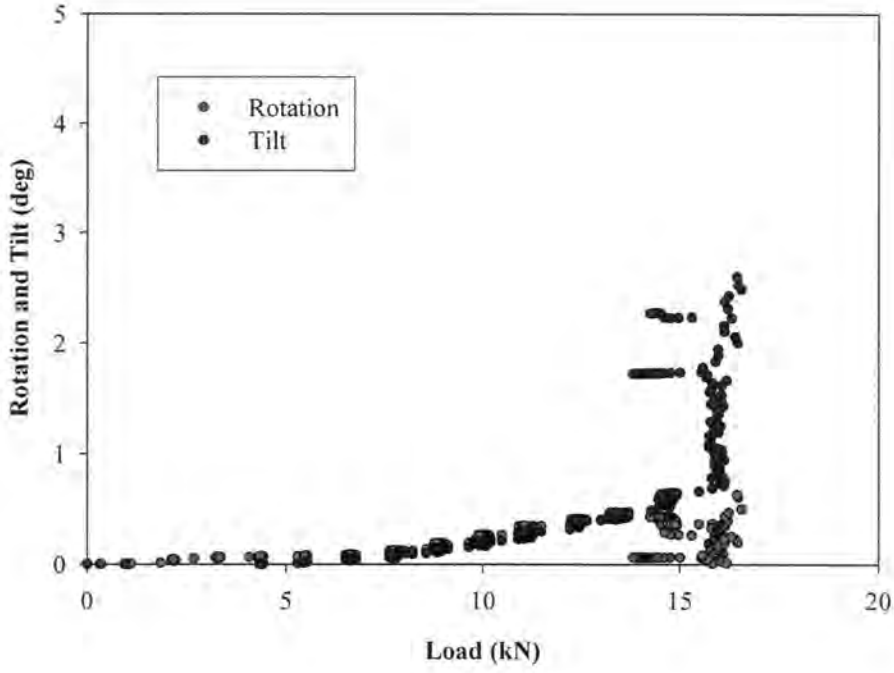

Figure 128 – Graph of Box Rotation and Tilt vs. Load for Glacial Till (Box 13)

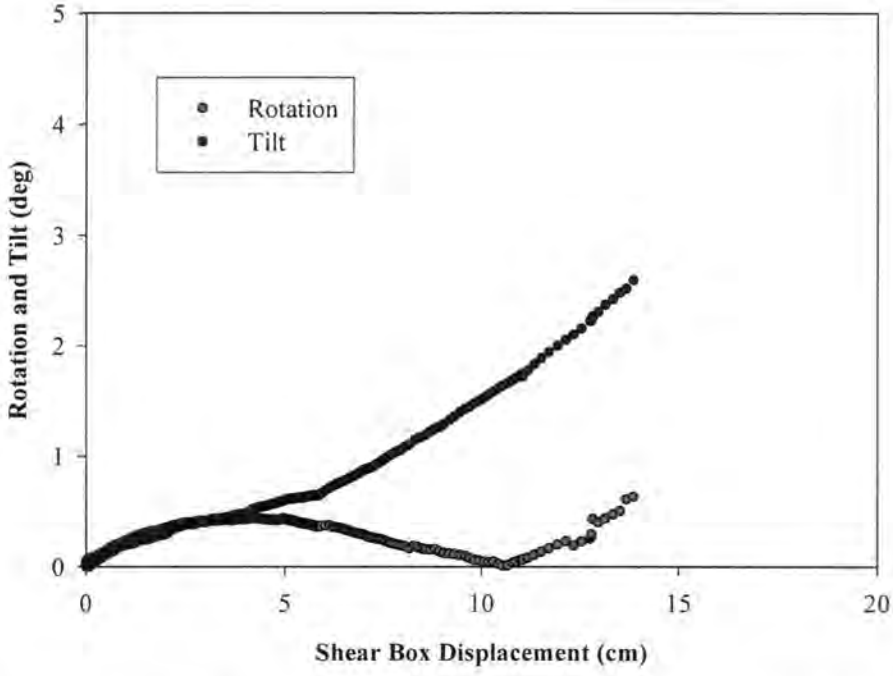

Figure 129 – Graph of Box Rotation and Tilt vs. Displacement for Glacial Till (Box 13)

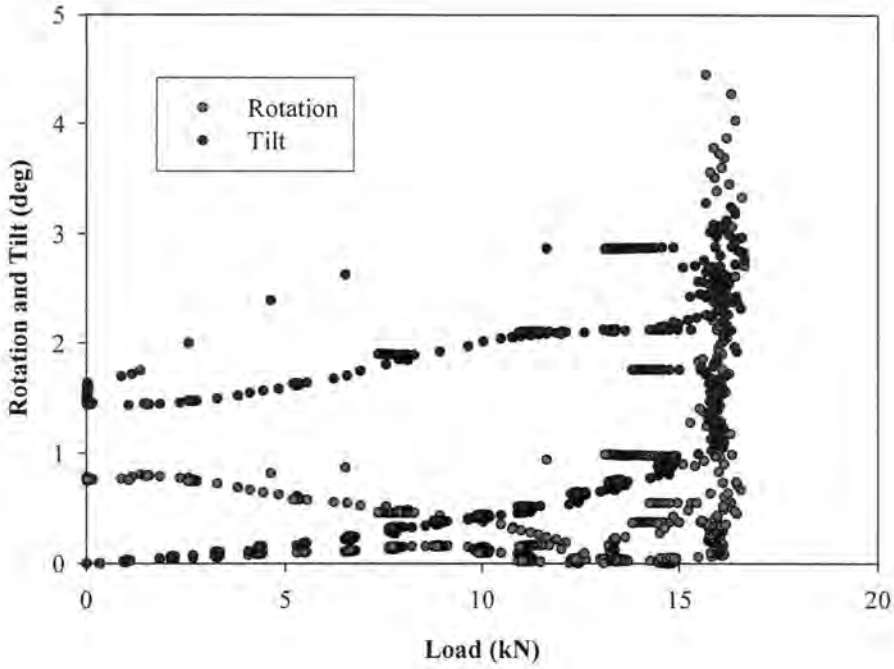

Figure 130 – Graph of Box Rotation and Tilt vs. Load for Glacial Till (Box 14)

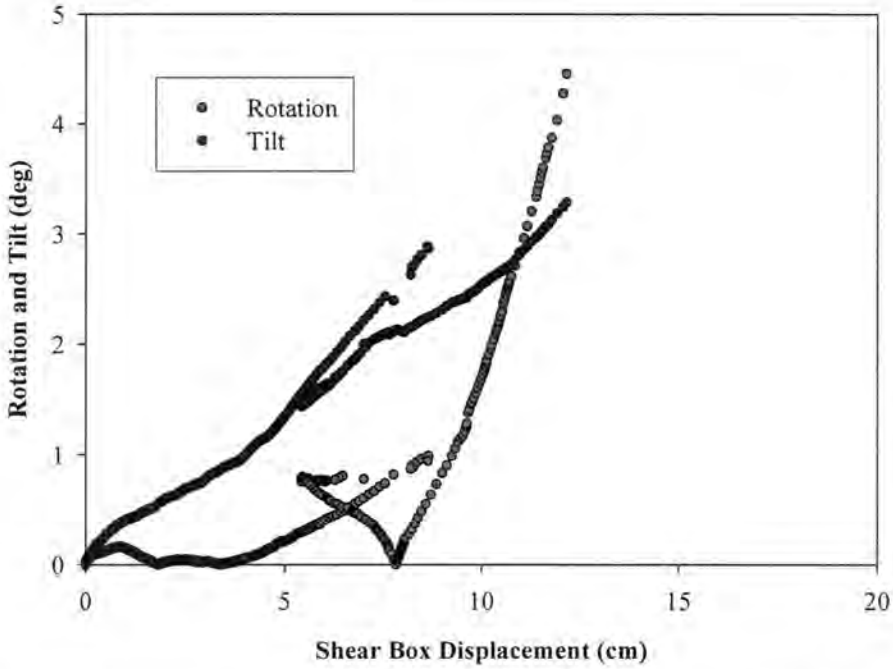

Figure 131 – Graph of Box Rotation and Tilt vs. Displacement for Glacial Till (Box 14)

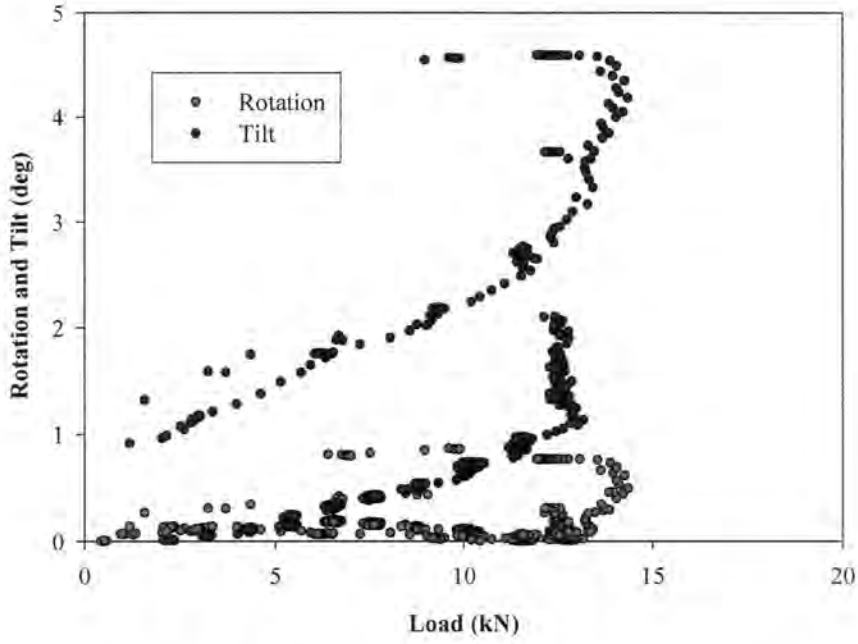

Figure 132 – Graph of Box Rotation and Tilt vs. Load for Weathered Shale (Box 10)

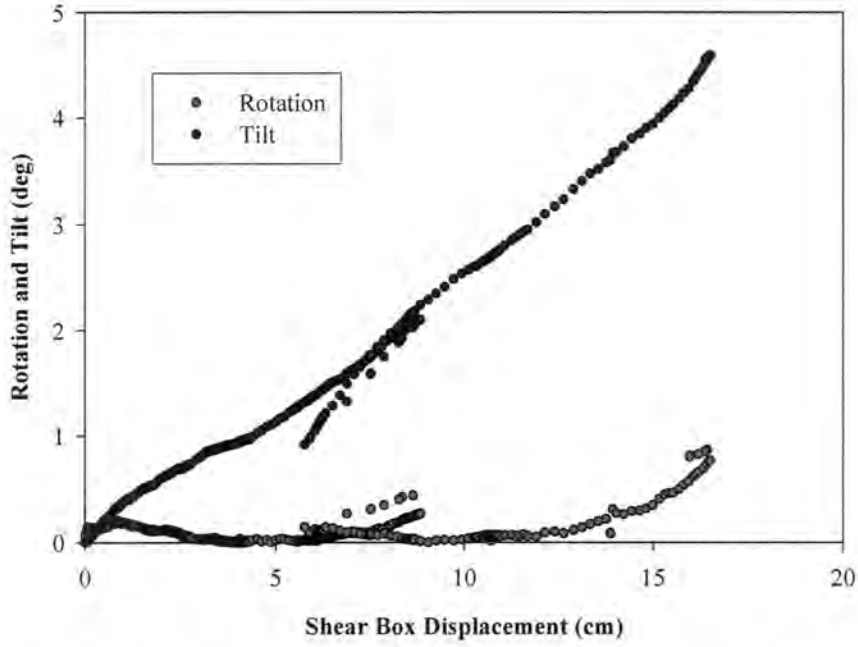

Figure 133 – Graph of Box Rotation and Tilt vs Displacement for Weathered Shale (Box 12)

PILE MOMENT DISTRIBUTIONS

Moment profiles along the entire length of piles, for the full range of loading, are provided in Figures 134 through 146. The depths of the y-axis are taken from the pile head (at the soil surface), and the loads provided in the legends of each figure represent the load applied to the shear box when the strain of pile reinforcement was measured. The measured strain of pile reinforcement was converted to bending moment through a moment-curvature analysis, documented in Chapter 3.

The figures provide the most influential evidence that the majority of piles failed due to mobilization of the moment capacity. The maximum measured moments for most single piles exceeded the section moment capacities, as shown in Figures 134 through 139. Approximately one half of the dual piles mobilized the full moment capacity, as well.

The location at which the maximum moment developed is additionally important to evaluating the performance of piles. Maximum moments are generally developed approximately 3 to 4 pile diameters from the load application. The research group observed maximum measured moments developed at approximately 4 pile diameters below the load application. The use of additional strain gauges near the maximum moment location facilitates a more accurate maximum moment depth. Nevertheless, the piles performed in accordance with generally accepted behavior.

The maximum moments and depths to the maximum moments are provided in Table 20. Additionally, the table provides the depths of plastic hinge development in terms of pile diameters below the shear surface.

Table 20 – Maximum Moments and Depths of Plastic Hinge Development

Pile	M_{max} (kN-m)	Depth (mm)*	Depth (Pile Diameters)**
4	2.60	965	3.34
5	2.24	1016	3.86
6	2.70	1016	3.69
8	2.13	1498	4.99
9	5.26	1067	2.71
10 A	2.44	965	3.34
10 B	1.86	787	1.81
11 A	2.12	813	2.01
11 B	2.60	1067	4.23
12	7.34	1524	5.43
13 A	0.75	1016	3.86
13 B	0.86	1016	3.79
14 B	2.29	1067	4.13

Notes:
* from pile head (soil surface)
** from shear surface

The negative strains measured in the length of pile subject to lateral soil movement, as seen in Figures 136 through 139, remain unexplained by the research group. Predicted bending moments associated with negative moment development due to pile rotation into the soil behind the piles are of significantly less magnitude than the moments corresponding to the strain mobilized in the reinforcement. Furthermore, despite the apparent mobilization of the cracking moment, cracking along the uppermost length of the piles was not observed during pile exhumation. The principal concern of the research group is that the strain follows a seemingly systematic pattern, in that the strains increase with increasing load and that the pattern occurs at multiple strain gauge levels. The issue is clearly more complicated than attributing the readings to poor strain gauge performance.

Negative strains were also measured near the tips of Piles 8 and 9 (Figures 137 and 138, respectively). The development of negative bending moments at these elevations is not unusual, but the conversion from measured strain to moment values is slightly erroneous.

The negative bending moments result in compression strains, where the neutral axis position is located at the center of the rebar. Upon cracking of the pile and shifting of the neutral axis position, however, tension is mobilized in the pile reinforcement. Tension strains are acquired, and the moment profiles experience a sign reversal at the particular gauge elevation. After a pile cracks, the employed moment-curvature analysis, from which strains are converted to moment, is valid only for the initial loading direction.

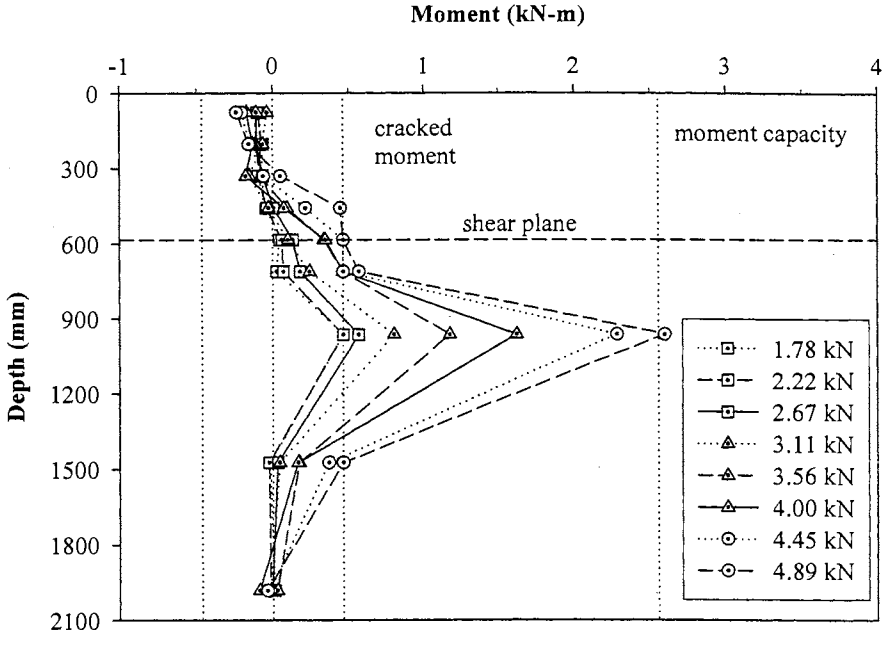

Figure 134 – Moment Profiles for Reinforced Loess (Pile 4)

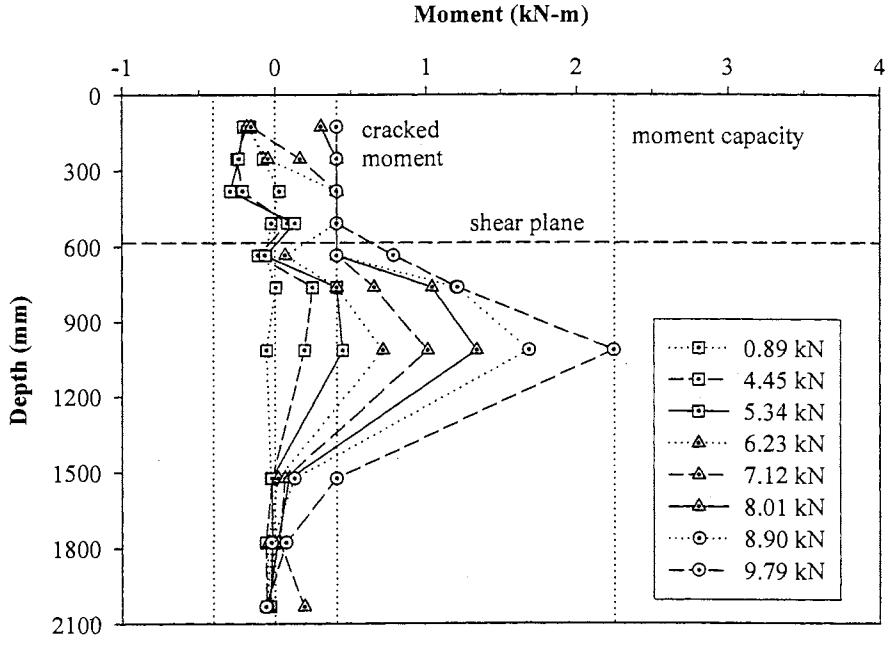

Figure 135 – Moment Profiles for Reinforced Glacial Till (Pile 5)

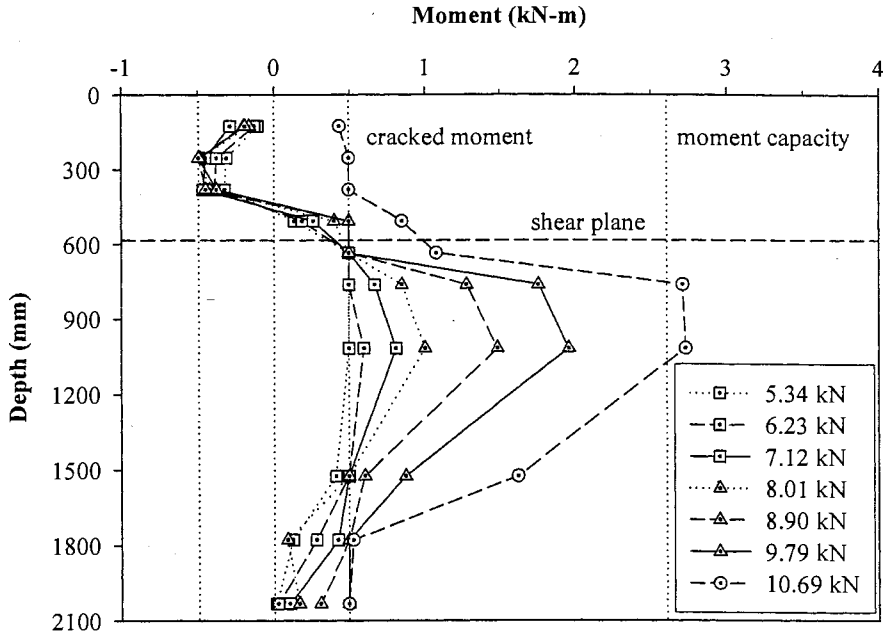

Figure 136 – Moment Profiles for Reinforced Weathered Shale (Pile 6)

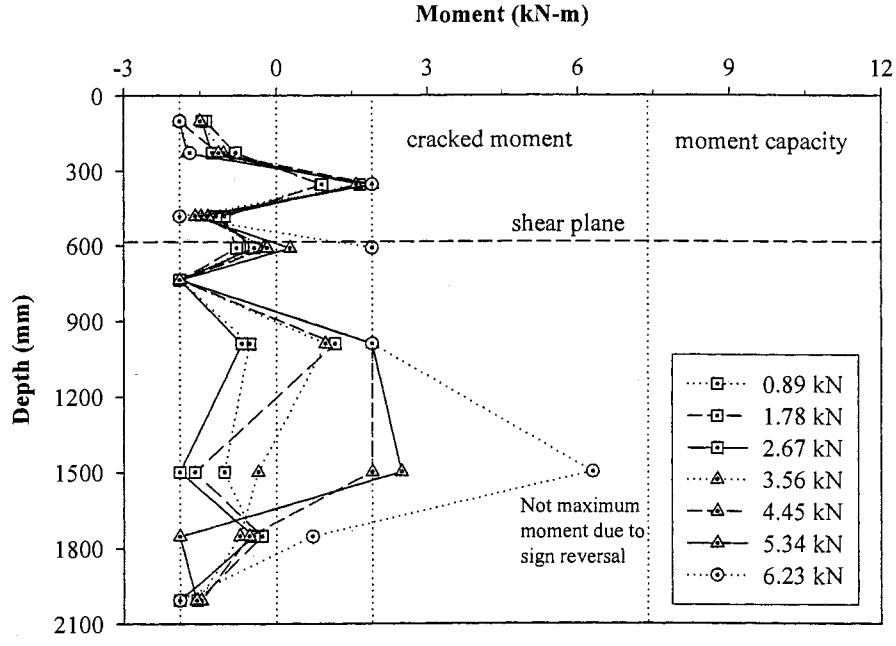

Figure 137 – Moment Profiles for Reinforced Loess (Pile 8)

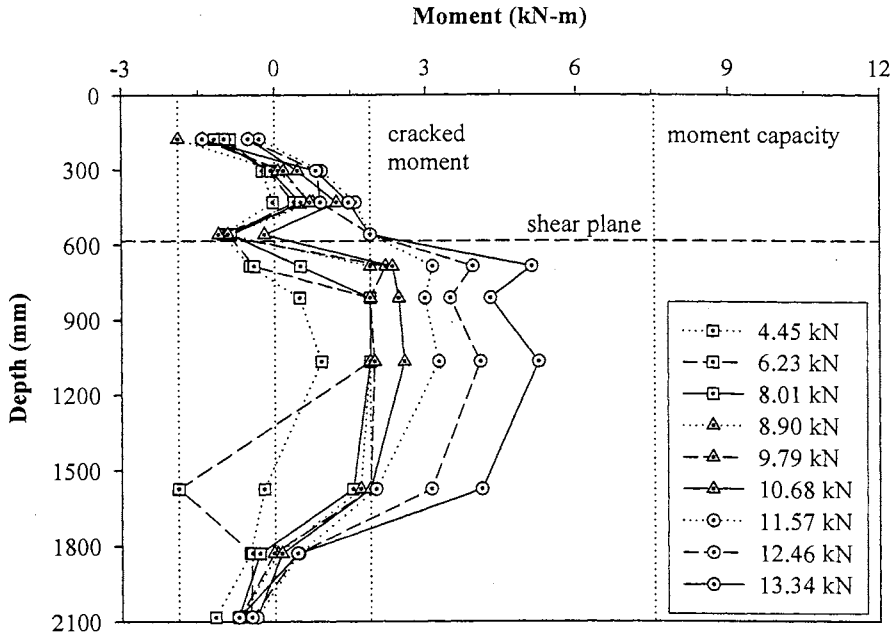

Figure 138 – Moment Profiles for Reinforced Glacial Till (Pile 9)

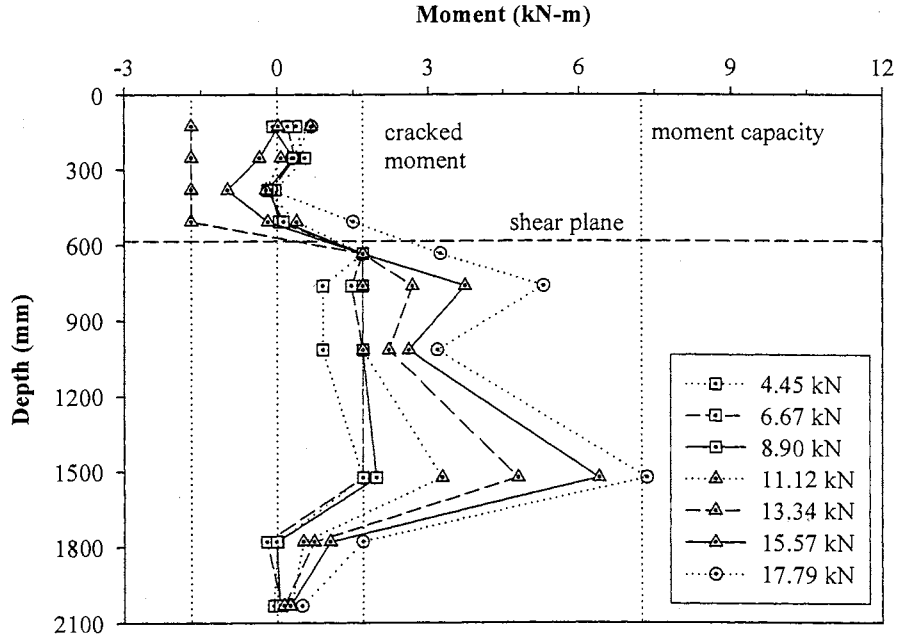

Figure 139 – Moment Profiles for Reinforced Weathered Shale (Pile 12)

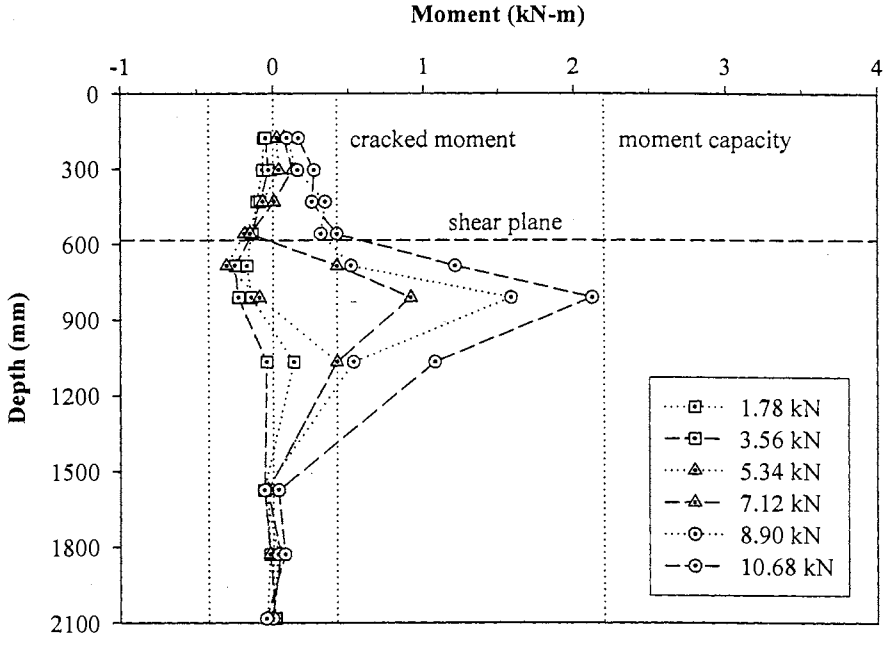

Figure 140 – Moment Profiles for Reinforced Loess (Pile 11 A)

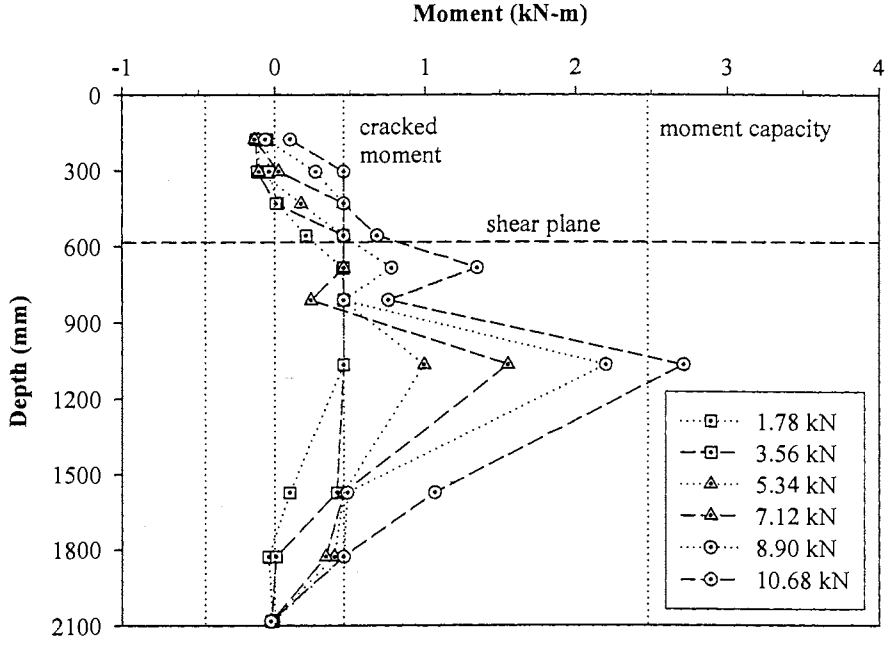

Figure 141 – Moment Profiles for Reinforced Loess (Pile 11 B)

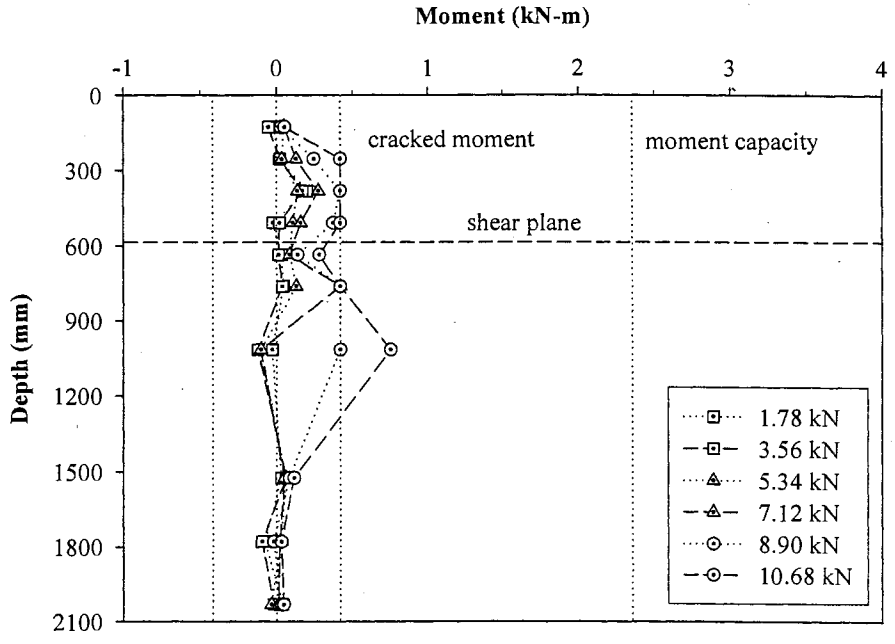

Figure 142 – Moment Profiles for Reinforced Glacial Till (Pile 13 A)

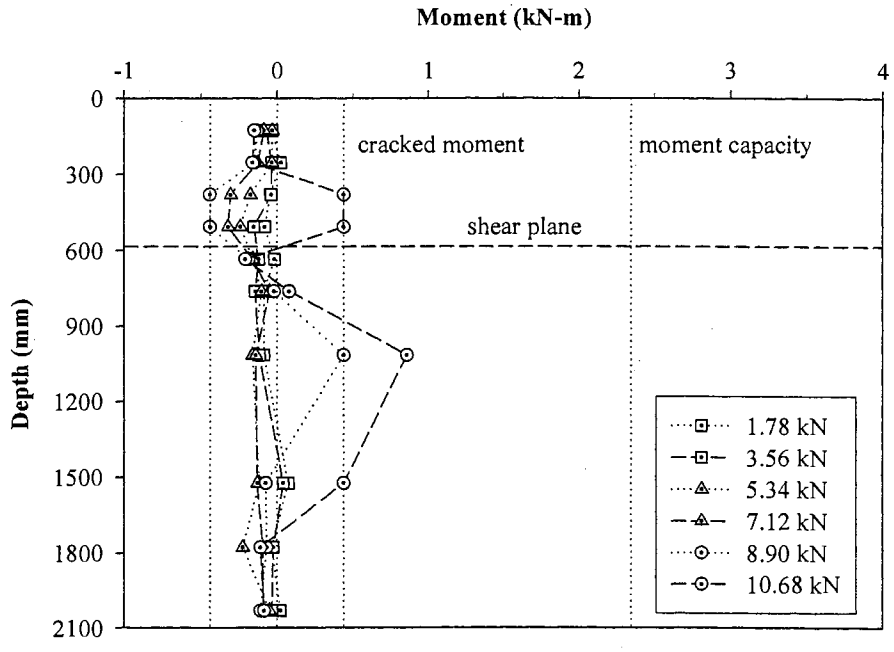

Figure 143 – Moment Profiles for Reinforced Glacial Till (Pile 13 B)

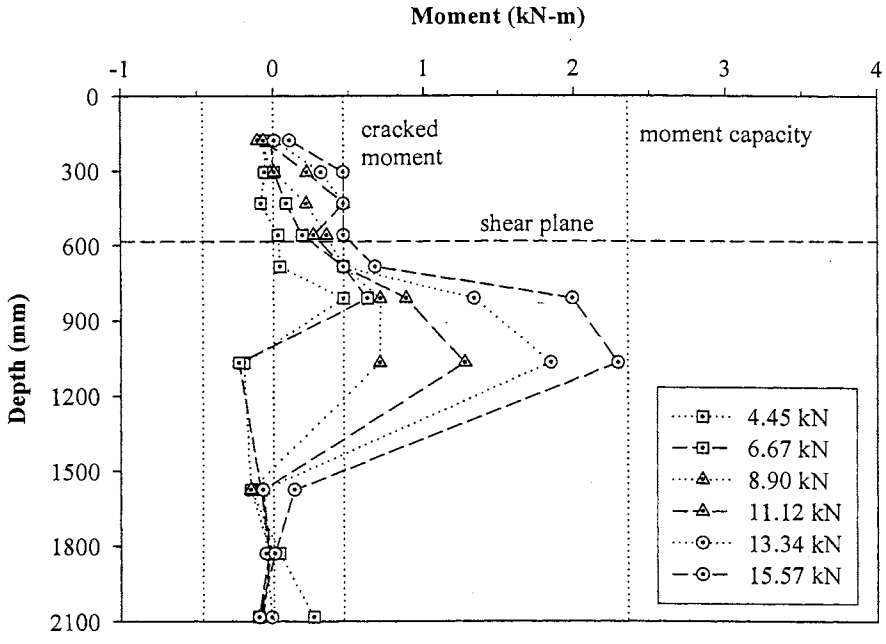

Figure 144 – Moment Profiles for Reinforced Glacial Till (Pile 14 B)

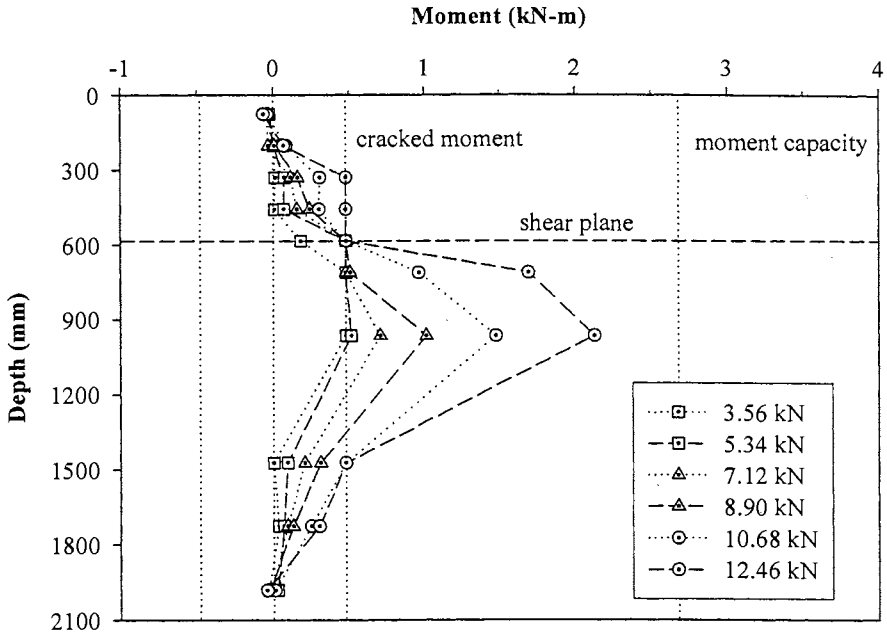

Figure 145 – Moment Profiles for Reinforced Weathered Shale (Pile 10 A)

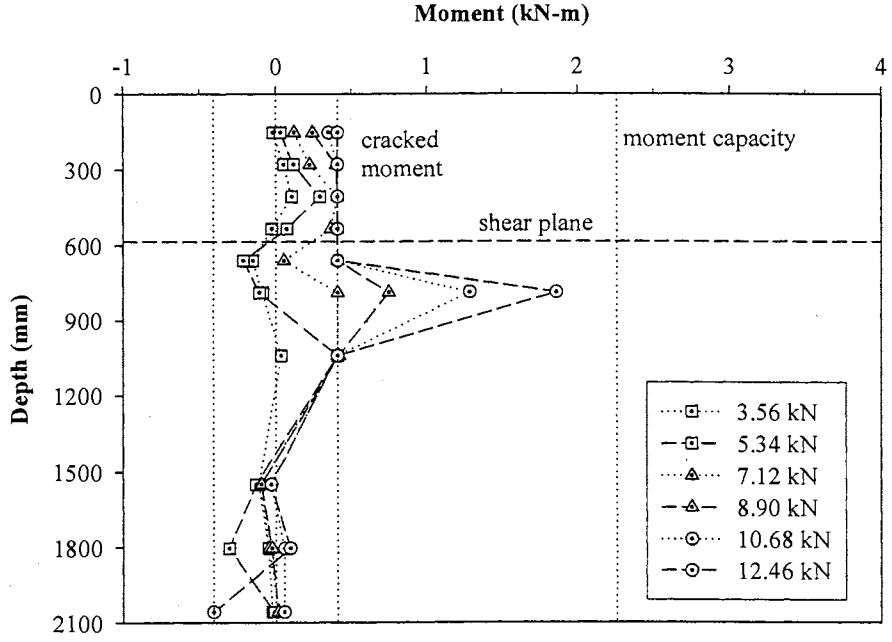

Figure 146 – Moment Profiles for Reinforced Weathered Shale (Pile 10 B)

PHOTOGRAMMETRY

The research group mounted cameras above the piles of each load test to document the observed behavior of pile heads and surface soil at different stages during pile loading. The pictures of Figures 150 through 159 effectively illustrate the gap formation between the pile head and surface soil. The pictures also indicate stress build-up around the piles. Radial cracking observed in front of the piles warrants a brief discussion on the relationship between radial and tangential stress, and the discussion is extended to include soil arching phenomena.

Relationship Between Radial and Tangential Stress

The major principal stress of soil at the upslope, soil-pile interface, applied in the radial direction of the pile and referred to as radial stress, increases during uniform lateral translation of soil. Cavity expansion theory suggests that an expanding cylinder in soil offers an elastic response mechanism of the soil, whereby the radial stress increases (Handy and White unpublished). The radial stress increase, directly related to the loading condition of the pile, is accompanied by a decrease in tangential stress of the same amount for a given radial distance from the cylinder. The tangential stress becomes negative after the radial stress exceeds two times the in-situ lateral stress. As soil is capable of withstanding negligible tension (i.e. not to exceed apparent cohesion, if applicable), tension cracks appear in the radial direction about the cavity. The series of tension cracks are also referred to as radial cracks. Figure 147 illustrates the relationship between radial and tangential stresses with Mohr's circle depiction of the change stress state with loading. Figure 148 shows the radial and tangential stresses of a single pile subject to lateral soil movement.

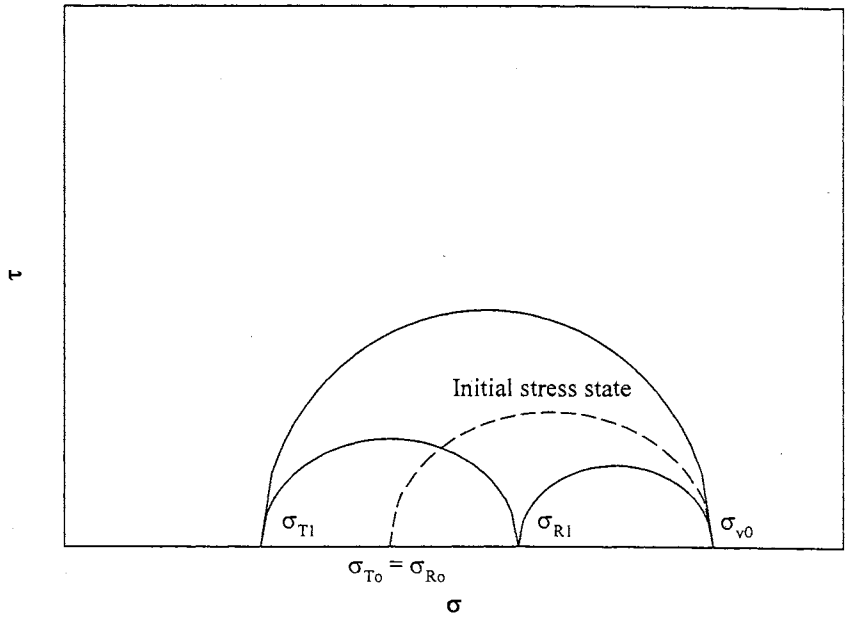

Figure 147 – Mohr's Circle Depiction of Stress State Change With Loading

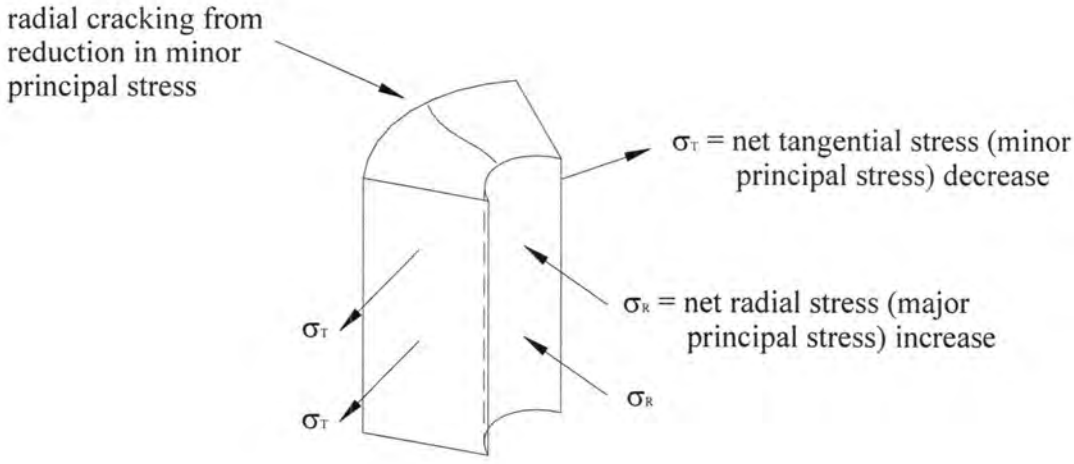

(a)

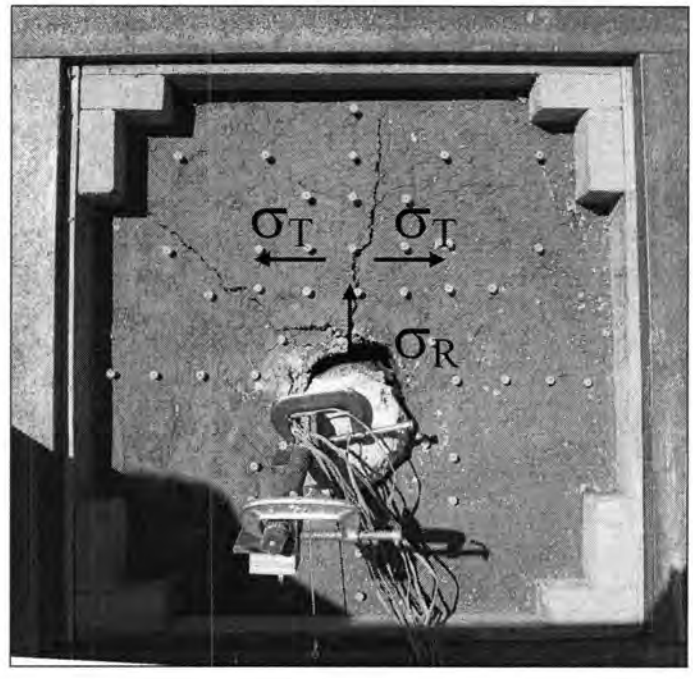

(b)

Figure 148 – Radial and Tangential Stresses of Single Piles Subject to Soil Movement

Grouped Piles Subject to Lateral Soil Movement and Soil Arching

Soil arching is the transfer of stresses from yielding soil to adjacent, non-yielding soil. The phenomenon is observed in the application of pile stabilization, where an arch occurs between stiff pile elements installed in a row. The influence of soil arching on pile stabilization generally benefits the stability of reinforced slopes. Unfortunately, research investigators and design engineers do not fully understand the conditions necessary for soil arching to occur or the quantitative effects of soil arching on the capacity of slope reinforcement.

Soil arching was observed in the pile load tests of multiple piles subject to lateral soil movement. The phenomenon was evidenced by an arch that developed between adjacent piles of the tests. The research group describes the formation of the arch in terms of radial and tangential stresses of soil. As for single piles subject to lateral soil movement, radial stresses develop in front of grouped piles. The difference between single piles and multiple piles subject to lateral soil movement is that the directions of the major principal stresses from multiple piles do not extend radially from the pile centers, but rather form an arch. The arch is the path of the major principal stress, and the direction perpendicular to the arch is direction in which the minor principal stress acts. The major principal stress increase is still accompanied by a decrease in the minor principal stress, and the reduced minor principal stresses that occur during loading result in tension cracks in the direction parallel to the major principal stress. The arch formation is illustrated in Figure 149.

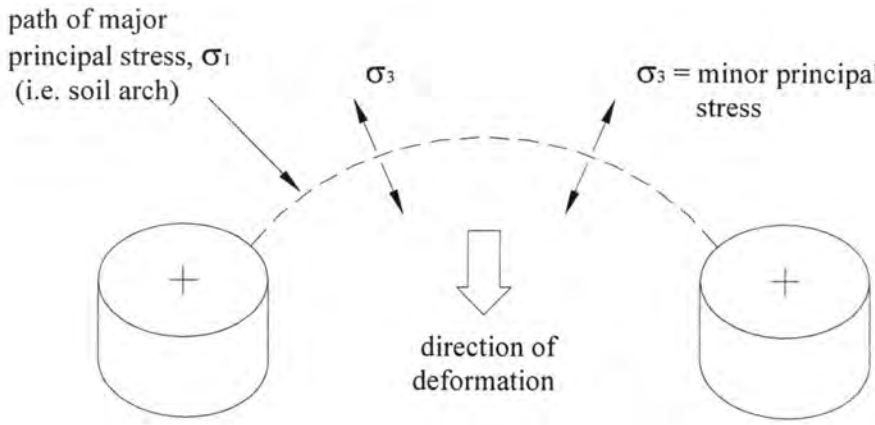

(a)

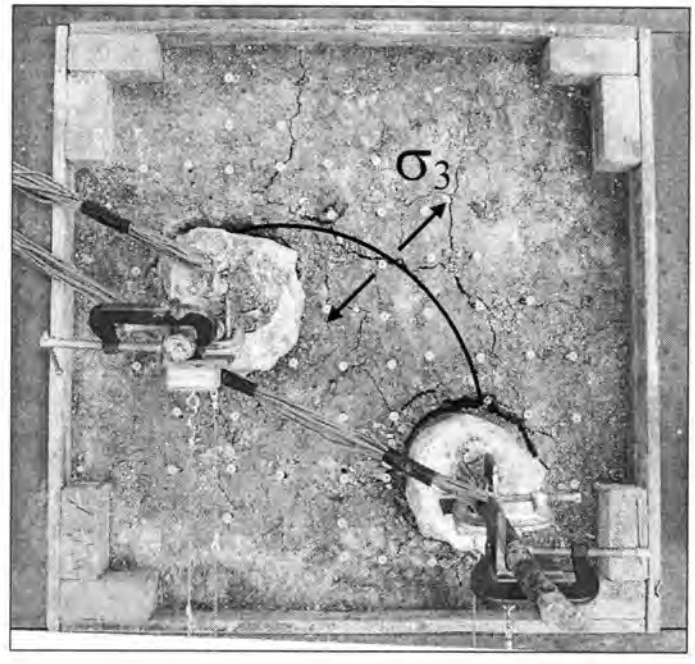

(b)

Figure 149 – Radial and Tangential Stresses of Multiple Piles Subject to Soil Movement

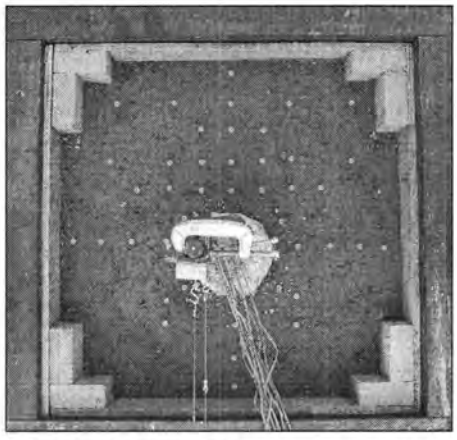

(a)

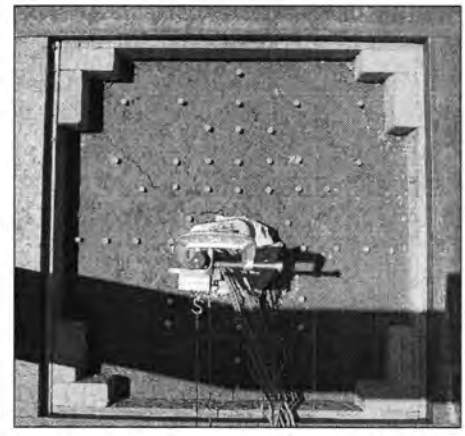

(b)

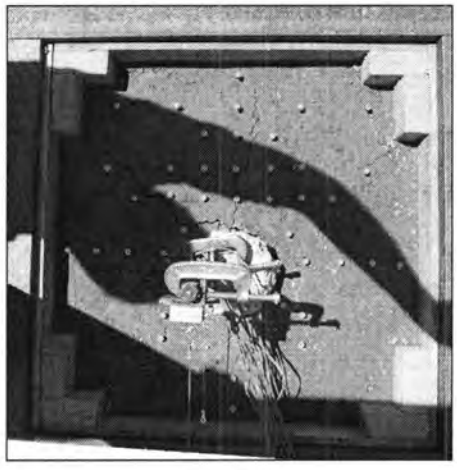

(c)

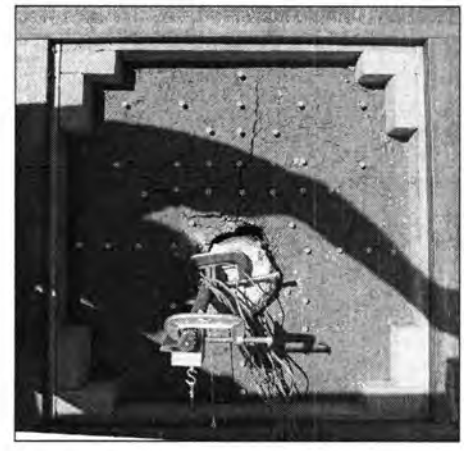

(d)

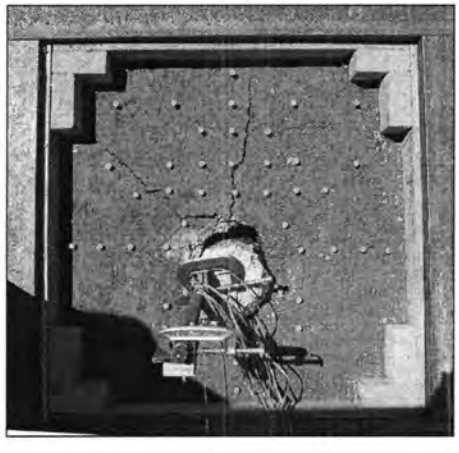

(e)

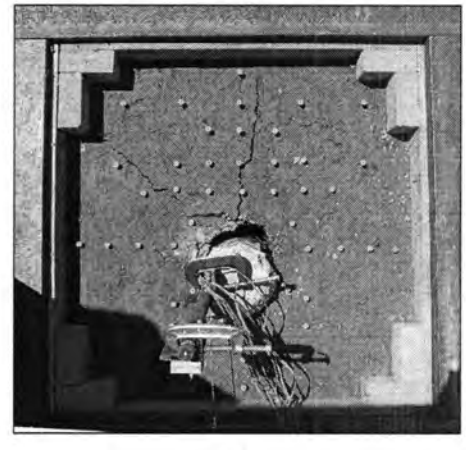

(f)

Figure 150 – Box 4 Photogrammetry Pictures (127-mm Pile in Loess)

(a) 0 cm; (b) 0 cm; (c) 5 cm; (d) 13 cm; (e) 15 cm; (f) 16 cm

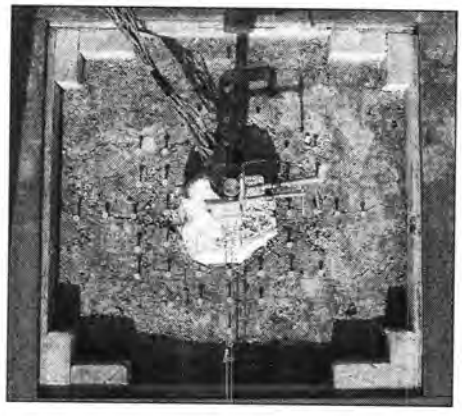

(a)

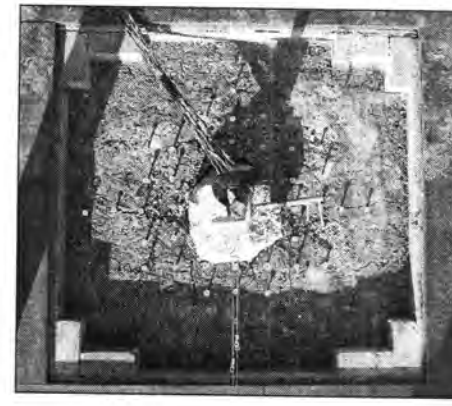

(b)

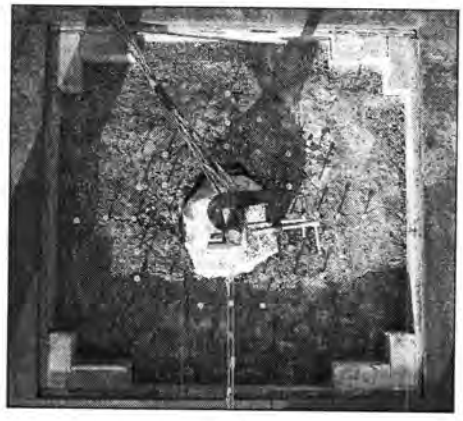

(c)

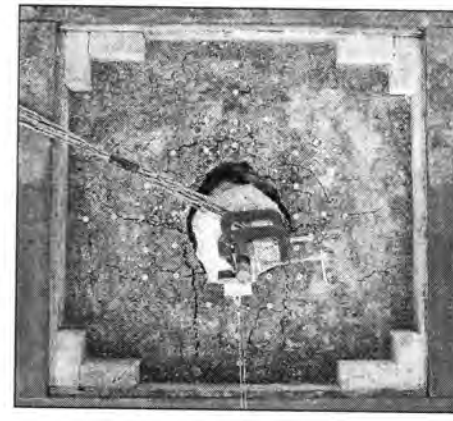

(d)

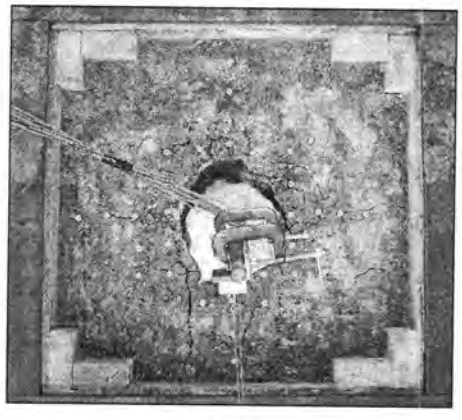

(e)

Figure 151 – Box 5 Photogrammetry Pictures (127-mm Pile in Glacial Till)

(a) 0 cm; (b) 2 cm; (c) 6 cm; (d) 13 cm; (e) 21 cm

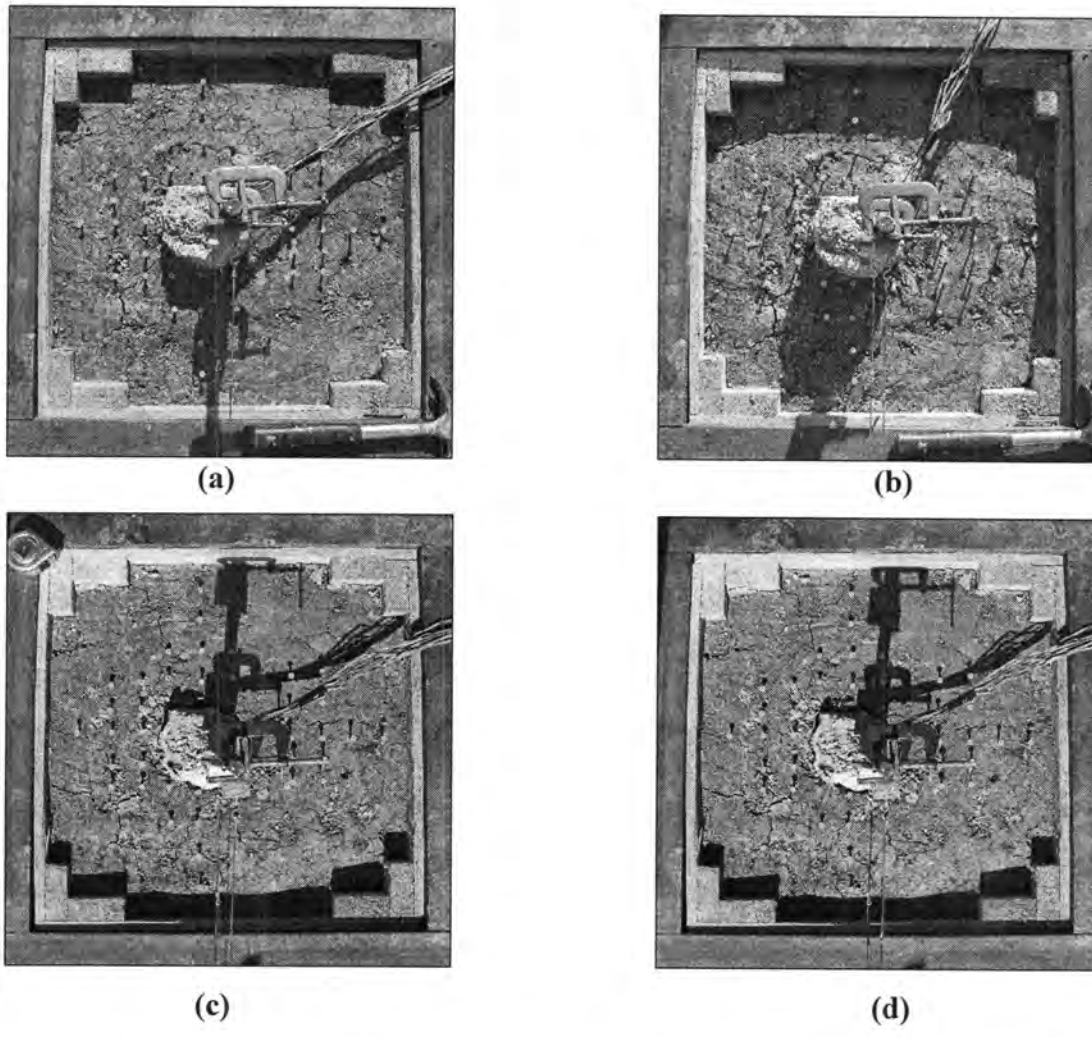

Figure 152 – Box 6 Photogrammetry Pictures (127-mm Pile in Weathered Shale)

(a) 0 cm; (b) 3 cm; (c) ~ 4 cm; (d) ~ 10 cm

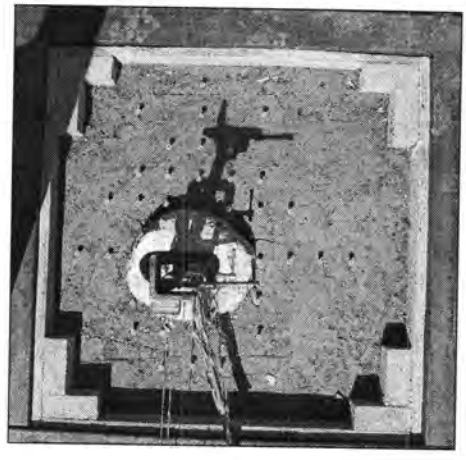

(a)

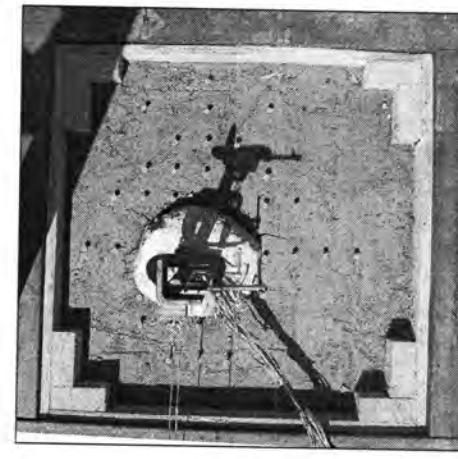

(b)

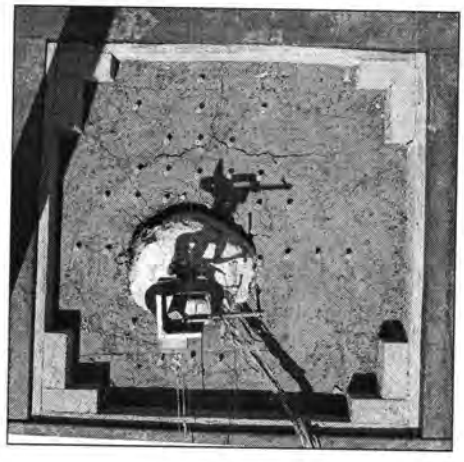

(c)

Figure 153 – Box 8 Photogrammetry Pictures (178-mm Pile in Loess)

(a) 0 cm; (b) 1 cm; (c) 3 cm

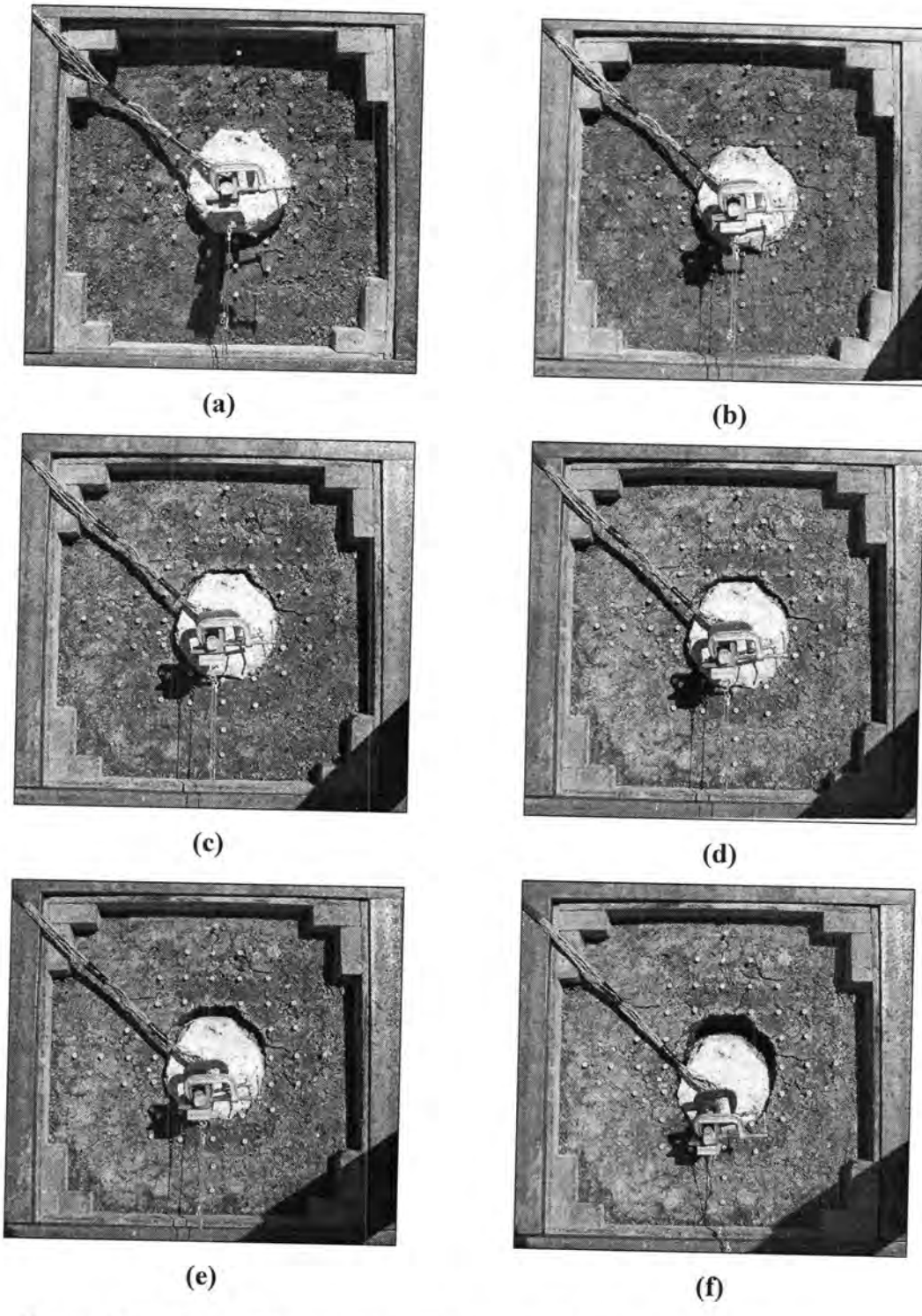

Figure 154 – Box 9 Photogrammetry Pictures (178-mm Pile in Glacial Till)

(a) 0 cm; (b) 4 cm; (c) 7 cm; (d) 8 cm; (e) 11 cm; (f) 17 cm

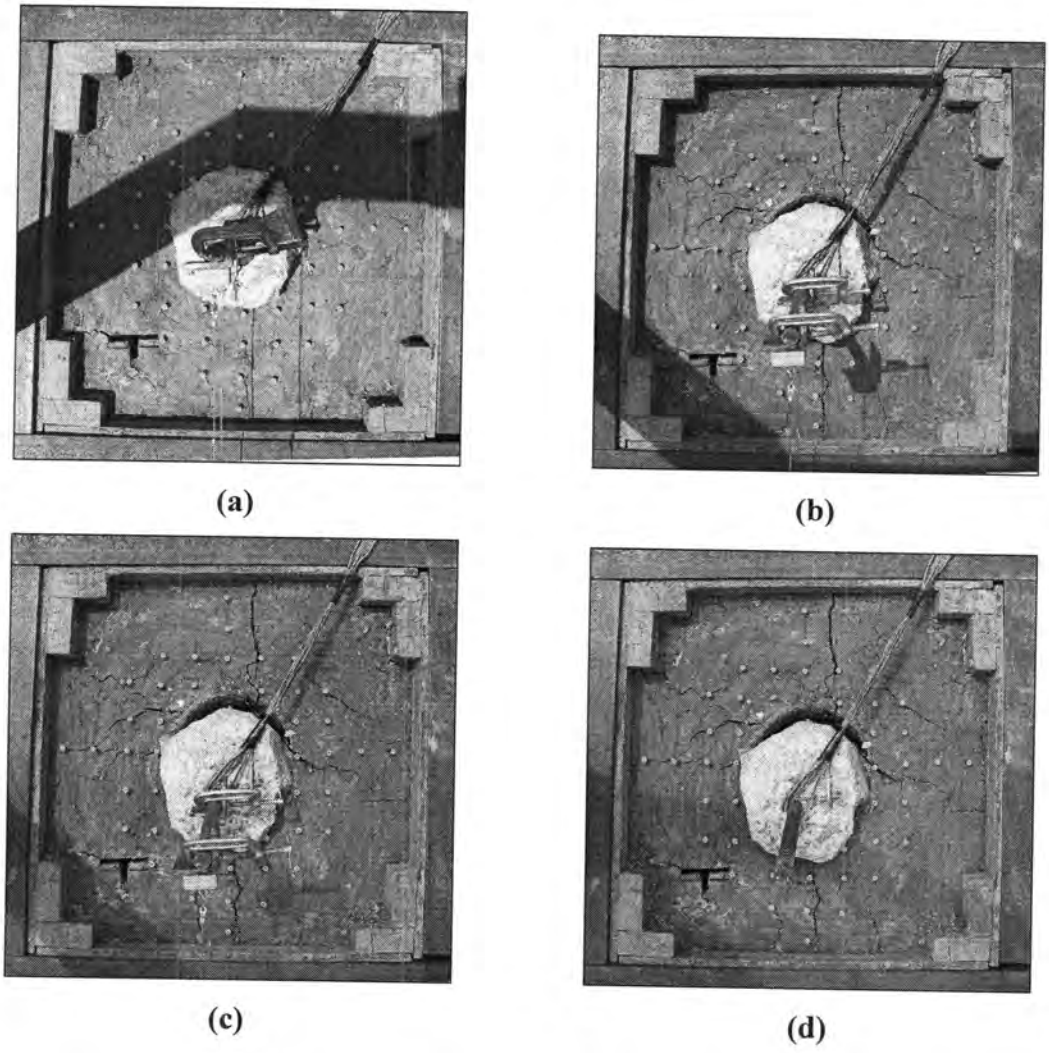

Figure 155 – Box 12 Photogrammetry Pictures (178-mm Pile in Weathered Shale)

(a) 0 cm; (b) 14 cm; (c) 19 cm; (d) 20 cm

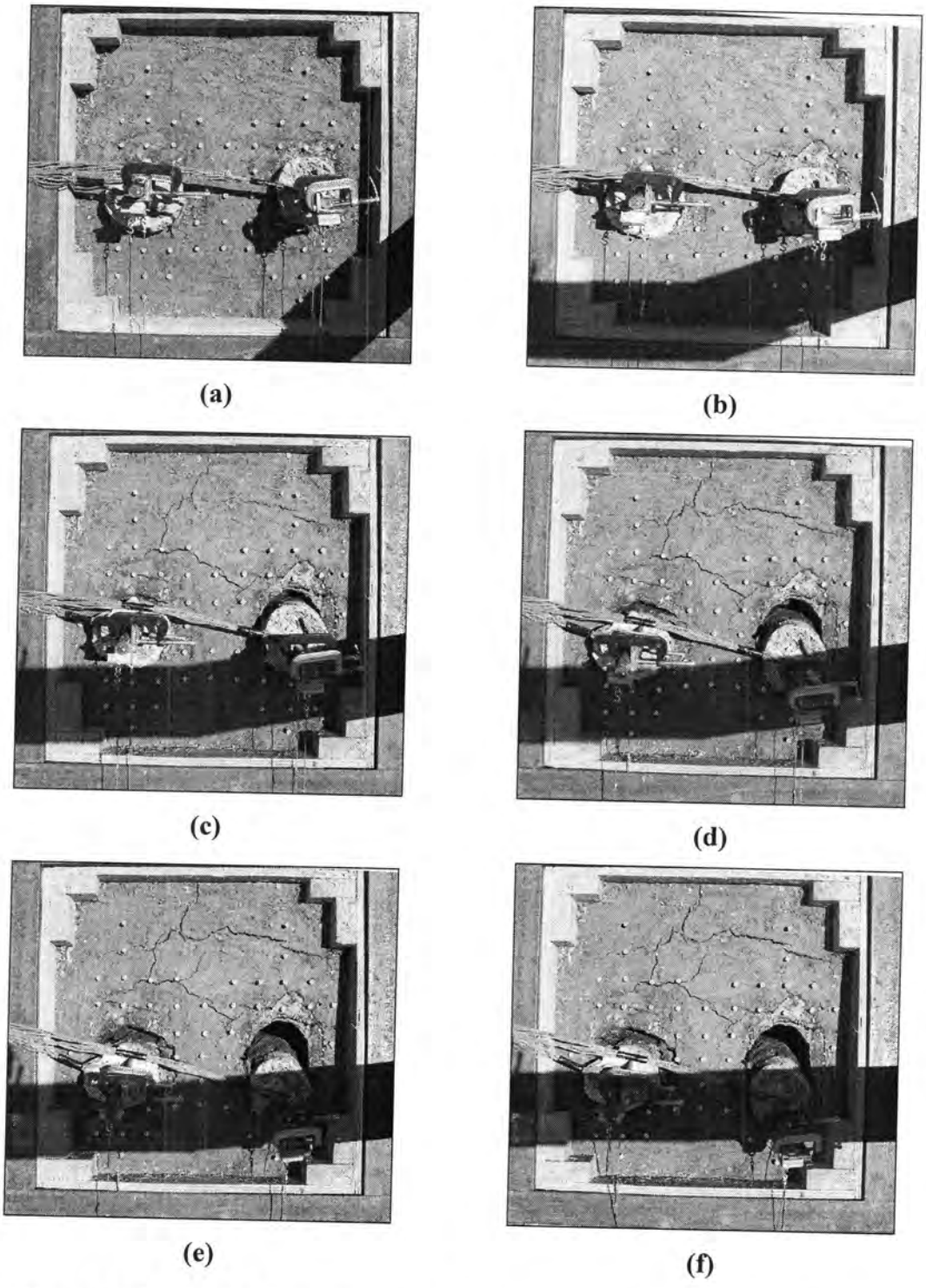

Figure 156 – Box 11 Photogrammetry Pictures [(2) 127-mm Piles in Loess]

(a) 0 cm; (b) 2 cm; (c) 11 cm; (d) 15 cm; (e) 23 cm; (f) 25 cm

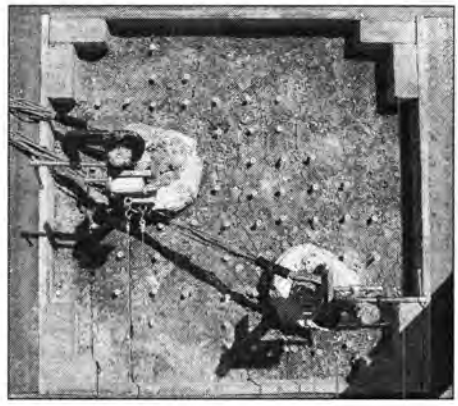

(a)

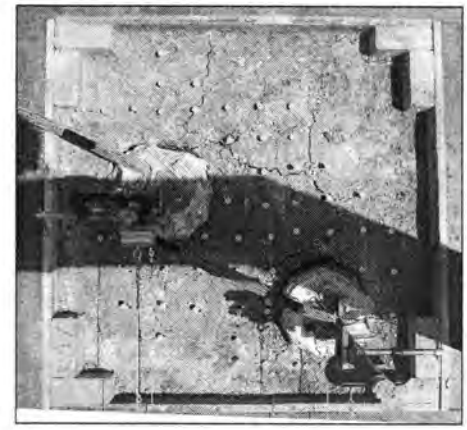

(b)

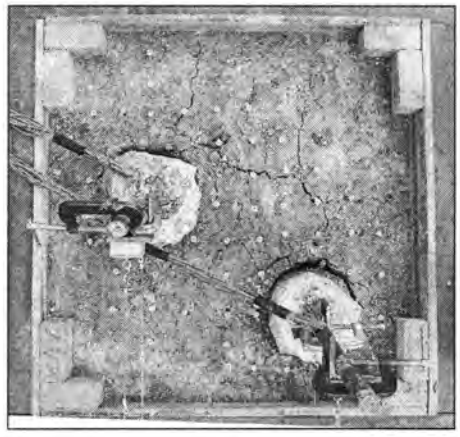

(c)

Figure 157 – Box 13 Photogrammetry Pictures [(2) 127-mm Piles in Glacial Till]

(a) 0 cm; (b) 10 cm; (c) 14 cm

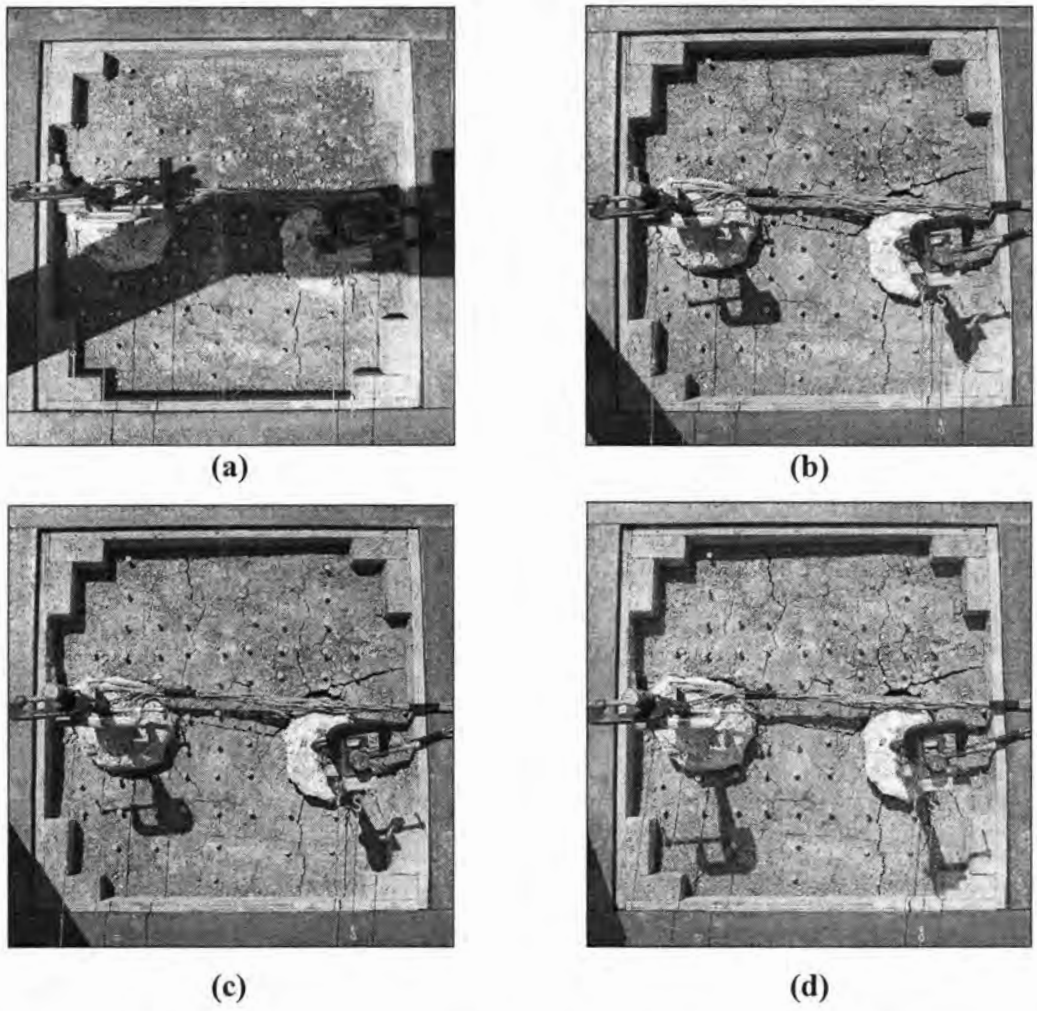

Figure 158 – Box 14 Photogrammetry Pictures [(2) 127-mm Piles in Glacial Till]

(a) 0 cm; (b) 8 cm; (c) 10 cm; (d) ~ 13 cm

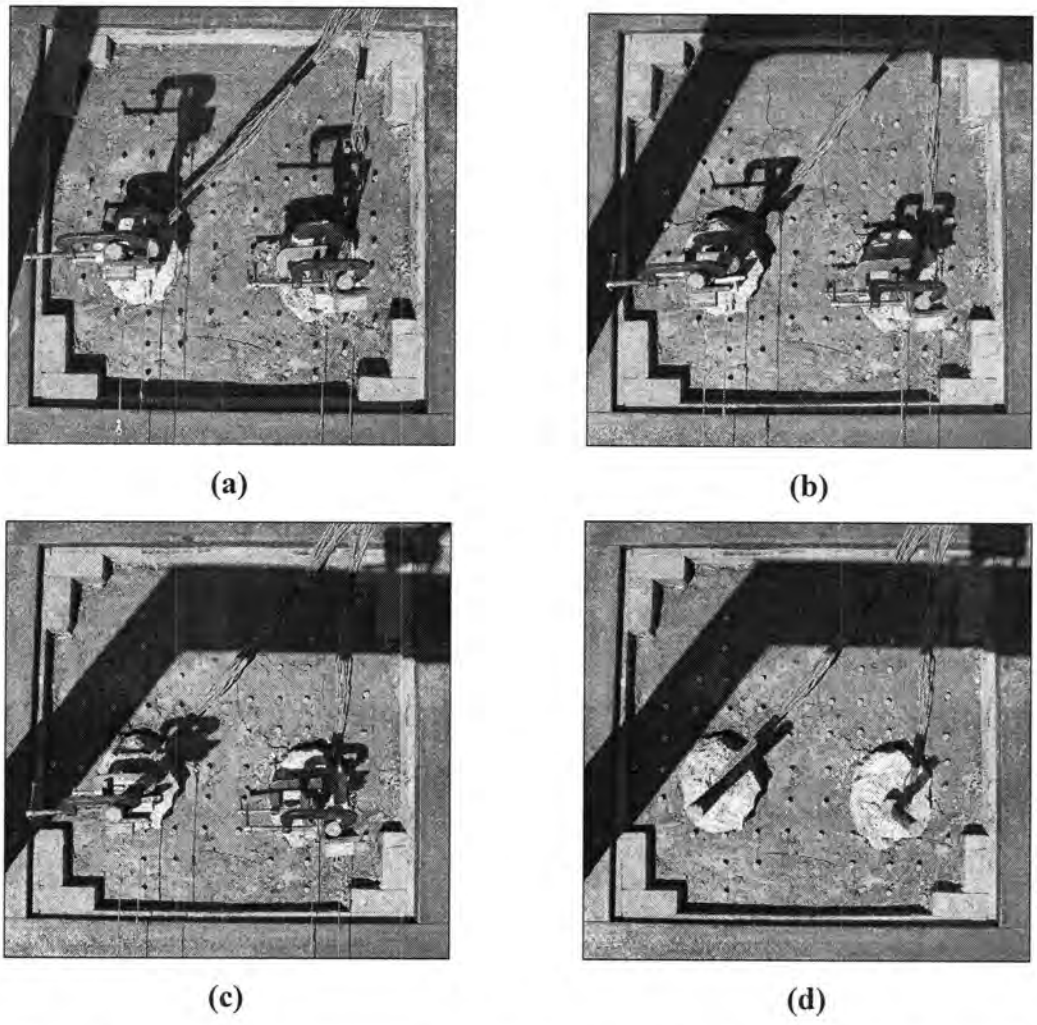

Figure 159 – Box 10 Photogrammetry Pictures [(2) 127-mm Piles in Weathered Shale]

(a) 0 cm; (b) 8 cm; (c) 15 cm; (d) End

SOIL SAMPLING

The compacted soil from select boxes was sampled after the performance of pile load tests. Sampling with Shelby tubes and in-situ testing devices offered evidence of soil conditions before and after loading of piles. Specifically, the research group evaluated moisture and density, strength profiles, and lateral earth pressure profiles.

Moisture and Density

Shelby tube samples were taken from select boxes, and ranges for unit weight and moisture contents were determined.

Table 21 – Measured Unit Weight and Moisture Content

Soil Type	γ_d (kN/m^3)	w (%)	n	$\gamma_{d,max}$ (kN/m^3)	w_{opt} (%)
Loess	13.8 – 14.8	25 - 35	5	15.6	18
Glacial Till	18.5 – 19.2	14 - 18	6	17.8	14
Weathered Shale	16.5 – 18.2	18 - 23	2	16.7	18

Notes:
n = number of samples

Dynamic Cone Penetrometer (DCP)

The dynamic cone penetrometer (DCP) is an instrument used principally for pavement evaluation and construction control. The data obtained in the field is most commonly used to develop pavement structural numbers, CBR, and elastic moduli values (ASTM 2003). The research group, for this project, used the dynamic cone penetrometer to evaluate the uniformity of soil within the soil boxes. Uniform CBR profiles suggest uniform density, whereas variable CBR profiles suggest variable density attributed to non-uniform compaction effort. The CBR values were developed from equations presented in ASTM D 6951-03 [Use of the Dynamic Cone Penetrometer in Shallow Pavement Applications] (ASTM 2002), as follows:

$$CBR = \frac{292}{DCP^{1.12}}, \text{ for loess} \tag{27}$$

$$CBR = \frac{1}{(0.017019 \cdot DCP)^2}, \text{ for glacial till and weathered shale} \tag{28}$$

Table 22 provides average DCP Index and CBR values for each soil type. The values are averages through the profile of the shear box soil and the soil of the control pads. Figures 160 through 162 show the CBR profiles for compacted loess, glacial till, and weathered shale.

Table 22 – Profile (915 mm) Average DCP Index and CBR Values

Soil Type	Test	Average DCP (mm/blow)	Average CBR
Loess	1	163	1.8
	4	198	1.0
	8	165	1.3
	11	150	1.2
Glacial Till	3	84	2.1
	5	74	2.5
	9	62	3.8
	14	74	3.0
Weathered Shale	2	71	2.6
	6	55	3.4
	12	59	3.3
	10	90	2.1

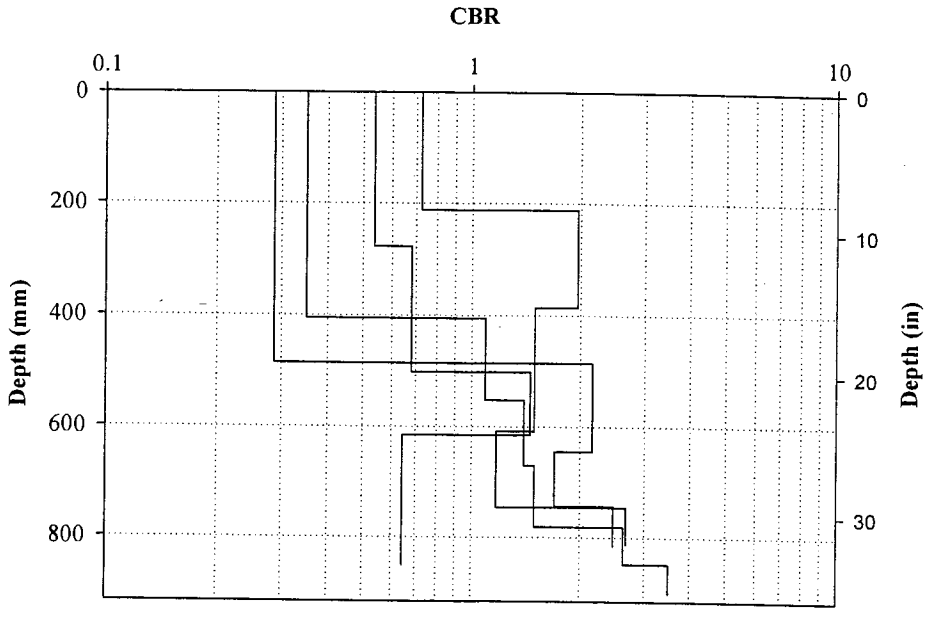

Figure 160 – DCP Results in Loess

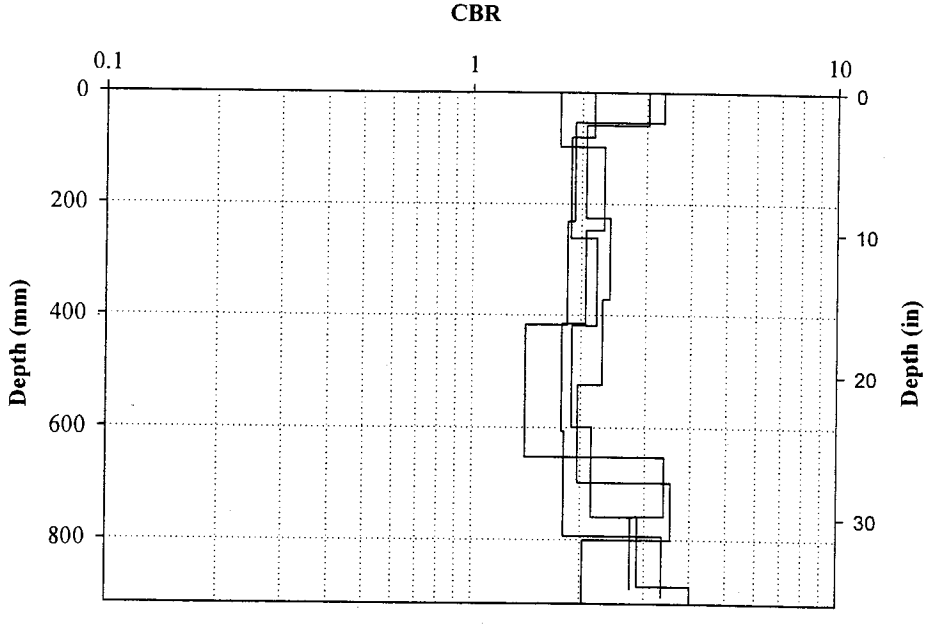

Figure 161 – DCP Results in Glacial Till

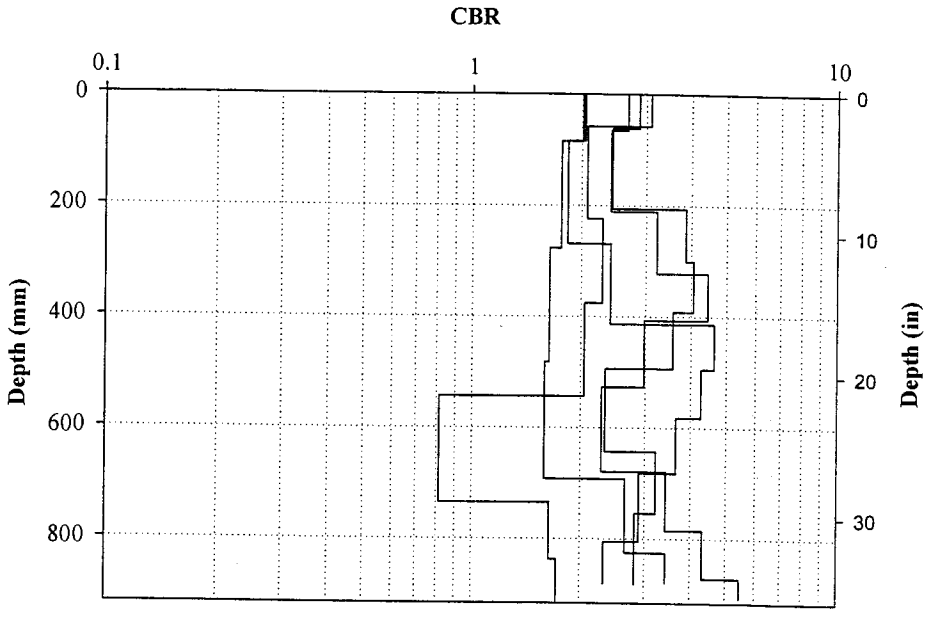

Figure 162 – DCP Results in Weathered Shale

K_o Stepped Blade

The Ko Stepped Blade was developed at Iowa State University to measure the in-situ lateral stress condition of soil. Soil pressures corresponding to known levels of disturbance are measured with pneumatic cells designed using a pressure-balance principle (Mings 1987). The relationship between soil disturbance and measured stress is subsequently used to extrapolate a pre-insertion (undisturbed) soil stress. The extrapolation principle is diagrammed in Figure 163.

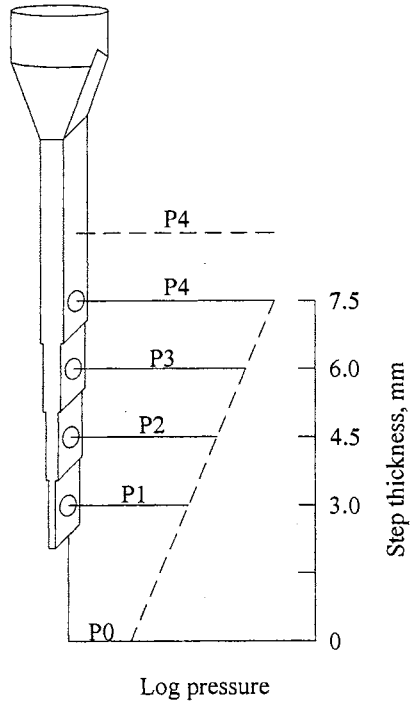

Figure 163 – Extrapolation Principle of K_o Stepped Blade (after Mings 1987)

The Ko stepped blade device is shown in Figure 164, and the Ko stepped blade test performance is shown in Figure 165. The Ko stepped blade test was performed in weathered shale, on four sides of a 178-mm pile.

Figure 164 – K_o Stepped Blade Device

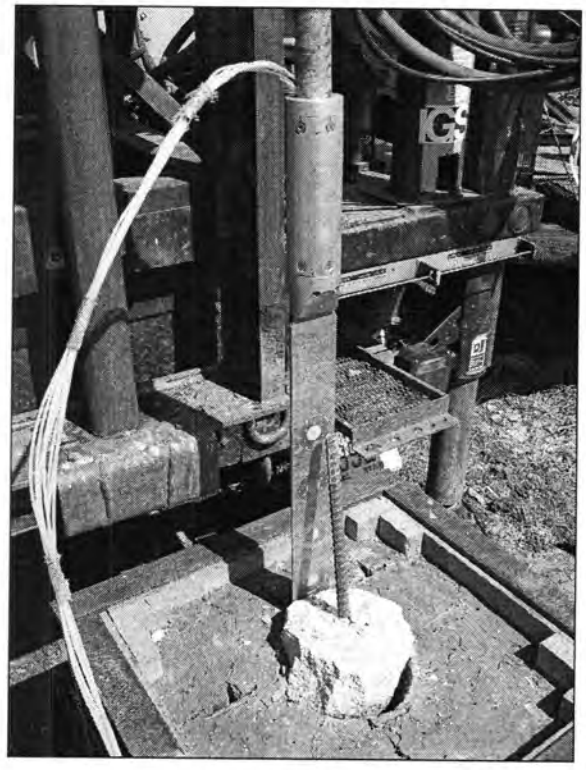

Figure 165 – K_o Stepped Blade Test Performance

The Ko stepped blade test was incorporated into the soil sampling plan to support the observed soil behavior around piles subject to lateral soil movement. The research group observed the formation of a gap at the soil surface at the front (i.e. load side) of the pile. The gap was a consequence of pile head rotation away from the load. Associated with the gaps are unloaded lengths of pile in the direction of shear box movement and low lateral soil pressures in front of the pile. Conversely, the research group observed bulging of soil behind the pile. Associated with the bulging soil are loaded lengths of pile in the direction opposing shear box movement and high lateral soil pressure behind the pile. At greater depths, the lateral soil pressure in front of the pile exceeds the lateral soil pressure behind the pile, confirming that the net load is applied to piles in the direction of lateral soil movement. Figures 166 and 167 show the formation of a gap and soil bulging observed during testing.

Figure 166 – Gap in Front of Pile (115-mm Pile in Glacial Till)

Figure 167 – Soil Bulging Behind Pile (115-mm Pile in Glacial Till)

Figures 168 through 171 show the extrapolation of lateral soil pressure at four locations within the weathered shale reinforced with a 178-mm pile. Figures 172 and 173 show the lateral stress profiles of the box. Figure 172 supports the previously discussed behavior of soil in front and behind the pile. The lateral stress in front of the pile is low at the top of the box and high at the bottom of the box, whereas the lateral stress behind the pile is high at the top of the box and low at the bottom of the box. The lateral stress on each side of the pile, as shown in Figure 173, is relatively constant with depth.

The magnitudes of lateral stress from the Ko Stepped Blade test, at first glance, appear high. The research group speculated that the cohesion of weathered shale was responsible the test results. The Rankine passive earth pressure was evaluated for the soil condition, as follows (Das 1999):

$$\sigma_p = \sigma_v K_p + 2c\sqrt{K_p} \qquad (29)$$

where, $\gamma = 17.5\ \text{kN/m}^3$

$c = 27.6$ kPa, from unconfined test

$K_p = 2.2$ for $\phi = 22°$

The Rankine passive earth pressure is shown on the lateral stress profiles of Figures 172 and 173. Despite the slightly-high lateral stress values from the tests, the qualitative information of the figures is valuable for understanding the system behavior.

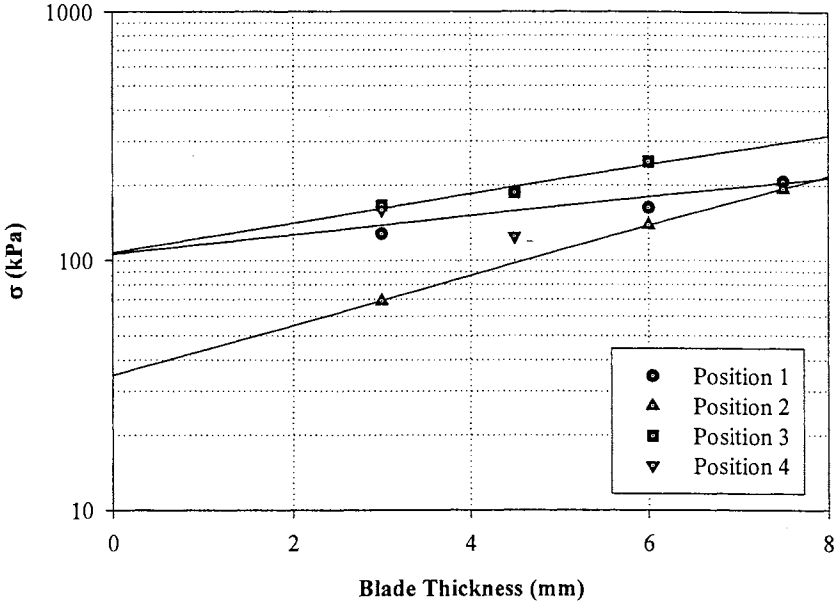

Figure 168 – Ko Stepped Blade Results (Behind Pile)

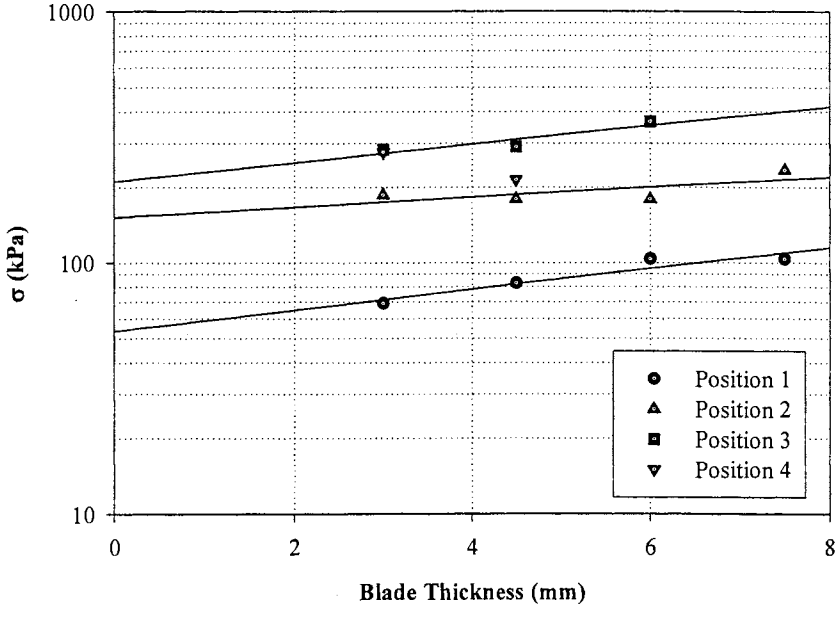

Figure 169 – Ko Stepped Blade Result (Front of Pile)

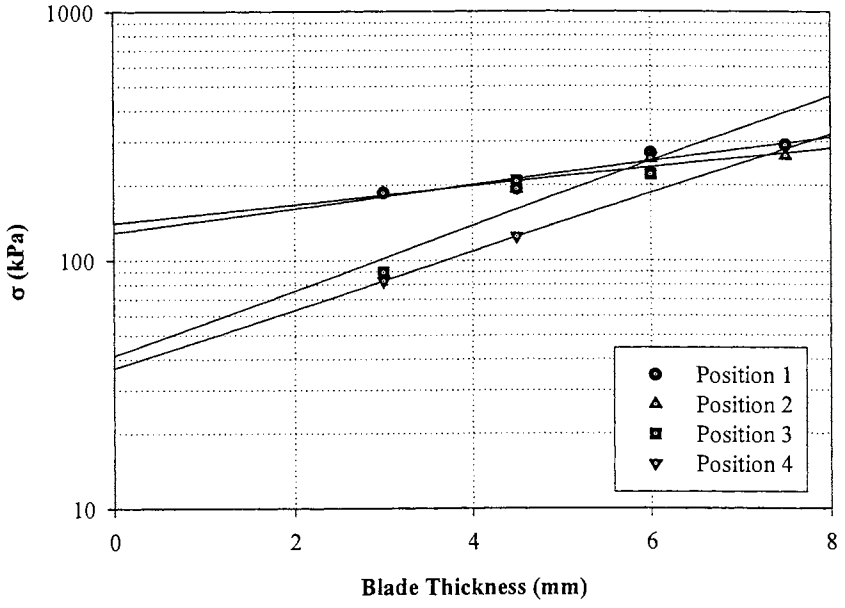

Figure 170 – Ko Stepped Blade Results (Left Side of Pile)

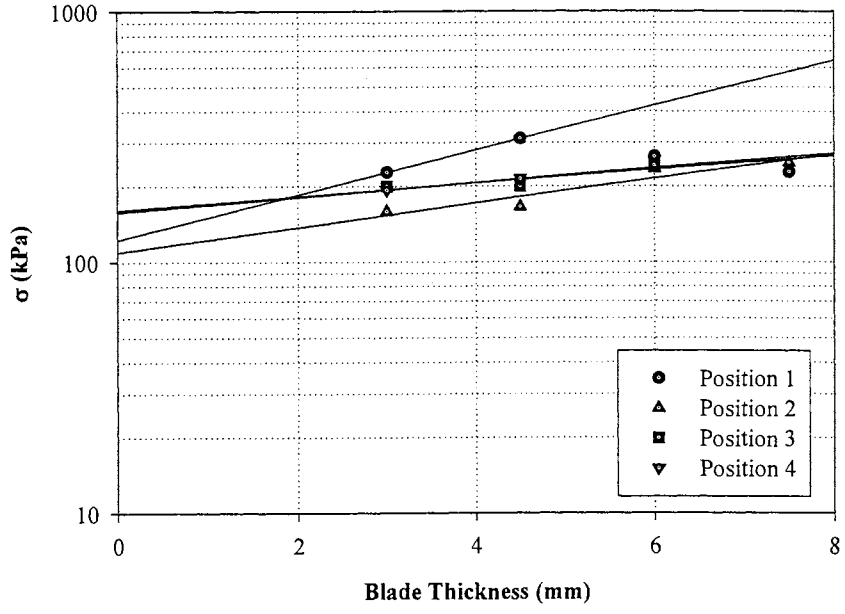

Figure 171 – Ko Stepped Blade Results (Right Side of Pile)

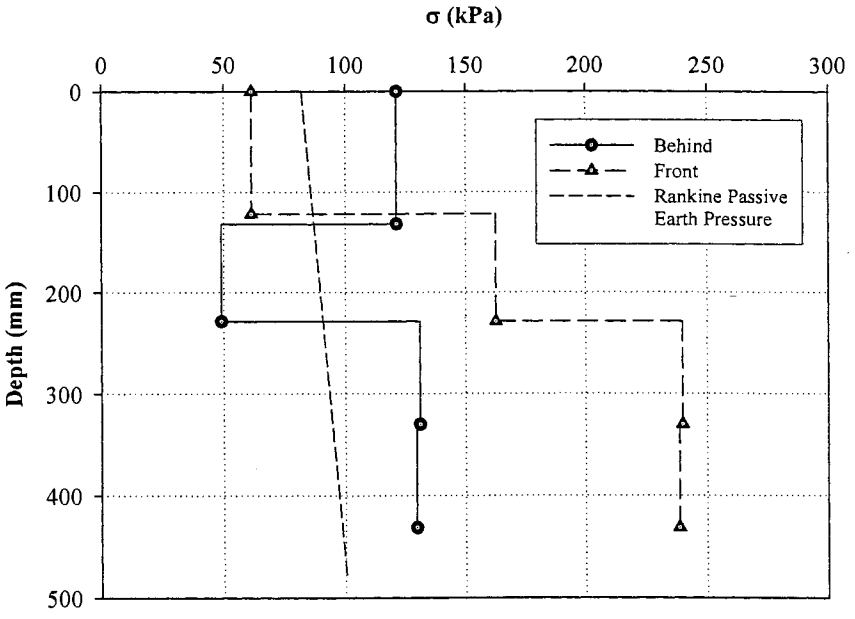

Figure 172 – Lateral Earth Pressure Profiles (Behind and Front of Pile)

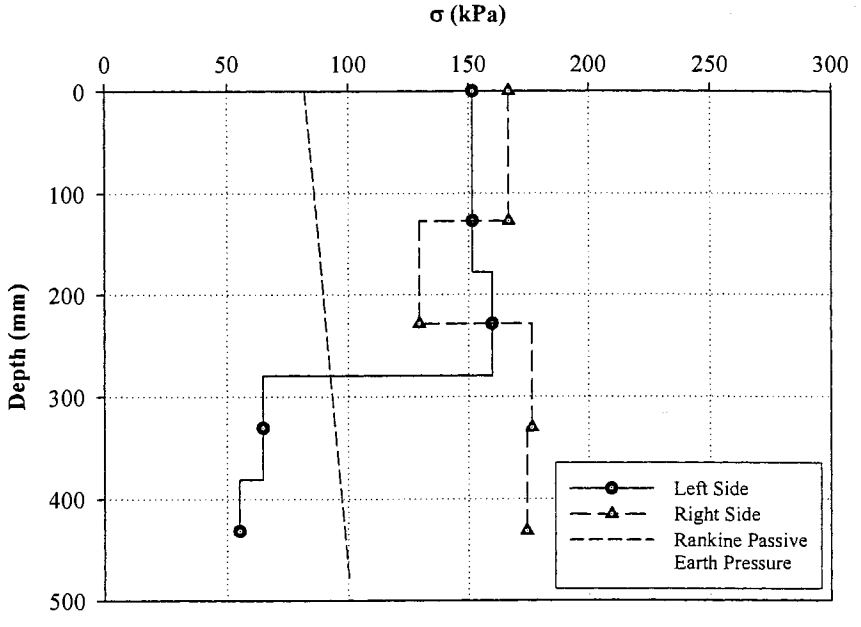

Figure 173 – Lateral Earth Pressure Profiles (Sides of Pile)

EXHUMATION OF PILES

The piles of each load test were exhumed to examine pile condition after failure, pile uniformity, and pile diameter. The exhumation of piles offered physical evidence of the failure of piles due to mobilization of the pile moment capacity. Figure 174 shows a representative pile failure. Moreover, the figure shows that the depth at which the maximum moment developed is approximately four pile diameters below the shear surface. The failure depth agrees with depths of maximum measured strain and, therefore, supports the load test results.

Figures 175 through 177 show that the installed piles were quite cylindrical. Irregularities of pile diameter with depth were of small magnitude, and circular pile sections for the load test analyses were employed with minimal consequence. The load test analysis required accurate pile dimensions for the development of unique moment-curvature relationships (see Appendix B). Upon exhumation of the piles, the piles were cleaned and the diameters were measured at several locations along the pile length. The measured pile diameters are provided in Table 23.

(a)

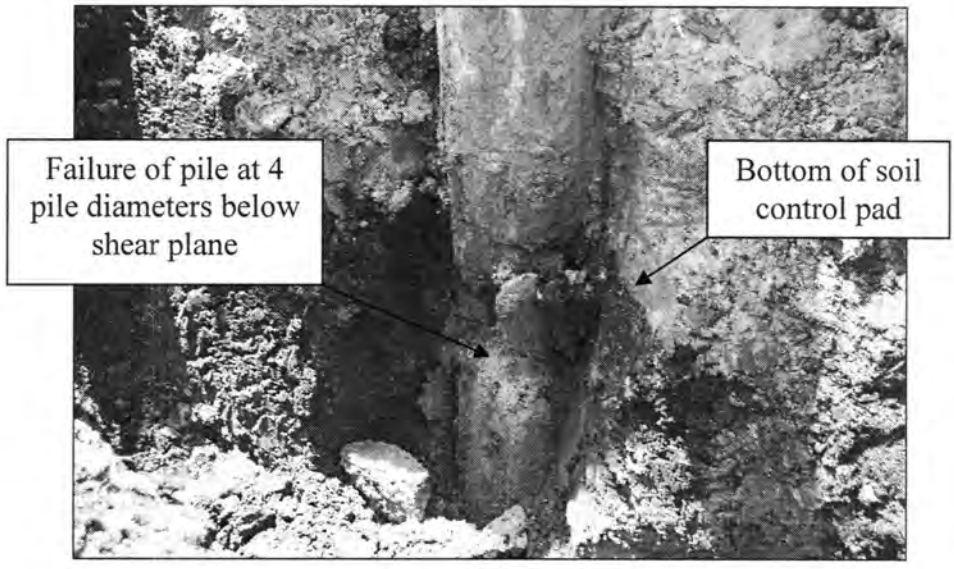

(b)

Figure 174 – Exhumation of Piles

(a) Exhumation of piles with excavator; (b) Location of maximum moment and pile failure

Figure 175 – Exhumed 127-mm Pile (Pile 5)

Figure 176 – Exhumed 178-mm Pile (Pile 9)

Figure 177 – (2) Exhumed 127-mm Piles (Pile 14 A and 14 B)

Table 23 – Measured Diameters of Exhumed Piles

Pile	Diameter (mm)
4	114
5	112
6	117
7	114
8	183
9	178
10 A	114
10 B	112
11 A	114
11 B	114
12	173
13 A	112
13 B	114
14 A	114
14 B	117

CHAPTER 5

LOAD TEST ANALYSIS AND DISCUSSION OF RESULTS

INTRODUCTION

The principal objectives of the load test analysis and characterization of load transfer of piles subject to lateral soil movement are: (1) to determine the load distributions induced on piles due to lateral soil movement, (2) to determine the ultimate soil pressure as a function of depth, and (3) to verify the predicted structural performance of pile elements under the loading conditions of slope reinforcement. The achievement of the analysis objectives supports the understanding of load transfer mechanisms of the system and the development of the proposed design methodology.

LOAD TEST ANALYSIS

Determination of Total Resisting Forces

The determination of total resisting forces, ΔF_R, is important for understanding the load transfer mechanisms of piles subject to downslope soil movement and the principal objective in designing pile stabilization. The total resisting forces, equal to the integration of loads developed along the length of pile subject to downslope soil movement, are directly incorporated into the limit equilibrium equations of global slope stability analyses to determine the factor of safety for the reinforced slope. In designing pile stabilization, an engineer uses the load development along a pile to calculate the total resisting force that acts to oppose slope movement. The analysis of load test data, however, is performed to

determine the load development along the pile. The total resisting forces therefore becomes an input of the analysis.

The total resisting forces for each test were determined by subtracting the loads applied to the system of the unreinforced tests from the loads applied to the system of the reinforced test. In recognizing the nonlinear behavior of the engineering materials, the respective loads were determined at equal shear box displacements. Additionally, the determination of total resisting forces was completed in terms of stress, where the load carried by soil in the reinforced soil tests was adjusted to account for the area replacement of soil with the pile element.

Estimation of Load Distributions with LPILE Software

Previous investigations of pile slope stabilization established that the load distributions developed along piles are linear or uniform with depth (see Chapter 2). The load test analysis was performed to show that the linear distribution of load is more appropriate for analyzing piles subject to lateral soil movement than the uniform distribution of load. The estimation of load distributions on piles from strain data is accomplished by differentiating the moment profiles of piles twice to obtain the load distribution. The use of LPILE software facilitates the progressive integration and differentiation to develop the relationship between pile load, shear, moment, and displacement with depth. Ultimately, total resisting forces were used to develop trial load distributions that vary linearly with depth along the piles of the pile load tests. The loads were applied to the pile system of experimental testing, and the measured pile response was compared to the LPILE-predicted response. Correlation of pile head deflection and maximum moment values suggests that the applied load of LPILE matches the applied load achieved during testing.

The Figures 188 through 213 compare measured and predicted values of pile head deflection and maximum moment as a function of total resisting force applied to the pile.

The predicted values of pile head deflection and maximum moment were obtained from the application of a distributed load on the pile varying from zero at the pile head to a maximum value at the failure surface. The measured pile head deflections and maximum moments were obtained from the load test results in Chapter 4.

Soil behavior of the soil control pads was modeled with p-y curves in LPILE. The user-defined p-y curves, empirically developed from laboratory stress-strain behavior, are shown in Figure 178.

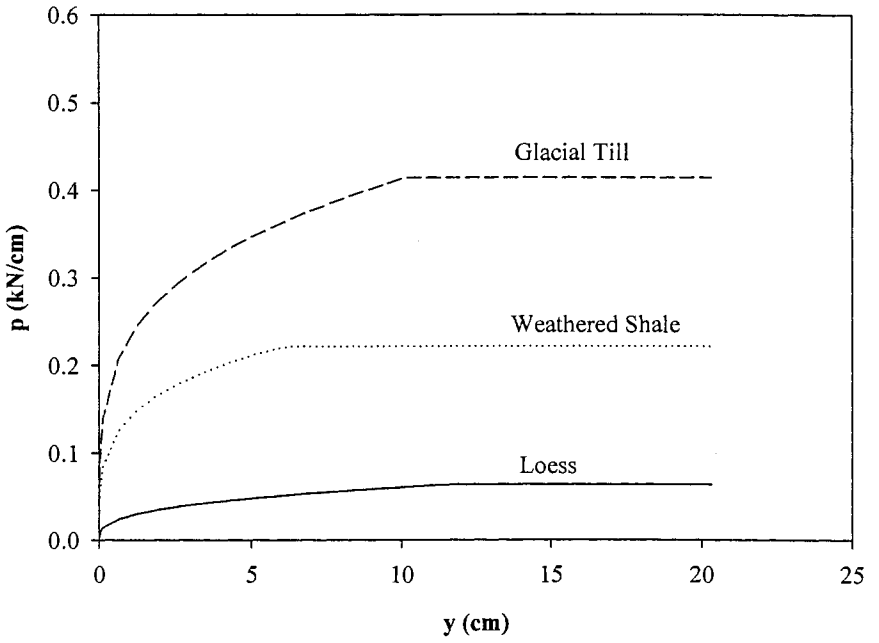

Figure 178 – User-Defined P-y Curves for Load Test Analyses

The research group attributed significant gap formation between piles and adjacent soil to the mobilization of pile moment capacities upon application of a peak load. Smaller gaps, with widths from 3 to 8 mm, developed at pre-peak loads. These gaps required that the research group conduct a sensitivity analysis to determine whether the gap formation was a factor in estimating load distributions. To account for the gaps, trial load distributions were applied to piles in LPILE as shown in Figure 179 (b). Figures 180 through 185 show that the

implementation of a gap in the analysis results in decreased pile head deflections and maximum moments, as anticipated. Moreover, the pile head deflections and maximum moment values are surprisingly not sensitive to small changes in gap length, L (defined in Figure 179). The load test analysis was thus performed by applying load distributions as shown in Figure 179 (a).

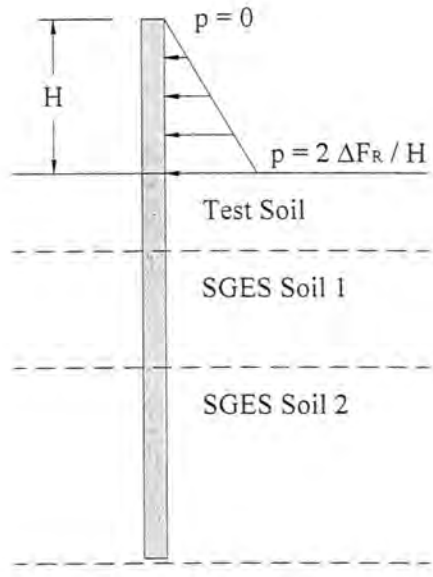

(a)

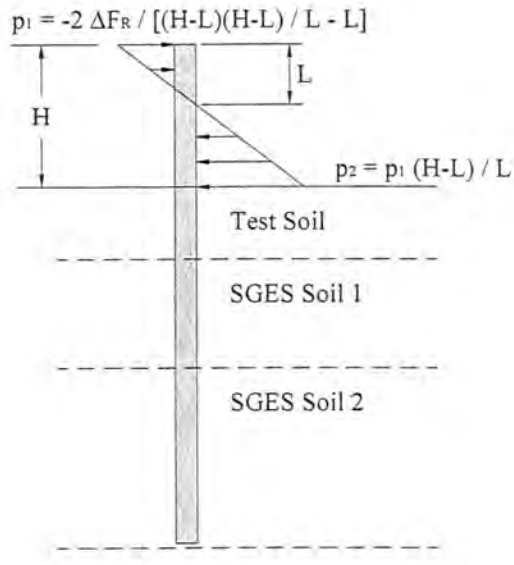

(b)

Figure 179 – LPILE Load Application

(a) Pre-peak load application; (b) Load application for gap

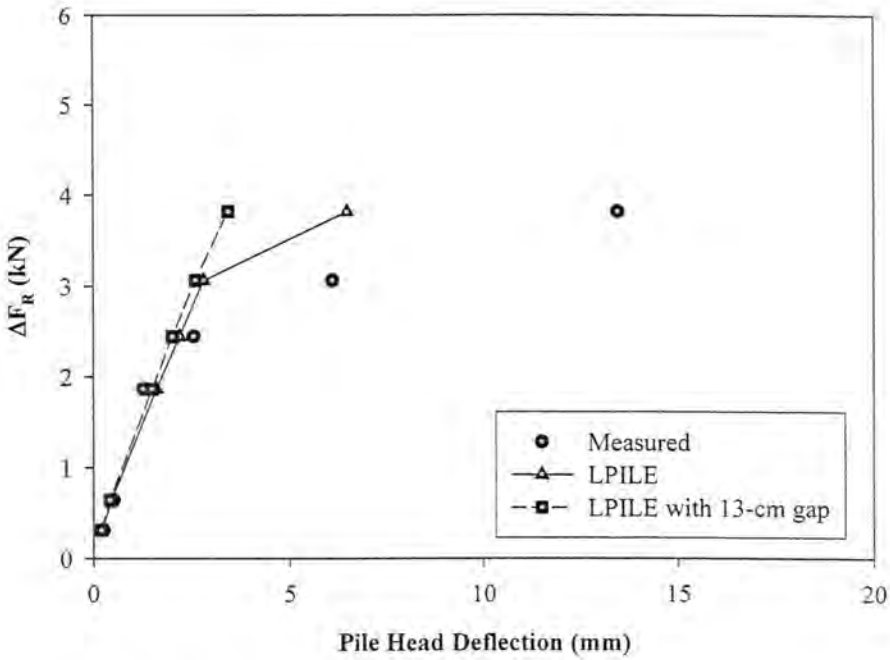

Figure 180 – Gap Sensitivity: Pile Head Deflections in Loess

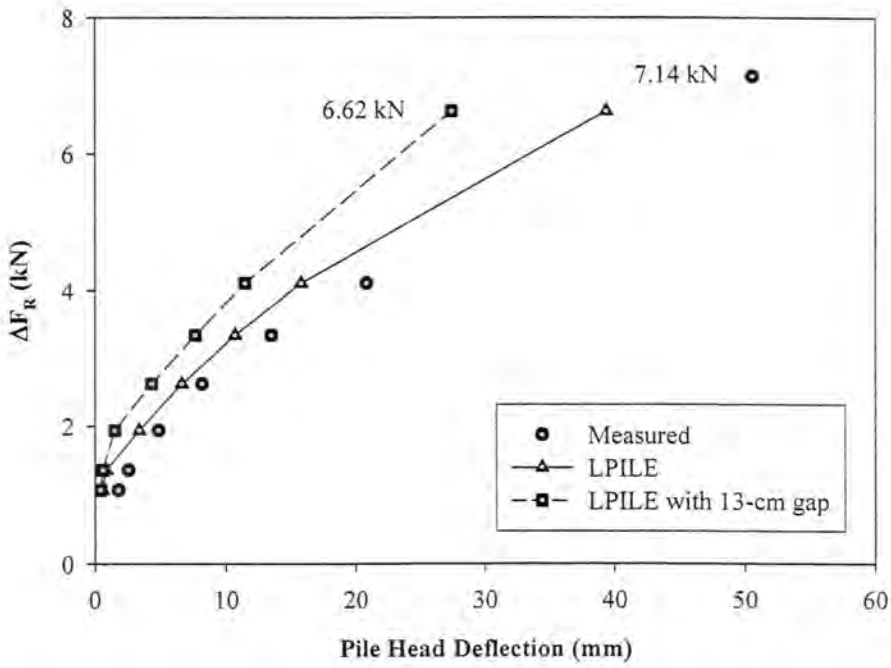

Figure 181 – Gap Sensitivity: Pile Head Deflections in Glacial Till

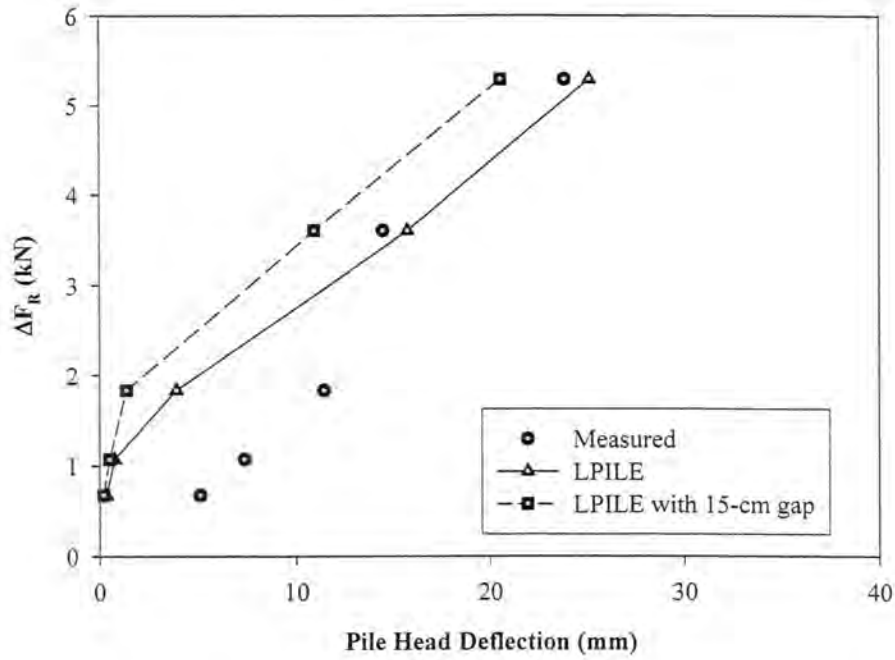

Figure 182 – Gap Sensitivity: Pile Head Deflections in Weathered Shale

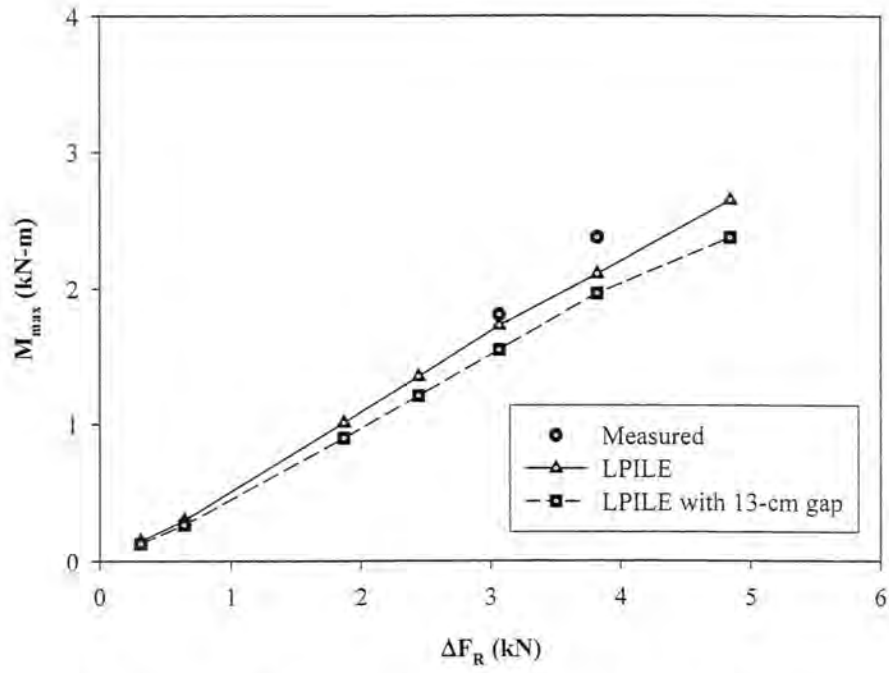

Figure 183 – Gap Sensitivity: Maximum Moments in Loess

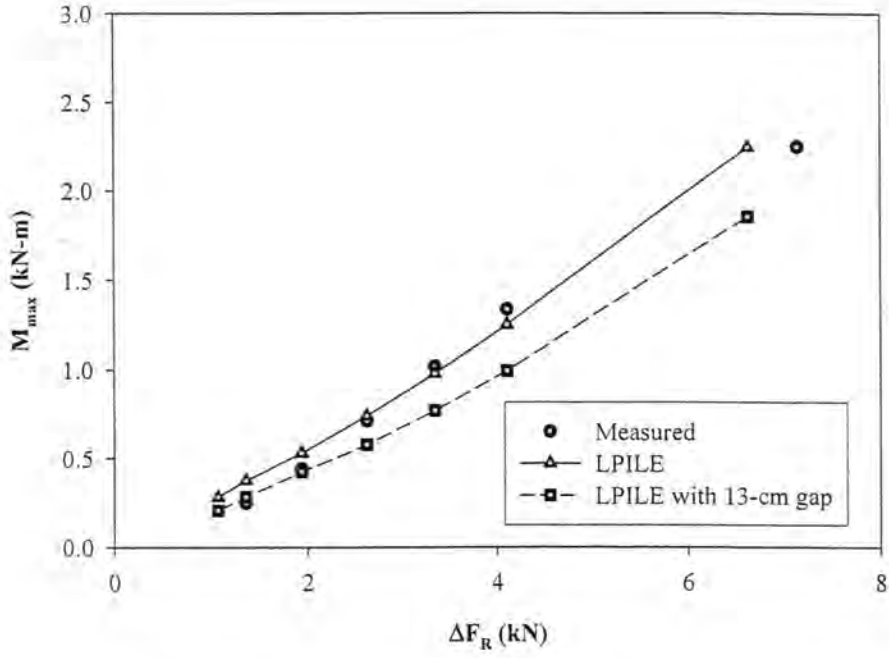

Figure 184 – Gap Sensitivity: Maximum Moments in Glacial Till

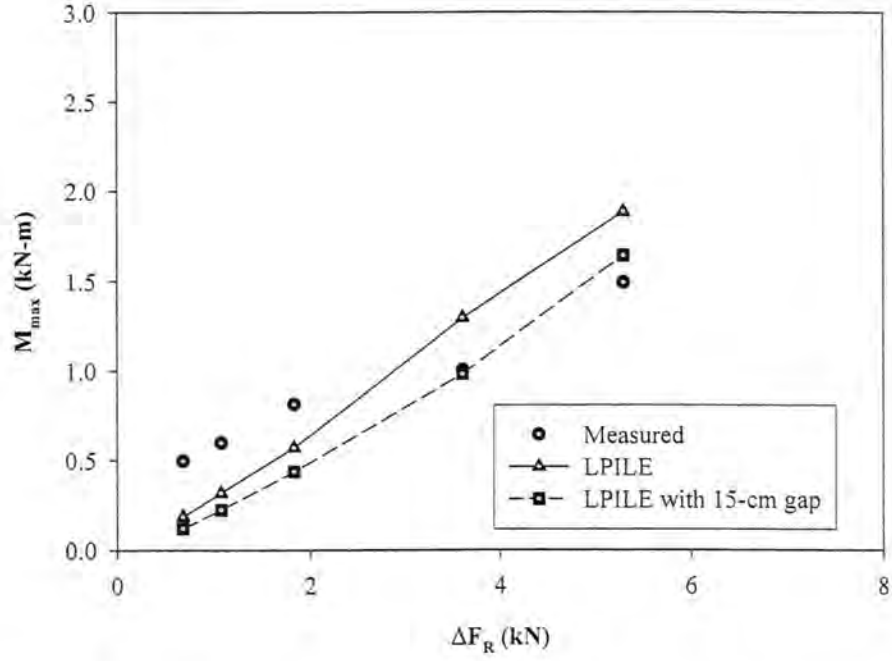

Figure 185 – Gap Sensitivity: Maximum Moments in Weathered Shale

Examination of the predicted pile head deflections indicates that LPILE oversimplifies the nonlinear load-pile head deflection relationship of the experimental reinforced soil system. The research group recognizes that the sudden drop in pile stiffness upon mobilization of the cracking moment (see Figure 58) is responsible for the near bilinear load-pile head deflection behavior exhibited in the figures of this section. Figures 186 and 187 show that typical plots of load (ΔF_R) versus pile head deflection are discontinuous and the discontinuities occur at the loads corresponding to the cracked moment. The *measured* data more accurately exhibits the nonlinearity of pile behavior, where the pile is surrounded by soil of nonlinear stress-strain behavior. The implications of pile behavior prediction with LPILE and the resulting relationship between load and pile head deflection are important, because seemingly poor correlation between measured and predicted pile behavior criteria is potentially explained by the simple model (i.e. no soil on the "downslope" side of the loaded pile) of LPILE software.

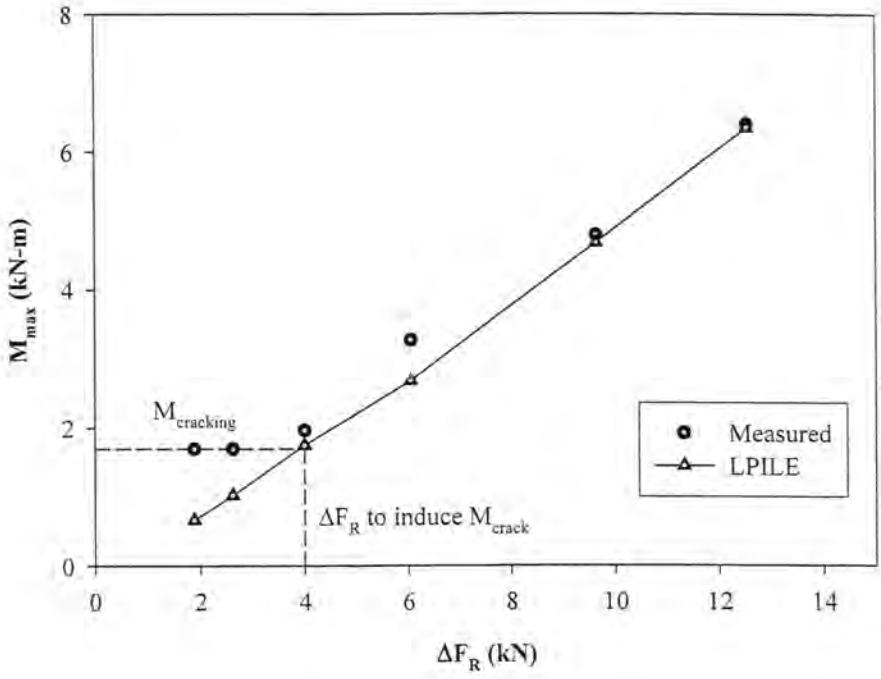

Figure 186 – Determination of Load that Develops Cracking Moment (Pile 12)

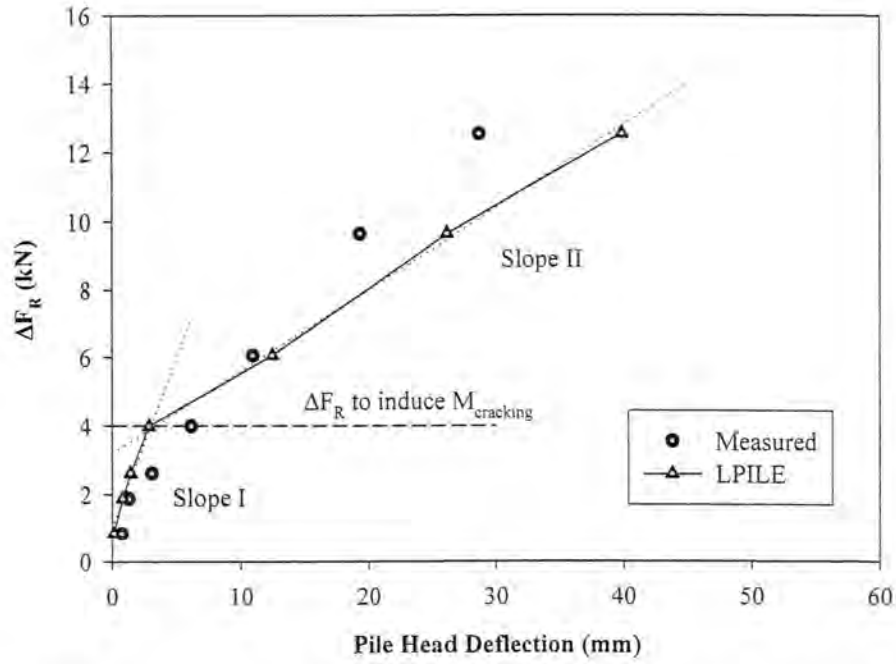

Figure 187 – Bilinear Pile Head Deflection Behavior of LPILE Calculations (Pile 12)

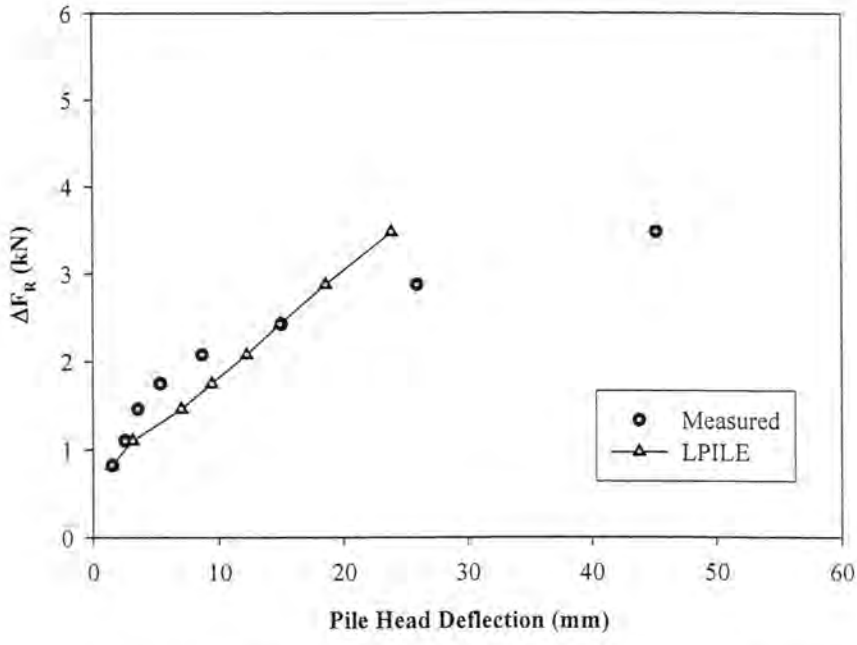

Figure 188 – Measured and Predicted Pile Head Deflections (Pile 4 in Loess)

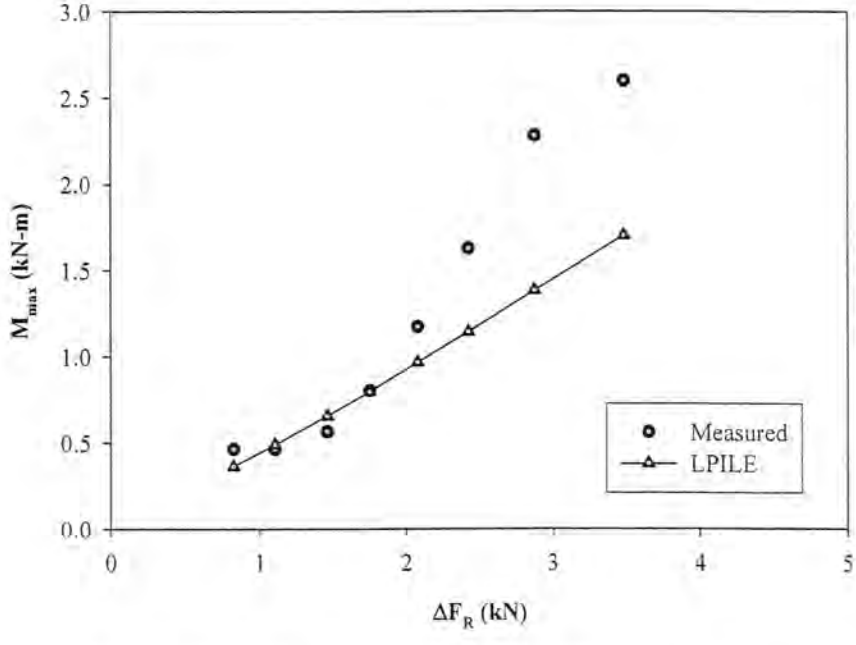

Figure 189 – Measured and Predicted Maximum Moments (Pile 4 in Loess)

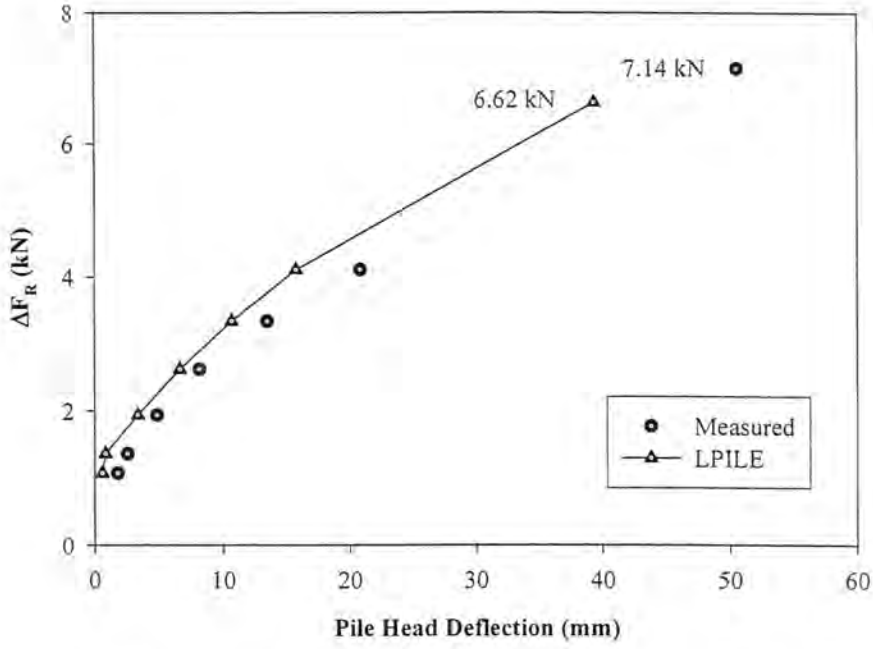

Figure 190 – Measured and Predicted Pile Head Deflections
(Pile 5 in Glacial Till)

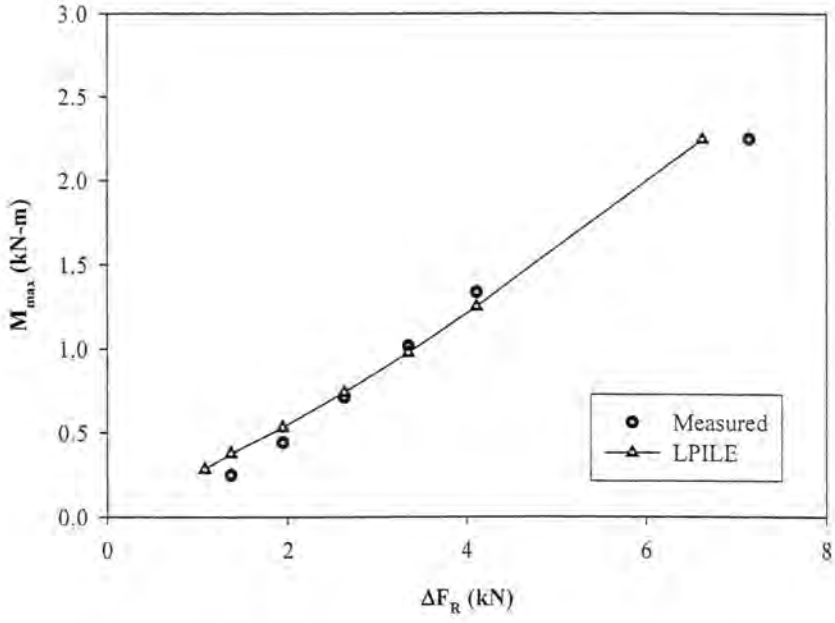

Figure 191 – Measured and Predicted Maximum Moments
(Pile 5 in Glacial Till)

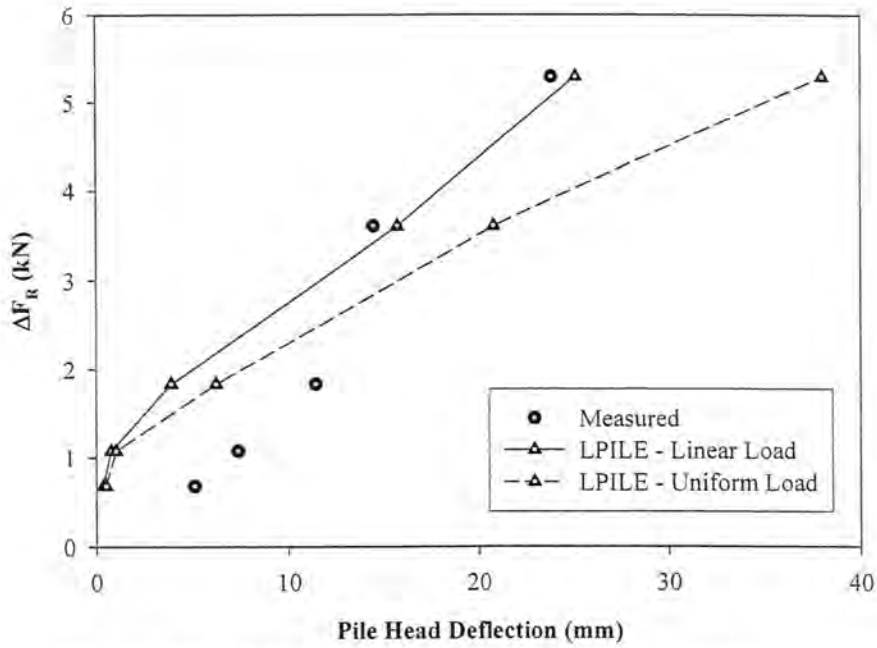

Figure 192 – Measured and Predicted Pile Head Deflections
(Pile 6 in Weathered Shale)

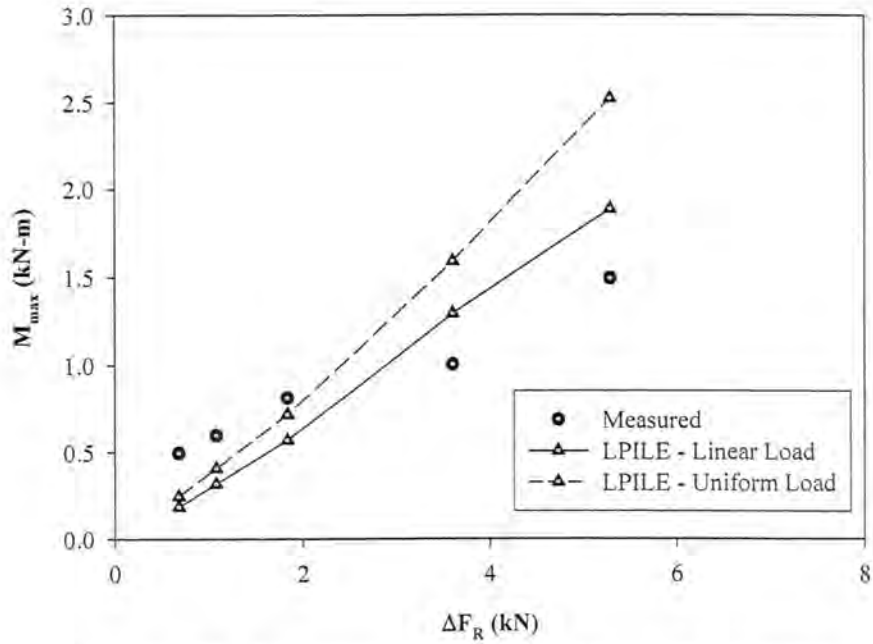

Figure 193 – Measured and Predicted Maximum Moments
(Pile 6 in Weathered Shale)

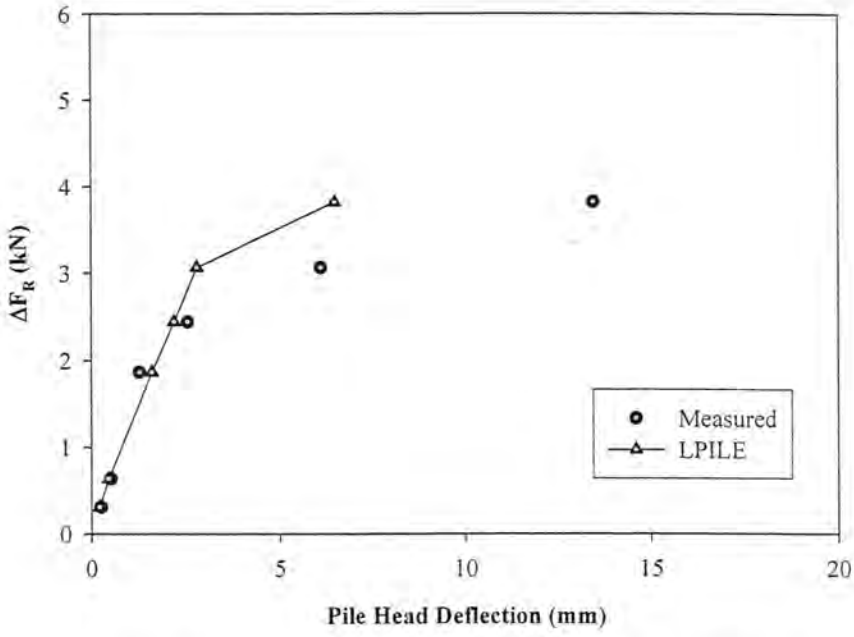

Figure 194 – Measured and Predicted Pile Head Deflections (Pile 8 in Loess)

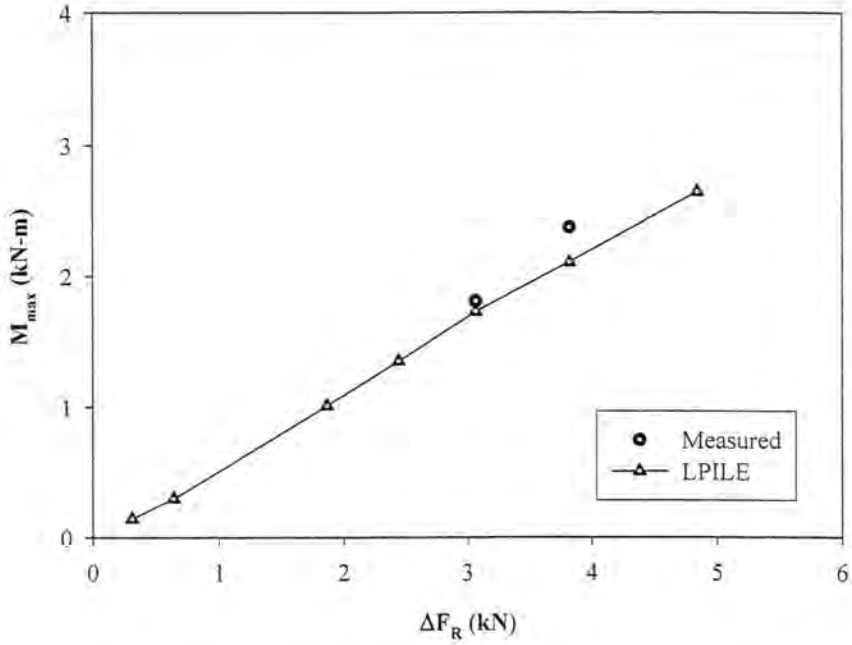

Figure 195 – Measured and Predicted Maximum Moments (Pile 8 in Loess)

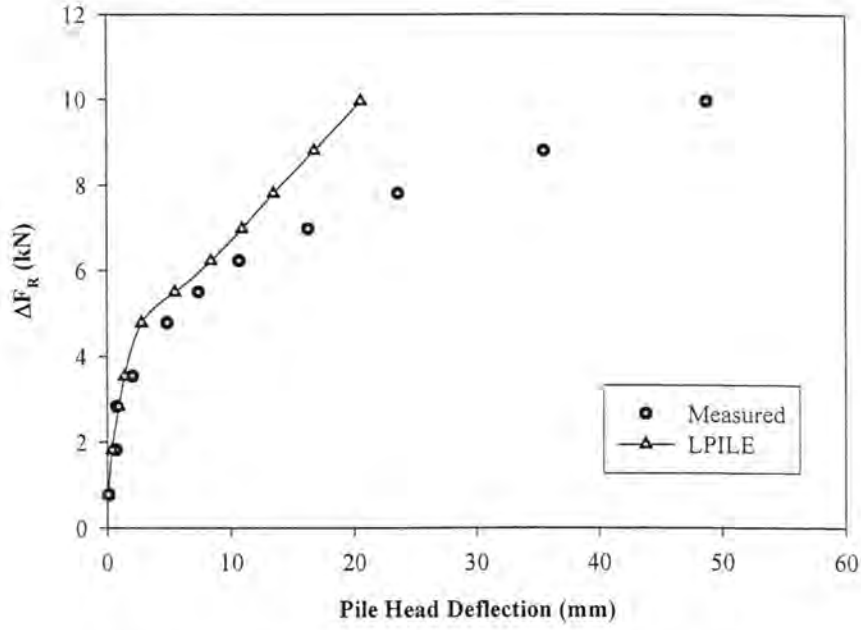

Figure 196 – Measured and Predicted Pile Head Deflections (Pile 9 in Glacial Till)

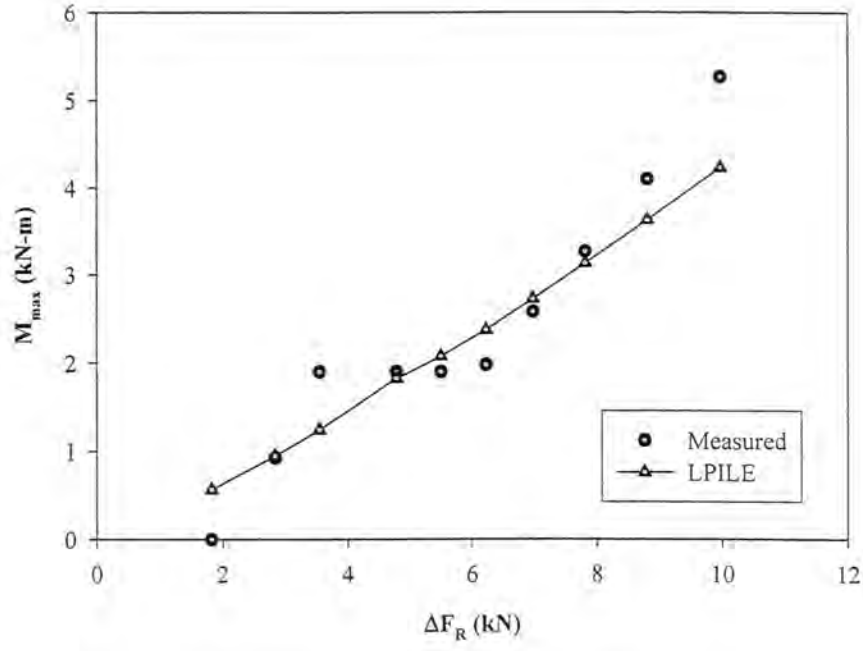

Figure 197 – Measured and Predicted Maximum Moments (Pile 9 in Glacial Till)

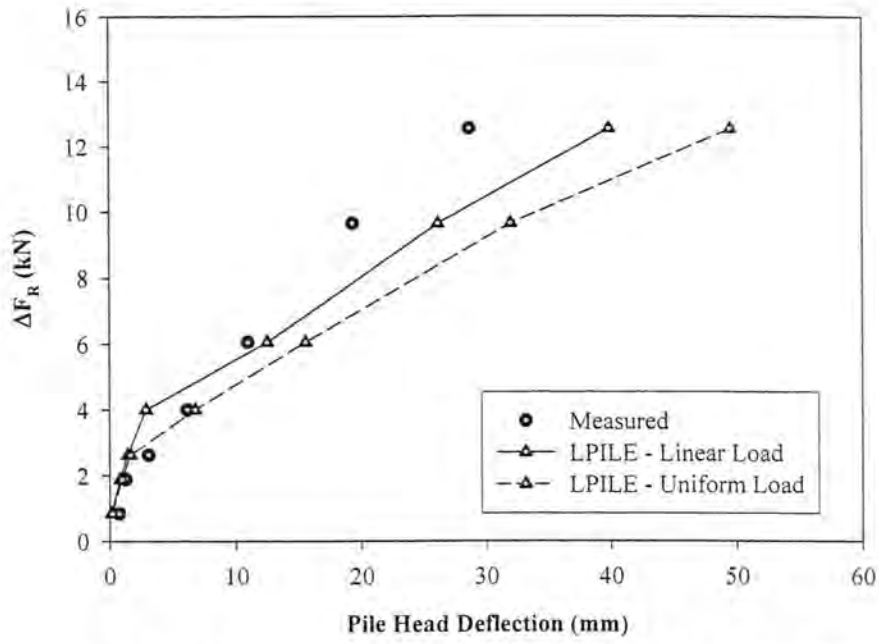

Figure 198 – Measured and Predicted Pile Head Deflections
(Pile 12 in Weathered Shale)

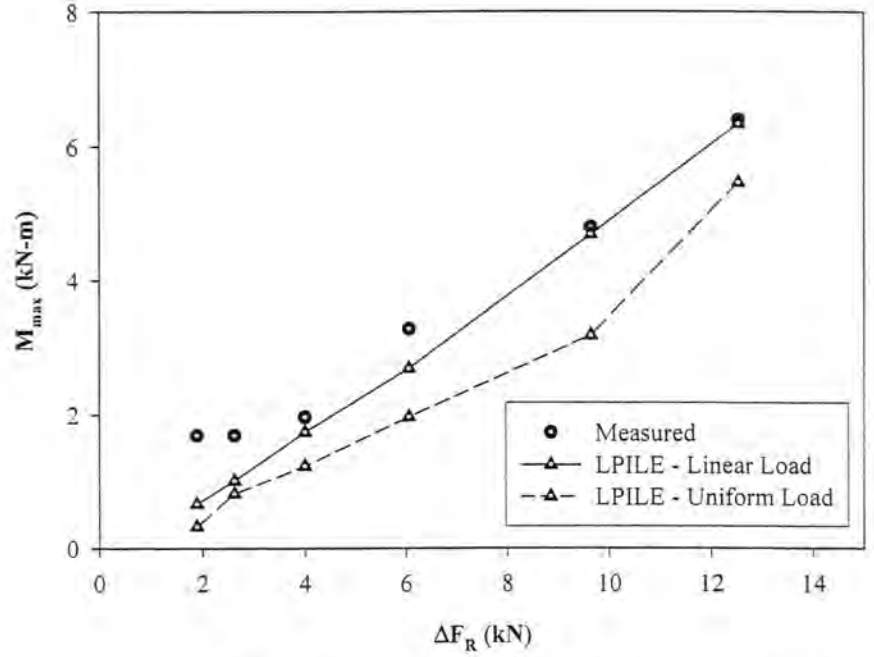

Figure 199 – Measured and Predicted Maximum Moments
(Pile 12 in Weathered Shale)

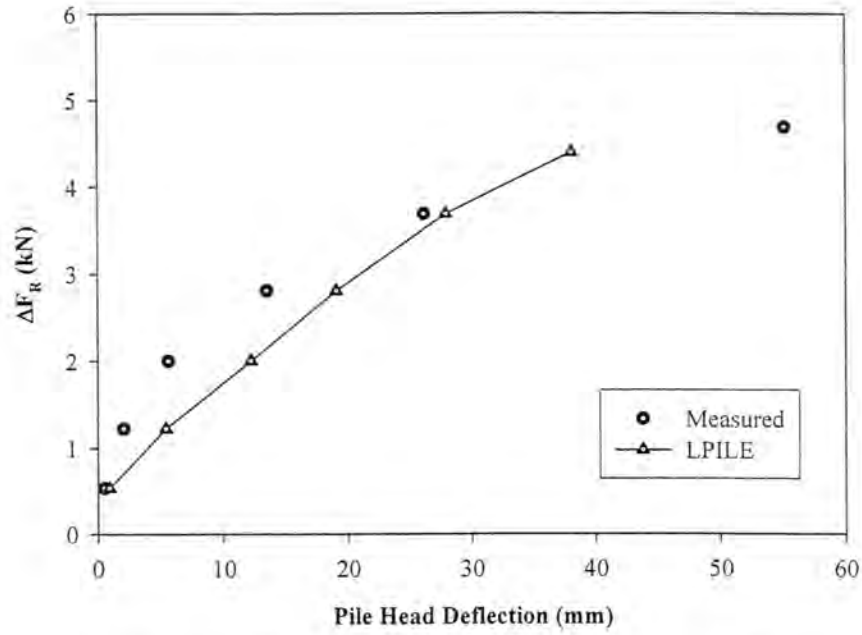

Figure 200 – Measured and Predicted Pile Head Deflections (Pile 11 A in Loess)

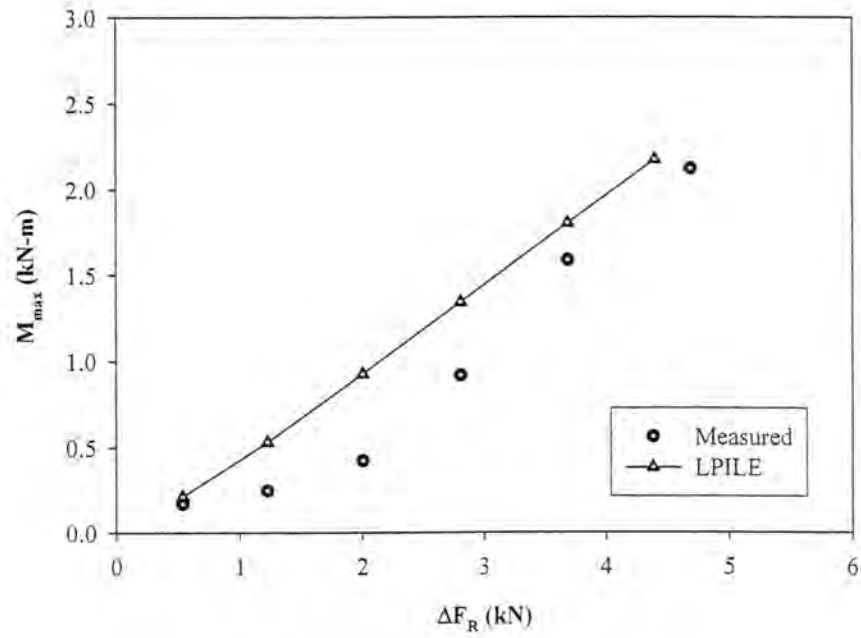

Figure 201 – Measured and Predicted Maximum Moments (Pile 11 A in Loess)

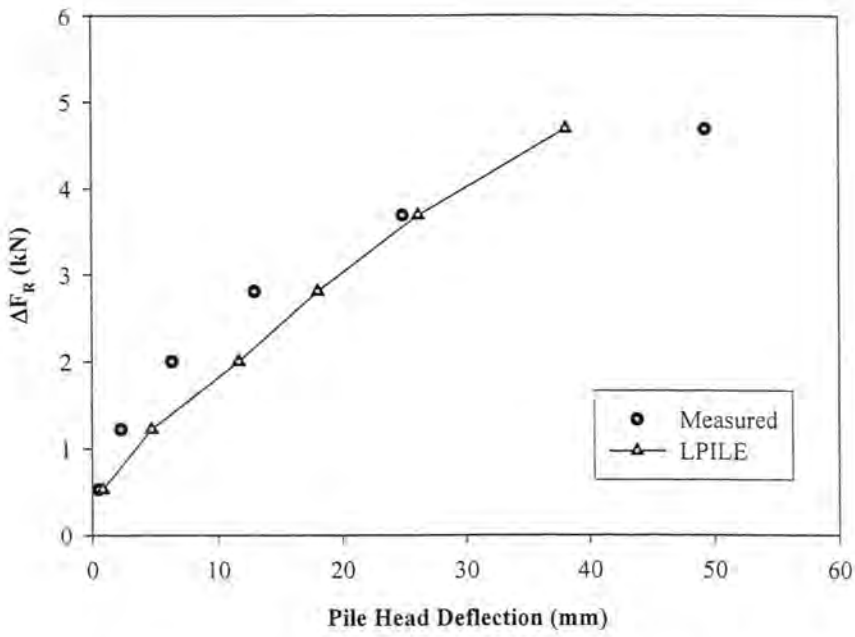

Figure 202 – Measured and Predicted Pile Head Deflections (Pile 11 B in Loess)

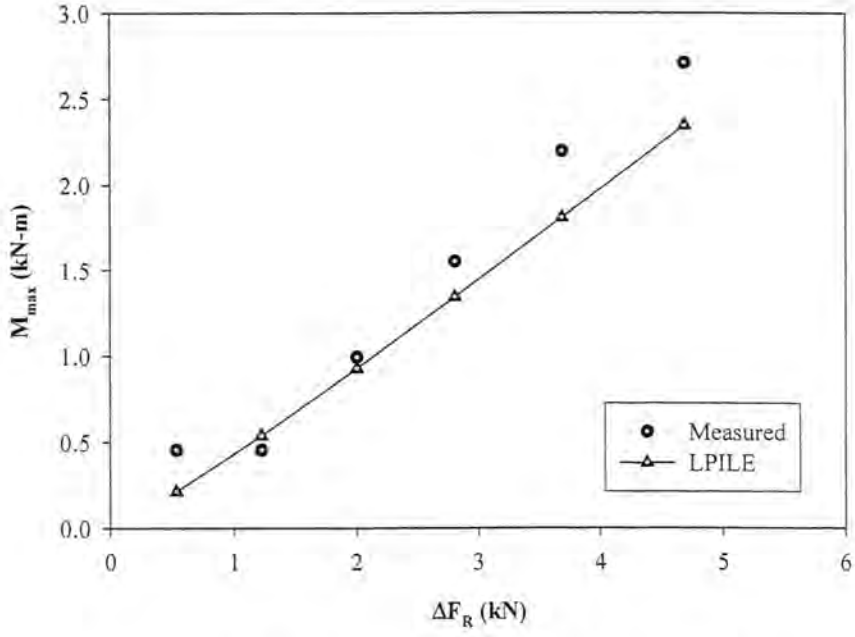

Figure 203 – Measured and Predicted Maximum Moments (Pile 11 B in Loess)

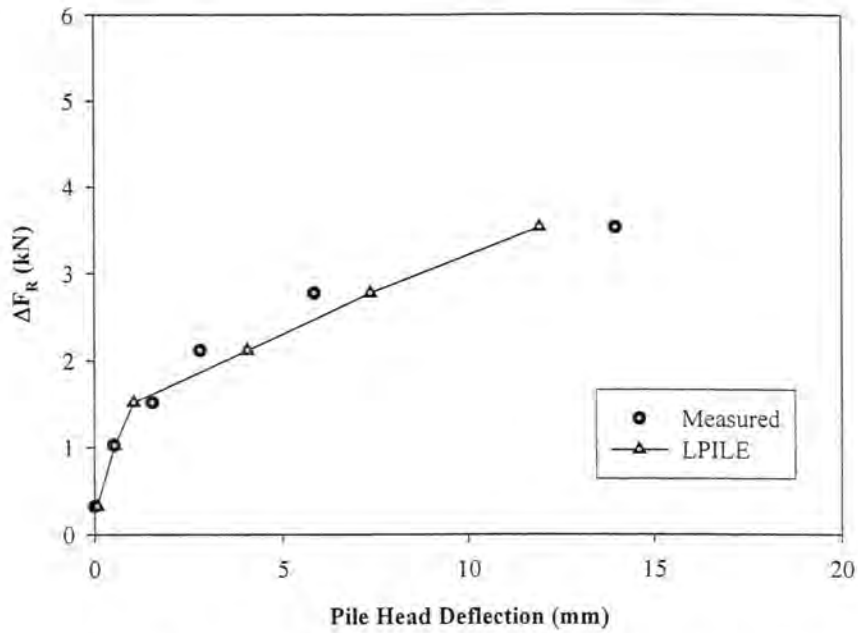

Figure 204 – Measured and Predicted Pile Head Deflections
(Pile 13 A in Glacial Till)

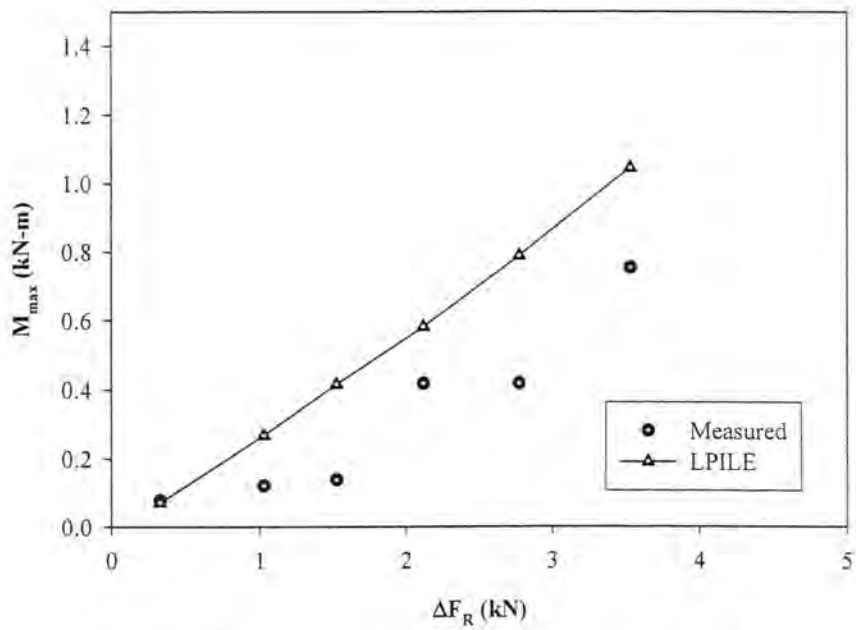

Figure 205- Measured and Predicted Maximum Moments
(Pile 13 A in Glacial Till)

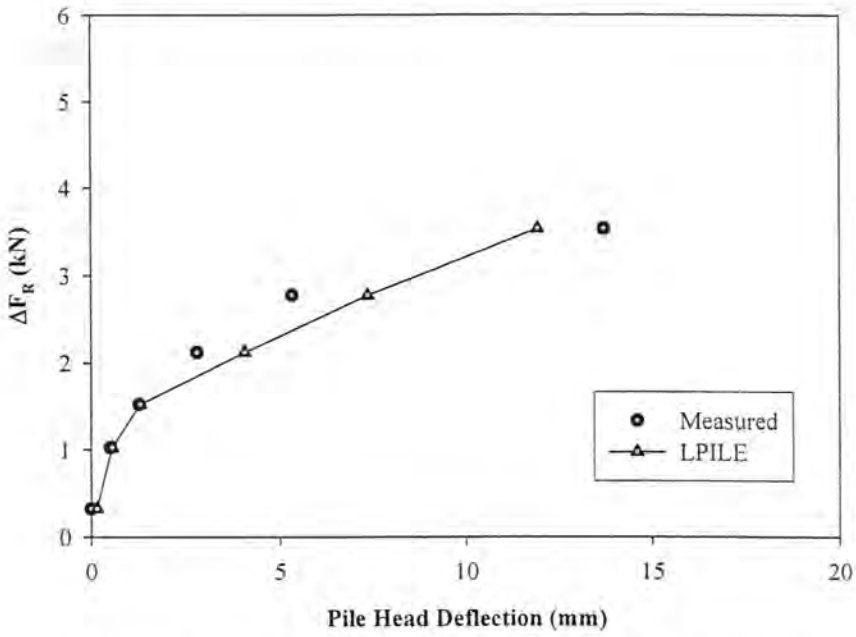

Figure 206 – Measured and Predicted Pile Head Deflections
(Pile 13 B in Glacial Till)

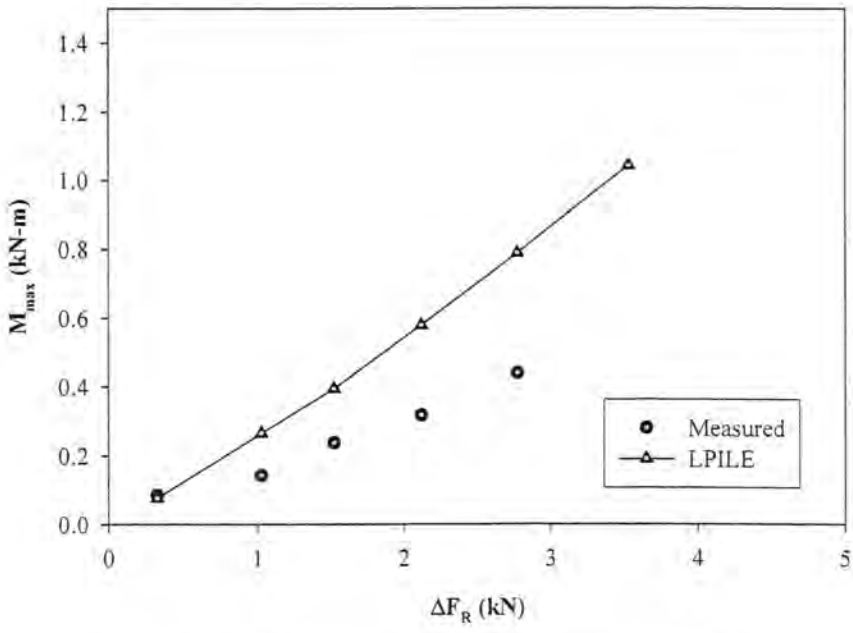

Figure 207 – Measured and Predicted Maximum Moments
(Pile 13 B in Glacial Till)

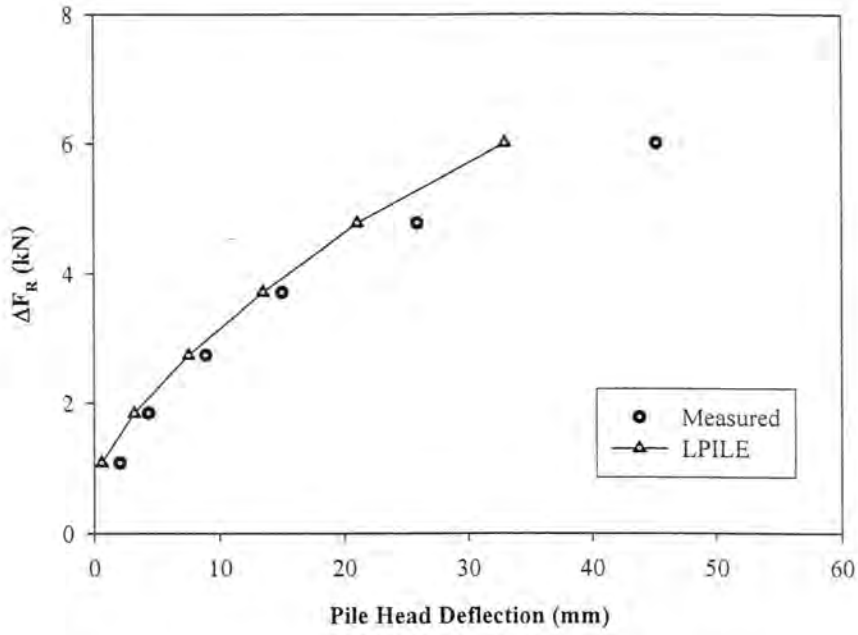

Figure 208 – Measured and Predicted Pile Head Deflections
(Pile 14 B in Glacial Till)

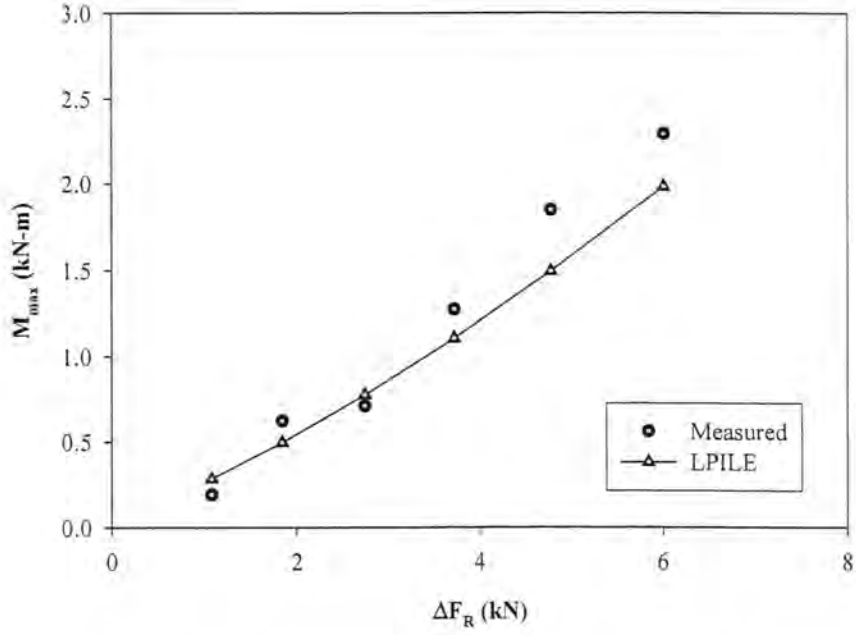

Figure 209 – Measured and Predicted Maximum Moments
(Pile 14 B in Glacial Till)

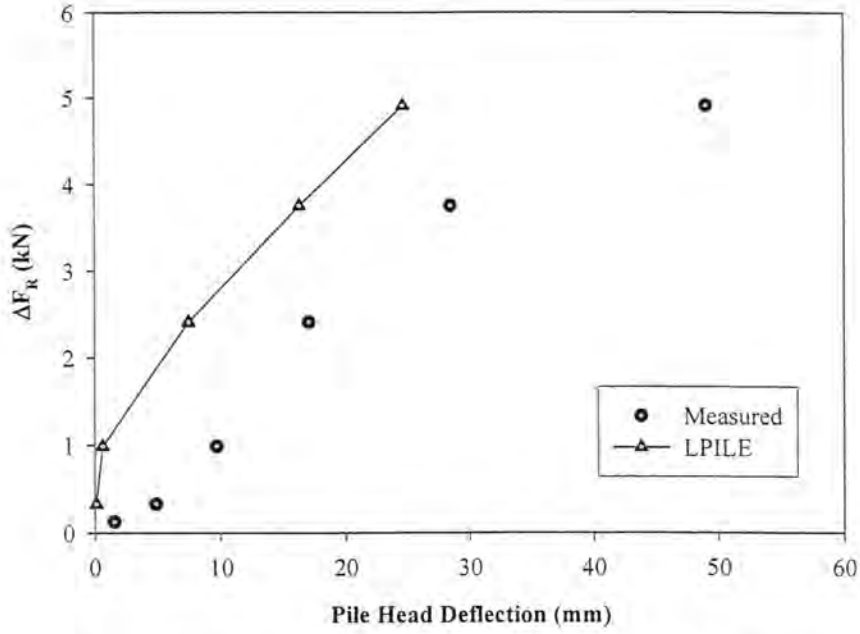

Figure 210 – Measured and Predicted Pile Head Deflections
(Pile 10 A in Weathered Shale)

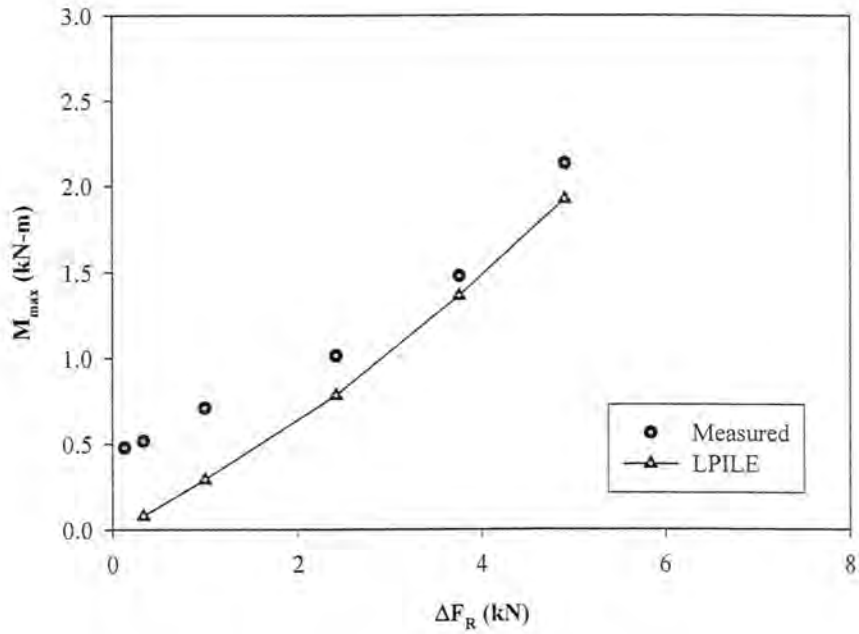

Figure 211 – Measured and Predicted Maximum Moments
(Pile 10 A in Weathered Shale)

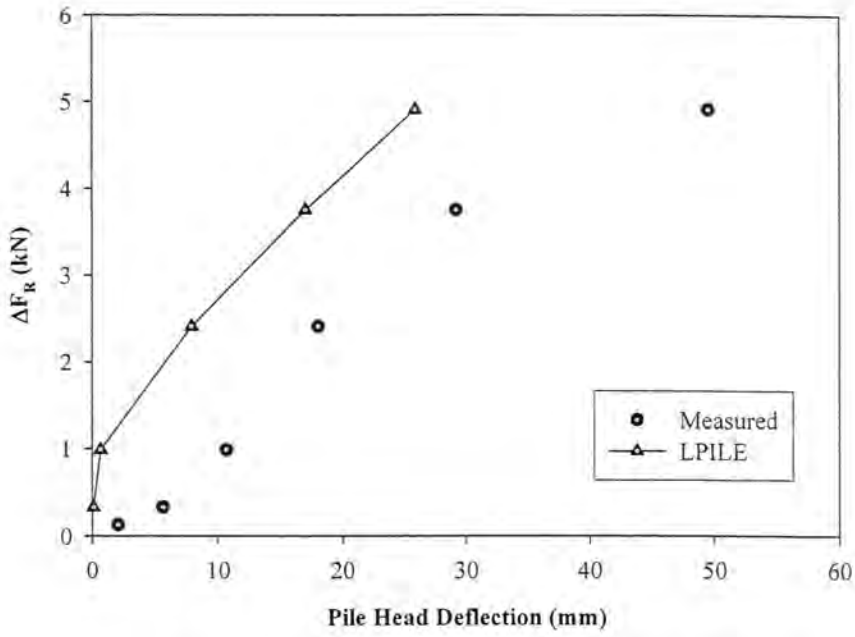

Figure 212 – Measured and Predicted Pile Head Deflections
(Pile 10 B in Weathered Shale)

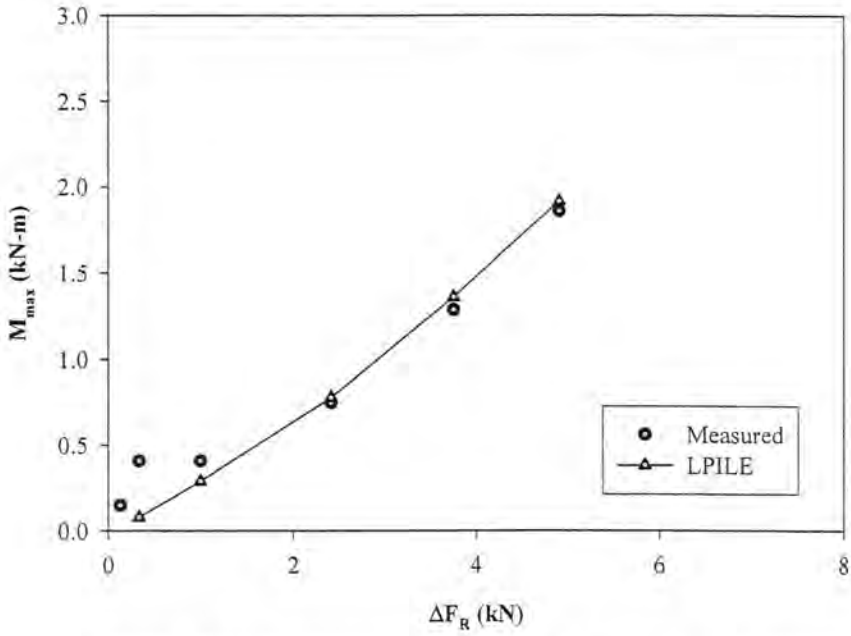

Figure 213 – Measured and Predicted Maximum Moments
(Pile 10 B in Weathered Shale)

The correlations of measured and predicted values of pile head deflection and maximum moment were linearized by plotting measured data against predicted data. The alternative plots are shown as Figures 214 through 239. The ideal correlation, in which measured data equals predicted data, is indicated by a 1:1 line, provided in the ensuing figures as a reference.

Correlation and regression predictability are closely related (Ott and Longnecker 2001). The proportionate reduction in error for a regression is the coefficient of determination, defined as follows (Ott and Longnecker 2001):

$$r^2 = \frac{SS(Total) - SS(Residual)}{SS(Total)} \tag{29}$$

where $SS(Total) = \Sigma_i (y_i - \bar{y}_i)^2$

$SS(Residual) = \Sigma_i (y_i - \hat{y}_i)^2$

y_i = measured value

$\bar{y}_i$ = average of measured values

$\hat{y}_i$ = predicted value

An r^2 value of zero indicates no predictive value and poor correlation, whereas an r^2 value of unity indicates perfect predictability and excellent correlation. The research group recognizes that the coefficient of determination depends on the number correlation points and the load (stage of loading) at which the pile behavior was compared. The calculated coefficients of determination are provided in Figures 214 through 239.

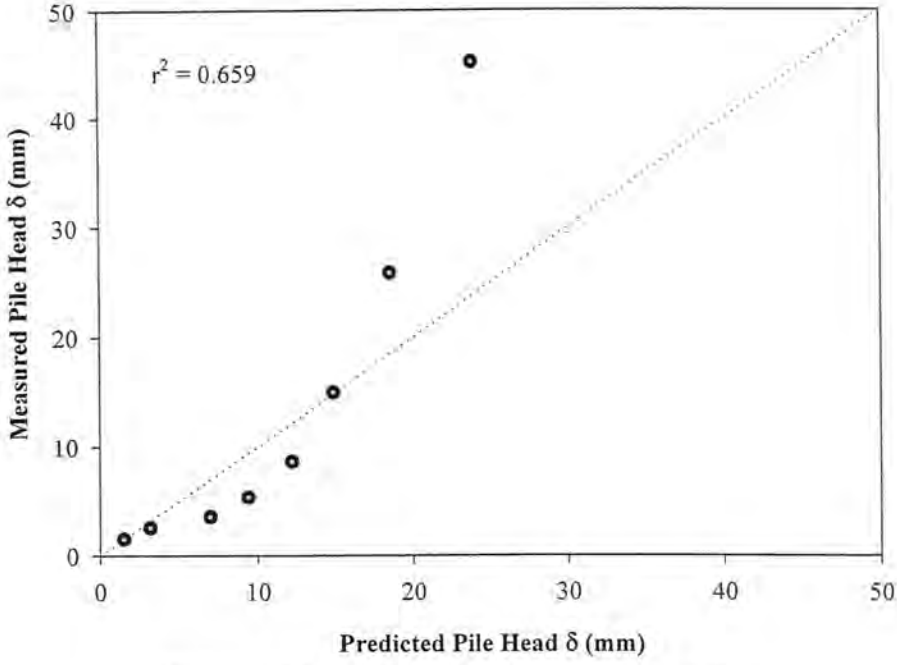

Figure 214 – Pile Head Deflection Correlation
(Pile 4 in Loess)

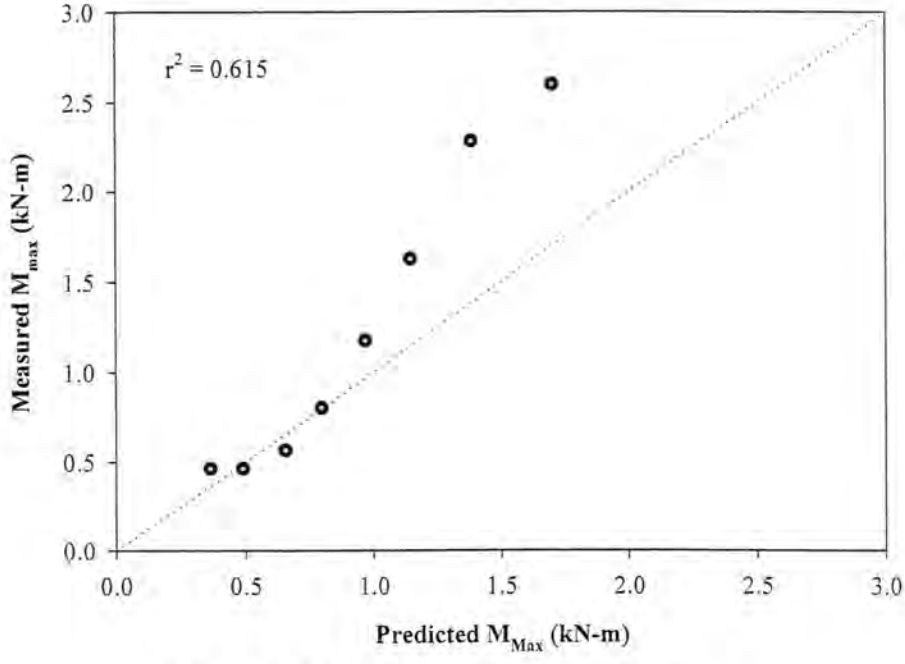

Figure 215 – Maximum Moment Correlation
(Pile 4 in Loess)

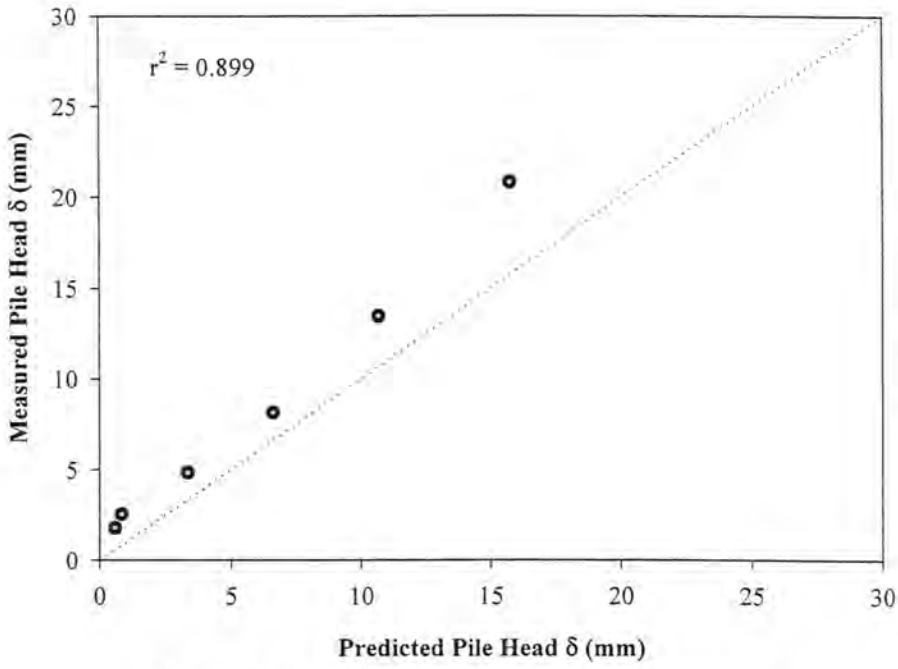

Figure 216 – Pile Head Deflection Correlation
(Pile 5 in Glacial Till)

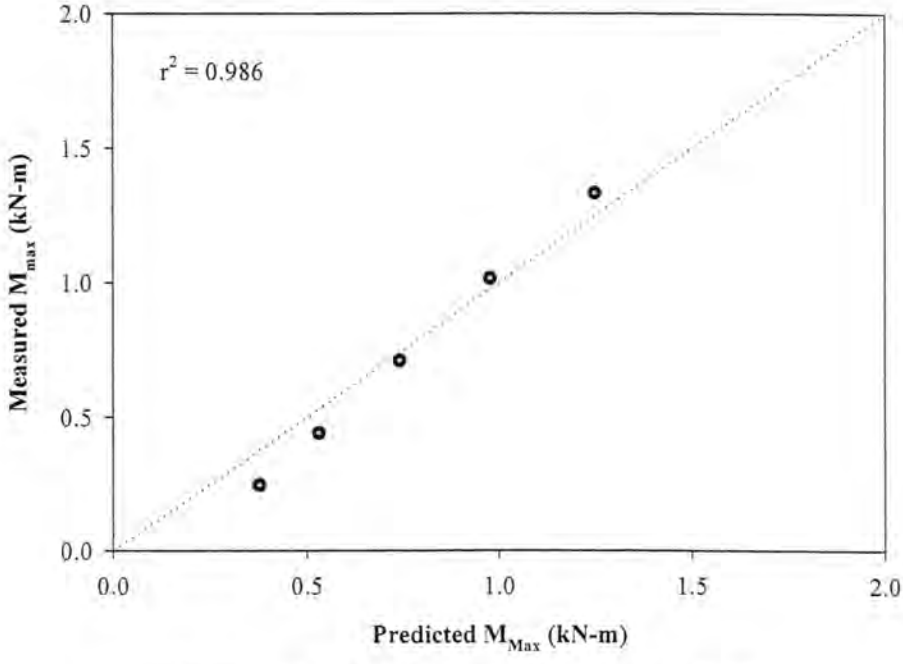

Figure 217 – Maximum Moment Correlation
(Pile 5 in Glacial Till)

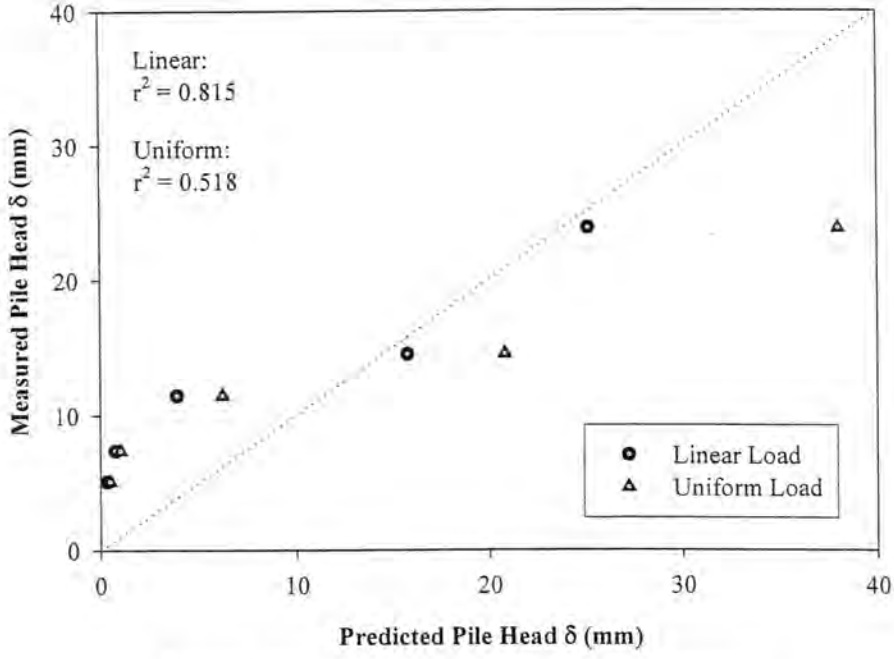

Figure 218 – Pile Head Deflection Correlation
(Pile 6 in Weathered Shale)

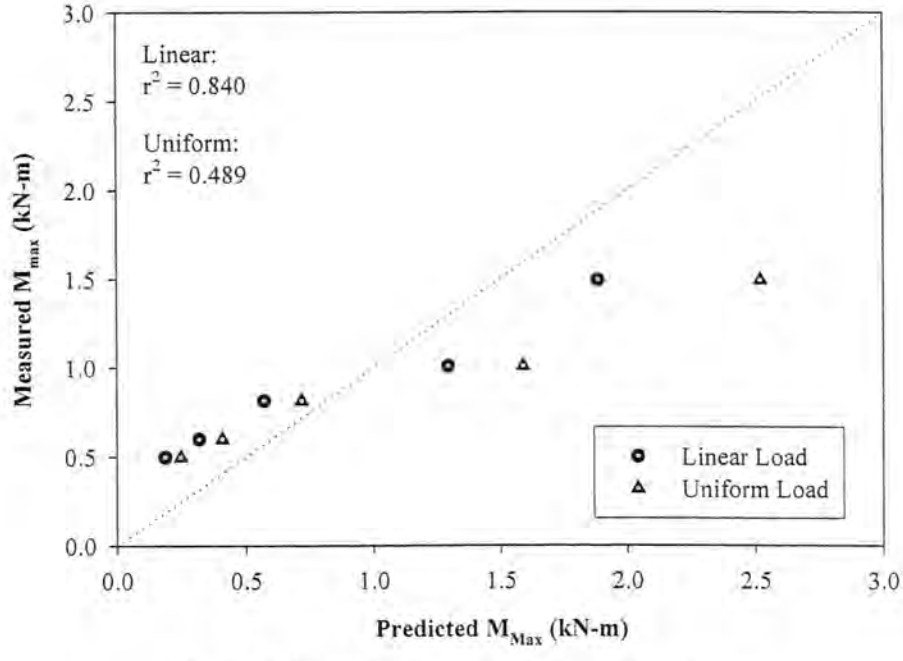

Figure 219 – Maximum Moment Correlation
(Pile 6 in Weathered Shale)

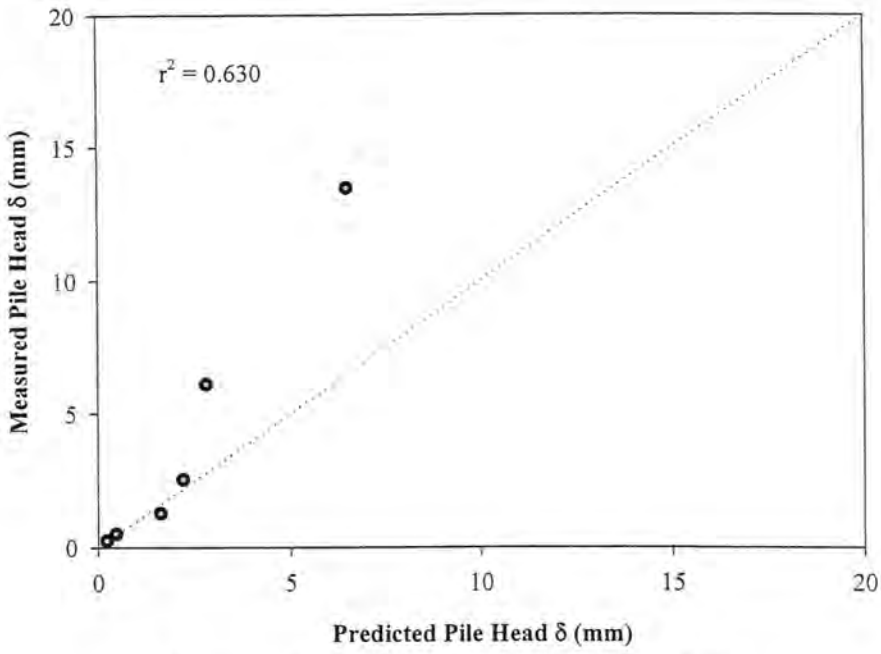

Figure 220 – Pile Head Deflection Correlation
(Pile 8 in Loess)

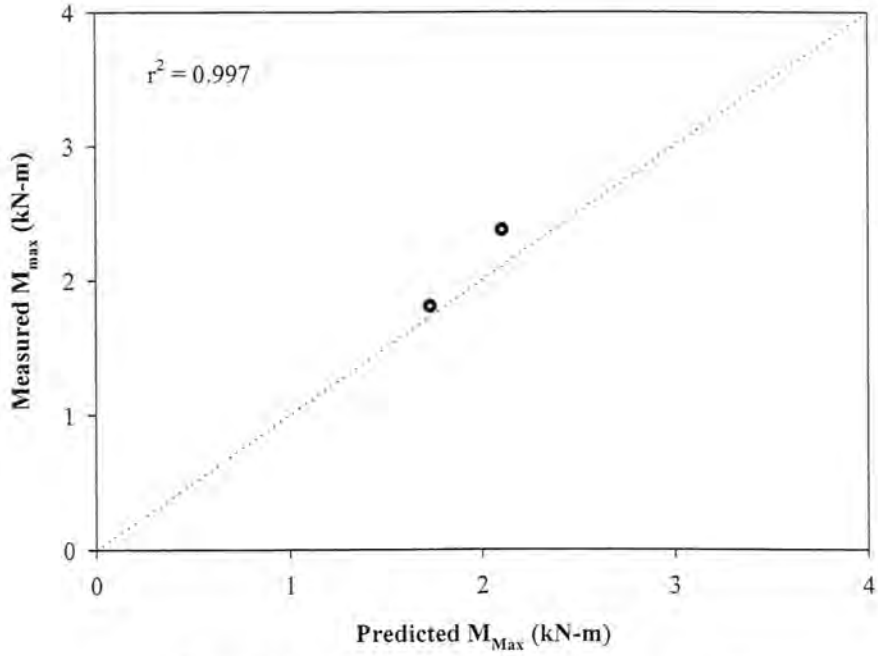

Figure 221 – Maximum Moment Correlation
(Pile 8 in Loess)

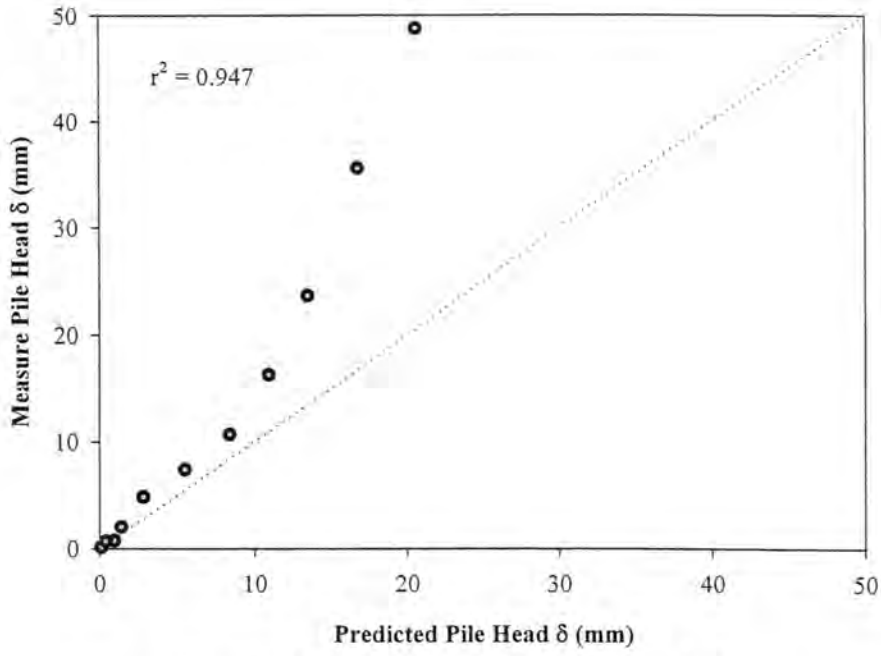

Figure 222 – Pile Head Deflection Correlation
(Pile 9 in Glacial Till)

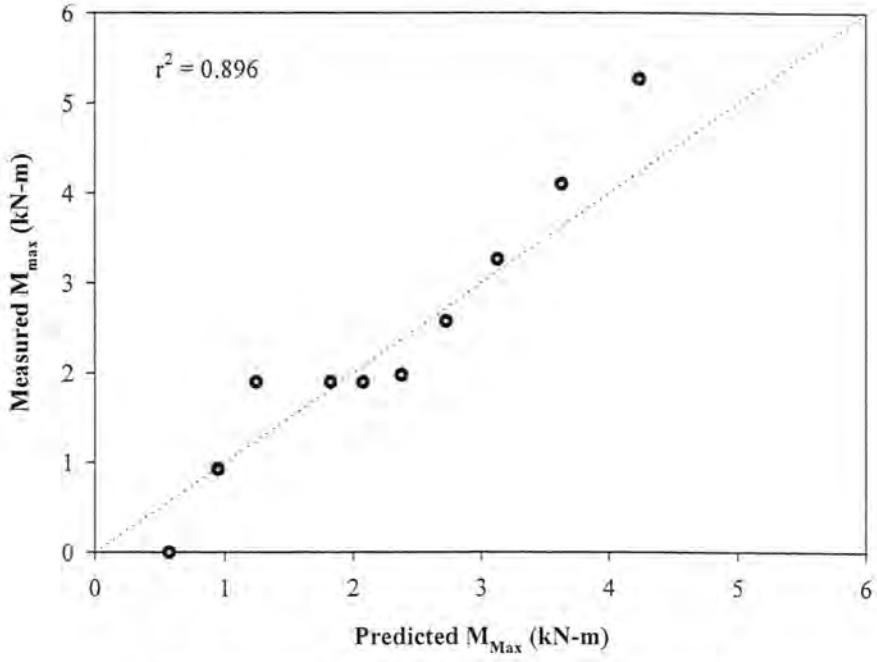

Figure 223 – Maximum Moment Correlation
(Pile 9 in Glacial Till)

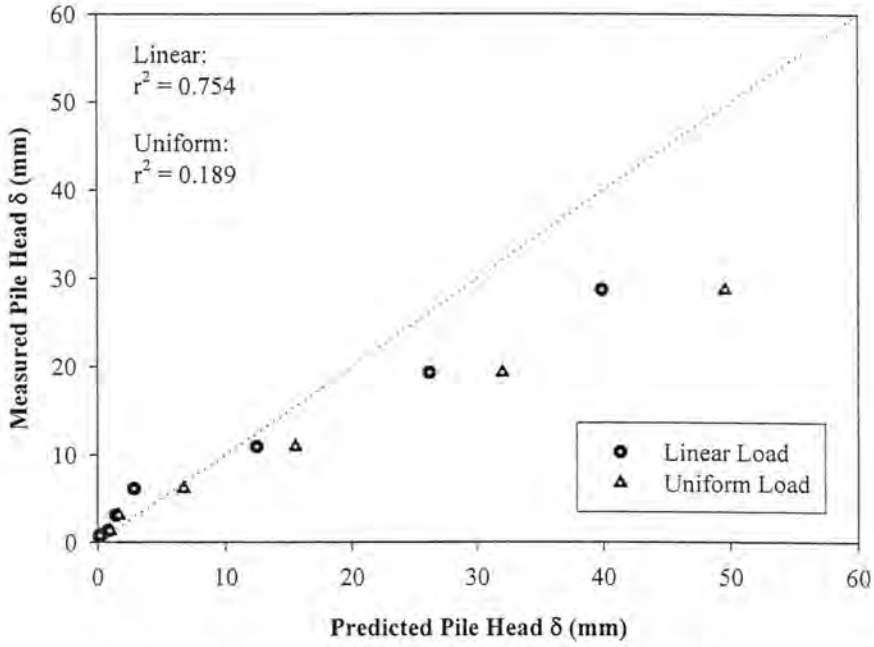

Figure 224 – Pile Head Deflection Correlation
(Pile 12 in Weathered Shale)

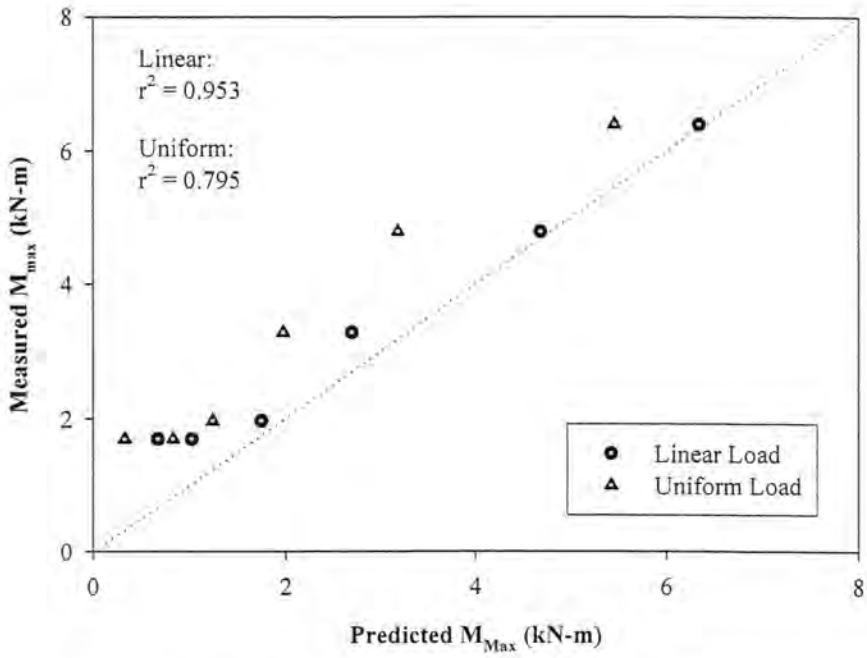

Figure 225 – Maximum Moment Correlation
(Pile 12 in Weathered Shale)

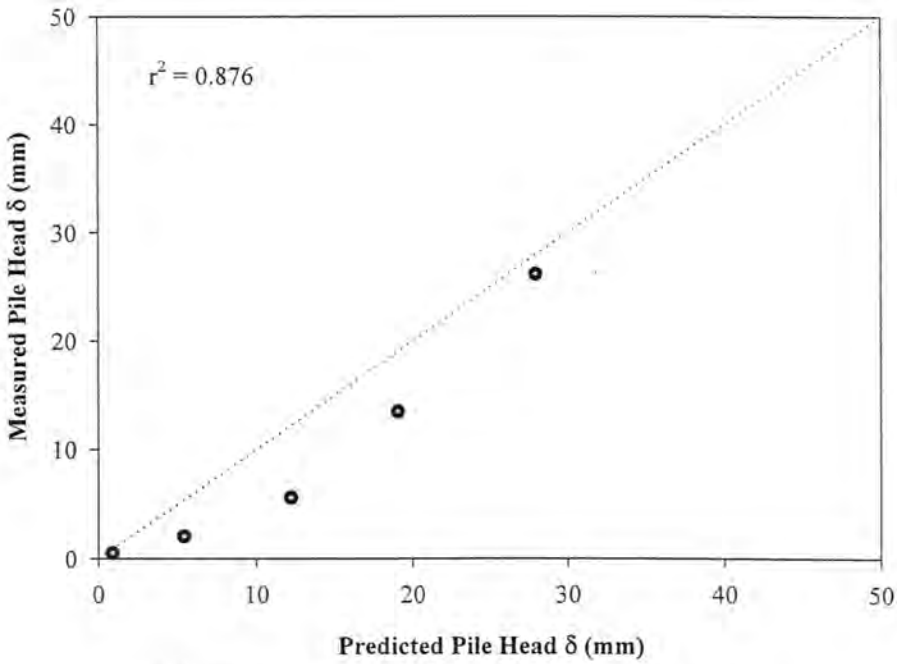

Figure 226 – Pile Head Deflection Correlation
(Pile 11 A in Loess)

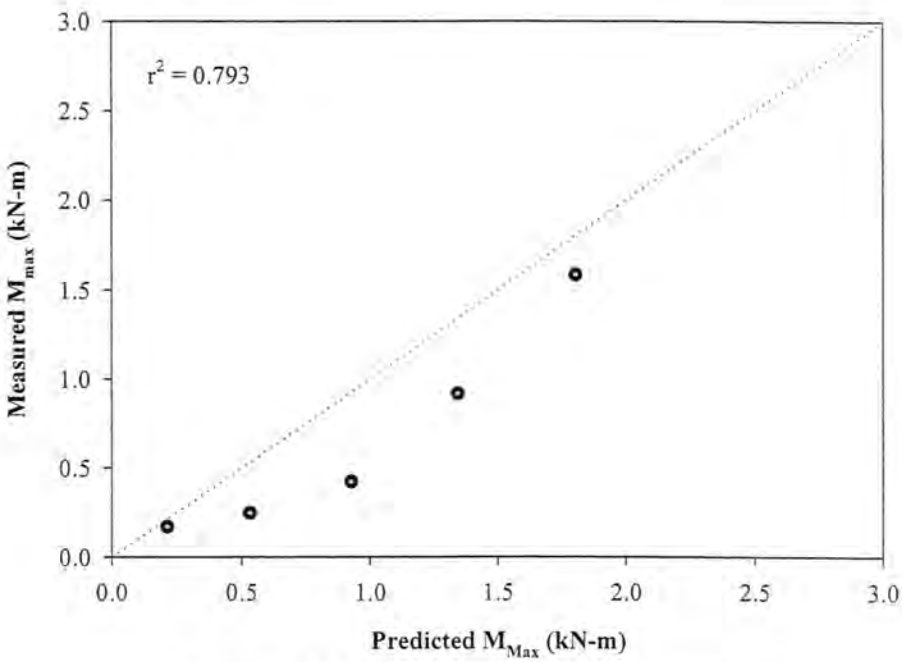

Figure 227 – Maximum Moment Correlation
(Pile 11 A in Loess)

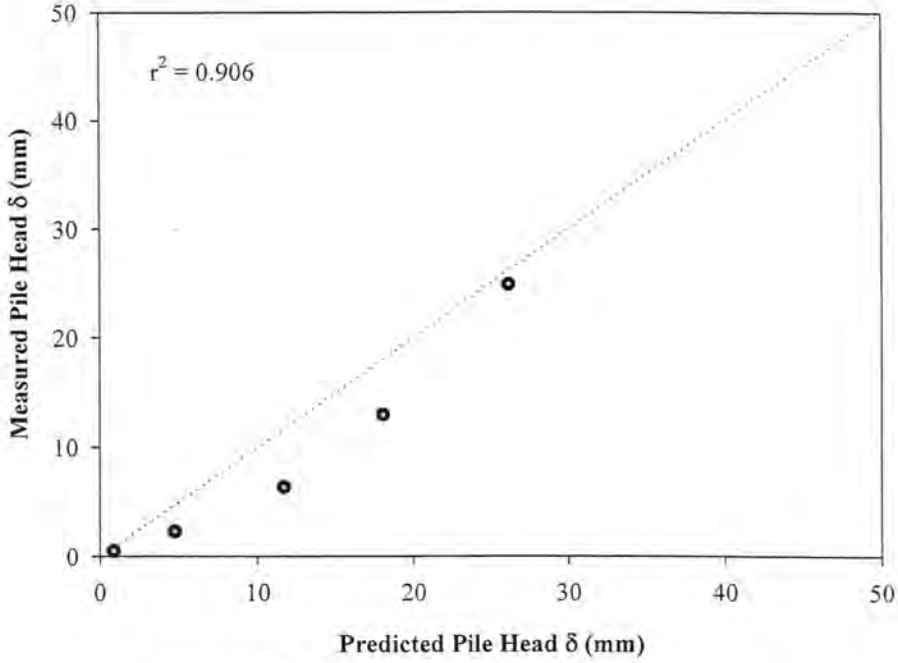

Figure 228 – Pile Head Deflection Correlation
(Pile 11 B in Loess)

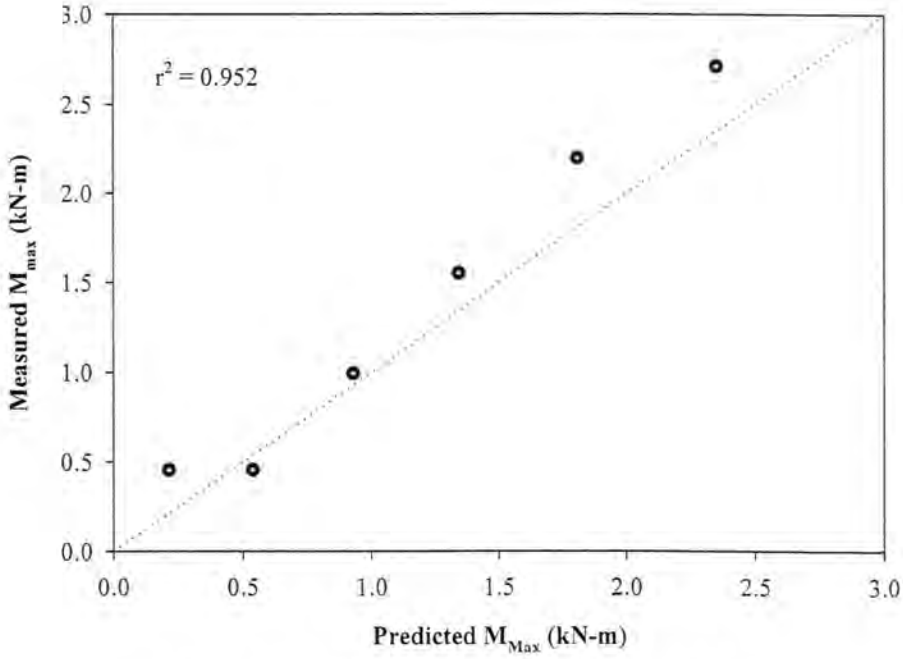

Figure 229 – Maximum Moment Correlation
(Pile 11 B in Loess)

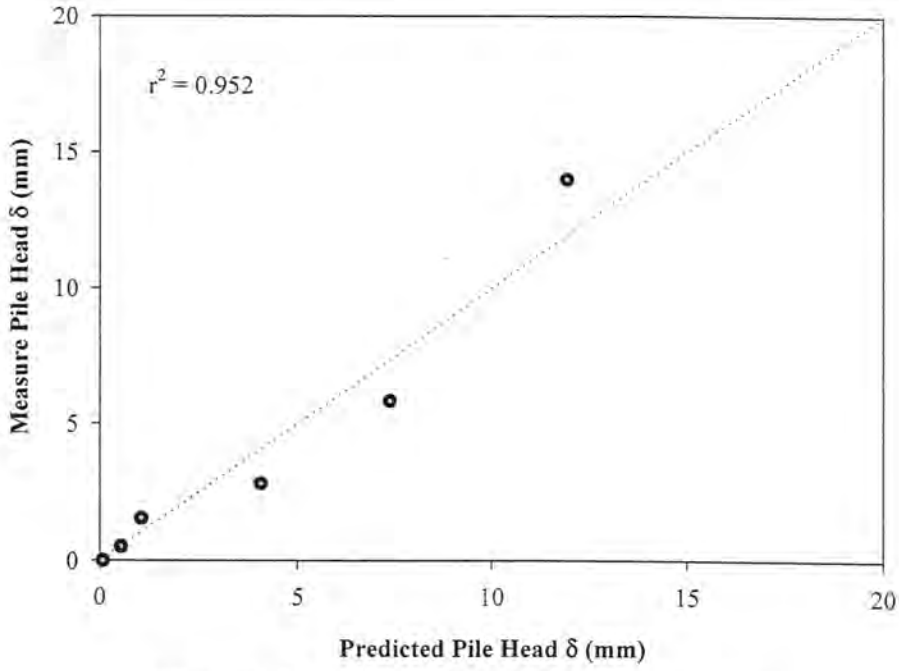

Figure 230 – Pile Head Deflection Correlation
(Pile 13 A in Glacial Till)

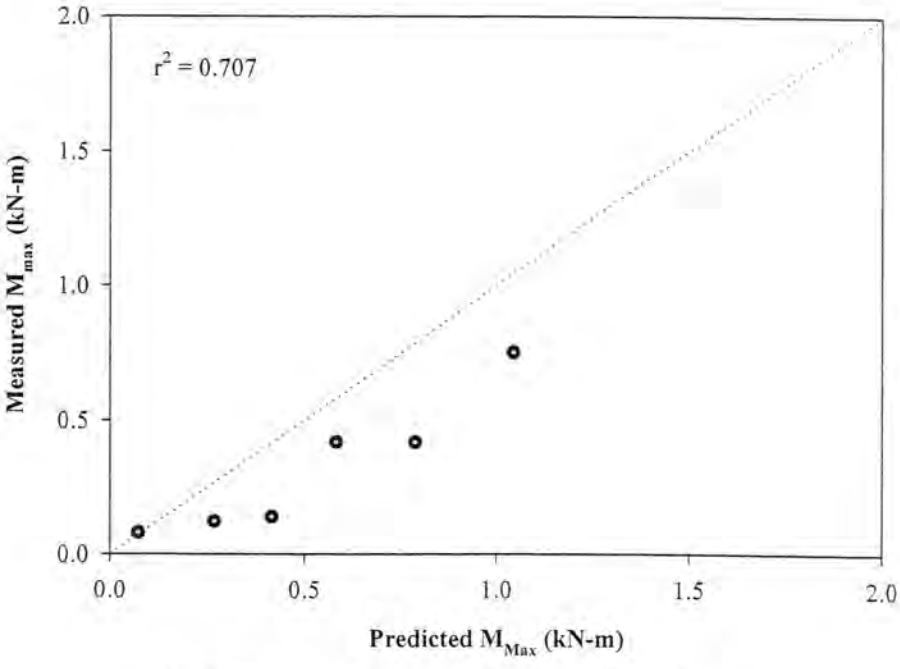

Figure 231 – Maximum Moment Correlation
(Pile 13 A in Glacial Till)

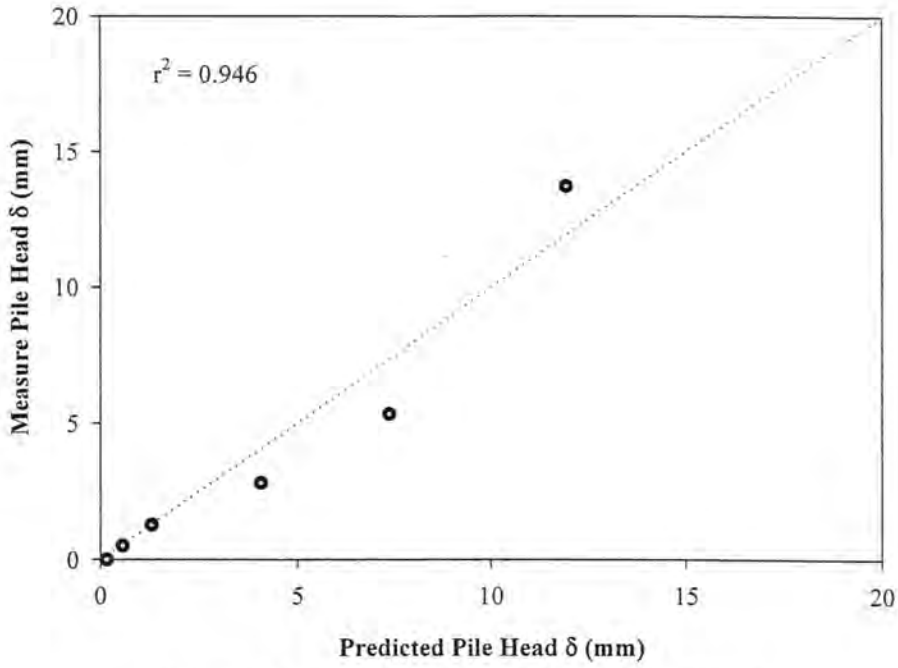

Figure 232 – Pile Head Deflection Correlation
(Pile 13 B in Glacial Till)

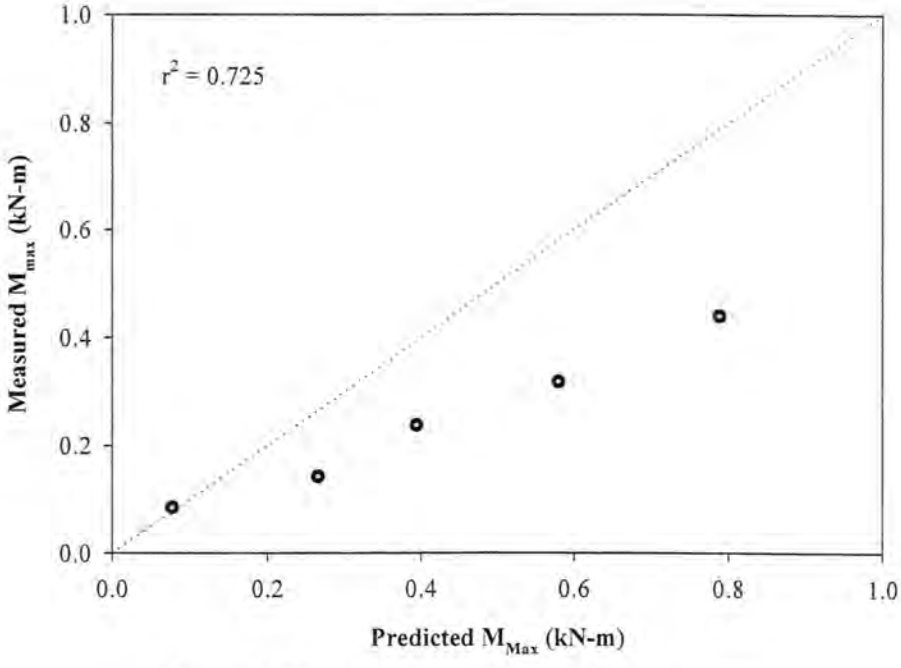

Figure 233 – Maximum Moment Correlation
(Pile 13 B in Glacial Till)

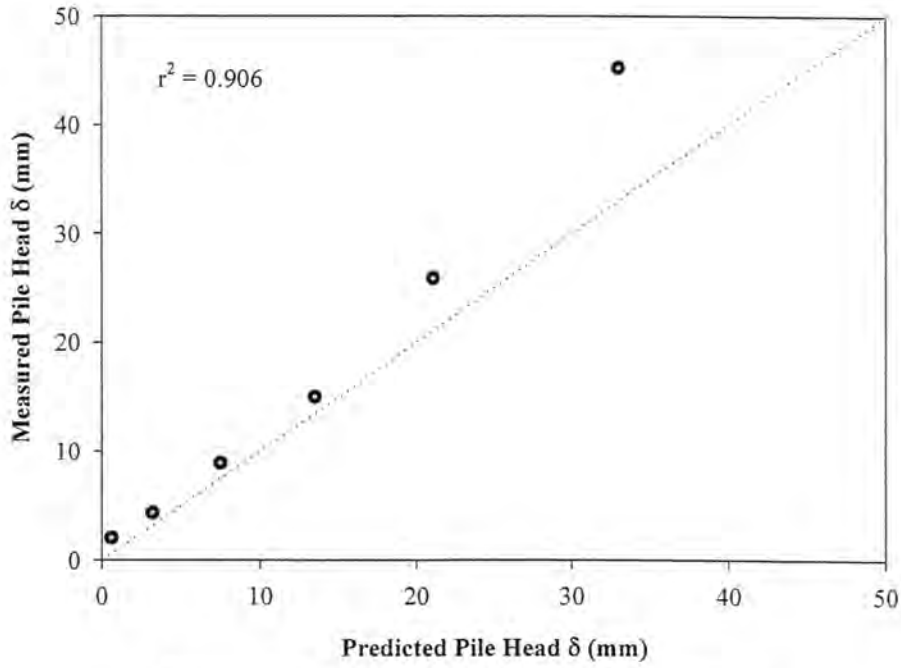

Figure 234 – Pile Head Deflection Correlation
(Pile 14 B in Glacial Till)

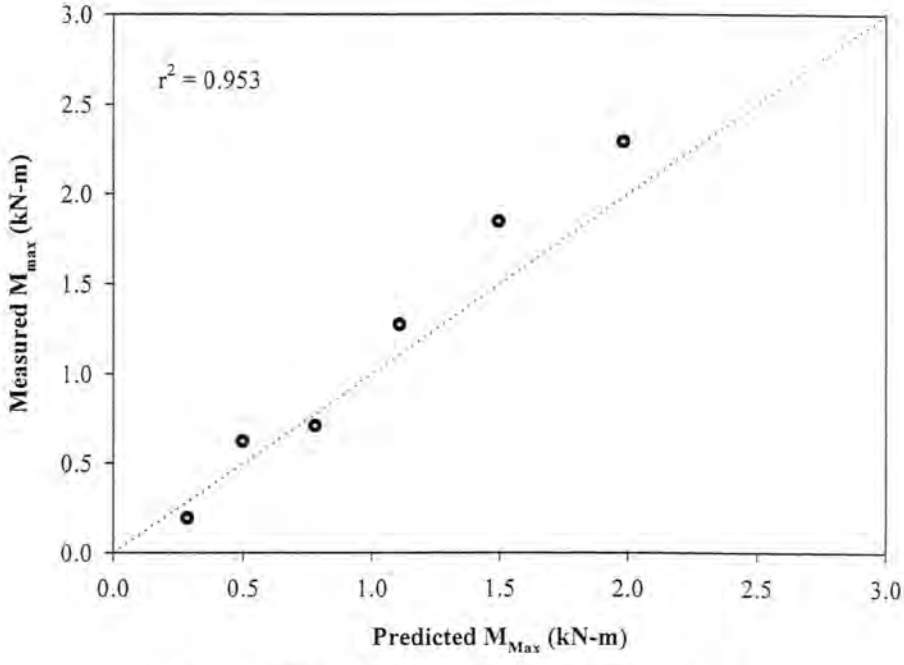

Figure 235 – Maximum Moment Correlation
(Pile 14 B in Glacial Till)

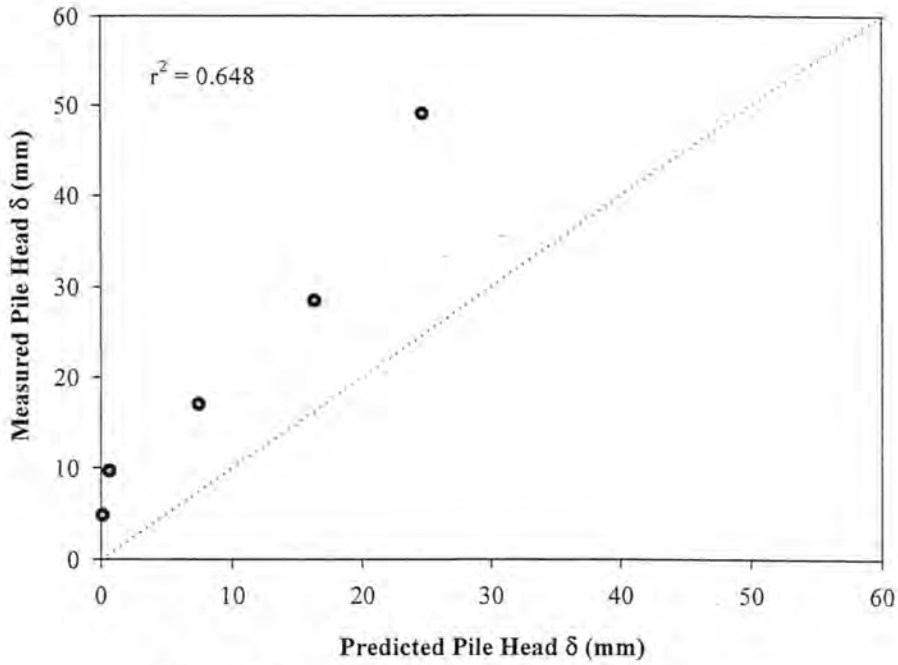

Figure 236 – Pile Head Deflection Correlation
(Pile 10 A in Weathered Shale)

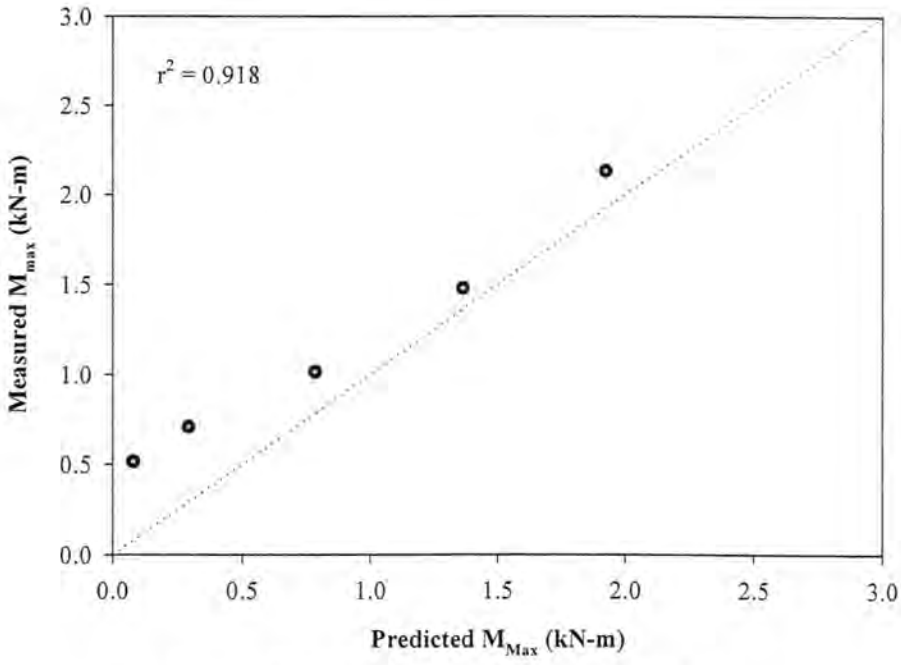

Figure 237 – Maximum Moment Correlation
(Pile 10 A in Weathered Shale)

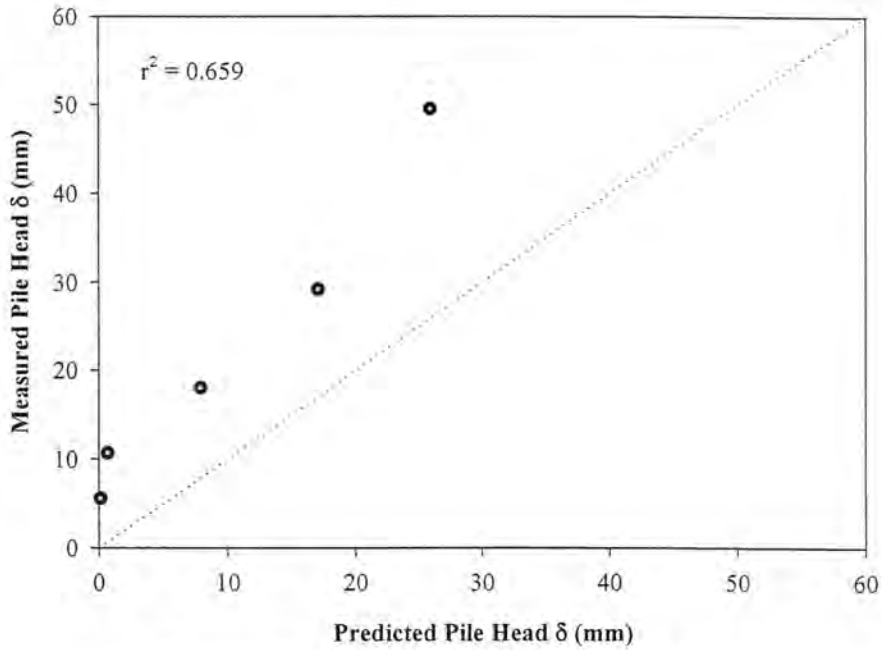

Figure 238 – Pile Head Deflection Correlation
(Pile 10 B in Weathered Shale)

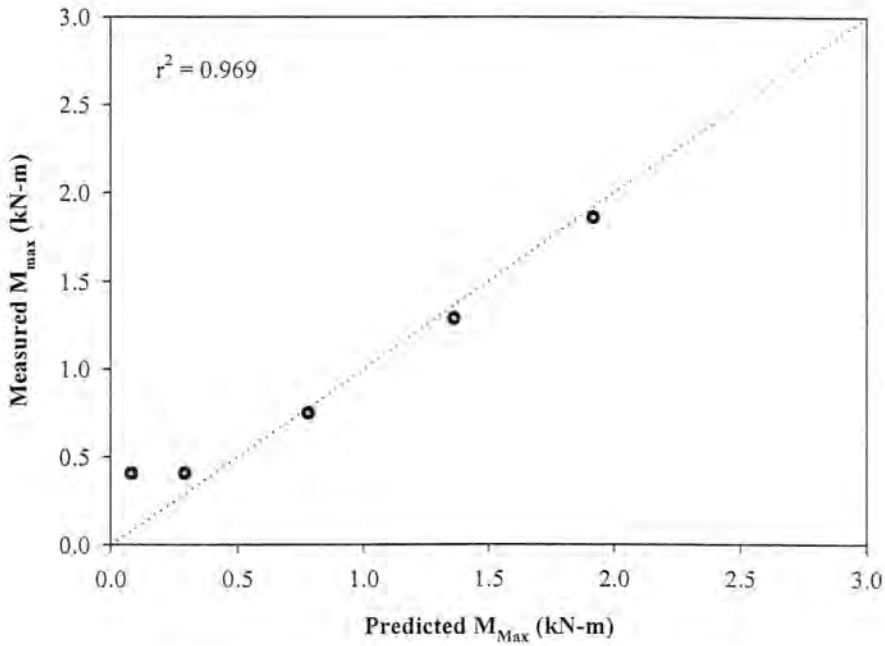

Figure 239 – Maximum Moment Correlation
(Pile 10 B in Weathered Shale)

The correlations of Figures 214 through 239 were reviewed and ranked, as follows: excellent, good, fair, poor, or very poor. The correlations generally correspond to r^2 values of 0.9, 0.7, 0.5, and 0.3 for excellent, good, fair, and poor, respectively. The analysis results were organized by soil type to assess the adequacy of the soil constitutive models and the validity of the trial load distributions. The correlation rankings are provided in Figures 240 through 242.

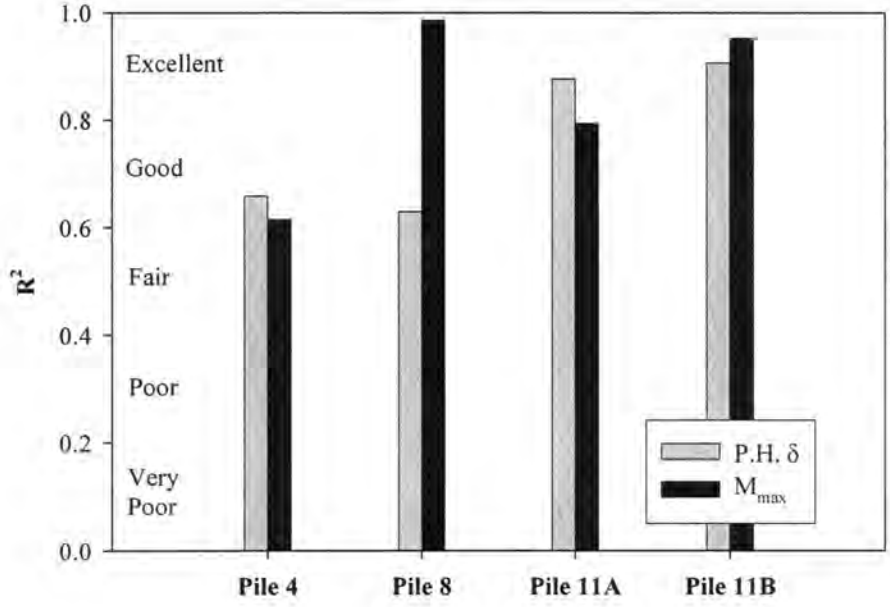

Figure 240 – Correlation of Pile Behavior in Loess

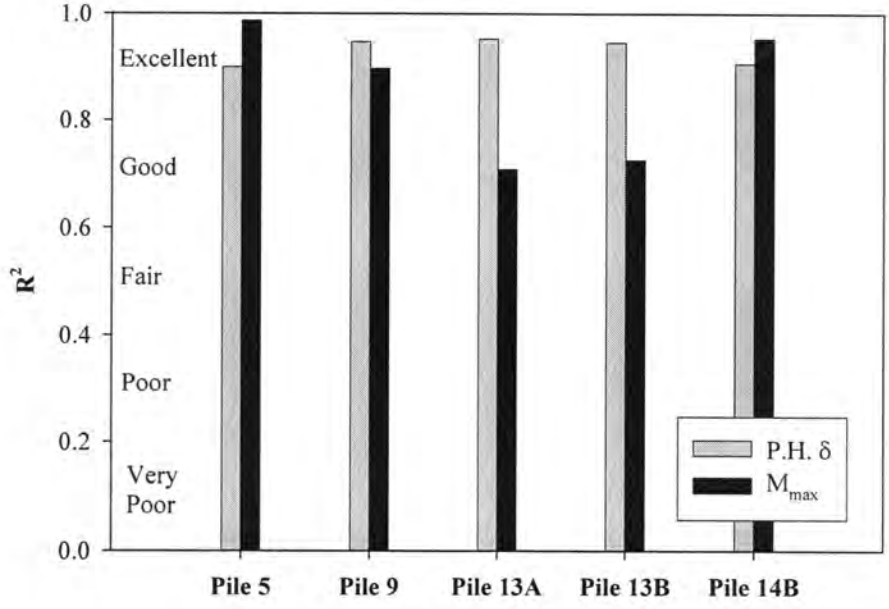

Figure 241 – Correlation of Pile Behavior in Glacial Till

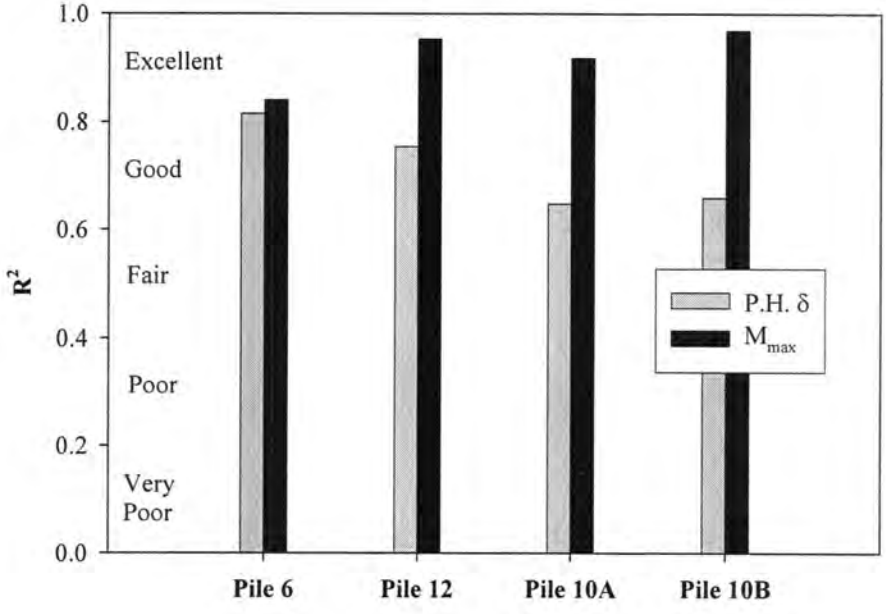

Figure 242 – Correlation of Pile Behavior in Weathered Shale

The analysis of piles installed in loess and glacial till shows that predicted pile behavior agrees with measured pile behavior. The research group concluded that linearly distributed loads can be used to analyze piles subject to lateral soil movement.

The analysis of piles installed in weathered shale shows relatively poor correlation of predicted and measured pile behavior for several tests. The research group does not attribute the poor correlation to the employed p-y curve for weathered shale, because the pile head deflections and maximum moments of Pile 12 (173-mm pile) are very well predicted. The linearly-varying trial load distributions were considered appropriate, because linear load distributions (as opposed to uniform load distributions) produced pile responses that more closely represented measured pile behavior (see Figures 192, 193, 198, 199, 218, 219, 224, and 225). Rather, the research group speculates that lack of correlation is due to the stiff load-displacement behavior of unreinforced weathered shale. A single test on unreinforced weathered shale is used to characterize the soil behavior, and a likely source of error is the determination of the total resisting forces applied to piles. The error source is more prevalent in tests containing weathered shale, because the changes in load over small displacements are much greater than those associated with loess or glacial till.

Verification of Predicted Structural Performance of Pile Elements

Figures 243 and 244 were developed to show the maximum moment achieved in the pile during loading. The measured maximum moments corresponding to the maximum applied load on the pile are plotted against the maximum moments predicted with LPILE for the appropriate load application. The plot indicates whether LPILE over-predicts or under-predicts the moment induced in a pile subject to a given loading. Additionally, the graphs show the cracking moment and the moment capacity of the pile section for each test pile. The location of the measured maximum moment on this continuum indicates the level of

bending stresses that were achieved during experimental testing and whether the loading of the system mobilized the ultimate soil pressure or the moment capacity of the pile sections.

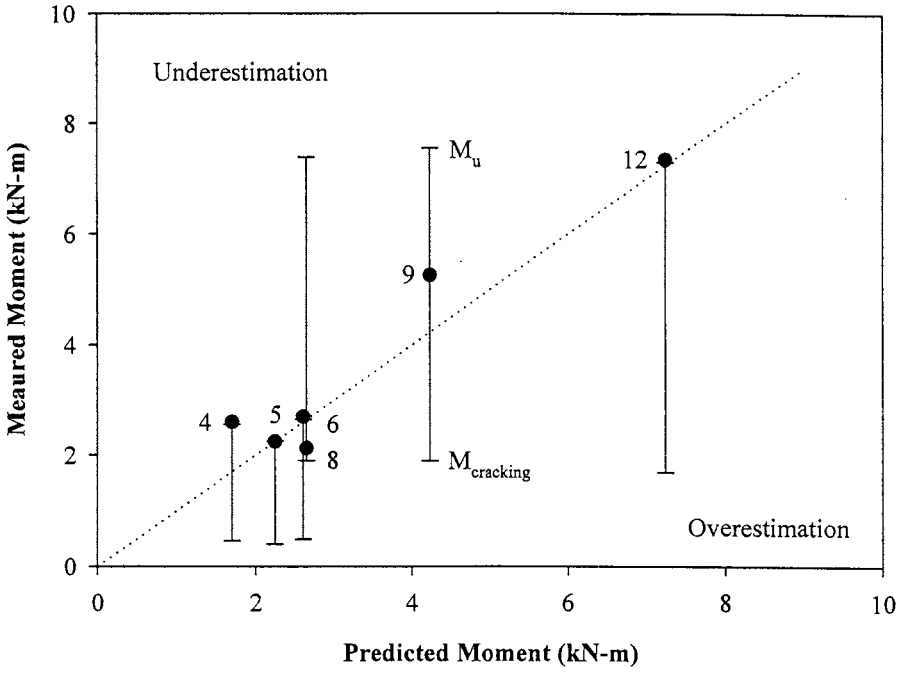

Figure 243 – Measured and Predicted Moments for Single Piles

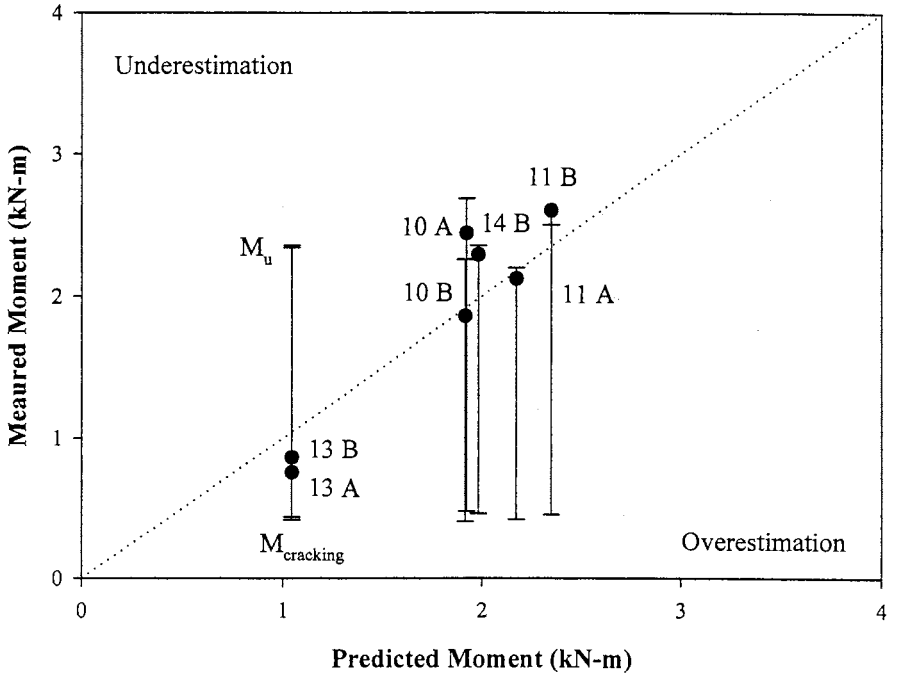

Figure 244 – Measured and Predicted Moments for Multiple Piles

DISCUSSION OF RESULTS

Comparison of Load Distributions with Existing Analytical Models

The load test analysis suggests that the load development on piles subject to lateral soil movement varies linearly with depth, as opposed to the development of uniform load distributions on piles. The figures of "Estimation of Load Distributions with LPILE Software" (Figures 188 through 213) support the claim of linearly distributed load application preceding the formation of a gap, in that the measured values of pile head deflection and maximum moment generally agree with those predicted by LPILE. The range of loading in LPILE ends at the mobilization of shear or moment capacities of pile sections, such that post-peak behavior was unanalyzed. The implementation of the study findings into a design methodology, nevertheless, focuses on the prediction of service loads which develop prior to failure of soil or pile elements. The prediction of gap formation and post-peak load distributions, although important for understanding pile behavior for the full range of loading, is not important for developing a design methodology based on strength limit states.

The principal consequence of failing to mobilize the ultimate soil pressure is the inability to directly deduce the ultimate soil pressure profile with depth. Existing analytical models and the proposed design methodology, however, assume that loads develop along piles as a factored ultimate soil pressure profile (Loehr and Bowders 2003). The research established that the loads developed along the piles vary linearly with depth, and the research group speculates that the ultimate soil pressure likely varies linearly with depth. The research group accepts the dependence of ultimate soil pressure on effective stress and considered using analytical models which incorporate overburden pressure (e.g. Ito and Matsui 1975, Brinch Hansen 1961) for designing pile stabilization. The results, however, do not document the conclusion that such analytical models are always more appropriate than those models which incorporate only undrained shear strength.

Extension of Pile Performance Prediction for Design of Alternative Pile Sections

The ability to accurately predict structural performance of pile sections is important for making stabilization with soil displacement grouted micropiles a robust slope remediation alternative. The benefits of designing piles to be weak or strong, depending on the controlling failure mechanism and required capacity of stabilizing piles, include the design of practical slope reinforcement systems and optimization of the designs to satisfy the cost constraints of the slope remediation.

The load test analysis required the validation of the predicted structural performance of the test piles. The analysis objective was achieved, as evidenced by the close correlation between measured maximum moments in failed piles (i.e. moment capacity) and the computed moment capacities of LPILE. Measured pile head deflections and bending behavior, which is highly dependent on pile flexural stiffness (changing with continued loading), was also well predicted with LPILE. As a result, LPILE is used to reliably analyze and design pile sections with alternative material properties and reinforcement arrangements.

CHAPTER 6

SDGM DESIGN METHODOLOGY

INTRODUCTION

The proposed design method offers a rational approach to slope stabilization with soil displacement grouted micropiles. The design methodology incorporates the following elements:

- Limit equilibrium analyses of unstable, unreinforced slopes
- Reinforcing effect of small-diameter pile elements, including structural capacity of the pile sections and the effect of the pile elements on the global stability of the reinforced slope
- Approach for designing pile sections, based on calculated moment capacities
- Recommendations for arrangement of piles on slopes

OVERVIEW OF LIMIT STATE DESIGN METHODOLOGY

To provide adequate stability for unstable slopes, inclusive of considering the potential failure of the reinforced slope, the proposed design procedure incorporates limit states. Specifically, the design procedure incorporates strength limit states that address potential failure mechanisms of pile-stabilized slopes. The possible modes of failure for slopes stabilized with pile elements include: (1) mobilization of the ultimate soil pressure and failure of the soil above the sliding surface, (2) passive failure of soil below the sliding surface due to insufficient anchorage, and (3) structural failure of individual pile elements due to bending forces developed in the piles that exceed the capacity of the pile sections.

The service limit states associated with the design of other earth and building structures are less important to the stabilization of nuisance slope failures. Small deformations of the slope are generally accepted, provided the slope maintains its primary function.

The presently discussed design procedure does not make the assumption that the stabilized slope moves sufficiently to mobilize the ultimate soil pressure along each pile element. Rather the design procedure assumes that a sufficient number of piles are installed to arrest slope movement before the ultimate soil pressure is allowed to develop. The unique stabilization approach, in which pile stability possibly controls the stabilization design, emphasizes the evaluation of limit states corresponding to the previously mentioned failure modes. The next section, based on the approach for designing recycled plastic pin stabilization (ref. Chapter 2), offers a step-by-step procedure for developing limit resistance curves.

DEVELOPMENT OF LIMIT STATES

Step 1 – Establish Design Input Variables

Step 1.a

Establish in spreadsheet software, to reference for subsequent calculations, the design input variables (see Figure 245).

The necessary soil parameters are:

- Effective cohesion, c'
- Effective internal friction angle, ϕ'
- Unit weight, γ
- Soil modulus, E_s

The necessary parameters related to properties and arrangement of pile elements are:

- Pile diameter, b
- Stiffness, EI

- Moment capacity, M_u
- Center-to-center spacing, D_1

Step 1.b

Calculate the Rankine passive, at-rest, and active lateral earth pressure (LEP) coefficients (K_p, K_o, and K_a, respectively) with Equations (30) through (32). Calculate the clear distance between piles, D_2, with Equation (33).

$$K_p = \tan^2(45 + \frac{\phi}{2}) \text{ for passive LEP,} \quad (30)$$

$$K_o = 1 - \sin\phi \text{ for at-rest LEP, and} \quad (31)$$

$$K_a = \tan^2(45 - \frac{\phi}{2}) \text{ for active LEP,} \quad (32)$$

$$D_2 = D_1 - b \quad (33)$$

Soil Properties	
c (kPa)	10.0
ϕ (deg)	14
γ_t (kN/m^3)	18.8
E_s (kPa)	20700

K_p	1.638
K_o	0.758
K_a	0.610

Pile Properties	
b (mm)	178
EI (kN-m^2)	657.3
M_u (kN-m)	25.90
D_1 (m)	0.91

D_2 (m)	0.73

Figure 245 – Calculation of Design Input Variables

Step 2 – Calculate Limit Soil Resistance

Step 2.a

Establish and calculate N_ϕ, J_1, J_2, and J_3 using Equations (34) through (37) (see Figure 246). The variables, each a function of the internal friction angle, are used solely to simplify

the later calculation of ultimate soil pressure. For the preliminary calculations, the units of internal friction angle are radians.

$$N_\phi = \tan^2(\frac{\pi}{4} + \frac{\phi}{2}), \tag{34}$$

$$J_1 = N_\phi^{1/2} \tan\phi + N_\phi - 1, \tag{35}$$

$$J_2 = 2\tan\phi + 2N_\phi^{1/2} + N_\phi^{-1/2}, \text{ and} \tag{36}$$

$$J_3 = N_\phi \tan\phi \tan(\frac{\pi}{8} + \frac{\phi}{4}), \tag{37}$$

N_ϕ	1.63825
$\tan\phi$	0.24933
$N_\phi \tan\phi$	0.40846
J_1	0.95738
J_2	3.83982
J_3	0.19922

Figure 246 – Calculation of Simplifying Variables

Step 2.b

For depths from the ground surface to the pile tip (6-m-length pile in this case), at approximately 0.2-m intervals, calculate the vertical overburden pressure, σ_v, with Equation (38). The uppermost depth is established at z = 0.001 m. The use of a non-zero value eliminates the "division by zero" error of spreadsheet software. Calculate the ultimate soil pressure, P_u, with Equation (39) (see Figure 247).

$$\sigma_v = \gamma z, \tag{38}$$

$$P_u(z) = c\,D_1\left(\frac{D_1}{D_2}\right)^{J_1}\left[\frac{1}{N_\phi \tan\phi}\left\{e^{\frac{D_1-D_2}{D_2}J_3} - 2\,N_\phi^{1/2}\tan\phi - 1\right\} + \frac{J_2}{J_1}\right] \qquad (39)$$

$$- c\left\{D_1\frac{J_2}{J_1} - 2\,D_2\,N_\phi^{-1/2}\right\} + \frac{\sigma_v}{N_\phi}\left\{D_1\left(\frac{D_1}{D_2}\right)^{J_1}\cdot e^{\frac{D_1-D_2}{D_2}J_3} - D_2\right\}$$

z = 0.001 m

Depth	Overburden Pressure	Ult Soil Pressure
z (m)	σ_v (kPa)	$P_u(z)$ (kN/m)
0.0	0.19	3.79
0.2	3.76	4.76
0.4	7.52	5.78
0.6	11.28	6.80
0.8	15.04	7.82
1.0	18.80	8.84
1.2	22.56	9.86
1.4	26.32	10.88
1.6	30.08	11.90
1.8	33.84	12.92
2.0	37.60	13.94

Figure 247 – Calculation of Ultimate Soil Pressure

Step 2.c

Establish potential sliding depths, Z_s, for which the limit soil resistance, F_S, is calculated. For relative ease of calculation, use sliding depths equal to the depths at which ultimate soil pressures are calculated as follows:

$$Z_s = z \qquad (40)$$

Step 2.d

Calculate the limit soil resistance, F_S, by integrating the ultimate soil pressure from the ground surface to each sliding depth. Use the trapezoidal rule of integration, as illustrated with Equation (41). Make certain that $F_S = 0$ at the ground surface.

$$F_S = F_{S,n-1} + \frac{(P_{u,n-1} + P_{u,n})}{2} \cdot (z_n - z_{n-1}) \quad (41)$$

Step 2.e

Divide the calculated limit soil resistance, F_S, by the pile spacing, D_1, to obtain limit soil resistance per unit length of slope, denoted F_S' (see Figure 248).

$$F_S'(\text{kN/m}) = \frac{F_S\ (\text{kN})}{D_1\ (\text{m})} \quad (42)$$

Depth	Overburden Pressure	Ult Soil Pressure	Slide Depths	Limit Soil Resistance	
z (m)	σ_v (kPa)	$P_u(z)$ (kN/m)	Z_s (m)	F_S (kN)	F_S' (kN/m)
0.0	0.19	3.79	0.0	0.00	0.00
0.2	3.76	4.76	0.2	0.81	0.89
0.4	7.52	5.78	0.4	1.87	2.05
0.6	11.28	6.80	0.6	3.13	3.44
0.8	15.04	7.82	0.8	4.59	5.04
1.0	18.80	8.84	1.0	6.26	6.87
1.2	22.56	9.86	1.2	8.13	8.93
1.4	26.32	10.88	1.4	10.20	11.21
1.6	30.08	11.90	1.6	12.48	13.71
1.8	33.84	12.92	1.8	14.96	16.44
2.0	37.60	13.94	2.0	17.65	19.39

Figure 248 – Calculation of Limit Soil Resistance

Step 3 – Calculate Limit Anchorage Resistance

Step 3.a

The maximum F_S value is located at the sliding depth equal to the pile length. Identify this value ($F_{S,max}$) for subsequent calculations (see Figure 249). Calculate the limit anchorage resistance, F_A, by subtracting the F_S value, for each sliding depth, from $F_{S,max}$. Calculation of the limit anchorage resistance in this manner is equivalent to integrating the ultimate soil pressure from each sliding depth to the pile tip.

Step 3.b

Divide the calculated limit anchorage resistance, F_A, by the pile spacing, D_1, to obtain limit anchorage resistance per unit length of slope, denoted F_A' (see Figure 249).

$$F_A'(\text{kN/m}) = \frac{F_A\ (\text{kN})}{D_1\ (\text{m})} \tag{43}$$

Slide Depths	Limit Soil Resistance		Limit Anchorage Resistance	
Z_s (m)	F_S (kN)	F_S' (kN/m)	F_A (kN)	F_A' (kN/m)
0.0	0.00	0.00	114.23	125.52
0.2	0.81	0.89	113.41	124.63
0.4	1.87	2.05	112.36	123.47
0.6	3.13	3.44	111.10	122.09
0.8	4.59	5.04		
1.0	6.26	6.87		
1.2	8.13	8.93		
1.4	10.20	11.21	104.03	114.32
1.6	12.48	13.71	101.75	111.81
1.8	14.96	16.44	99.27	109.08
2.0	17.65	19.39	96.58	106.13
2.2	20.54	22.57	93.69	102.95
2.4	23.63	25.97	90.59	99.55
2.6	26.93	29.60	87.30	95.93
	30.44	33.45	83.79	92.08
	34.14	37.52	80.09	88.01
	38.05	41.82	76.17	83.71
3.4	42.17	46.34	72.06	79.19
3.6	46.49	51.08	67.74	74.44
3.8	51.01	56.05	63.22	69.47
4.0	55.74	61.25	58.49	64.28

$F_{S,max} - F_S = F_A$
$F_A = 114.23 - 0.81$ kN

At $Z_s = 6$ m,
$F_S = 114.23$ kN

Figure 249 – Calculation of Limit Anchorage Resistance

Step 4 – Calculate Limit Member Resistance

Step 4.a

Calculate the polynomial constants in Equation (44), f_1 and f_2, using Equations (45) and (46). Also calculate the characteristic length, β, with Equation (47), based on relative stiffness of the soil and the pile (see Figure 250).

$$P_u = f_1 + f_2 z \tag{44}$$

$$f_1 = c D_1 \left(\frac{D_1}{D_2}\right)^{J_1} \left[\frac{1}{N_\phi \tan\phi}\left\{e^{\frac{D_1-D_2}{D_2}J_3} - 2 N_\phi^{1/2} \tan\phi - 1\right\} + \frac{J_2}{J_1}\right] \tag{45}$$

$$- c\left\{D_1 \frac{J_2}{J_1} - 2 D_2 N_\phi^{-1/2}\right\}$$

$$f_2 = \frac{\gamma}{N_\phi}\left\{D_1 \left(\frac{D_1}{D_2}\right)^{J_1} \cdot e^{\frac{D_1-D_2}{D_2}J_3} - D_2\right\} \tag{46}$$

$$\beta = \sqrt[4]{\frac{E_s}{4 E_p I_p}} \tag{47}$$

f_1 (kN/m)	10.69
f_2 (kN/m^2)	5.10
β (m^{-1})	1.68

Figure 250 – Calculation of Polynomial Constants and Characteristic Length

Step 4.b

For each potential sliding depth, calculate the maximum moment developed along the pile with Equation (51). This step requires preliminary calculation of A, B, and z2 with Equations (48) through (50).

$$A = \frac{Z_s}{12E_pI_p\beta^3}\{3(2+\beta Z_s)f_1 - Z_s(3+2\beta Z_s)f_2\} \quad (48)$$

$$B = \frac{-(Z_s)^2}{12E_pI_p\beta^2}(3f_1 - 2Z_sf_2) \quad (49)$$

$$z_2 = \frac{1}{\beta}\tan^{-1}\frac{A+B}{A-B} \quad (50)$$

$$M_{max} = -2E_pI_p\beta^2 e^{-\beta z_2}(A\sin\beta z_2 - B\cos\beta z_2) \quad (51)$$

Step 4.c

Calculate the reduction factor, α, by which the ultimate soil pressure is increased or, more commonly, decreased. The reduction factor is given by Equation (52) and varies with the depth to the sliding surface, Z_S.

$$\alpha = \frac{M_u}{M_{max}} \quad (52)$$

Step 4.d

Calculate the limit member resistance, F_M, for each potential sliding depth, by multiplying the reduction factor, α, and the limit soil resistance, F_S (see Equation (53)).

$$F_M = \alpha F_S \quad (53)$$

Step 4.e

Divide the calculated limit member resistance, F_M, by the pile spacing, D_1, to obtain limit member resistance per unit length of slope, denoted F_M' (see Figure 54).

$$F_M'(kN/m) = \frac{F_M(kN)}{D_1(m)} \quad (54)$$

					Limit Member Resistance	
A (m)	B (m)	z_2 (m)	M_{max} (kN-m)	α	F_M (kN)	F_M' (kN/m)
0.000	0.000	0.464	0.021	1241.26	0.00	0.00
0.000	0.000	0.385	0.530	48.84	39.69	43.62
0.001	-0.001	0.326	1.288	20.10	37.54	41.26
0.001	-0.001	0.283	2.236	11.58	36.20	39.78
0.002	-0.001	0.251	3.319	7.80	35.81	39.35
0.002	-0.001	0.227	4.466	5.66	36.24	39.82
0.003	-0.001	0.209	5.643	4.46	37.46	41.16
0.003	-0.002	0.195	6.824	3.69	39.49	43.40
0.004	-0.002	0.185	7.606	3.41	42.49	46.70
0.004	-0.002	0.178	8.290	3.12	46.74	51.37
0.004	-0.002	0.174	8.664	2.99	52.75	57.97
0.004	-0.002	0.174	8.651	2.99	61.49	67.57
0.004	-0.002	0.180	8.175	3.17	74.87	82.28
0.003	-0.002	0.193	7.166	3.61	97.34	106.97
0.003	-0.001	0.224	5.568	4.65	141.58	155.58

At $Z_S = 0.2$ m, $F_S = 0.81$ kN

$F_M = \alpha F_S$
$F_M = 48.84 \times 0.81$ kN

Figure 251 – Calculation of Limit Member Resistance

Step 5 – Plot Composite Limit Resistance Curve

The composite limit resistance, used for designing slope reinforcement, is the minimum of the limit resistances for the three respective failure modes (i.e. F_R = minimum(F_S, F_A, F_M)) (see Figure 252). Plot the composite limit resistance as a function of sliding depth, Z_s (see Figure 253).

$F_R = \min(F_S, F_A, F_M)$

Composite Limit Resistance	
F_R (kN)	F_R' (kN/m)
0.00	0.00
0.81	0.89
1.87	2.05
3.13	3.44
4.59	5.04
6.26	6.87
8.13	8.93

Figure 252 – Calculation of Composite Limit Resistance

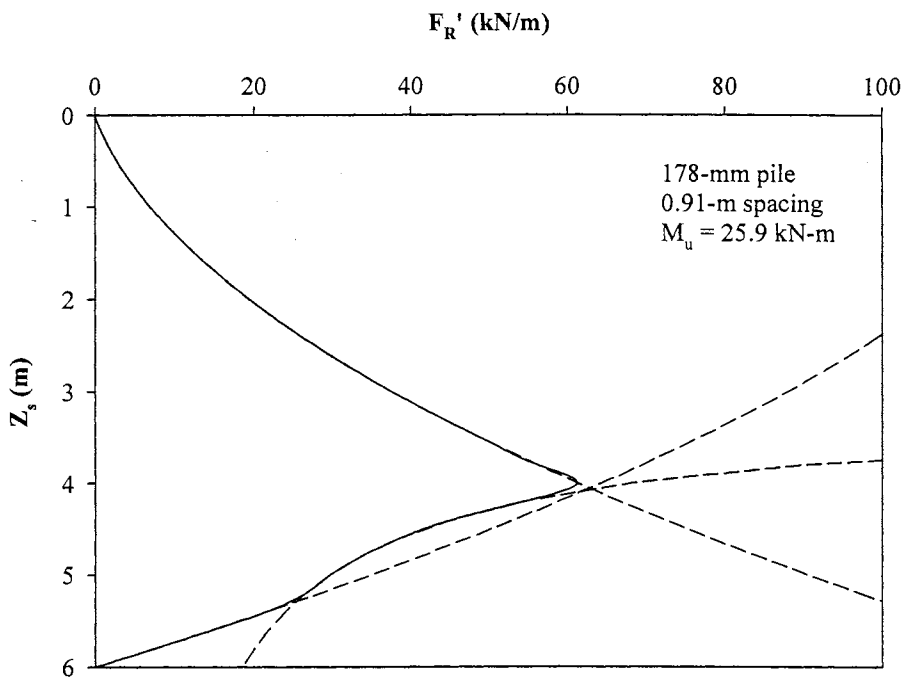

Figure 253 – Composite Limit Resistance Curve

DESIGN PROCEDURES

The design protocol, detailed in the ensuing sections, proceeds with the following steps:

1. Global stability analysis for unreinforced slope
2. Calculation of required stabilizing force
3. Development of composite limit resistance curves
4. Calculation of required number of rows and piles
5. Global and local stability analyses for reinforced slope
6. Material cost analysis

Step 1 – Perform the Global Stability Analysis for Unreinforced Slope

The performance of slope stability analyses for the unreinforced slope is necessary to evaluate the condition of the slope. A detailed analysis, performed in conjunction with a slope investigation, aids in establishing the cause of instability and effective remediation alternatives. Site investigations that encounter high groundwater tables, for example, may suggest that reduced effective stresses are responsible for slope instability. The influence of the groundwater table elevation on the stability of a slope is easily verified by performing multiple stability analyses. Subsurface drainage may be considered to be a primary remediation alternative when groundwater causes slope instability. Subsurface drainage fails to improve the stability of slopes, however, when groundwater has little effect on the unstable slope. Rather, the performed analyses may suggest that slope geometry and/or weak slope soils are responsible for slope instability. In this case, slope reinforcement and use of piles for slope stabilization may be considered to be a potential remediation alternative. Perform the stability analysis of the unreinforced slope to indicate the required capacity of slope reinforcement. In addition to the factor of safety, document the forces driving and resisting slope movement and the depths to the failure surface along the slope profile. The stability analysis may involve the documentation of multiple failure surfaces, where the

failure surface of the unreinforced slope does not necessarily match the failure surface of the reinforced slope.

Step 2 – Calculate the Required Stabilizing Force

The stability of an unreinforced slope and global stability specifications control the required capacity of slope reinforcement. Use the total resisting and driving forces (ΣFR and ΣFD, respectively) from the stability analysis and the target factor of safety to calculate the required stabilizing force, ΔFR (see Equation (55)).

$$\Delta F_R = FS \cdot \Sigma F_D - \Sigma F_R \text{ , per unit length of slope} \qquad (55)$$

where, ΔF_R = total stabilizing force,

ΣF_R = total resisting force (unreinforced slope),

ΣF_D = total driving force (unreinforced slope), and

FS = factor of safety

The achievement of ΔFR with the installation of piles necessarily satisfies the established stability requirements for the slope.

Step 3 – Develop Composite Limit Resistance Curves

Develop the limit resistance curves for soil displacement grouted micropiles, as presented earlier in this chapter. Table 24 provides the moment capacities and stiffness values of several steel-reinforced pile sections, determined from a pile section analysis with LPILE. The table values are inputs for developing composite limit resistance curves. Design charts (i.e. prepared composite limit resistance curves for select soil parameters and pile sections) are provided in Appendix D for the convenient design of pile size, spacing, and reinforcement.

Table 24 – Properties of SDGM Sections

		M_u (kN-m)		EI (kN-m^2)	
b (mm)	**Reinforcement**	**Unfactored**	**Factored**	**Uncracked**	**Cracked**
102	(1) No. 19	1.634	1.362	129	28
127	(1) No. 19	3.015	2.512	316	60
127	(1) No. 25	3.238	2.699	316	77
127	102-mm Pipe*	13.375	11.146	316	n/a
178	(1) No. 19	7.189	5.991	1210	161
178	(1) No. 25	8.144	6.787	1210	224
178	(1) No. 32	8.688	7.240	1210	276
178	(4) No. 19	15.598	12.998	1380	488
178	152-mm Pipe*	31.554	26.295	1380	n/a
203	(1) No. 25	11.667	9.723	2070	316
203	(1) No. 32	12.536	10.446	2070	402
203	(4) No. 25	31.840	26.533	2580	1090

Notes:
Concrete strengths are 27.6 MPa
Steel yield strengths are 413.7 MPa
Factored moment capacity uses FS = 1.2
* Pipe thicknesses are 3 mm

Step 4 – Calculate the Required Number of Rows and Piles

Step 4.a

The sliding depths along the slope width are variable, and the use of a single F_R' value for all pile rows oversimplifies the calculation of the required number of rows. Rather, the accurate estimation of the total stabilizing force, ΔF_R, requires the determination of unique stabilizing forces, F_R', obtained from the composite limit resistance curve for sliding depths at each pile row location. The process of identifying limit resistances at each pile row location facilitates the effective and reliable design of pile stabilization. The pile row locations are generally established to maximize F_R'. When the limit soil resistance controls the design, for example, pile rows may be installed on the slope at a location where the sliding depth is largest, ensuring that the limit member resistance does not control the reinforcement stability and stabilization design.

Calculate the required number of pile rows with Equation (56), based on the required stabilizing force of the reinforcement, ΔF_R, and the limit resistances for individual rows of piles, F_R'.

$$n = \frac{\Delta F_R}{F_R'} \tag{56}$$

where n = number of required pile rows

The number of pile rows is conservatively rounded (e.g. n = 2.4 → 3 pile rows required), and a new factor of safety is later calculated based on the achieved ΔF_R.

Step 4.b

Calculate the required number of piles with the number of required pile rows, the pile spacing, and the length of slope needing stabilization (see Equation (57)).

$$\text{Number of Piles} = \frac{\text{Slope length}}{D_i} \cdot n \tag{57}$$

Step 5 – Perform Global and Local Stability Analyses for Reinforced Slope

Step 5.a

Calculate the factor of safety for the reinforced slope with Equation (58), based on the achieved ΔF_R. The computed factor of safety is likely greater than the target factor of safety, because the design methodology conservatively rounds the required number of pile rows.

$$FS = \frac{\Sigma F_R + \Delta F_R}{\Sigma F_D} \tag{58}$$

Step 5.b

Ensure the local stability of the reinforced slope. Identify potential failure surfaces that exist above or below stabilizing piles (see Figure 254), and verify that the factors of safety corresponding to the failure surfaces exceed the stability requirements.

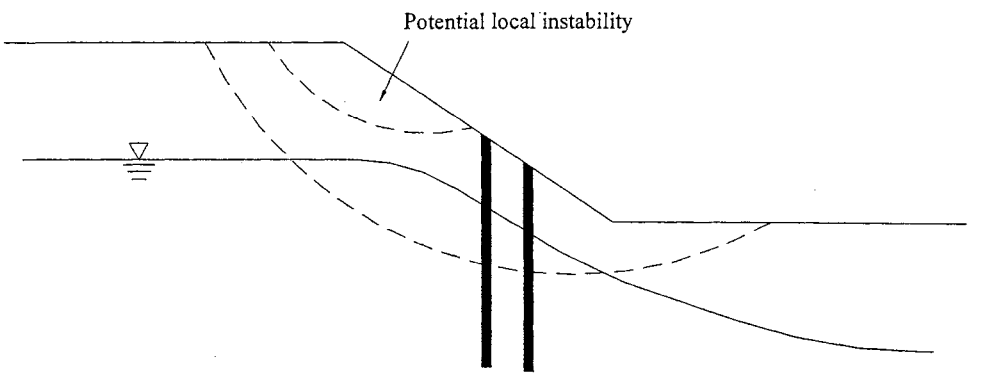

Figure 254 – Local Instability of Reinforced Slope

The recommended layout of soil displacement grouted micropiles employs equilateral spacing, such that the stabilization system achieves maximum benefit from soil arching. Equilateral spacing of SDGM reinforcement is illustrated in Figure 255.

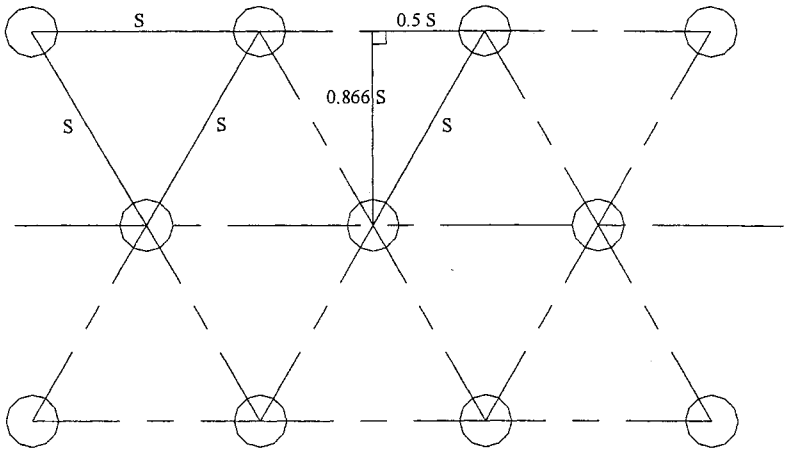

Figure 255 – Equilateral Spacing of SDGM Reinforcement

Step 6 – Perform Material Cost Analysis

Evaluate the cost effectiveness of the design option by performing a material cost analysis. Establish and apply unit prices to the calculated material quantities for the number of piles required to stabilize the unstable slope. A general equation for the material cost of pile stabilization is provided in Equation (59).

$$\text{Cost} = \text{Unit Price} \cdot \frac{\text{Quantity}}{\text{Piles}} \cdot \text{Piles} \tag{59}$$

SAMPLE DESIGN

The sample design demonstrates the stabilization potential of small-diameter pile elements and the effectiveness of the proposed stabilization approach. The demonstration also compares the remediation method with conventional remediation practices of local transportation agencies to show that pile stabilization is recurrently more appropriate than excavation (i.e. benching and/or slope flattening) and construction of drainage structures.

Slope Description

Low shear strength parameters associated with weathered shale result in slope instability throughout Iowa. Remediation of the slope failures is uniquely challenging, because conventional remediation practices may fail to address the cause of instability. Conventional remediation practices target drainage as a general cause of instability, as opposed to low shear strength of slope soil. Slope reinforcement and, more specifically, pile stabilization is likely more effective in preventing continued slope movements in weak soil.

The emblematic slope used to demonstrate the proposed design methodology stands with a maximum height of 6 meters and slope of 3.5:1 (21-m width). The slope geometry is typical of slopes along transportation corridors in Iowa. The slope consists of weathered shale, and residual shear strength parameters for the material were obtained by conducting ring shear tests on weathered shale samples from a project site in Ottumwa, Iowa. The groundwater table was adjusted to provide a factor of safety equal to unity. The location of the groundwater table is sufficiently low to support pile stabilization as the appropriate remediation alternative over the construction of drainage structures.

Step 1 – Global Stability Analysis for Unreinforced Slope

Global stability analyses were performed with SLOPE/W, a slope stability software program, to evaluate the stability of the unreinforced slope. The anticipated failure surface is provided in Figure 256. The forces resisting and driving slope movement, along with corresponding factors of safety, for several limit equilibrium methods are provided in Table 25.

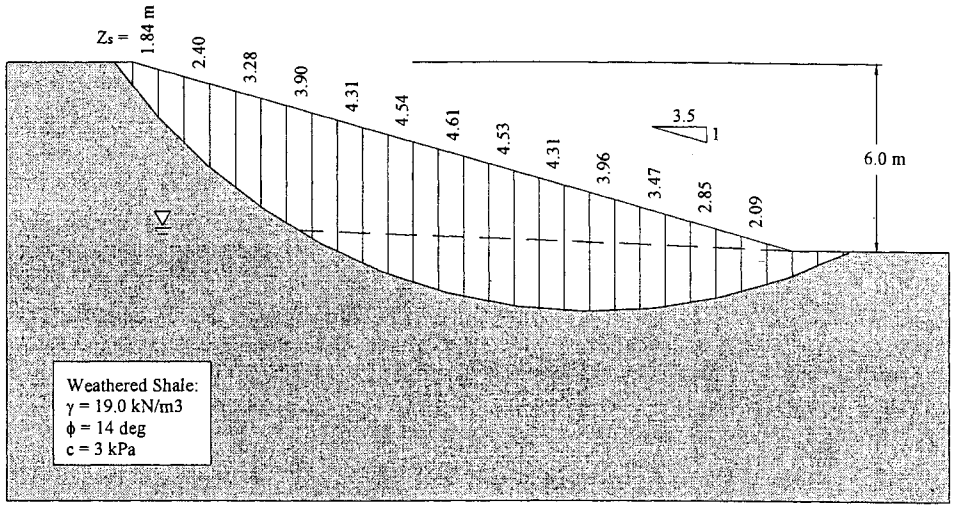

Figure 256 – Potential Failure Surface

Table 25 – Stability Parameters for Unreinforced Slope

(kN/m)	Ordinary Method	Bishop's Simplified	Janbu's Method
ΣF_R*	6755	7348	340.2
ΣF_D*	6549	6549	328.6
FS	1.03	1.12	1.03

Notes:
* Moments for Ordinary and Bishop's methods

Step 2 – Calculation of Required Stabilizing Force

The total required stabilizing force, ΔF_R, is determined with the forces of Table 25 and a factor of safety equal to 1.3.

$$\Delta F_R = FS \cdot \Sigma F_D - \Sigma F_R$$

$$\Delta F_R = 1.3 \cdot 328.6\,kN/m - 340.17\,kN/m$$

$$\Delta F_R = 87.1\,kN/m$$

Step 3 – Development of Composite Limit Resistance Curves

The composite limit resistance curves indicate that member resistance controls the design, such that a second design option employs steel pipe reinforcement. The two stabilization design options of different steel reinforcement are developed herein. The composite limit resistance curves are provided in Figures 257 and 258.

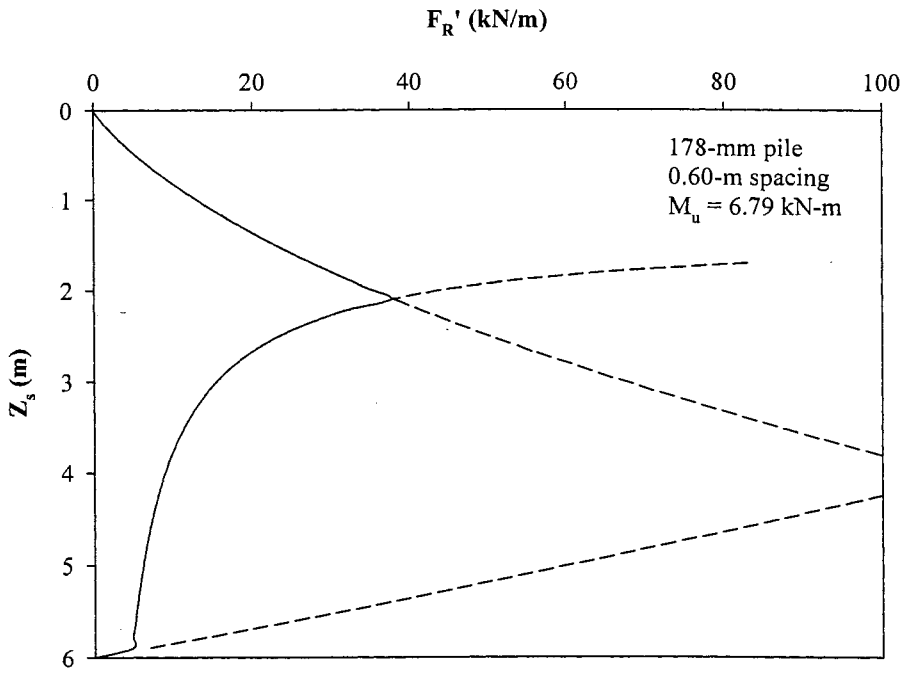

Figure 257 – Limit Resistance Curves for 178-mm Pile with Centered No. 25

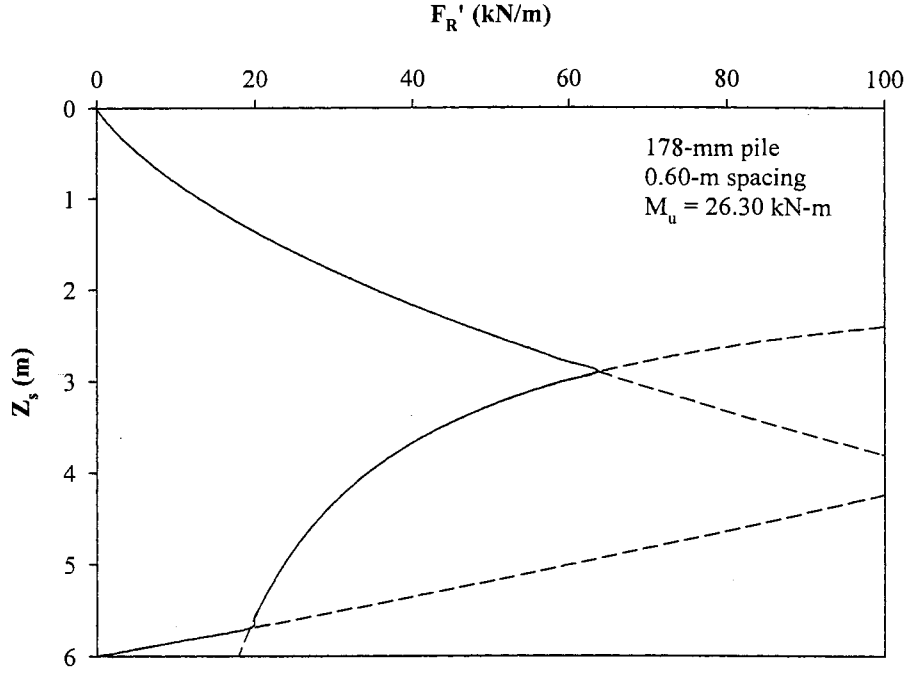

Figure 258 – Limit Resistance Curves for 178-mm Pile with 152-mm Steel Pipe

Step 4 – Calculate the Required Number of Rows and Piles

Step 4.a

Table 26 – Stabilizing Forces Along Sliding Depths of Slope Profile

Z_S (m)	178-mm Pile (1) No. 25	178-mm Pile 152-mm Pipe
2.09	37.57	—
2.85	17.84	60.10
3.47	11.30	43.74
3.96	8.85	—
4.31	7.81	—
ΔF_R	83.37	103.84
n	5	2

Notes:
Units of kN/m
Z_S values from Figure 227
n = number of required rows
ΔF_R = sum of stabilizing forces for each row

Step 4.b

The required number of piles was calculated for a 91-m (300-ft) slope length.

$$\text{Number of Piles} = \frac{\text{Slope length}}{D_1} \cdot n$$

$$\text{Number of Piles} = \frac{91\,\text{m}}{0.60\,\text{m}} \cdot 5 = 758 \text{ piles for centered No. 25 reinforcement}$$

$$\text{Number of Piles} = \frac{91\,\text{m}}{0.60\,\text{m}} \cdot 2 = 303 \text{ piles for 152 - mm pipe reinforcement}$$

Step 5 – Global and Local Stability Analyses for Reinforced Slope

Step 5.a

$$FS = \frac{\Sigma F_R + \Delta F_R}{\Sigma F_D}$$

$$FS = \frac{340.2 + 83.4}{328.6} = 1.29 \text{ for centered No. 25 reinforcement}$$

$$FS = \frac{340.2 + 103.8}{328.6} = 1.35 \text{ for 152 - mm pipe reinforcement}$$

Step 5.b

Local stability in ensured by performing a stability analysis in which potential failure surfaces are limited to a particular location. The rows of piles are simply modeled by high strength soil, such that a failure surface generated by slope stability software will not pass through the piles. The likely failure surface for local instability, shown in Figure 259, corresponds to a factor of safety of 1.35.

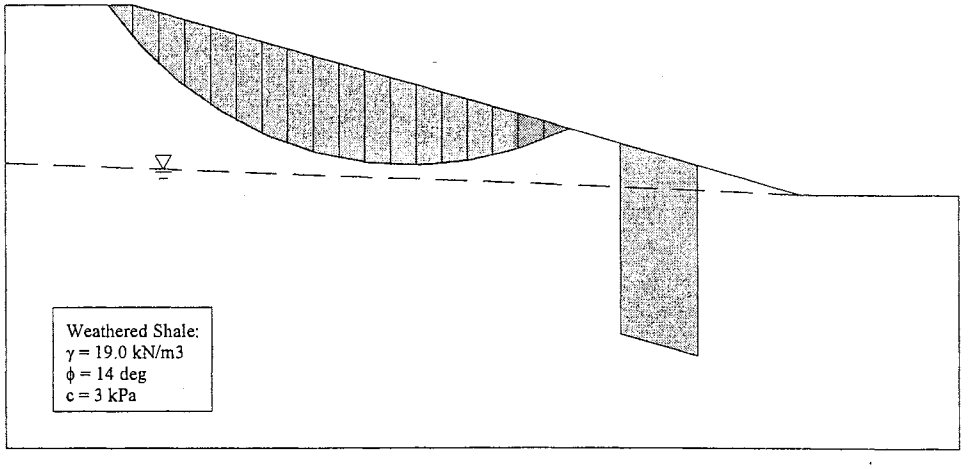

Figure 259 – Failure Surface for Local Instability

Step 7 – Material Cost Analysis

The unit costs and total material costs are developed in Table 27.

Table 27 – Material Cost Analysis

	178-mm Pile (1) No. 25	**178-mm Pile 152-mm Pipe**
No. Piles (per 91-m slope)	758	303
Grout volume (m^3)	113.7	45.5
Grout cost ($)	8,900	3,500
Steel cost ($)	19,000	45,500
Material cost (per 91-m slope)	27,900	49,000
Material cost (per m^2)	14.00	24.60

Notes:
Unit costs: \$78 / m^3 grout, \$25 / No. 25, \$150 / 152-mm pipe

CHAPTER 7

CONCLUSIONS

INTRODUCTION

It is apparent, from examples in literature and from pile load tests performed at the Iowa State University Spangler Geotechnical Experimentation Site, that small-diameter pile elements provide effective passive resistance to lateral soil movement. Traditional procedures for designing pile stabilization involve the design of large-diameter, heavily-reinforced pile sections, such that the bending moment induced by the application of the ultimate soil pressure does not exceed the moment capacity of the proposed section. An alternative stabilization approach, presented in the thesis, employs small-diameter pile elements. The thesis outlines a rational design procedure for slope reinforcement with *soil displacement grouted micropiles* and discusses the benefits associated with implementing the unconventional remediation method into slope stabilization practices.

SUCCESSES OF RESEARCH

The program of work accomplished in the research study includes the performance of a comprehensive literature review on the state of knowledge of slope stability and slope stabilization, the preparation and performance of 14 full-scale pile load tests, the analysis of load test results, and the development of a design methodology for implementing the technology into current practices of slope stabilization.

The load transfer of piles subject to lateral soil movement associated with unstable slopes has been the focus of international analytical and experimental studies. The results of

this research project, however, represent a significant contribution to the ongoing evaluation of pile stabilization. The experimental testing plan, executed in a controlled environment, involved testing full-scale pile elements subject to uniform lateral translation of soil and incorporated three critical parameters of pile stabilization (e.g. soil type, pile size, pile spacing).

The main conclusions developed from the research study are summarized as follows:

CONCLUSIONS

Review of Literature

- Prediction of lateral soil movement profiles is difficult, and alternative design and analysis methods of pile stabilization incorporate a limit state methodology.
- Ultimate soil pressures are most easily and most reliably obtained from p-y relationships, but p-y curves necessitate prohibitively-expensive pile load tests.
- Other researchers have established approximations for ultimate soil pressure in terms of standard soil properties and stress conditions.
- Recent investigations have established the feasibility of stabilizing relatively shallow slope failures with slender pile elements.

Laboratory Investigation

- Load-displacement (p-y) curves are empirically developed from unconfined and consolidated-undrained (CU) triaxial compression test results.

Field Investigation

- Slender pile elements are effectively installed with simple construction equipment (i.e. small drill rig and concrete mixer) and minimal labor.

- Displacement and strain gauges indicate the load-displacement behavior of reinforced soil and indirectly indicate the loads induced on piles due to lateral soil movement, respectively.
- The 115-mm-diameter piles offered considerable resistance to lateral soil movement. The 178-mm-diameter piles offered additional resistance, beyond that achieved with smaller pile elements.
- Installation and loading of multiple piles offered some evidence of soil arching and increased capacity due to group effects.
- Gap formation occurred at the front of piles, and the relative displacement of shear boxes and pile heads indicated behavioral stages of pile loading.
- Section moment capacities were mobilized in most pile elements, and the failure of the pile elements was supported by observation of cracked piles upon exhumation.

Analytical Investigation

- Load distributions induced on piles due to lateral soil movement vary linearly with depth.
- Ultimate soil pressures were not mobilized during the performance of pile load tests. The pressures, however, are presumably proportional to the loads induced on piles subject to lateral translation of soil and therefore vary linearly with depth.
- Structural performance of pile elements under the loading conditions of slope reinforcement is effectively predicted with LPILE software.

Design and Feasibility Investigation

- Design of pile stabilization with soil displacement grouted micropiles is performed with relative ease.

- The proposed design methodology is robust, in that the method is readily adaptable to achieve reinforcement requirements for a wide range of slope failure conditions. Piles are potentially designed to be strong or weak, depending on the project-specific requirements and the preferences of the design engineer.
- Designs of pile stabilization with soil displacement grouted micropiles are cost-effective with regards to material costs. The pile elements are installed with traditional engineering materials (i.e. concrete, steel), and the installation does not require specialized equipment.

CHAPTER 8

RECOMMENDATIONS

IMMEDIATE IMPACT

The research study established the feasibility of slope stabilization with small-diameter pile elements, and the research group recommends that pilot studies of slope reinforcement with soil displacement grouted micropiles be performed to more fully understand and verify the load transfer mechanisms of the stabilization system.

LONG-TERM IMPACT

Current practices of slope remediation often fail to address the cause of slope instability. Construction of drainage structures, for example, is ineffective in stabilizing a slope with a low groundwater table and low shear strength parameter values. As a result, select slope failures are repaired on multiple occasions. As evidence of the efficiency and cost-effectiveness of stabilization of nuisance slope failures with soil displacement grouted micropiles is accumulated, local transportation agencies will more readily employ the remediation alternative. Employment of the technology is important, because the technology is often more appropriate for stabilizing shallow slope failures.

FUTURE INVESTIGATION

The recommendations for future research include the monitoring of pilot studies of slope reinforcement with soil displacement grouted micropiles, supplementary experimental studies, and advanced numerical studies, as follows:

Slope Stabilization and Monitoring Studies

- Develop site-specific stabilization designs based in-situ soil tests (e.g. borehole shear test, K_o stepped blade test) and pile load tests.
- Monitor slope movement and load transfer of the stabilization system with inclinometers, piezometers, daily rainfall records, strain measurements, and survey markers.

Experimental Studies

- Directly measure load-displacement (p-y) relationships of soil, and correlate p-y curves with standard soil properties. Develop ultimate soil pressure (P_u) envelopes with respect to overburden and/or confining stress for given soil and pile properties.
- Perform pile load tests on battered and truncated piles to investigate the influence of orientation on the stabilization potential of slender pile elements. This experimental study is the next most important task for improving remediation with soil displacement grouted micropiles.

Numerical Studies

- Perform 3-D finite element analyses of experimental testing of this research study. The analyses serve as calibration for constitutive models of engineering materials and boundary conditions of slope reinforcement.
- Perform 3-D finite element analyses of slope reinforcement to investigate the complicating issues of slope stabilization, as follows:
    - Numerical investigations (3-D FEA) indicate the influence of interactions between adjacent piles, namely soil arching.

- The imposition of displacement compatibility between piles and adjacent soil results in stress concentrations of which current analytical models fail to consider.

REFERENCES

Abramson, L. W., Lee, T. S., Sharma, S. and Boyce, G. M. (2002). *Slope Stability and Stabilization Methods*, 2nd Ed., John Wiley & Sons, Inc., New York.

Anderson, W. I. (1998). *Iowa's Geological Past: Three Billion Years of Change*, University of Iowa Press, Iowa City.

ASTM C128, 2002. Specific Gravity and Absorption of Fine Aggregate. American Standard Testing Methods.

ASTM D698, Method A, 2000. Standard Test Method for Moisture-Density Relations of Soils and Soil-Aggregate Mixtures. American Standard Testing Methods.

ASTM D2487, 2000. Standard Test Method for Classification of Soils for Engineering Purposes. American Standard Testing Methods.

ASTM D4318, 2000. Standard Test Method for Liquid Limit, Plastic Limit, and Plasticity Index of Soils. American Standard Testing Methods.

ASTM D6951, 2003. Standard Test Method for Use of the Dynamic Cone Penetrometer in Shallow Pavement Applications. American Standard Testing Methods.

Barrett, R. K., Ruckman, A. C., Myles, B. and Steward, J. (2002). "Launched soil nails stabilize embankments." *http://www.soilnaillauncher.com* , Date accessed May 12, 2004.

Benedict, C., Haider, T. and Byle, M. (2001). "Compaction grout columns for track support." *Foundations and Ground Improvement*, ASCE, 113, 74-88.

Bransby, M. F. and Springman, S. (1999). "Selection of load-transfer function for passive lateral loading of pile groups." *Comput. Geotech.*, 24 (3), 155-184.

Broms, B. B. (1964a). "Lateral resistance of piles in cohesionless soils." *Journal of the Soil Mechanics and Foundation Division*, ASCE, Vol. 90, SM3, 123-156.

Broms, B. B. (1964b). "Lateral resistance of piles in cohesive soils." *Journal of the Soil Mechanics and Foundation Division*, ASCE, Vol. 90, SM2, 27-63.

Coduto, D. P. (2001). *Geotechnical Engineering: Principles and Practices*, 2nd Ed., Pearson Education, New York.

COM624 (1993). "Laterally loaded pile analysis program for the microcomputer." *FHWA-SA-91-048*, Computer program documentation, by S. T. Wang and L. C. Reese.

Crozier, M. J. (1986). "Landslides - causes, consequences and environment." *Croom Helm*, London, 252.

CTRE (2003), "Flowable mortar helps prevent settling of bridge approaches." *Technology News*, June.

Das, B. M. (1999). *Principles of Foundation Engineering*, 4th Ed. PWS Publishing Co., Boston.

Davidson, D. T. (1960). "Geologic and engineering properties of pleistocene materials in Iowa." *Iowa Highway Research Board, Bulletin 20.*

Davies, J. P., Loveridge, F. A., Patterson, D. and Carder, D. (2003). "Stabilization of a landslide on the M25 highway London's main artery." http://www.hatch.ca/Infrastructure/, Date accessed July 18, 2004.

Elias, V. and Juran, I. (1991). "Soil nailing for stabilization of highway slopes and excavations." *Report, FHWA-RD-89-198.*

Elias, V., Christopher, B. R. and Berg, R. R. (2001). "Mechanically stabilized earth walls and reinforced soil slopes design and construction guidelines." *Report, FHWA-NHI-00-043.*

FLAC (2004). *FLAC/Slope User's Guide*, 2nd Ed., Itasca Consulting Group, Inc., Minneapolis.

Forrester, K. (2001). *Subsurface Drainage for Slope Stabilization*, ASCE Press, New York.

Fox, N. S. and Cowell, M. J. (1998). *Geopier Foundation and Soil Reinforcement Manual.* Geopier Foundation Company, Inc., Scottsdale.

Fukuoka, M. (1977). "The effects of horizontal loads on piles due to landslides." *Proceedings, 9th International Conference on Soil Mechanics and Foundation Engineering*, Tokyo, 27-42.

Handy, R. L. and White, D. J. (unpublished). "Stress zones near displacement piers: radial cracking and wedging."

Hansen, B. (1961). "The ultimate resistance of rigid piles against transversal forces." *Bulletin No. 12*, Danish Geotechnical Institute, Copenhagen.

Holtz, R. D., Christopher, B. R., and Berg, R. R. (1997). *Geosynthetic Engineering*, BiTech Publishers Ltd., Richmond.

Hong, L. (2003). "Laterally loaded intermediate cast-in-drilled-hole (CIDH) concrete piers: evaluation of scale and base shear effects." Master's thesis submitted to the Department of Civil, Construction and Environmental Engineering, Iowa State University, Ames, IA.

Ito, T. and Matsui, T. (1975). "Methods to estimate lateral force acting on stabilizing piles." *Soils and Foundations*, 15 (4), 43-59.

Ito, T., Matsui, T. and Hong, P. W. (1981). "Design method for stabilizing piles against landslide – one row of piles." *Soils and Foundations*, 21 (1), 21-37.

Loehr, J. E., Bowders, J. J. and Salim, H. (2000). "Slope stabilization using recycled plastic pins-constructability," *Final Report, Missouri DOT RDT 00-007.*

Loehr, J. E. and Bowders, J. J. (2003). "Slope stabilization using recycled plastic pins-assessment in varied site conditions," *Final Report, Missouri DOT RDT 03-016.*

Lohnes, R. A., Kjartanson, B. H., and Barnes, A. (2001). "Regional approach to landslide interpretation and repair," *Final report, Iowa DOT Project TR-430.*

Mings, C.L. (1987). "Ko stepped blade tests in alluvial clay." Master's thesis submitted to the Department of Civil, Construction and Environmental Engineering, Iowa State University, Ames, IA.

Mitchell, J. K. (1993). *Fundamentals of Soil Behavior*, 2nd Ed., John Wiley & Sons, Inc., New York.

Nilson, A. H. (1997). *Design of Concrete Structures*, 12th Ed., McGraw Hill Companies, Inc., New York.

Ott, R. L. and Longnecker, M. (2001). *Statistical Methods and Data Analysis*, 5th Ed., Duxbury, Pacific Grove.

Pan, J. L., Goh, A. T. C., Wong, K. S. and Teh, C. I. (2002). "Ultimate soil pressures for piles subjected to lateral soil movements." *Journal of Geotechnical and Geoenvironmental Engineering, June*, 530-535.

Pearlman, S. L. and Withiam, J. L. (1992). "Slope stabilization using in situ earth reinforcements." *Presented at ASCE Conference*, Berkeley.

Polster, D. F. (2003). "Soil bioengineering for slope stabilization and site restoration." *Mining and the Environment III*, May 25-28.

Popescu, M. (1994). "A suggested method for reporting landslide causes." *Bull IAEG*, 50, 71-74.

Poulos, H. G. and Davis, E. H. (1980). *Pile Foundation Analysis and Design*, John Wiley & Sons, Inc., New York.

Poulos, H. G. (1995). "Design of reinforcing piles to increase slope stability." *Canadian Geotechnical Journal*, 37, 890-897.

Reese, L. C., William, R. C. and Koop, F. D. (1974). "Analysis of laterally loaded piles in sand." *Proceedings, 6th Offshore Technology Conference*, Vol. 2, 473-483.

Reese, L. C. and Allen, J. D. (1977). *Drilled Shaft Design and Construction Guidelines Manual*, Vol. 2, U.S. Department of Transportation Offices of Research and Development Implementation Division HDV-22.

Reese, L. C. and Wang, S. T. (2000). *LPILE Plus 4.0 Technical Manual.* Ensoft, Inc.

Robertson, P. K. and Campanella, R. G. (1983). "Interpretation of the Cone Penetrometer Test." *Canadian Geotechnical Journal*, Vol. 20, No. 4, 718-745.

Robertson, P. K., Campanella, R. G., Brown, P. T., Grof, I. and Hughes, J. M. (1985). "Design of axially and laterally loaded piles using in situ tests: a case history." *Canadian Geotechnical Journal*, Vol. 22, No. 4, 518-527.

Robertson, P. K., Davies, M. P. and Campanella, R. G. (1987). "Design of laterally loaded driven piles using the flat dilatometer." *Geotechnical Testing Journal*, ASCE, Vol. 149, No. 89, 30-38.

Rogers, C. D. F. and Glendinning, S. (1997). "Stabilization of shallow slope failures with lime piles." *Transportation Research Record*, 1589, 83-91.

Santi, P. M. (2001). "Horizontal wick drains as a cost-effective method to stabilize landslides." *Geotechnical News*, Vol. 17, No. 2, 44-46.

Schlagbaum, T. (2002). "Economic impact of self-consolidating concrete (SCC) in ready mixed concrete." First North American Conference on the Design and Use of Self-Consolidating Concrete, November 12-13.

Schlosser and Francois (1991). "Recommendations Clouterre." *Report, U.S. Department of Transportation, NTIS No. PB94-109980.*

Sotir, R. B. and Gray, D. H. (1996). *Biotechnical and Soil Bioengineering Slope Stabilization: A Practical Guide for Erosion Control*, John Wiley & Sons, Inc., New York.

Spiker, E. C.and Gori, P. L. (2003). "National landslide hazards mitigation strategy – a framework for loss reduction." U.S. Geological Survey, Circular 1244, 4-13.

Viggiani, C. (1981). "Ultimate lateral load on piles used to stabilize landslides." *Proceedings, 10th International Conference on Soil Mechanics and Foundation Engineering,* Stockholm, Vol. 3, 555-560.

Walker, B. and Fell, R. (1987). *Soil Slope Instability and Stabilization.* A.A.Balkema Publishers, Rotterdam.

Wong, D. O., FitzPatrick, B. T. and Wissman, K. J. (2004). "Stabilization of retaining walls and embankments using rammed aggregate piers. *Geotechnical Engineering in Transportation Projects*, ASCE, 126 (2), 1866-1875.

Wu, T. H. (1995). "Evaluation of remedial measures for embankment failures." *Report, FHWA/OH-95019.*

ACKNOWLEDGMENTS

The author wishes to express his deepest gratitude to his major advisor, Dr. David White, for his guidance during this study. Dr. White demonstrated, beyond technical insight, his enthusiasm for geotechnical engineering research. The opportunity to work for such a model has been the highlight of my academic career.

Dr. Muhannad Suleiman was an invaluable resource throughout the study. Dr. Suleiman worked closely with the author in developing the research program, performing pile load tests, and interpreting the study results.

The author would also like to thank advisory committee members Dr. Vern Schaefer and Dr. Thomas Rudolphi for their contribution to the research.

Special recognition goes to Iowa State University graduate and undergraduate students Mohamed Mekkawy, Sherry Voros, Matz Jungman, and Martinique Martineau for their assistance during the field testing phase of the project.

APPENDIX A

P-Y CURVES FOR ISU SGES

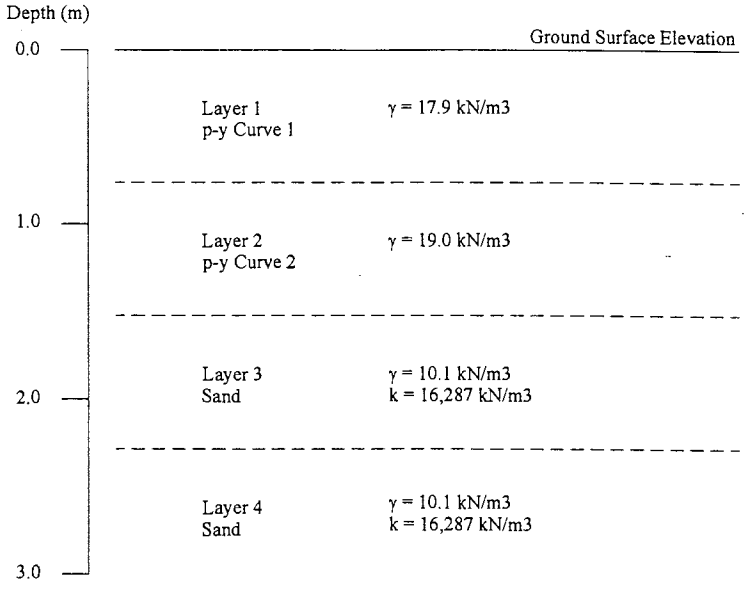

Figure 260 - Iowa State University SGES Soil Profile

Table 28 - Iowa State University SGES p-y Curves

p-y Curve 1		p-y Curve 2	
y (cm)	**p (kN/m)**	**y (cm)**	**p (kN/m)**
0.0	0.0	0.0	0.0
0.2	35.4	0.3	65.0
0.5	50.6	1.0	125.2
1.0	73.4	2.9	173.7
2.2	96.8	4.7	191.4
3.5	111.2	6.6	201.6
4.7	121.5	8.4	207.9
5.9	128.9	10.3	213.7
7.2	133.5	12.2	217.7
8.4	137.7	14.0	220.8
9.7	140.8	15.9	223.6
10.9	143.1	17.8	225.4
12.2	144.1	19.7	227.1
13.4	145.4	21.5	227.5
14.7	146.4	23.4	227.8
15.3	146.4	25.2	228.4
15.9	146.4	25.9	228.5

APPENDIX B

MOMENT-CURVATURE GRAPHS PER PILE

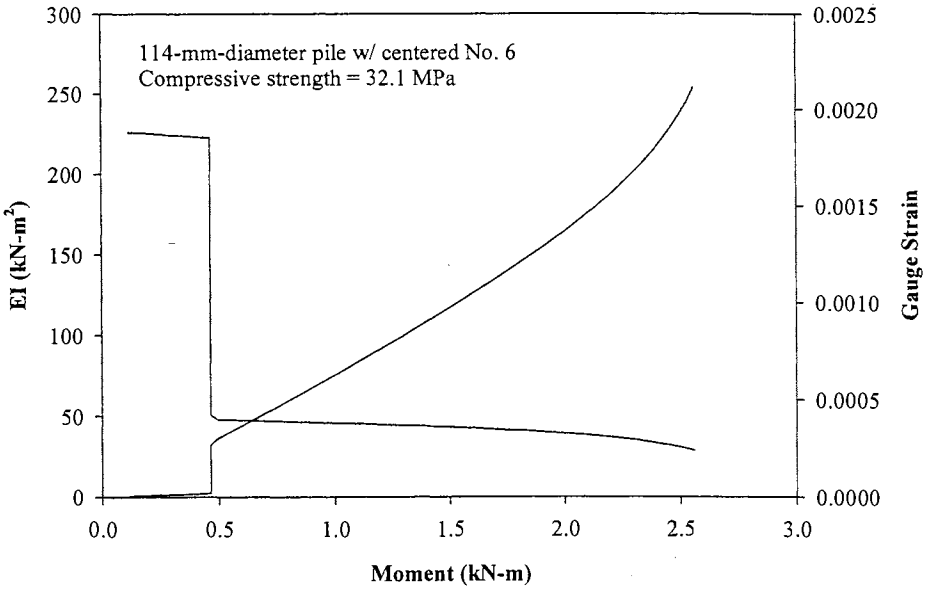

Figure 261 – Graph of Stiffness and Strain vs. Moment (Pile 4)

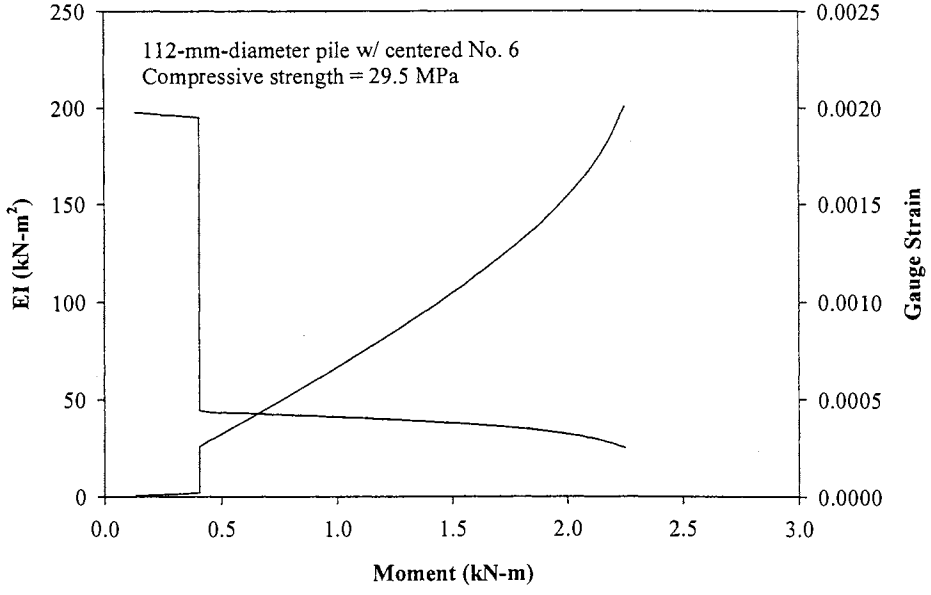

Figure 262 – Graph of Stiffness and Strain vs. Moment (Pile 5)

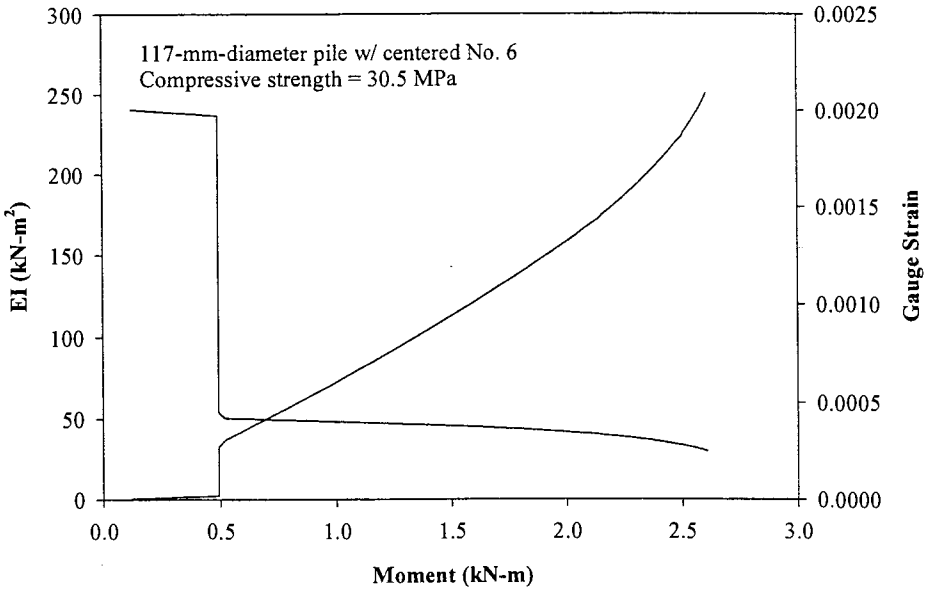

Figure 263 – Graph of Stiffness and Strain vs. Moment (Pile 6)

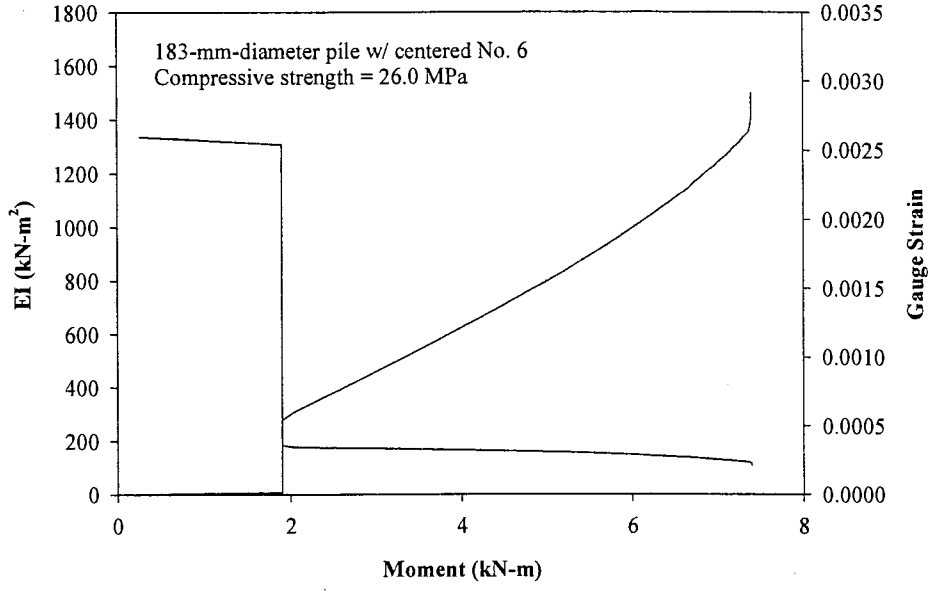

Figure 264 – Graph of Stiffness and Strain vs. Moment (Pile 8)

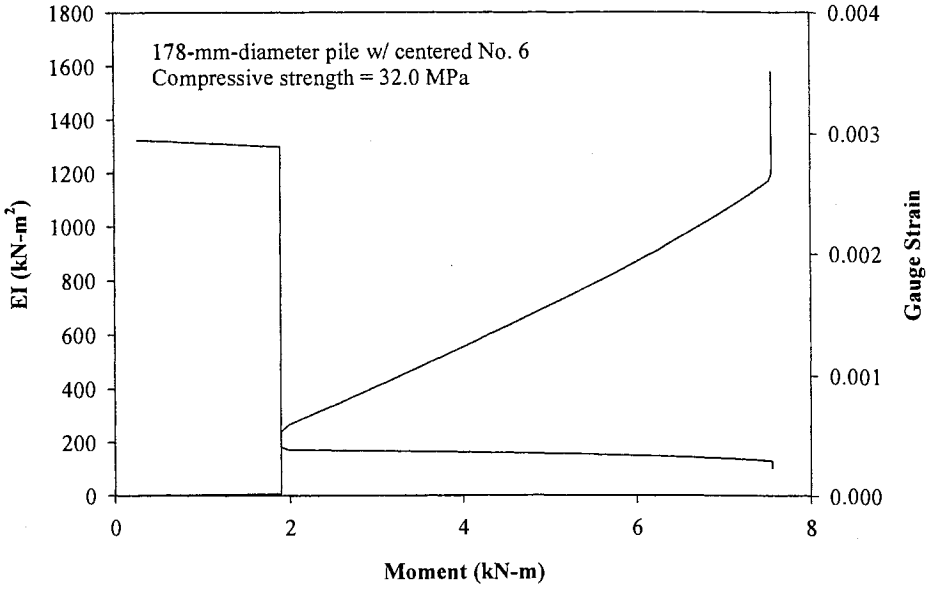

Figure 265 – Graph of Stiffness and Strain vs. Moment (Pile 9)

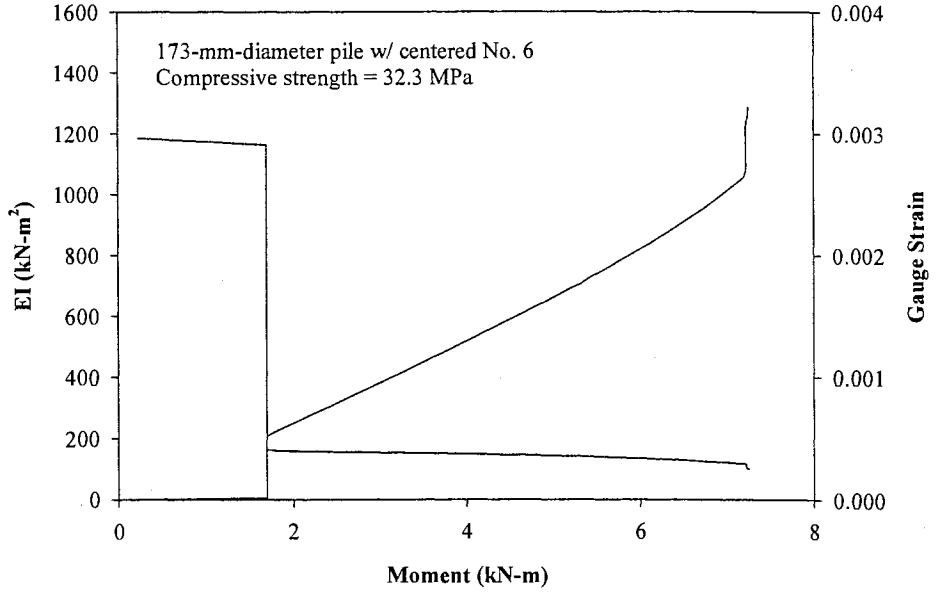

Figure 266 – Graph of Stiffness and Strain vs. Moment (Pile 12)

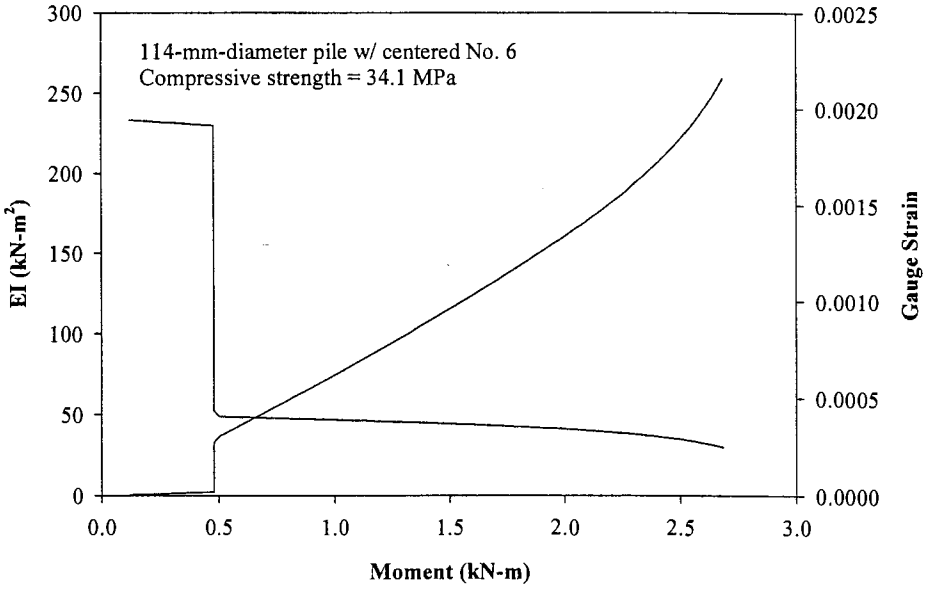

Figure 267 – Graph of Stiffness and Strain vs. Moment (Pile 10 A)

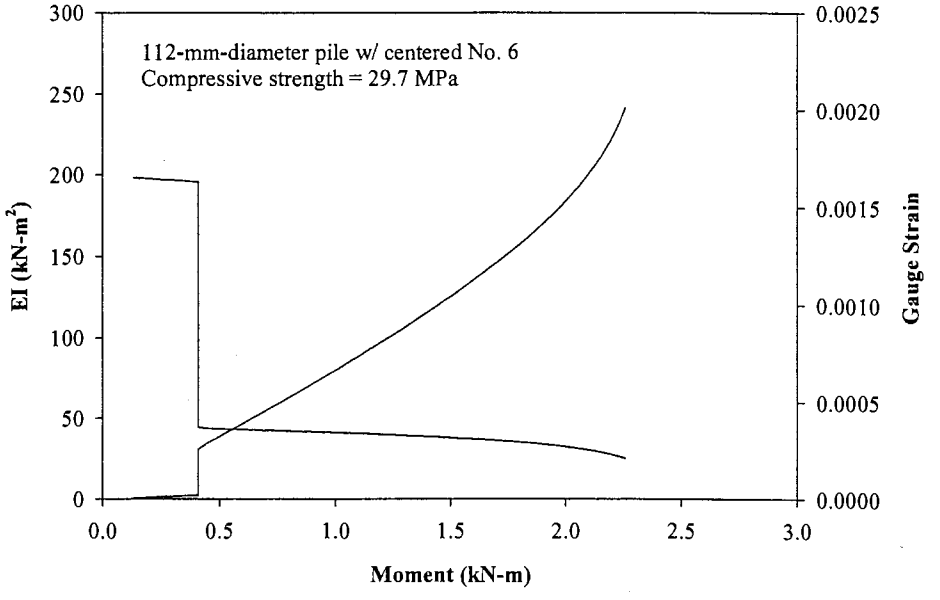

Figure 268 – Graph of Stiffness and Strain vs. Moment (Pile 10 B)

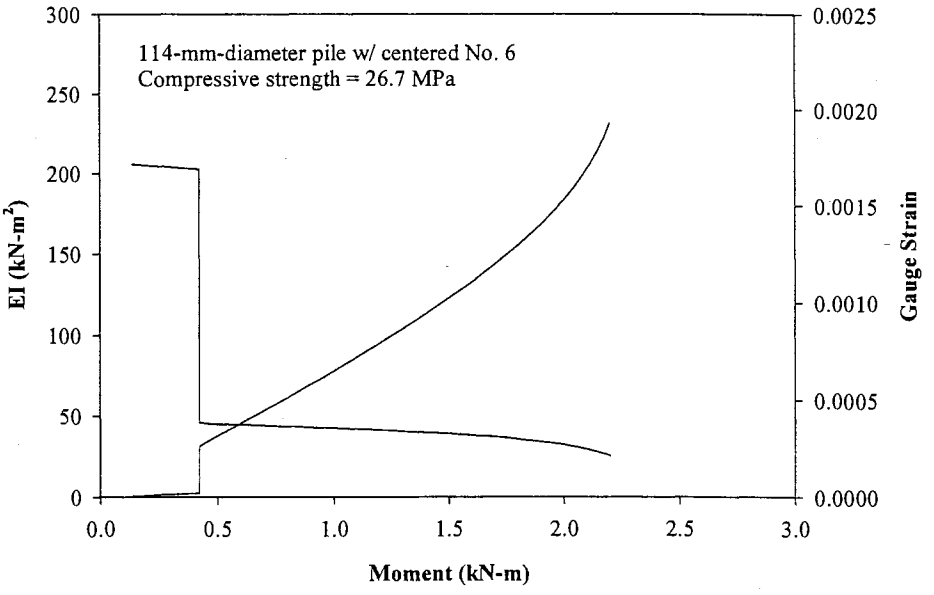

Figure 269 – Graph of Stiffness and Strain vs. Moment (Pile 11 A)

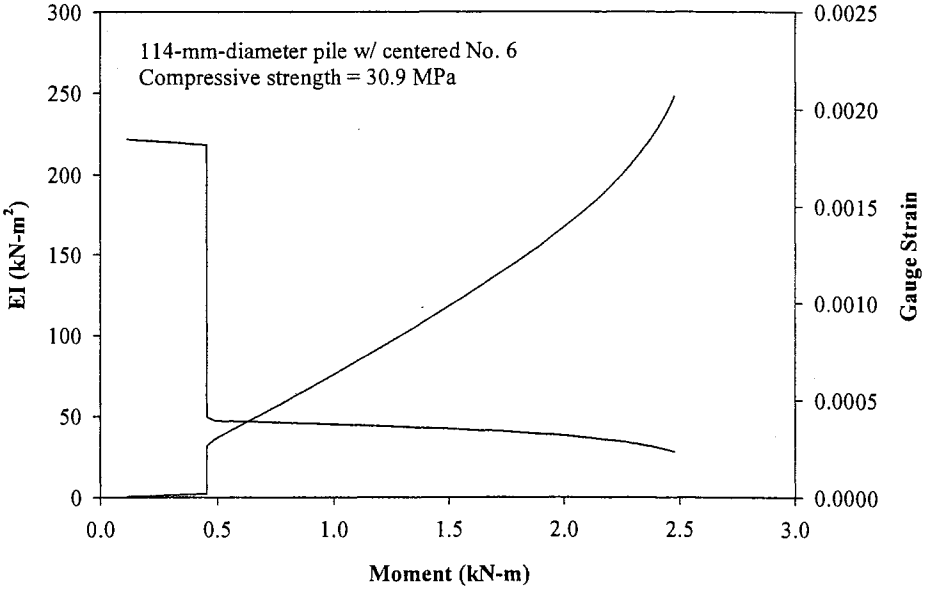

Figure 270 – Graph of Stiffness and Strain vs. Moment (Pile 11 B)

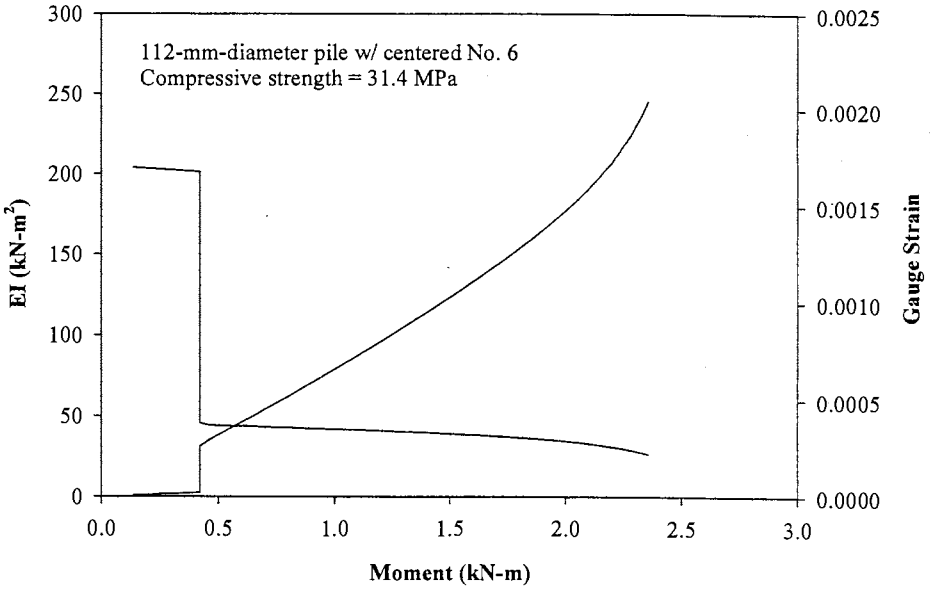

Figure 271 – Graph of Stiffness and Strain vs. Moment (Pile 13 A)

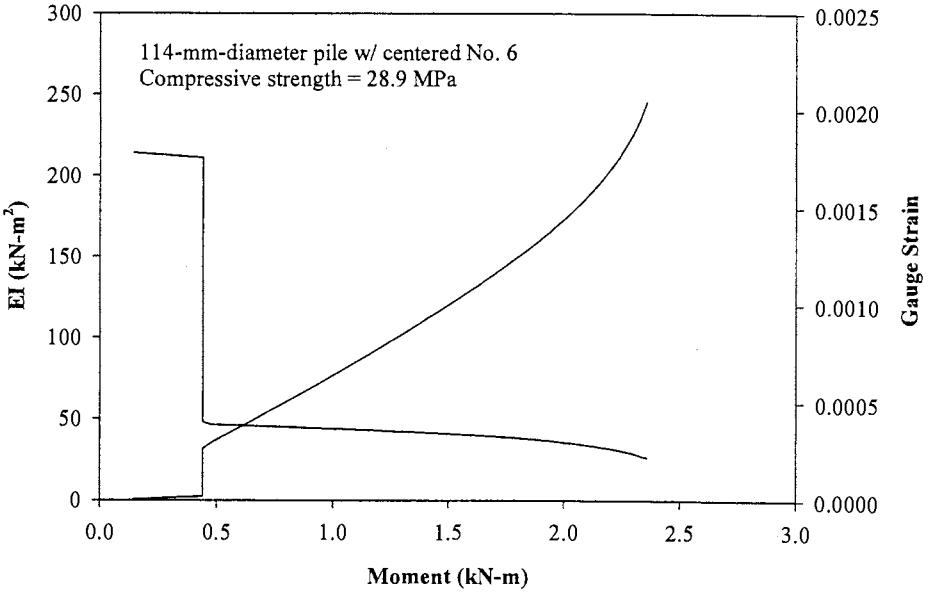

Figure 272 – Graph of Stiffness and Strain vs. Moment (Pile 13 B)

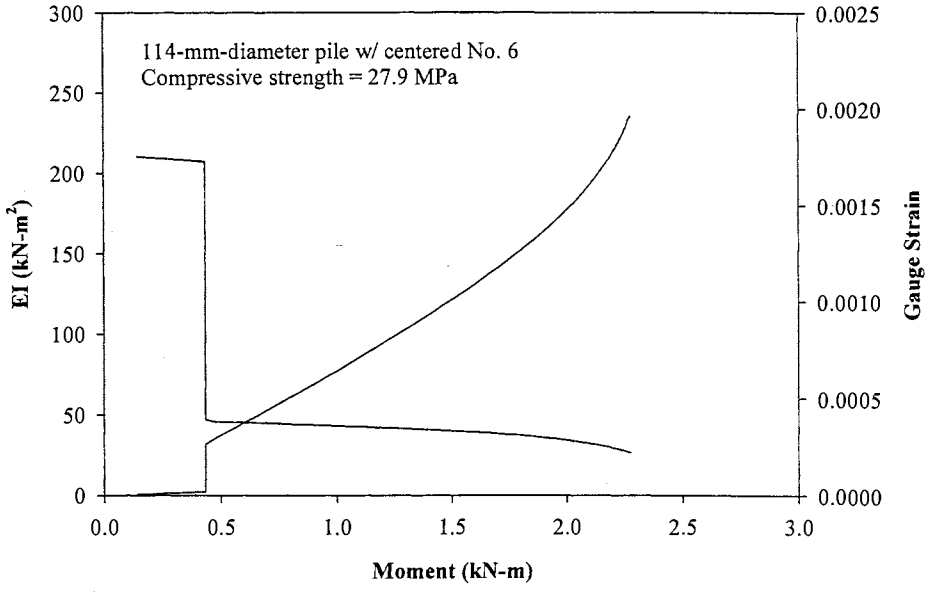

Figure 273 – Graph of Stiffness and Strain vs. Moment (Pile 14 A)

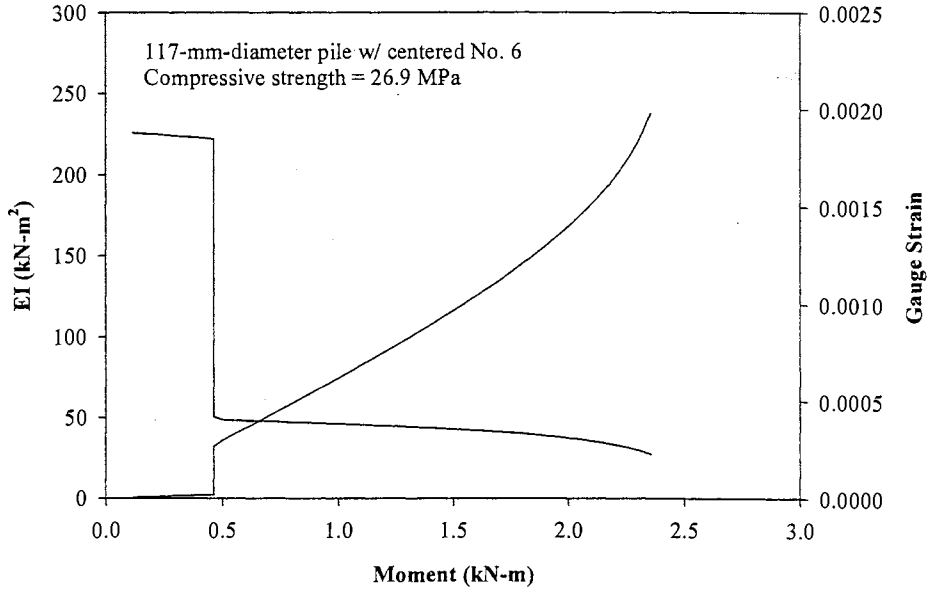

Figure 274 – Graph of Stiffness and Strain vs. Moment (Pile 14 B)

APPENDIX C

PILE LOAD TEST DATA

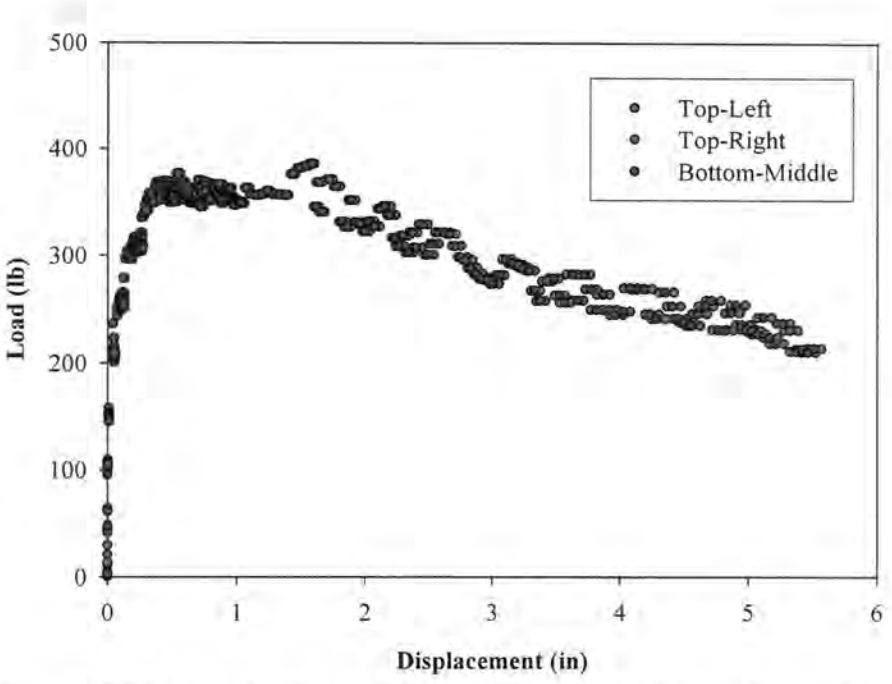

Figure 275 – Graph of Load vs. Displacement for Unreinforced Loess

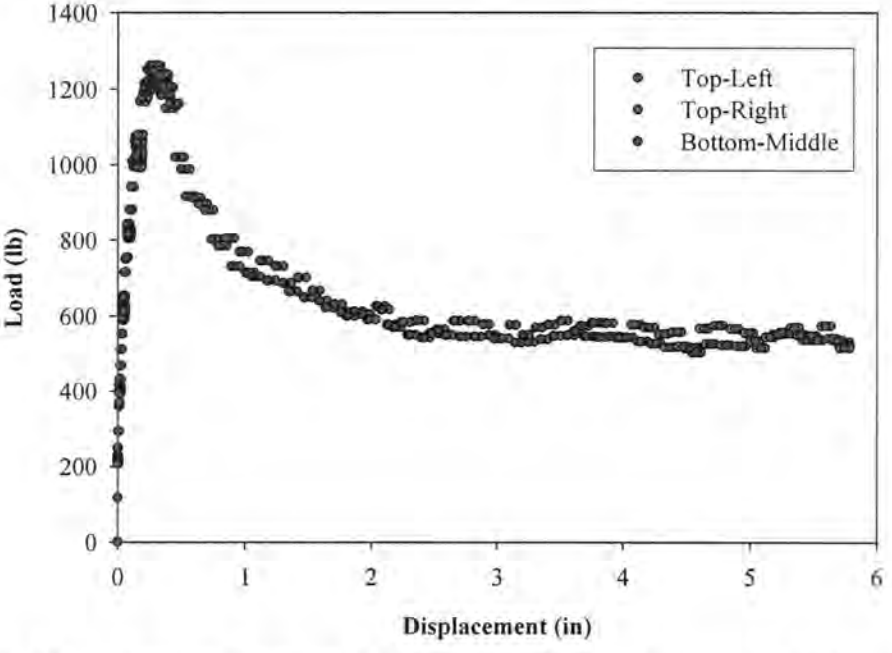

Figure 276 – Graph of Load vs. Displacement for Unreinforced Weathered Shale

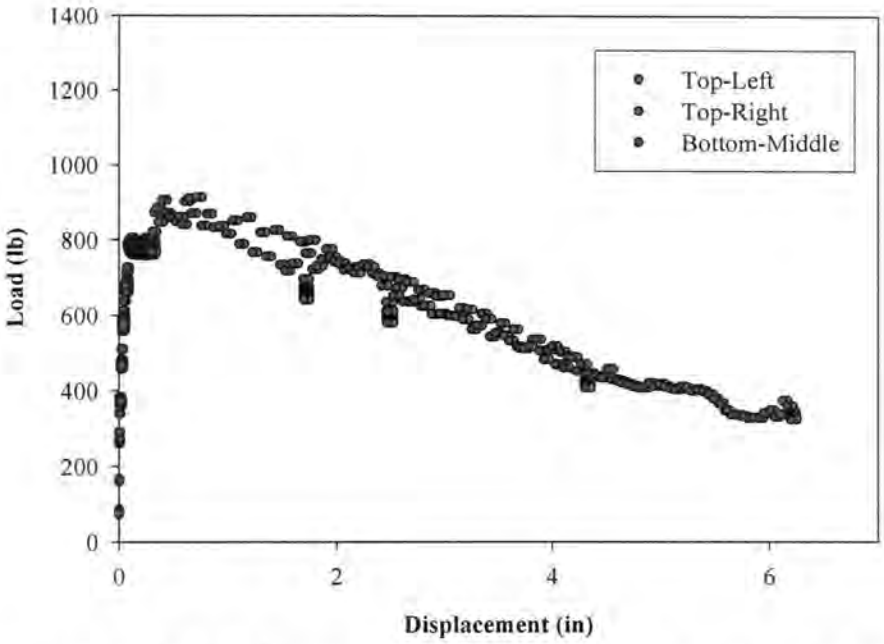

Figure 277 – Graph of Load vs. Displacement for Unreinforced Glacial Till

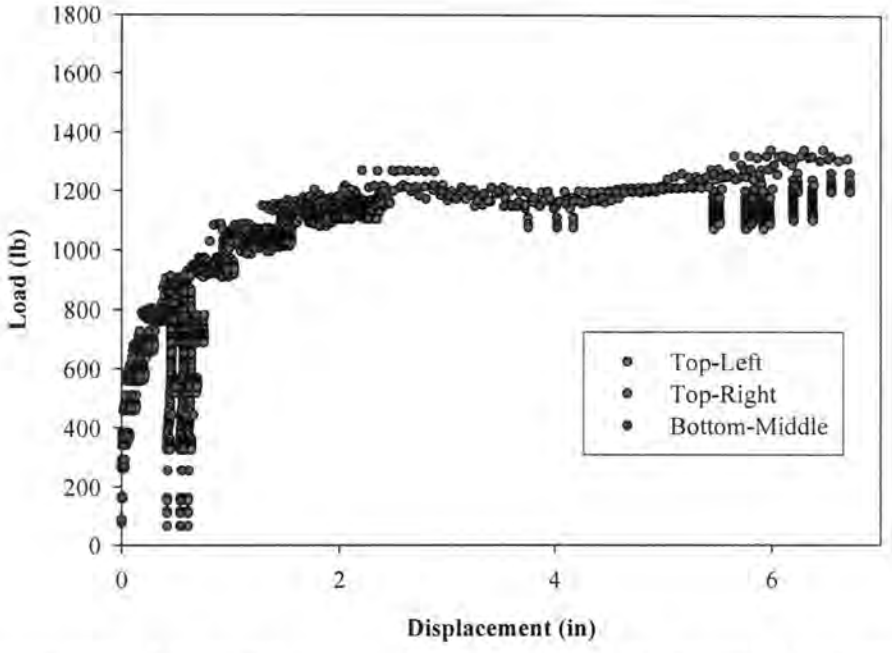

Figure 278 – Graph of Load vs. Displacement for Reinforced Loess (Pile 4)

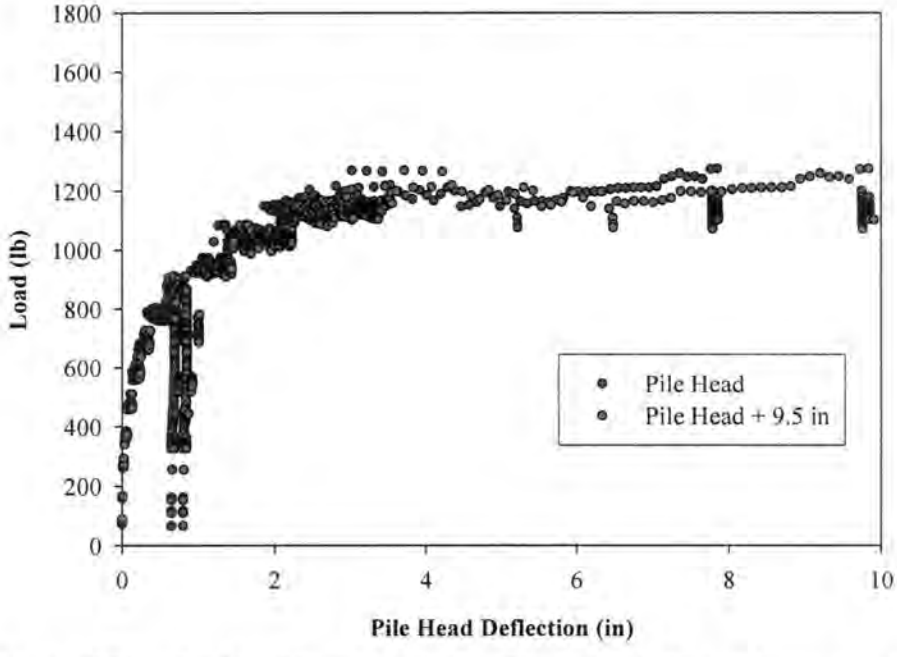

Figure 279 – Graph of Load vs. Deflection for Reinforced Loess (Pile 4)

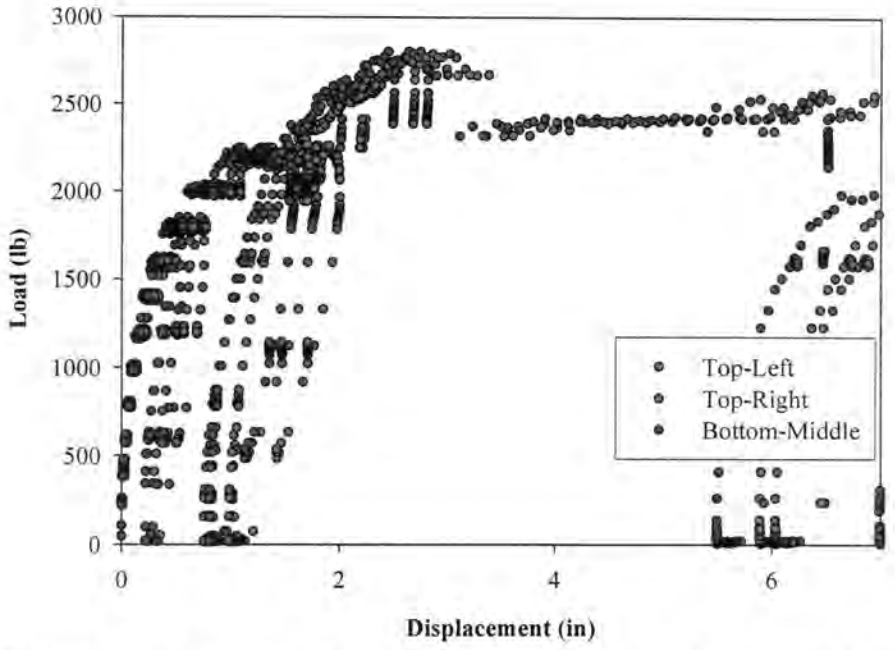

Figure 280 – Graph of Load vs. Displacement for Reinforced Weathered Shale (Pile 6)

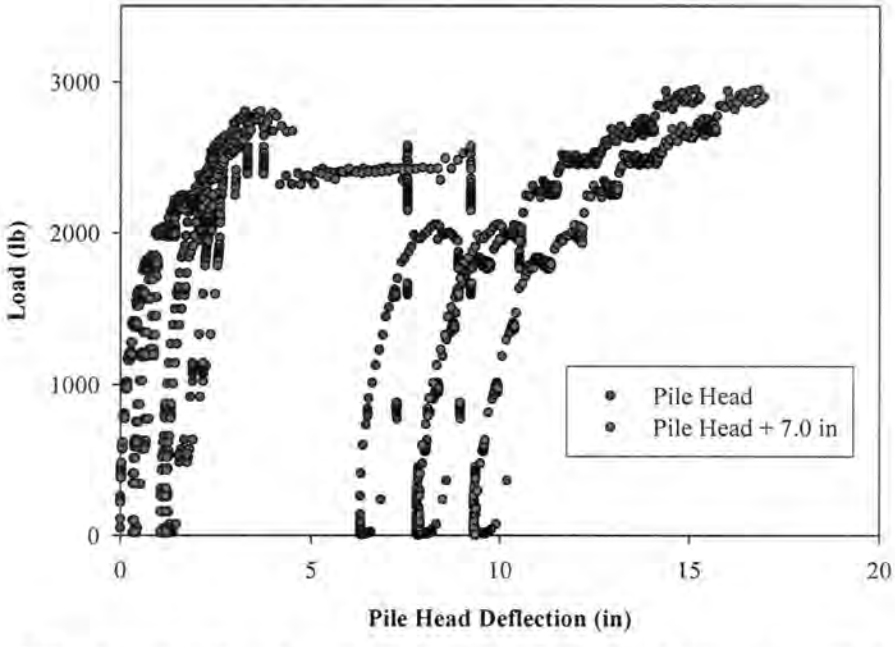

Figure 281 – Graph of Load vs. Deflection for Reinforced Weathered Shale (Pile 6)

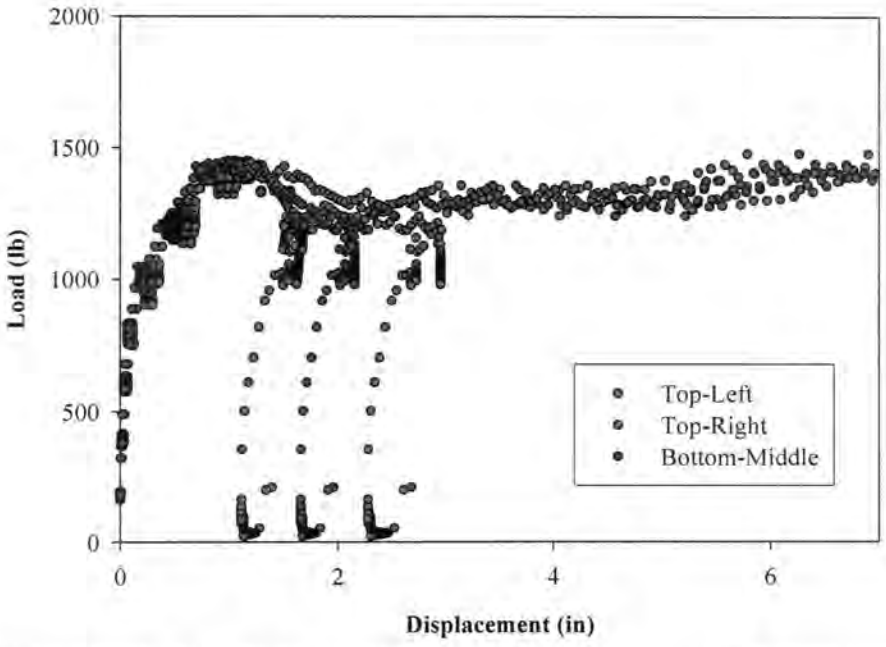

Figure 282 – Graph of Load vs. Displacement for Reinforced Weathered Shale (Pile 7)

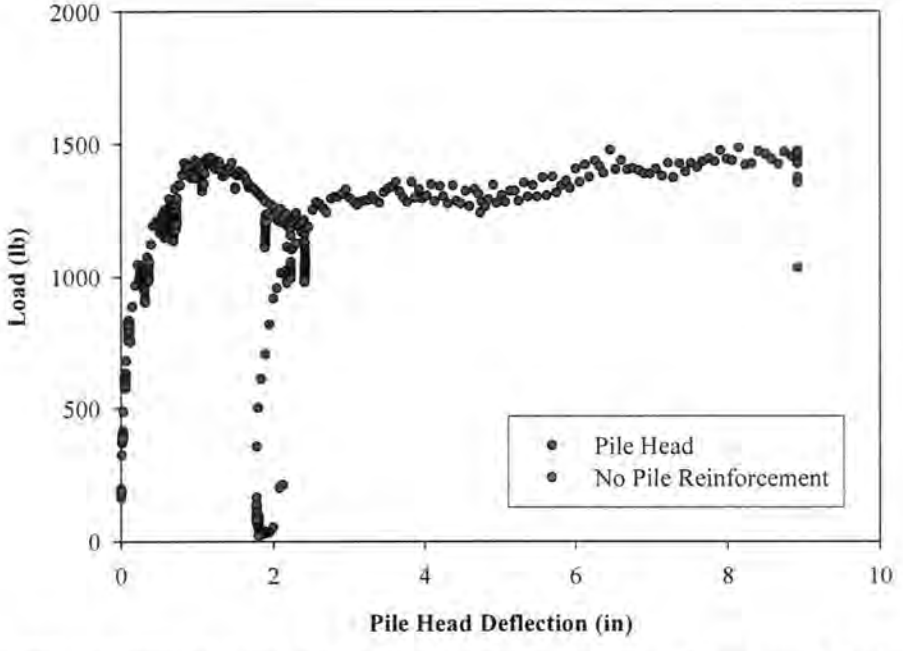

Figure 283 – Graph of Load vs. Deflection for Reinforced Weathered Shale (Pile 7)

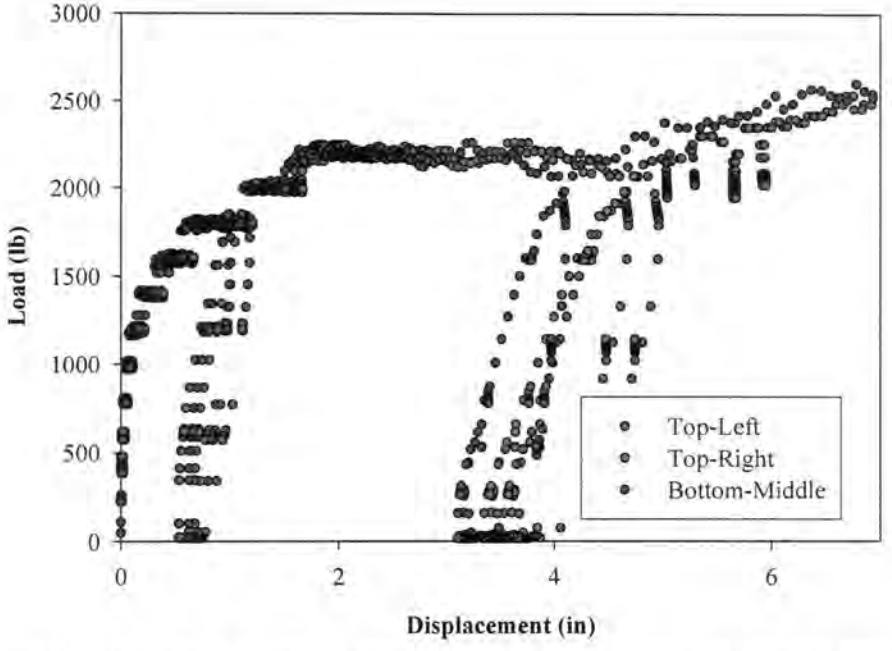

Figure 284 – Graph of Load vs. Displacement for Reinforced Glacial Till (Pile 5)

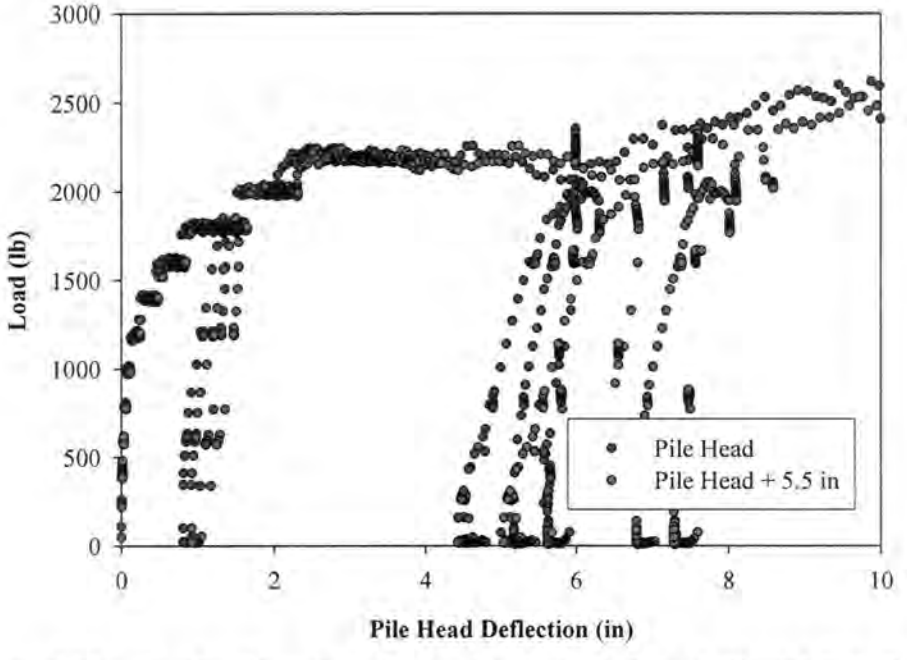

Figure 285 – Graph of Load vs. Deflection for Reinforced Glacial Till (Pile 5)

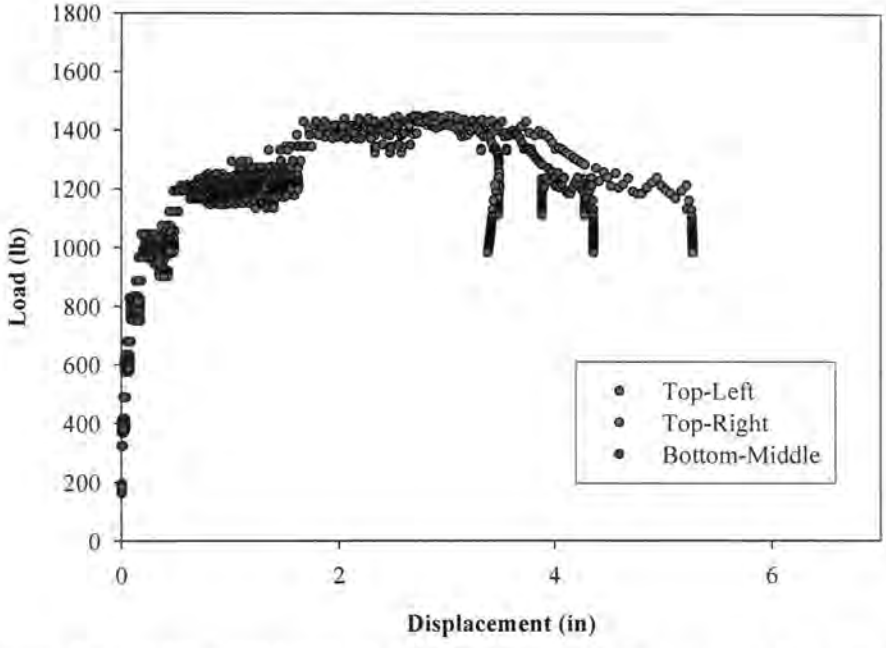

Figure 286 – Graph of Load vs. Displacement for Reinforced Loess (Pile 8)

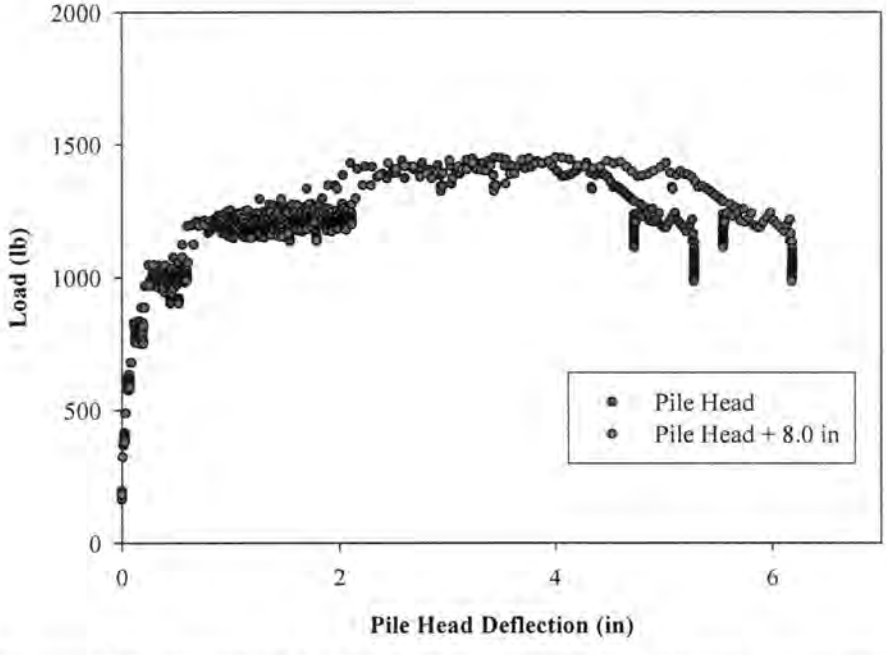

Figure 287 – Graph of Load vs. Deflection for Reinforced Loess (Pile 8)

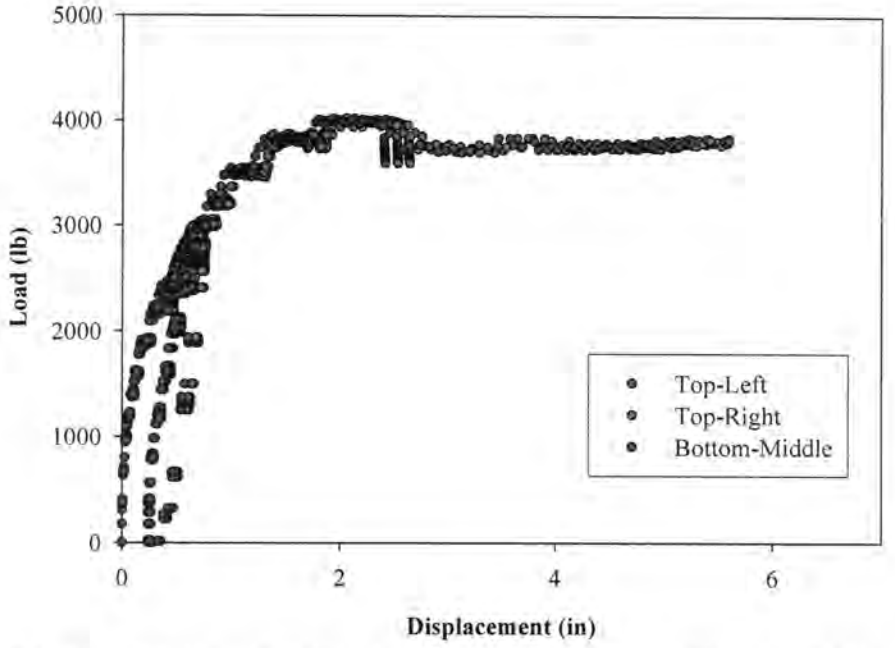

Figure 288 – Graph of Load vs. Displacement for Reinforced Weathered Shale (Pile 12)

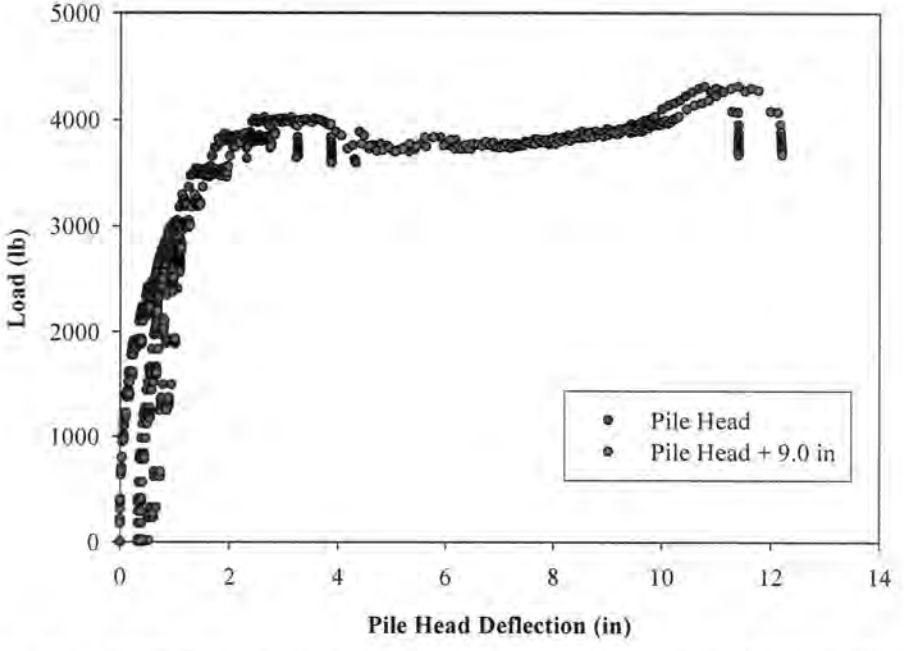

Figure 289 – Graph of Load vs. Deflection for Reinforced Weathered Shale (Pile 12)

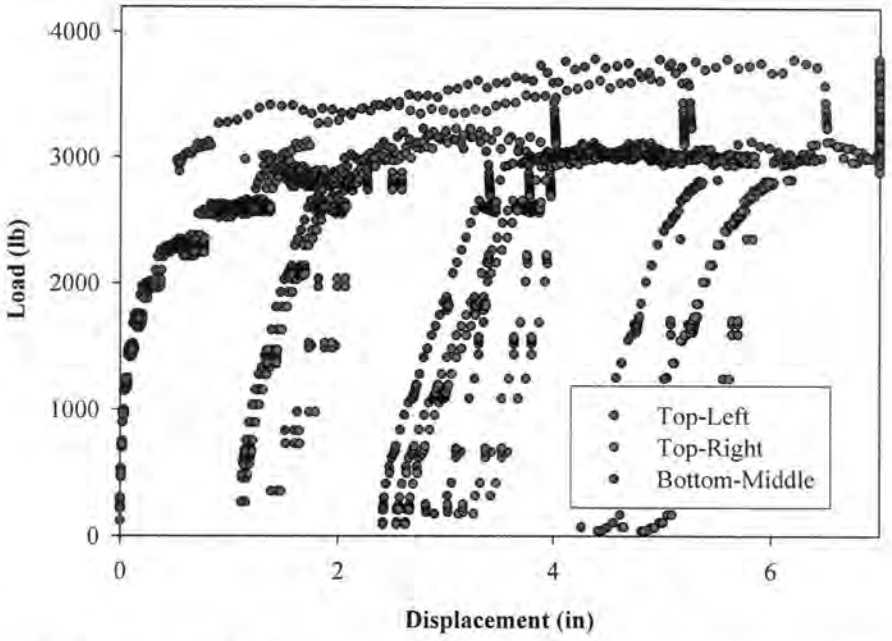

Figure 290 – Graph of Load vs. Displacement for Reinforced Glacial Till (Pile 9)

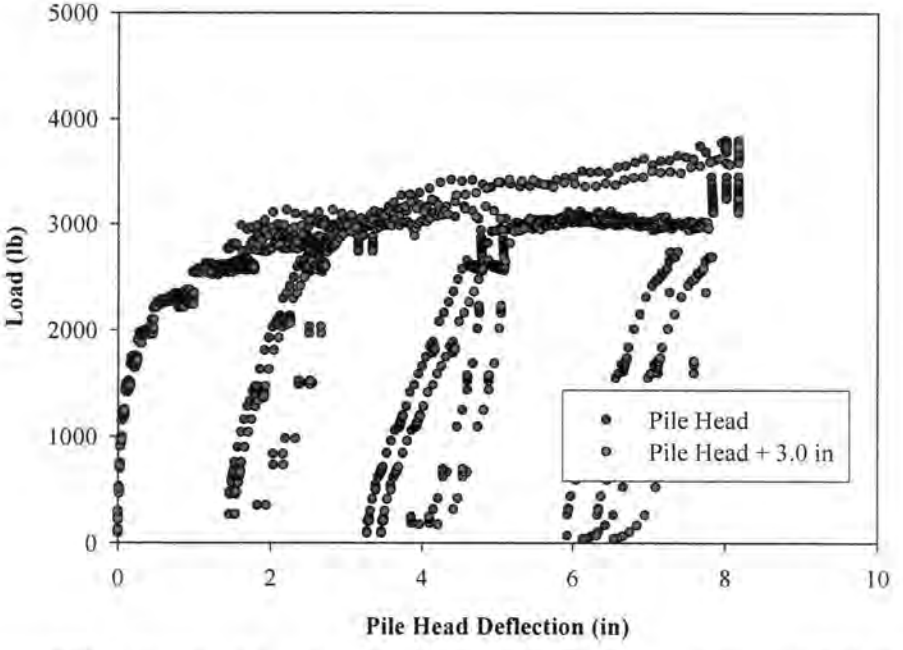

Figure 291 – Graph of Load vs. Deflection for Reinforced Glacial Till (Pile 9)

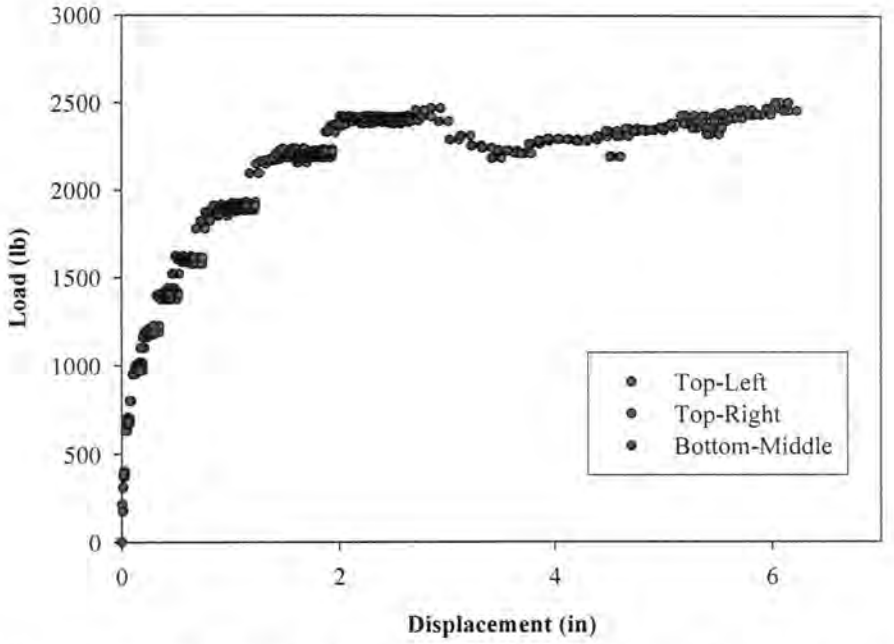

Figure 292 – Graph of Load vs. Displacement for Reinforced Loess (Piles 11 A and B)

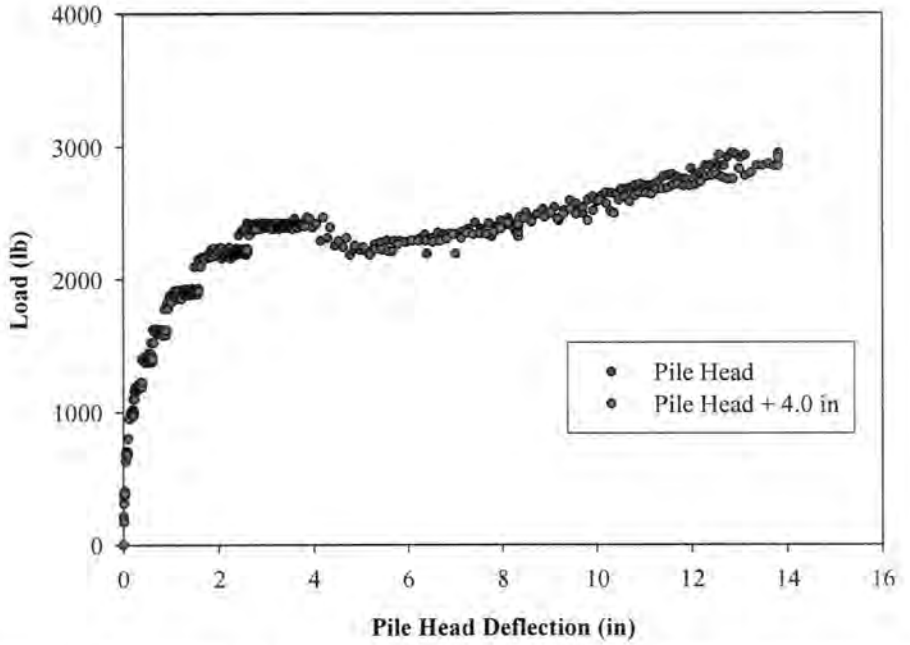

Figure 293 – Graph of Load vs. Deflection for Reinforced Loess (Pile 11 A)

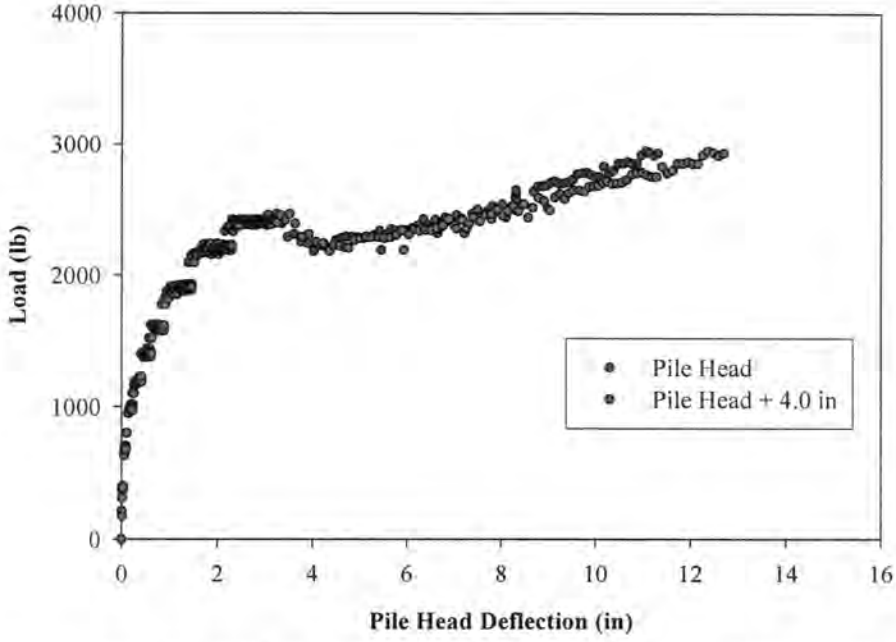

Figure 294 – Graph of Load vs. Deflection for Reinforced Loess (Pile 11 B)

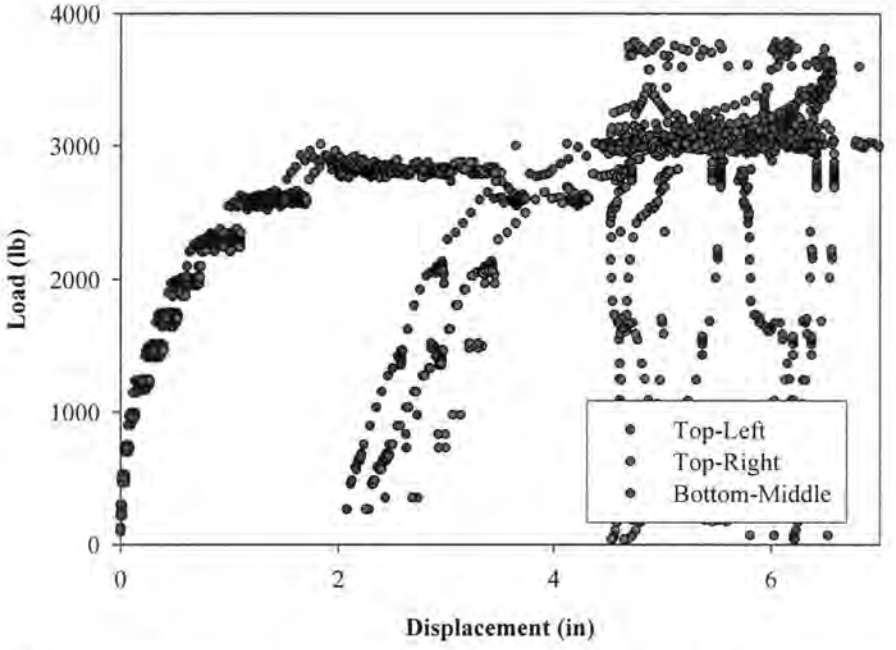

Figure 295 – Graph of Load vs. Displacement for Weathered Shale (Piles 10 A and B)

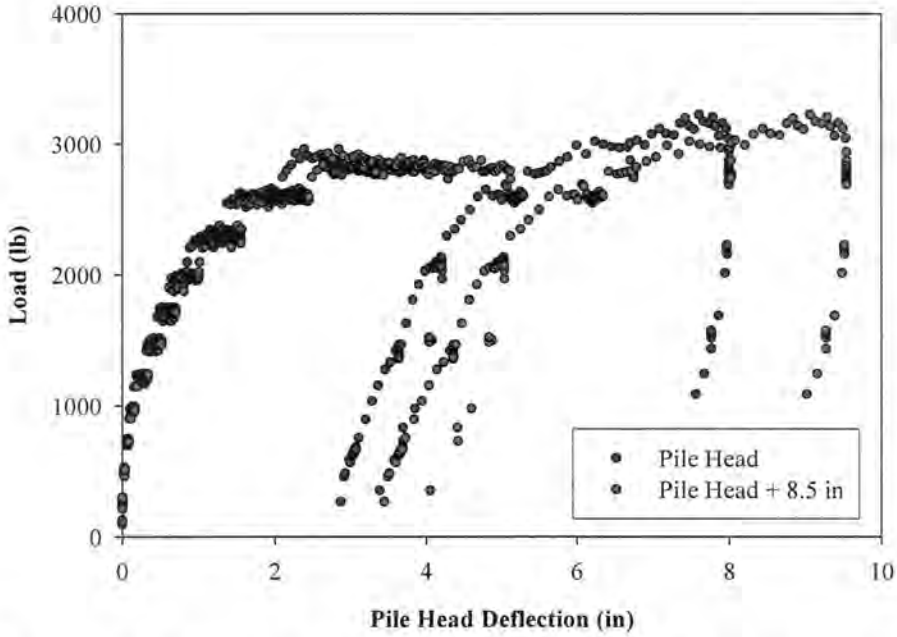

Figure 296 – Graph of Load vs. Deflection for Reinforced Weathered Shale (Pile 10 A)

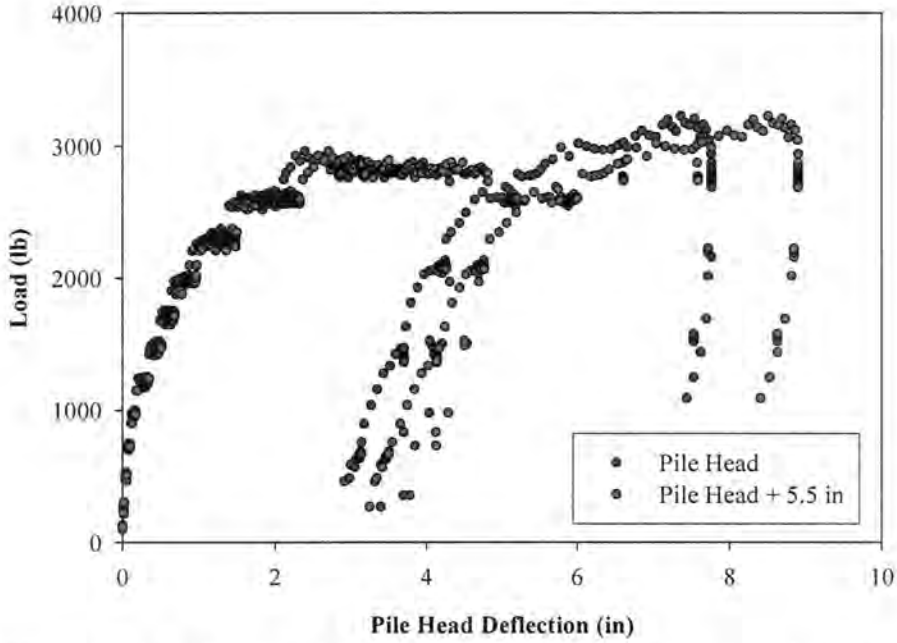

Figure 297 – Graph of Load vs. Deflection for Reinforced Weathered Shale (Pile 10 B)

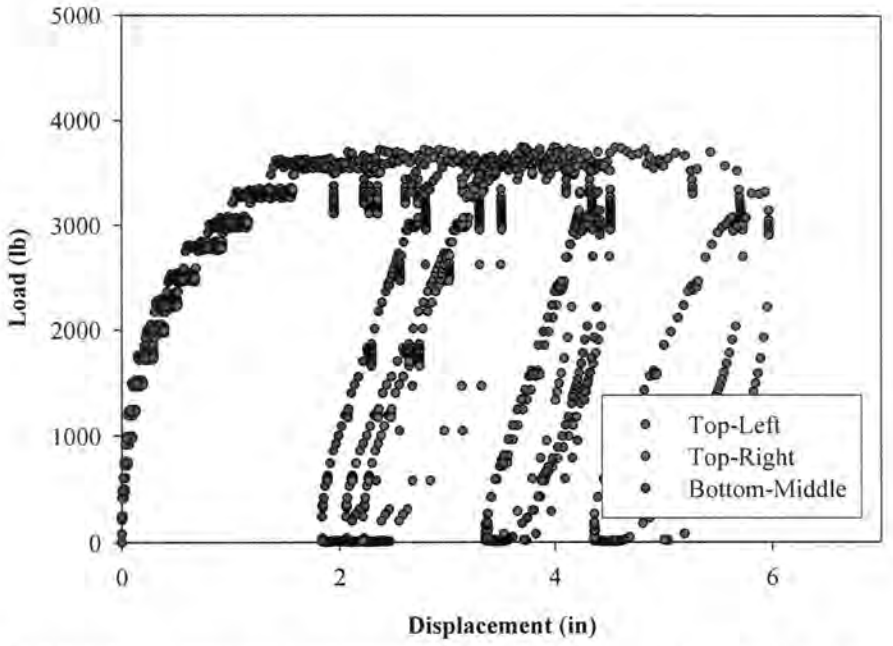

Figure 298 – Graph of Load vs. Displacement for Reinforced Glacial Till (Piles 14 A and B)

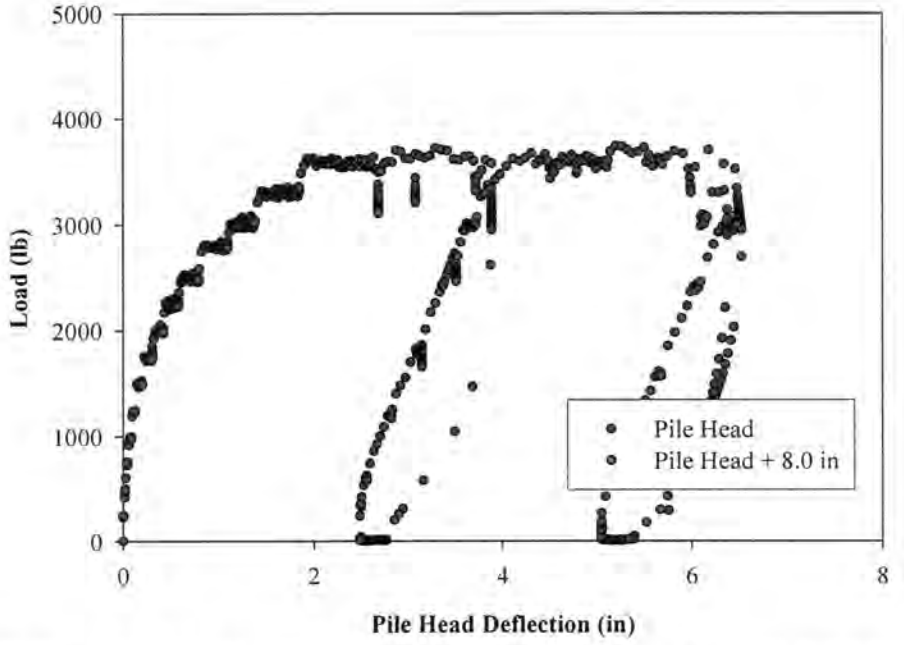

Figure 299 – Graph of Load vs. Deflection for Reinforced Glacial Till (Pile 14 A)

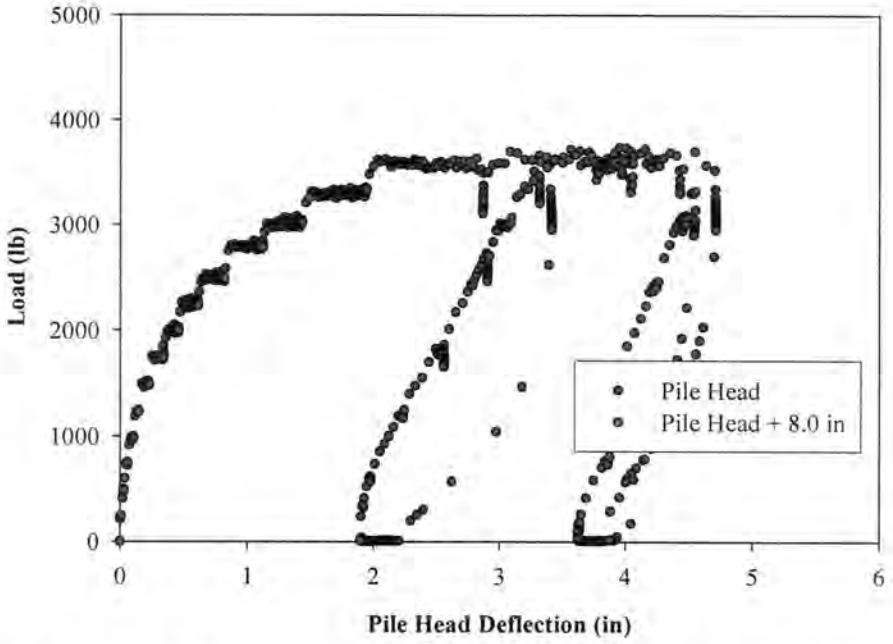

Figure 300 – Graph of Load vs. Deflection for Reinforced Glacial Till (Pile 14 B)

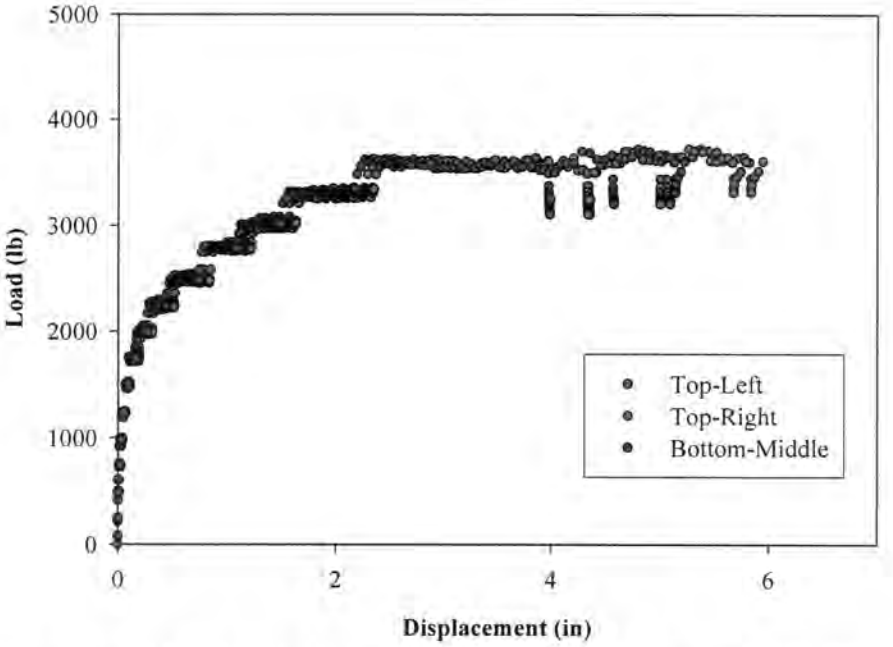

Figure 301 – Graph of Load vs. Displacement for Reinforced Glacial Till (Piles 13 A and B)

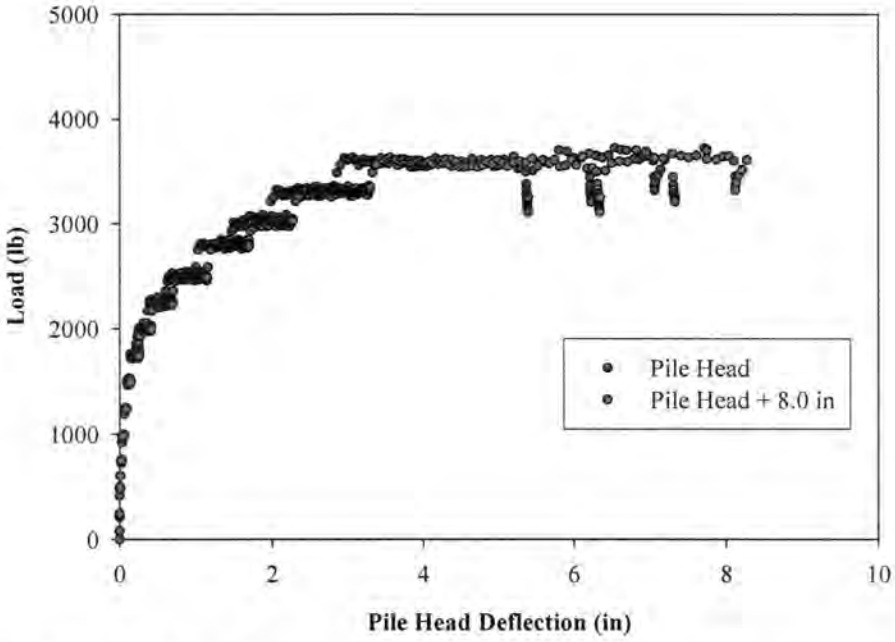

Figure 302 – Graph of Load vs. Deflection for Reinforced Glacial Till (Pile 13 A)

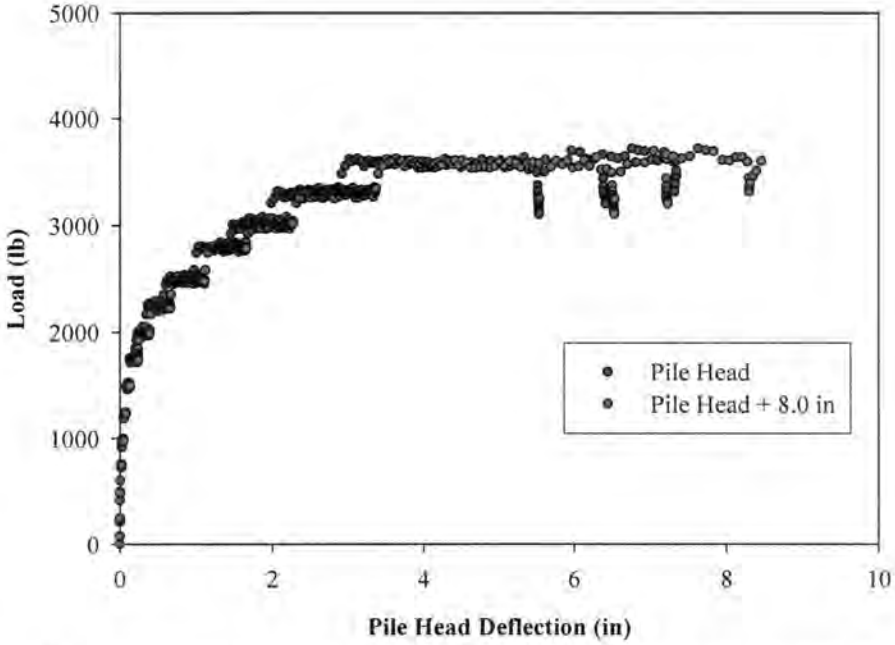

Figure 303 – Graph of Load vs. Deflection for Reinforced Glacial Till (Pile 13 B)